Studies on immunoreceptor activation and SARS-CoV-2 RBD/ACE2 interactions



Michael Ian Barton

St Catherine's College

University of Oxford

A thesis submitted for the degree of Doctor in Philosophy

Hilary Term 2022

Acknowledgments

First, I would like to thank Anton van der Merwe for supervising me during my DPhil. When I first joined his group in late 2016 for a short three-month project, I could not have imagined that I would start and complete a DPhil. Having spent the previous year doing a PGCE in secondary school teaching I really wanted to get back to lab work and after a couple of months Anton agreed to take a chance and employ me as a research assistant. He then encouraged me to apply for DPhil positions to start at the end of 2017. Although I was accepted onto the Sir William Dunn School of Pathology DPhil program, I was not successful in acquiring funding. Once again Anton decided to support me by continuing to employ me as a research assistant during my DPhil, which I am extremely grateful for.

I also need to give a big thank you to Eleanor Denham who agreed to supervise me when I joined the lab even though I did not have much recent lab experience. She subsequently taught me a large amount of immunology and lab techniques including tissue culture, which was new to me. I also want to thank both Marion H Brown and Omer Dushek for regular discussions of my work and supporting me throughout my time in the lab. I have closely collaborated with both in the production of this thesis.

I would also like to thank my transfer examiners Professor Simon Davis and Associate Professor Marco Fritzsche and my confirmation examiners Professor David Vaux and Associate Professor Geraldine Gillespie who were very supportive and helped shape my priorities during my DPhil. I also thank my final viva examiners Professor Simon Davis and Professor Peter Steinberger for studying the work in this thesis and discussing it with me.

I also want to thank all the past and present members of the Molecular Immunology Group. They were all very friendly and lunchtime chat has been a big highlight of my time in the lab. As is often the case in science due to funding and the nature of 4-year DPhils I now find

myself in the position of longest serving lab member. However, I have really enjoyed the spirit of the lab which has always been really supportive and collaborative but there has never been pressure to produce as much data as possible at all costs. We have also had lots of fun lab events including organizing the departmental Christmas party one year which (while a lot of work) was also great fun to do together.

In general, progress on my DPhil was going well until the start of 2020. Then COVID hit, and although it delayed my submission date by six months, it gave me the opportunity to collaborate with my father. He has always supported me to do what I enjoy doing the most. Although I have never wanted to follow him into bioinformatics, from him I inherited my interest in science and all things practical. I of course also want to thank my mother for all her support, especially with my Dyslexia. Without her fighting my corner and providing that early support in school I would not have been able to write this thesis.

However, the pandemic did not leave me unscathed, and Ines and I had to postpone our wedding originally planned for the summer of 2020 to 2021. Thankfully we were able to get married in 2021 and had a fantastic day in Scotland despite most of Ines' family not being able to travel from Spain due to restrictions at the time. Ines is my best friend, and I don't think I can emphasize enough how lucky I am for her love and support over the last ten years but particularly during my DPhil. It's no exaggeration to say that I would not have been able to complete it without her help. I also need to highlight her help in making sense of and proofreading the whole thesis, which was a huge amount of work.

I feel very privileged to have met incredibly generous people and had amazing opportunities presented to me throughout my life. We all live in increasingly uncertain times with big challenges facing us and I therefore wish nothing but peace and happiness to all who read this.

Abstract

The immune system must maintain a very fine balance recognising threats without damaging healthy cells and it uses cell surface non-catalytic tyrosine phosphorylated receptors (NTRs) to achieve this. In order to study this complex behaviour this work has taken a reductionist approach, using artificial systems in order to control as many variables as possible. The use of a generic cell surface ligand system to activate NTRs has suggested that they share a common mechanism for activation and shed light on specific characteristics of this mechanism. While NTRs are significantly different in terms of sequence homology they share similar structural characteristics which make them sensitive to receptor ligand dimensions. I was also able to show that altering the valency of the ligand could improve activation, but this was not due to clustering of the receptor. The mobility of the ligand was shown not to influence activation. Finally, changing the affinity of the ligand suggests the presence of a kinetic proofreading step during receptor activation.

This system was then applied to the accessory immune receptors CD5 and CD6. Until now, they have been very difficult to understand as they have been reported to both increase and decrease TCR activation. Using a combination of the generic ligand system and mutagenesis I was able to identify and characterise activatory and inhibitory effects of CD5 and CD6. The activatory effect was dependent on ligand engagement and expression of the TCR and comprised of contributions from both the extracellular domain through adhesion and signalling through the cytoplasmic tail. The inhibitory effects were independent of ligand engagement and, in the case of CD6, required the cytoplasmic tyrosine residue 489. CD5 was also suggested to exhibit a dual role with the extracellular domain inducing activation and the cytoplasmic tail responsible for inhibition.

Lastly, due to the emergence of the SARS-CoV-2 virus, the focus of my study shifted from receptor-ligand interactions in the immune response to characterise the effect of common mutations on the interaction of the SARS-CoV-2 Spike protein and its cell surface receptor on human cells ACE2. I purified and obtained detailed affinity data for nine ACE2 missense variants which are present in the human population plus one found through *in silico* saturation mutagenesis. I then purified and obtained detailed affinity and kinetic data for nineteen RBD constructs which contain mutations found in the common SARS-CoV-2 variants of concern (Alpha, Beta, Gamma, Delta, and Omicron).

Publications resulting from this thesis

Denham, E. M., **Barton, M. I**., Black, S. M., Bridge, M. J., de Wet, B., Paterson, R. L., van der Merwe, P. A., & Goyette, J. (2019). A generic cell surface ligand system for studying cell–cell recognition. *PLOS Biology*.

Barton, M. I., Macgowan, S., Kutuzov, M., Dushek, O., Barton, G. J., & van der Merwe, P. A. (2021). Effects of common mutations in the SARS-COV-2 spike RBD and its ligand the human ACE2 receptor on binding affinity and kinetics. *eLife*.

Macgowan, S. A., **Barton, M. I**., Kutuzov, M., Dushek, O., Van Der Merwe, P. A., & Barton, G. J. (2022). Missense variants in human ACE2 strongly affect binding to SARS-CoV-2 Spike providing a mechanism for ACE2 mediated genetic risk in Covid-19: A case study in affinity predictions of interface variants. *PLOS Computational Biology*.

In draft:

Barton, M. I., & van der Merwe, P. A. Review article. The importance of receptor ligand complex dimensions in the immunological synapse.

Barton, M. I., Denham, E. M., van der Merwe, P. A., & Goyette, J. Physical requirements for immune receptor triggering.

Barton, M. I., Perticucci, E., Denham, E. M., Brown, M. H., & van der Merwe, P. A. Applying a generic ligand system to better understand CD5 and CD6.

List of Figures

Figure 1.1: Kinetic segregation model diagram 15

Figure 1.2: Relative size of common leucocyte surface proteins 22

Figure 1.3: Antibody binding to its epitope and an Fc receptor simultaneously 27

Figure 1.4: Effect of elongation on the activation of the inhibitory receptor KIR2DL1 29

Figure 1.5: Receptor ligand dimensions are key for Immunotherapy 33

Figure 3.1: Cartoon diagram of the generic ligand system showing the key components 64

Figure 3.2: Purification of monovalent Strep-Tactin SpyCatcher 69

Figure 3.3: Calculating the average number of binding sites per ligand cell, short ligand or long ligand coupled with monovalent Strep-Tactin SpyCatcher 72

Figure 3.4: Checking expression levels of SIRPβ1, Siglec 14, NKp44 and TREM-1 plus the adaptor DAP12 74

Figure 3.5: Comparison of conjugate formation using monovalent Strep-Tactin SpyCatcher coupled to short and long ligand cells 75

Figure 3.6: Conjugate formation of four receptors with short or long ligand cells coupled with monovalent Strep-Tactin SpyCatcher 78

Figure 3.7: Stimulation assay comparison using monovalent Strep-Tactin SpyCatcher coupled to short and long ligand cells 80

Figure 3.8: Stimulation versus Conjugation assay comparison using monovalent Strep-Tactin SpyCatcher coupled to short and long ligand cells 81

Figure 3.9: Stimulation and conjugation assays using the same receptor and CHO cells within one experiment shows the same result as the combined data from multiple experiments 83

Figure 3.10: Conjugation assays on ice and at 37 °C in a water bath for monovalent Strep-Tactin SpyCatcher coupled to CHO short or long ligand cells shows the same pattern of ligand length sensitivity 85

Figure 3.11: Comparison of SIRPβ1, Siglec 14, NKp44 and TREM-1 shows short receptors are more potent in inducing signalling than long receptors 87
Figure 4.1: Purification of tetravalent Strep-Tactin SpyCatcher 96
Figure 4.2: Calculating the average number of binding sites per short ligand cell coupled with monovalent or tetravalent Strep-Tactin SpyCatcher 99
Figure 4.3: Conjugate formation of four receptors with short ligand cells coupled with monovalent or tetravalent Strep-Tactin SpyCatcher 101
Figure 4.4: Stimulation assay comparison using monovalent or tetravalent Strep-Tactin SpyCatcher coupled to short ligand cells 102
Figure 4.5: Stimulation versus Conjugation assay comparison using monovalent or tetravalent Strep-Tactin SpyCatcher coupled to short ligand cells 104
Figure 4.6: Conjugation assay on ice and at 37 °C in a water bath for monovalent versus tetravalent Strep-Tactin SpyCatcher highlights that the monovalent stimulation is still equal to or superior at equivalent conjugate formation 107
Figure 4.7: The SFK inhibitor (A-419259 trihydrochloride) prevents signalling from THP-1 cells but does not prevent receptor-ligand engagement measured by receptor downregulation 108
Figure 4.8: Calculating the average number of binding sites per short ligand cell coupled with monovalent or trivalent Strep-Tactin SpyCatcher 110
Figure 4.9: Stimulation assay comparison using monovalent or trivalent Strep-Tactin SpyCatcher coupled to short ligand cells 111
Figure 4.10: Calculating the average number of binding sites per ligand cell, short ligand or long ligand coupled with tetravalent Strep-Tactin SpyCatcher 113
Figure 4.11: Conjugate formation of four receptors with short or long ligand cells coupled with tetravalent Strep-Tactin SpyCatcher 114

Figure 4.12: Stimulation assay comparison using tetravalent Strep-Tactin SpyCatcher coupled to short and long ligand cells 117
Figure 4.13: Stimulation versus conjugation assay comparison using tetravalent Strep-Tactin SpyCatcher coupled to short and long ligand cells 118
Figure 4.14: Expression levels of the four ligand anchors, CD80, LAIR-1, CD43 and CD52 119
Figure 4.15: Calculating the number of biding sites per ligand cell, Short (CD80-SpyTag), LAIR-1-SpyTag, CD43-SpyTag and CD52-SpyTag coupled with monovalent or tetravalent Strep-Tactin SpyCatcher 121
Figure 4.16: Measuring the mobility of four ligand anchors presenting the SpyTag 122
Figure 4.17: Time course assay showing the ligand anchor half-life on the plasma membrane 124
Figure 4.18: Comparison of the ability for four ligand anchors to form conjugates and stimulate the SIRPβ1 receptor with monovalent Strep-Tactin SpyCatcher 126
Figure 4.19: Conjugation, stimulation, and stimulation versus conjugation assay comparison for CD80-SpyTag, LAIR-1-SpyTag, CD43-SpyTag and CD52-SpyTag ligand anchors coupled with monovalent or tetravalent Strep-Tactin SpyCatcher interacting with cells expressing SIRPβ1 receptor 129
Figure 4.20: Stimulation comparison of SIRPβ1, Siglec 14, NKp44 and TREM-1 with ligand cells expressing CD80-SpyTag, LAIR-1-SpyTag, CD43-SpyTag and CD52-SpyTag coupled with either monovalent or tetravalent Strep-Tactin SpyCatcher 130
Figure 4.21: Purification of monovalent streptavidin SpyCatcher 132
Figure 4.22: Purification of tetravalent streptavidin SpyCatcher 133
Figure 4.23: Calculating the average number of binding sites per ligand cell, short ligand coupled with monovalent or tetravalent Strep-Tactin or streptavidin SpyCatcher 135

Figure 4.24: Comparison of SIRPβ1 and Siglec 14 behaviour when engaged with monovalent or tetravalent Strep-Tactin or streptavidin 137
Figure 4.25: SpyCatcher fusion protein coupling efficiency comparison 142
Figure 5.1: Cartoon representing the experimental set up to engage the TCR in combination with CD5 and CD6..... 147
Figure 5.2: Cross-reactivity between WT CD6 and endogenously expressed hamster CD166 151
Figure 5.3: Blocking WT CD6 prevents cross reactivity with hamster CD166 on CHO cells 153
Figure 5.4: WT CD5 and CD6Δd3 show different dependences on ligand length..... 156
Figure 5.5: Expression check for NFkB reporter Jurkat cells expressing the 1G4 TCR..... 157
Figure 5.6: Mutations in CD6 tail tyrosine residues modify its behaviour..... 159
Figure 5.7: Expression check for No TCR Jurkat cells 161
Figure 5.8: CD5 and CD6 constructs cannot stimulate without the TCR..... 162
Figure 5.9: Producing No TCR Jurkat cells reconstituted with the 1G4 TCR 165
Figure 5.10: Reconstituting No TCR cells with 1G4 TCR plus CD5 and CD6 constructs rescues the stimulatory effect..... 166
Figure 5.11: Expression test for endogenous CD5 in the Jurkat reporter and No TCR Jurkat cells. 168
Figure 5.12: CD6Δd3 is both stimulatory and inhibitory in the context of TCR activation.. 171
Figure 5.13: Removing the cytoplasmic tail of CD6Δd3 abolishes the inhibitory effect..... 172
Figure 5.14: The effect of CD6Δd3 can be mimicked by the three-domain chimeric receptor CD5/CD6 Tail..... 174
Figure 5.15: Activation of WT CD5 shows only minor effects as activatory, and inhibitory roles mask each other..... 176

Figure 5.16: Activation of CD5 No Tail shows the inhibitory role of the CD5 tail 177
Figure 5.17: Mutating the CD6 tail tyrosine residues Y629 and Y662 does not strongly influence activation 179
Figure 5.18: Mutating the CD6 tail tyrosine residue Y489 mimics the CD6Δd3 No tail 181
Summary Figure 5.19: Comparison of the effect of CD5 and CD6 constructs on the minimum and maximum response in reporter Jurkat cells expressing the 1G4 TCR 183
Figure 5.20: Summary diagram for CD6Δd3 and CD6Δd3 No Tail effects on TCR activation 186
Figure 5.21: Summary diagram for WT CD5 and CD5 No Tail effects on TCR activation . 190
Figure 6.1: SARS-CoV-2 RBD variants 195
Figure 6.2: Purification of SARS-CoV-2 receptor binding domain and soluble human ACE2 197
Figure 6.3: Purification of soluble human ACE2 variants E37K, T27R, G326E and D355N 200
Figure 6.4: Purification of soluble human ACE2 variants E35K, F40L, S19P, P389H, E329K and K26R 201
Figure 6.5: Purification of Alpha, Beta, Gamma and EK/NY SARS-CoV-2 RBD variants . 203
Figure 6.6: Purification of E484K, K417N, K417T, KN/EK, KT/EK and S477N SARS-CoV-2 RBD variants 204
Figure 6.7: Purification of E484Q, L452R, LR/EQ, SN/EK, T478K and LR/TK SARS-CoV-2 RBD variants 205
Figure 6.8: Example data set for RBD binding captured WT ACE2 208
Figure 6.9: WT RBD binding to WT and ten ACE2 variants 210
Figure 6.10: Anti ACE2 Antibody (NOVUS AC384-NBP2-80038) binding to WT and ten ACE2 variants 211

Figure 6.11: Fitting kon and koff for WT RBD binding WT ACE2 216
Figure 6.12: WT and E484K/N501Y binding WT ACE2 over a range of immobilisations .217
Figure 6.13: Effect of RBD variants binding WT ACE2 including Alpha, Beta, and Gamma 219
Figure 6.14: Continued, effect of RBD variants binding WT ACE2 including Epsilon, Kappa, Delta, and Omicron.....221
Figure 6.15: RBD variants binding S19P and K26R ACE2 variants 223

List of Tables

Table 2.1 List of different SpyCatcher fusion proteins with the subunits required to make them.....51

Table 6.1: Summary of the ten ACE2 variants highlighting the predicted and measured ΔΔG values 213

Table 6.2: Summary of the binding parameters for RBD WT and nineteen variants.....227

Table 6.3: Summary of the ΔG values for nineteen RBD variants binding ACE2 WT plus ACE2 S19P and ACE2 K26R.....228

Abbreviations

ALCAM	Activated leukocyte cell adhesion molecule
ACE2	Angiotensin-converting enzyme 2
ADCC	Antibody dependent cellular cytotoxicity
ADCP	Antibody dependent cellular phagocytosis
APCs	Antigen presenting cells
k_{on}	Association rate
BP	Binding protein
BLI	Bio-layer interferometry
BFP	Bio membrane force probe
BiTEs	Bi-specific T-cell engagers
BBB)	Blood-brain barrier
cad-AJs	Cadherin-based cadherin junction
CAR	Chimeric antigen receptor
CHO	Chinese Hamster Ovary
CDC	Compliment-dependent cytotoxicity
ΔG	Delta G
EGFR	Epidermal growth factor
EBV	Epstein-Barr virus
ERM	Ezrin/Radixin/Moesin
DAMPs	Damage-associated molecular patterns
K_D	Dissociation constant
k_{off}	Dissociation rate
DAP10	DNAX-activating protein of 10kDa
DAP12	DNAX-activating protein of 12kDa
FKBP	FK506 binding protein
FRB	FKBP-binding domain
FACS	Fluorescence-activated cell sorting
FRAP	Fluorescence recovery after photobleaching
FBS	Foetal bovine serum
FcRγ	Gamma subunit of the immunoglobulin Fc receptor
GPCRs	G-protein-coupled receptors
GWAS	Genome-wide association studies
gMFI	Geometric mean fluorescence intensity
GUVs	Giant unilamellar vesicles
GPI	Glycosylphosphatidylinositol
gnomAD	Genome Aggregation Consortium Database
EC50	Half maximal response
ImmTACs	Immune mobilising monoclonal T-cell receptors against cancer
IS	Immunological synapse
ITTM	Immunoglobulin tail tyrosine motif
ITAMs	Immunoreceptor tyrosine-based activatory motifs
ITIMs	Immunoreceptor tyrosine-based inhibitory motifs
ITSMs	Immunoreceptor tyrosine-based switch motifs
KIR	Killer cell lectin-like receptors
KS	Kinetic segregation model
MHC	Major histocompatibility complex
mTOR	Mammalian target of rapamycin

MCSP	Melanoma chondroitin sulfate proteoglycan
MLL-5	Mixed lineage leukemia-5
NK	Natural killer
NKp44	Natural killer receptor 44
NTR	Non-catalytic tyrosine-phosphorylated receptor
NHL	Non-Hogkins lymphoma
k_{obs}	Observed-on rate
pMHC	Peptide loaded major histocompatibility complex
PGN	Peptidoglycan
PMBCs	Peripheral blood mononuclear cells
PCNA	Protein proliferating cell nuclear antigen
RBD	Receptor binding domain
RPTP	Receptor protein tyrosine phosphatase
PGLYRP1	Recognition protein 1
Tregs	Regulatory T cells
RU	Response units
RTX	Rituximab
SRCR	Scavenger receptor cysteine rich
SARS-CoV-2	Severe acute respiratory syndrome coronavirus 2
scFv	Single-chain variable fragment
SNP	Single nucleotide polymorphism
SAP	SLAM-associated protein
SHIP-1	SH2 domain-containing inositol 5'-phosphatase 1
SHP-1	SH2-containing protein tyrosine phosphatase-1
SHP-2	SH2-containing protein tyrosine phosphatase-2
Siglec 14	Sialic acid-binding immunoglobulin-type lectin 14
SIRPβ1	Signal regulatory protein β1
SLAM	Signalling lymphocytic activation molecule
SCD	Single chain dimer
SCT	Single chain trimer
SEC	Size exclusion chromatography
SFKs	Src family kinases
SH2	Src homology 2
SD	Standard deviation
sSTII	Single Strep-Tag-II tag
SLBs	Supported lipid bilayers
SPR	Surface plasmon resonance
STAR	Synthetic T cell receptor and antigen receptor
TDBs	T cell-dependent bispecific antibodies
TCR)	T cell receptor
TIRF	Total internal reflection fluorescence
TMPRSS2	Transmembrane protease, serine 2
TREM-1	Triggering receptor expressed on myeloid cells 1
tSTII	Twin Strep-Tag-II tag
WT	Wild type

Table of Contents

Acknowledgments II

Abstract IV

Publications resulting from this thesis VI

List of Figures VII

List of Tables XIII

Abbreviations XIV

Table of Contents XVI

Chapter 1 - Introduction 1

1.1. Introduction to the immune system 1

1.1.1. T cell development 2

1.1.2. Regulation of T cell activation 2

1.2. Non-catalytic tyrosine-phosphorylated receptors 3

1.2.1. Tyrosine motifs involved in NTR signalling 4

1.2.2. NTR-associated adaptor proteins 6

1.2.3. Src family kinases (SFKs) 6

1.2.4. Membrane associated phosphatases 7

1.3. Models to explain NTR triggering 8

1.3.1. Conformational change/mechanical force 9

1.3.2. Induced clustering/aggregation 12

1.3.3. Kinetic segregation 14

1.4. Studies on the impact of receptor-ligand dimensions on the immune response 20

1.4.1. Close contact formation and adhesion molecules 20

1.4.2. The effect of receptor ligand size on TCR activation 23

1.4.3. The effect of receptor ligand size on other activatory NTR members 25

1.4.4. The effect of receptor ligand size on inhibitory NTR members 28

1.4.5. The effect of receptor ligand size on non-NTR cell surface molecules 30

1.5. Therapeutic relevance of receptor ligand dimensions 31

1.5.1. Antibodies targeting tumour markers 31

1.5.2. Bispecific T-cell dependent antibodies 32

1.5.3. Chimeric antigen receptors (CARs) 34

1.6. The CD5 and CD6 co-receptors 36

1.6.1. CD5 and CD6 role in T cell development and differentiation 37

1.6.2. Role of CD5 and CD6 in disease 38

1.7. SARS-CoV-2 39

1.7.1. SARS-CoV-2 structure and cell entry 40

1.7.2. Immune response 41

1.7.3. Origins of SARS-CoV-2 41

1.8. Aims 42

Chapter 2 - Materials and Methods 43

2.1. Constructs 43

2.1.1. Receptors....43
2.1.2. Adaptors....43
2.1.3. Ligand anchor constructs....44
2.1.4. SpyCatcher fusion proteins....46
2.1.5. ACE2 and RBD variant constructs....47
2.2. Cell culture....48
2.2.1. THP-1 cell lines....48
2.2.2. CHO cell lines....48
2.2.3. HEK293F suspension cell culture....48
2.2.4. Transduction of THP-1 or Jurkat cells....48
2.2.5. Transfection of CHO cells with various ligand anchors....49
2.2.6. Transfection of HEK293F suspension cells....49
2.3. Flow cytometry....50
2.3.1. Checking receptor and adaptor expression....50
2.3.2. Checking ligand anchor expression....50
2.3.3. FACS sorting of ligand anchor expressing CHO cells....51
2.4. Protein expression and purification....51
2.4.1. Expression and purification of monovalent, trivalent, and tetravalent Strep-Tactin SpyCatcher and streptavidin SpyCatcher....51
2.4.2. GFP-SpyCatcher....52
2.4.3. RBD and ACE2 purification from HEK293F suspension cell supernatant....52
2.5. Cellular assays....53

2.5.1. Coupling SpyCatcher fusion proteins to CHO cells 53
2.5.2. Biotin-4-fluorescein quenching assay 53
2.5.3. Calculating the number of binding sites per coupled CHO ligand cell 54
2.5.4. Down-regulation of generic ligand anchors 56
2.5.5. Measuring the number of 9V-HLA-A*02 per cell 56
2.5.6. THP-1 cell assays 56
2.5.7. Jurkat NFκB eGFP and Jurkat cells not harbouring an eGFP reporter assays 57
2.5.8. Conjugation assays 57
2.5.9. Stimulation assays 58
2.5.10. Fluorescence recovery after photobleaching (FRAP) 59
2.6. Surface plasmon resonance (SPR) 60
2.6.1. SPR data fitting 61
Chapter 3 - Developing a generic ligand system to study the effect of ligand length on NTR activation 63
3.1. Introduction 63
3.1.1. Challenges to studying NTRs 63
3.1.2. The generic ligand system 65
3.1.3. Selected NTRs for this study 66
3.1.4. Key findings 67
3.2. Results 68
3.2.1. Purification of monovalent Strep-Tactin SpyCatcher 68

3.2.2. Developing a method to calculate the average number of available generic ligands on CHO ligand cells to study NTR ligand length 70

3.2.3. Long ligands are superior binders in conjugate assays 76

3.2.4. Despite less efficient conjugation short ligands trigger stronger activation 79

3.2.5. Short receptors are more sensitive than long receptors 84

3.3. Discussion 88

Chapter 4 - Extending the generic ligand system to study the effect of ligand valency, mobility, and affinity on NTR activation 92

4.1. Introduction 92

4.1.1. Ligand valency 92

4.1.2. Ligand mobility 93

4.1.3. Ligand affinity 94

4.1.4. Key findings 95

4.2. Results 95

4.2.1. Measuring the average number of monovalent and tetravalent ligands presented on ligand cells 97

4.2.2. Tetravalent ligands are superior binders in conjugate formation assays 100

4.2.3. Despite less efficient conjugation, monovalent ligands trigger equal or stronger activation 103

4.2.4. Increasing ligand valency results in NTR downregulation 106

4.2.5. Trivalent Strep-Tactin is equivalent to tetravalent Strep-Tactin 109

4.2.6. NTR activation is still sensitive to changes in ligand length even with multivalent ligands 112
4.2.7. Initial characterisation of ligand anchors of different mobility and stability at the membrane 116
4.2.8. Altering ligand anchors has no clear impact on NTR activation 125
4.2.9. Confirmation that the CD80 ligand anchor does not influence receptor clustering 127
4.2.10. Altering the affinity of the ligand shows evidence that kinetic proof reading is important for NTR activation 131
4.3. Discussion 138
Chapter 5 - Applying the generic ligand system to better understand the behaviour of CD5 and CD6 145
5.1. Introduction 145
5.1.1. Key findings 148
5.2. Results 149
5.2.1. CD6 cross-reacts with hamster CD166 on CHO cells 149
5.2.2. CD5 and CD6 are not canonical activatory receptors and they differ in their sensitivity to ligand length 154
5.2.3. Expression of CD6 in Jurkat cells inhibits TCR activation in a ligand independent manner 158
5.2.4. Jurkat activation by CD5 and CD6 engagement requires TCR expression. 163
5.2.5. Both CD5 and CD6 receptors have an inhibitory effect on TCR activation. 167
5.2.6. Factorial stimulation assays confirm dual behaviour of CD6. 169

5.2.7. The CD5 and CD6 cytoplasmic tails mediate their inhibitory functions, but their contributions to co-stimulatory functions are more challenging to characterise. 170

5.2.8. The Y629 and Y662 residues in the CD6 cytoplasmic tail may be important in localising stimulatory molecules to the TCR. 180

5.2.9. The Y489 residue in the CD6 cytoplasmic tail is responsible for much of the inhibitory effect observed 182

5.3. Discussion 184

Chapter 6 - How variants in SARS-CoV-2 RBD domain and its ligand ACE2 change the binding affinity and kinetics 191

6.1. Introduction 191

6.1.1. SPR is the gold standard to quantify protein binding affinity and kinetics 196

6.1.2. Key findings 198

6.2. Results 198

6.2.1. Production of SARS-CoV-2 receptor binding domain (RBD) 198

6.2.2. Production of soluble human ACE2 199

6.2.3. Production of ten ACE2 variants 202

6.2.4. Production of sixteen RBD variants 206

6.2.5. Validating the ACE2/SARS-CoV-2 RBD SPR binding assay 206

6.2.6. Testing the prediction that specific ACE2 variants could significantly increase or decrease RBD binding 207

6.2.7. Expanding the assay to common ACE2 variants and calibrating the prediction algorithm 212

6.2.8. Effect of emergent SARS-CoV-2 RBD variants on binding WT and common ACE2 variants 214

6.2.9. The combined effect of RBD variants binding common ACE2 variants S19P and K26R 222

6.3. Discussion 229

Chapter 7 - General Discussion 233

7.1. Improving immunotherapies 233

7.2. CD5 and CD6 immunotherapies 235

7.3. Applications for RBD/ACE2 binding data 236

Bibliography 238

Chapter 1 - Introduction

1.1. Introduction to the immune system

The environment we live in continuously bombards the body with microorganisms. While many are benign and some beneficial, a percentage can cause disease. If these pathogens get past the initial defences such as the skin and mucus membranes it is the role of the highly complex immune systems to eliminate the threat (Murphy K., 2011). These systems also work to identify and destroy dysfunctional cells which could lead to cancer (De Visser et al., 2006).

The immune systems can be split into the innate and adaptive immune system (Murphy K., 2011). The initial response to a pathogen will come from the innate immunity. This rapid response is launched predominantly by macrophages, neutrophils, natural killer (NK) cells and the complement system. The slower adaptive response requires the mobilisation of many different cell types but allows for a memory of that specific pathogen to be retained. This allows for a very swift and effective response should the same pathogen be detected again.

All immune cells must sense their environment in order to perform their role. The cell surface of a leukocyte is covered in an array of different receptors which are critical for sensing their environment (Barclay et al., 1997). This can involve receptors that detect soluble molecules secreted from cells, for example inflammatory cytokines or damage-associated molecular patterns (DAMPs), released by damaged or dying cells (Cerami, 1992; Hernandez et al., 2016). Other receptors can bind membrane bound ligands on an opposing cell surface (Dushek et al., 2012). Perhaps the most important example of this is the interaction between the major histocompatibility complex (MHC) and the T cell receptor (TCR) (Murphy K., 2011). During infection, antigen presenting cells can present foreign peptides derived from the pathogen on their MHC. A T cell can then use its unique TCR to bind the peptide loaded

MHC (pMHC). The activation of the TCR leads to cellular proliferation which can then clear the remaining infected cells (Murphy K., 2011).

1.1.1. T cell development

T cells are a key component of the adaptive immune system. There are two common types which are critical when mounting an immune response, the CD4+ helper cells and the CD8+ cytotoxic cells. These cells differentiate from haematopoietic cells in the thymus (Murphy K., 2011). The naive T cells can each produce a unique TCR. They then undergo positive selection to ensure the TCR can recognise MHC followed by negative selection to remove any TCRs which strongly react to self-peptides (Klein et al., 2014). The self-peptides are presented via the MHC molecules which are expressed in thymic epithelial cells. Naive T cells bind the pMHC and will undergo apoptosis if they produce strong activation (Hogquist & Jameson, 2014).

The CD4+ T cells are known as T helper cells as they mainly act via release of specific cytokines that target other immune cells. They can further differentiate into specific subsets such as Th1 and Th17 cells, which target intracellular bacteria; Th2, which specialises in parasite defence; and regulatory T cells (Tregs), which act to prevent over activation of the immune system (Zhou et al., 2009). Conversely, CD8+ T cells (also known as cytotoxic T cells) act directly on virus infected or cancerous cells via release of perforin and granzymes which results in target cell apoptosis (Harty et al., 2003).

1.1.2. Regulation of T cell activation

Due to their potential to destroy host cells T cells must be kept under very fine control. Therefore, activation is highly regulated to prevent pathogenic effector functions. This is the basis for autoimmune diseases like multiple sclerosis. However, the lack of these T cell effector functions can lead to cancer (Fletcher et al., 2010; Xing & Hogquist, 2012).

Signalling induced via the pMHC-TCR binding produces the primary signal required for cellular activation. However, this is aided by co-stimulatory receptors like CD28 which binds CD80 and CD86 (Azuma et al., 1993; Chen & Flies, 2013; June et al., 1987). Costimulatory ligands are also upregulated during inflammation to enhance T cell responses. Finally, T cell activation can be maintained though cytokine responses (Curtsinger & Mescher, 2010). There are also co-inhibitory receptors such as PD-1, CTLA-4 and LAIR-1 which are thought to recruit inhibitory molecules such as phosphatases to the site of TCR engagement (Long, 2003). Taken together these different signals are integrated to produce a controlled and effective immune response to pathogens and cancer while preventing damage to healthy cells.

1.2. Non-catalytic tyrosine-phosphorylated receptors

While immune cells have many receptors on their surface which can be classified in different ways, a subset of over one hundred immune receptors has been defined under the term non-catalytic tyrosine-phosphorylated receptors (NTRs) (Dushek et al., 2012). This definition is not based on their sequence homology, but on key structural features they all share. As a result, these receptors come from several different immune receptor families. NTRs can be activatory, inhibitory or both (Dushek et al., 2012).

NTRs have a relatively small extracellular domain which is highly variable due to rapid evolution to combat pathogen escape. Importantly, this domain typically binds surface associated ligands (for example, pMHC in the case of the TCR). Of the NTRs where the structure of both receptor and ligand is known, the vast majority have relatively small dimensions and span a total distance of 10-20 nm between opposing membranes (Dushek et al., 2012).

The extracellular domain is linked to a single pass transmembrane region and a structurally disordered cytoplasmic tail. The tail, while often short, is key to their function. It has no

intrinsic tyrosine kinase catalytic domains, which means that they cannot initiate downstream signalling directly. However, it contains tyrosine residues arranged in specific motifs which, when phosphorylated by Src-family tyrosine kinases, recruit Src homology 2 (SH2) containing proteins from the cytosol (Schlessinger, 1994). Alternatively, many activatory NTRs present tails too short to contain the tyrosine motifs, and instead they associate through electrostatic interactions via their transmembrane domains with adaptor proteins that have these tyrosine motifs (Beth et al., 2005).

1.2.1. Tyrosine motifs involved in NTR signalling

There are three main types of tyrosine motifs: immunoreceptor tyrosine-based activatory motifs (ITAMs), immunoreceptor tyrosine-based inhibitory motifs (ITIMs) and immunoreceptor tyrosine-based switch motifs (ITSMs). Upon receptor binding, these motifs are phosphorylated by tyrosine kinases such as Src family kinases (SFKs), which interact with the inner leaflet of the plasma membrane (Cooper & Qian, 2008). If the phosphorylation state of the receptor is maintained for long enough it can initiate downstream signalling. To balance this activation, receptor protein tyrosine phosphatase (RPTPs) such as CD45 and CD148 act to dephosphorylate the receptor and return the system to its resting state (Dushek et al., 2012).

ITAMs are composed of two tyrosine residues, each contained within their own short Yxx(L/I)x sequence (where x corresponds to any amino acid), that are spaced six to eight residues apart (Cambier, 1995). Phosphorylation of these tyrosine residues leads to the recruitment of kinases with two tandem SH2 domains such as Syk and ZAP70 which subsequently leads to downstream activation of the immune response (Chan et al., 1991; Kihara & Siraganian, 1994; Narula et al., 1995). Activatory NTRs may contain a single ITAM, but greater numbers are present in adaptors such as DAP12, which forms a dimer with

one ITAM per chain (Lanier, 2009) or in the TCR complex, which contains a total of ten ITAMs (Guy & Vignali, 2009).

HemiTAMs are a type of ITAM with an almost identical sequence of YxxL but consisting of a single tyrosine residue instead of two. They are mostly restricted to the Killer cell lectin-like receptors (KIR) and C-type lectin subfamilies of NTRs (Robinson et al., 2006). Another well described activatory motif is the YxNM immunoglobulin tail tyrosine motif (ITTM). Most notably this is found in the key co-receptor CD28 and the adaptor DAP10. Once phosphorylated it acts to recruit proteins such as Grb2 and PI3K to aid cellular activation (Lanier, 2009).

ITIMs are only subtly different to ITAMs. They consist of a single canonical sequence (S/I/V/L)xYxx(I/V/L) (Masao et al., 1997). Upon phosphorylation they recruit phosphatases such as SH2-containing protein tyrosine phosphatase-1 or -2 (SHP-1 or SHP-2, respectively) or SH2 domain-containing inositol 5'-phosphatase 1 (SHIP-1) (D'Ambrosio et al., 1995; Masao et al., 1997; Vély et al., 1996). Thus, they have an inhibitory effect on cellular activation.

ITSMs are again a single tyrosine-based motif, but in their case with the canonical sequence TxYxx(I/V) (Shlapatska et al., 2001). Upon phosphorylation they recruit the SH2 containing SLAM-associated protein (SAP), which acts as a scaffold for the recruitment of SFKs such as Fyn (Cannons et al., 2011). Without the presence of the SAP molecules the ITSM can switch to recruit SHP-1, SHP-2, and SHIP-1 phosphatases. This ability to recruit both activatory and inhibitory molecules allows NTRs that contain them, such as the signalling lymphocytic activation molecule (SLAM) family receptors, to exert fine control of immune activation (Cannons et al., 2011; Veillette et al., 2009).

1.2.2. NTR-associated adaptor proteins

The NTR-associated adaptors do not contain any extracellular domains but are anchored in the membrane via a transmembrane region and contain an unstructured cytoplasmic tail. The most well-known adaptor is the CD3ζ which is a key component of the TCR complex. It contains 3 ITAMs and forms a homodimer via a disulphide bond above the transmembrane region (Call & Wucherpfennig, 2004).

In the case of DNAX-activating protein of 12kDa (DAP12) it has a single ITAM motif and forms a homodimer in the membrane (Call & Wucherpfennig, 2007). It contains an aspartic acid residue in the centre of its transmembrane region which allows it to associate with lysine or arginine residues found in the transmembrane of activating NK receptors and other NTRs (Feng et al., 2006; Lanier, 2009; Lanier et al., 1998).

The γ subunit of the immunoglobulin Fc receptor (FcRγ) has a similar structure and contains a single ITAM. It also forms a homodimer but has been shown to form a heterodimer with the CD3ζ chain (Orloff et al., 1990). It is most well-known for associating with NTRs in the Fc and NK receptor subfamilies.

DNAX-activating protein of 10kDa (DAP10) is also a homodimer but it contains a YxxM motif (Call & Wucherpfennig, 2007) It is less common compared to the other adaptors discussed so far but it does associate with the NK receptor NKG2D (Lanier, 2009; J. Wu et al., 1999).

1.2.3. Src family kinases (SFKs)

The Src family is comprised of eleven tyrosine kinases that have a common basic structure comprised of one SH2 and one SH3 domain linked to a kinase domain. They interact with the plasma membrane via a myristoylated or palmitoylated region which is incorporated into the inner membrane leaflet (Koegl et al., 1994; Resh, 1999). The activity of the kinase is

regulated by the phosphorylation and dephosphorylation of tyrosine residues. This means that in addition to regulation at the level of the receptor/adaptor complex via their tyrosine motifs, there is an extra layer of regulatory phosphorylation on the kinases themselves.

One such example is the SFK Lck, which contains two key regulatory tyrosine residues: Y394 and Y505 (D'Oro et al., 1996). The Y505 residue is the target of regulation by Csk, an inhibitory kinase (Bergman et al., 1992; Okada et al., 1991). Upon phosphorylation of this residue it can bind to the SH2 domain of Lck through an intramolecular interaction inactivating its kinase activity (W. Xu et al., 1999). This negative regulation by Csk is reversed by CD45, which can dephosphorylate Y505, returning Lck to a primed, activatable state (McNeill et al., 2007). As for Y394, it can be phosphorylated by another Lck via trans autophosphorylation, which leads to full activation (Yamaguchi & Hendrickson, 1996). Importantly, this activity is also countered via CD45 dephosphorylation (McNeill et al., 2007). This is how a balance of activatory, and inhibitory factors can regulate Src family kinases. This balance of signals is thought to maintain an activation threshold for kinases and so differences in the localisation of the kinase and phosphatase are key to their function (Davis & van der Merwe, 2011; Hermiston et al., 2009; McNeill et al., 2007).

1.2.4. Membrane associated phosphatases

As seen above, the role of CD45 and CD148 as both activators and inhibitors emphasises the complexity of NTR signalling. Receptor protein tyrosine phosphatases (RPTPs) are key regulators of the immune cells to prevent unwanted off target activation and preventing abnormal responses (Hermiston et al., 2009). Phosphatases such as CD45 and CD148 are highly expressed, large membrane proteins. CD45 has a number of different splice variants with sizes of the extracellular domain ranging from 28-50 nm (Barclay et al., 1997; McCall et al., 1992). Similarly, CD148 contains between 8-10 fibronectin domains in addition to a mucin-like domain which makes its extracellular domain approximately 47-55 nm (Cordoba

et al., 2013). Both proteins have a single pass transmembrane region and then a cytoplasmic phosphatase domain close to the inner leaflet of the membrane.

These phosphatases are not regulated in the same way as the Src family kinases, and their large extracellular domains are not known to bind any specific ligands. Therefore, the majority of evidence points towards them being constitutively active, with their large extracellular domain (much larger than that of their substrates: NTRs and kinases) as a way to spatially exclude them from close-contact areas during receptor ligand engagement at cell-cell interfaces (Cordoba et al., 2013; Irles et al., 2003; Lin & Weiss, 2003; Varma et al., 2006). This observation also forms the basis for the kinetic segregation model (KS), which is one of the main theories as to how NTRs are activated and will be discussed in detail (Davis & van der Merwe, 1996).

1.3. Models to explain NTR triggering

As stated so far, for NTRs to become activated the tyrosine motifs in their intracellular tails must be phosphorylated for long enough to initiate downstream signalling. I will refer to this event as the "triggering" of the receptor. To achieve this the balance of influences from the kinase and phosphatase in the proximity of the NTR must be shifted towards a kinase dominated environment. However, the mechanism by which this triggering of the receptor occurs is subject to a number of competing models (Choudhuri & van der Merwe, 2007). This debate has focused on the TCR but is likely applicable to any member of the NTR family. The main models fall into three groups, conformational change/mechanical force, induced clustering/aggregation, and segregation. The literature has not yet come to a consensus and it is possible that the real answer is a mechanism that combines different traits from each model (Dushek et al., 2012).

1.3.1. Conformational change/mechanical force

This model is based on the idea that a conformational change upon receptor ligand binding is important for NTR activation as has been demonstrated for G-protein-coupled receptors (GPCRs) (Rosenbaum et al., 2009). This means that the receptors must switch between two states. For example, in the inactive state, the tyrosine motifs on the receptor are inaccessible to SFKs whereas in the active state the tyrosine motifs are accessible. Then, upon ligand binding, the NTR must transition to an active state to allow phosphorylation. This model requires that SFK activity dominates in the cell in order to maintain the phosphorylation state of any receptor in its active state long enough to trigger downstream signalling, otherwise the receptors would be immediately switched off via RPTP activity (Dushek et al., 2012).

This idea was first proposed for the TCR, where the ITAM motifs on the CD3ζ adaptor chains are held close to the inner membrane via electrostatic interactions with the lipids, preventing SFK activity. Ligand binding would then lead to changes in the lipid composition around the TCR and release the CD3ζ chains in order for SFK-mediated phosphorylation to take place (Aivazian & Stern, 2000; Kuhns & Davis, 2008; C. Xu et al., 2008). However, later studies have shown that the release of the CD3ζ chains occurs post phosphorylation rather than it being the trigger (Fernandes et al., 2010; H. Zhang et al., 2011). Also, while it is possible that the unstructured cytoplasmic domains of the TCR complex associate with the membrane, this observation has not been reproduced for other NTR tails and their adaptors. Furthermore, there is the issue of the large diversity of extracellular domains across the NTRs, which is difficult to reconcile with a conformational change mechanism which must be highly conserved and reliable (Dushek et al., 2012; Springer, 1990).

An alternative mechanism invoking conformational change postulates a role for mechanical force (Choudhuri & van der Merwe, 2007). Initial work on the forces induced upon close contact formation suggested that the TCR-pMHC interaction formed a ring of binding that

would then be trafficked to a central cluster (Grakoui et al., 1999). The symmetry of this close contact could produce an equal force in all directions, helping to maintain the cell in position during ligand engagement. The interaction of relatively small molecules such as the TCR-pMHC was predicted to lead to a repulsive force due to the physical repulsion produced by the larger glycocalyx as the two membranes formed a close contact, thereby putting strain on the receptor ligand interaction. This has been possible to study using atomic force microscopy to measure the force T cells experience upon TCR-pMHC binding at the single molecule scale (Puech et al., 2011). However, in terms of the NTR family it is difficult to see how such a force could be passed through the membrane when the extracellular and intracellular domains of NTRs are linked by flexible hinge regions and transmembrane domains.

It is intuitive that when receptor ligand interactions occur between cells this would produce a mechanical force (Ma et al., 2012). However, it is not so clear how that force would be recognised and lead to activation of the receptor. One system used CD4 primary T cells which could interact with beads coated in anti-CD3 attached to a bio membrane force probe (BFP) (Husson et al., 2011). The interacting cells transitioned though three distinct phases: a latency phase; a pushing phase and a pulling phase, the latter of which was suggested to be a form of antigen discrimination. Another study showed that when primary human T-cells settled onto special surfaces containing pillars with anti-CD3 and anti-CD28, it was possible to measure a traction force (Bashour et al., 2014). There was also evidence that at the locations of force generation there was a concentration of SFK activity but not ZAP70 which is subsequently recruited to phosphorylated NTRs. Staining for SFKs showed that they were localised within areas of force generation and PP2 inhibition of SFKs lead to a reduction in the force produced.

It also appears that the type of force applied is important as inducing a high frequency pulling force on the TCR-pMHC interaction lead to a calcium influx which is an early marker of cellular activation (Pryshchep et al., 2014). This calcium response was further enhanced by CD8 binding. Interestingly, decreasing the frequency of the force application reduced the response and continuous cell-cell close contact prevented receptor activation. There was also some evidence that the calcium influx could only occur in regions of the membrane experiencing this pulling force.

If mechanical force is key to NTR activation, there is little evidence that NTRs directly interact with the cytoskeleton, therefore what could translate the pulling force into receptor activation? One mechanism to explain this is force sensitive ion channels such as Piezo1, which can be activated with small perturbations to the cell membrane (Syeda et al., 2016). There is also evidence that when 3T3 fibroblasts are engaged via the TCR, with a single-chain variable fragment (scFv) for CD3 and a force is applied via a micropipette a calcium influx is seen (Y.-C. Li et al., 2010). Interestingly, this is not found with scFv's binding to other surface molecules such as CD28, ICAM-2 and CD62L. However, it has been shown that the magnitude of the force provided by adhesion molecules such as LFA-1 can act to fine tune TCR activation (Ma et al., 2022).

Interestingly, mechanical force generated by the cytoskeleton has been suggested to play a role in B cell antigen discrimination for clonal selection (Natkanski et al., 2013). Forces generated by the cytoskeleton lead to invagination of the area of the membrane where the BCR-antigen interaction is occurring. Therefore, only high affinity interactions that can withstand this mechanical test would activate the cells. There is also evidence that the stiffness of the substrate presenting the antigen is important for activation of both the TCR and BCR (Judokusumo et al., 2012; Wan et al., 2013). However, while the polyacrylamide

gels used to present the substrates in these studies can mimic the physiological stiffness of a cell membrane, it is difficult to compare the results to a physiological cell-cell interaction.

Overall, it is widely accepted that when immune cells interact with antigen presenting cells (APCs), forces will be produced that can be mediated by the cytoskeleton. However, it has been challenging to create systems that can study the importance of these forces for signalling while balancing the physiological relevance of the experimental set up with the need for accurate force measurements.

1.3.2. Induced clustering/aggregation

This category of model assumes that more than one NTR is required for triggering and that clustering or aggregation of the NTRs leads to triggering. This clustering of receptors would produce a high density of signalling motifs which would allow for SFKs, which associate with these motifs, to trans-autophosphorylate each other and phosphorylate NTRs more efficiently.

Supporting this model is early evidence that simply crosslinking of NTRs is sufficient to cause triggering, as seen with both the TCR and BCR (Bunnell et al., 2002; Campi et al., 2005; Kaye & Janeway, 1984; Woodruff et al., 1967). It is also well known that receptor binding leads to clustering due to the opposing membranes being held at the optimum length for more interactions to take place (Cartwright et al., 2014; Paszek et al., 2014; Schmid et al., 2016). More recently, with advances in high resolution microscopy it has been possible to see micro clusters and even nano clusters of TCRs (Pageon et al., 2016). TCRs in larger, denser clusters were shown to be more likely to be activated upon ligand binding. This suggests only signalling competent clusters of receptors with sufficient density can trigger, which constrains ligand recognition to only those that can form dense clusters. Importantly, they showed that these clusters were formed prior to engagement and therefore phosphorylation.

Mathematical modelling has also been used to better understand the behaviours of SFKs when surrounded by a high concentration of substrates. Due to the trans-autophosphorylation needed to activate SFKs this kind of environment can lead to a positive feedback loop where the SFKs are maintained in the active state. This would facilitate receptor triggering to commence and be maintained (Cooper & Qian, 2008). This idea has been successfully tested using an *in vitro* reconstituted system with only Lck kinase and CD3ζ adaptor on supported lipid bilayers (SLBs) (Hui & Vale, 2014). They showed that clustering Lck and CD3ζ is sufficient to induce phosphorylation. This could be controlled by the addition of Csk or CD45.

Nevertheless, a key issue with the clustering model is that there is a large body of evidence that very low numbers or even a single TCR binding a single ligand can lead to triggering and cellular activation (J. Huang et al., 2013; Irvine et al., 2002; Ma et al., 2008; Purbhoo et al., 2004; Sykulev et al., 1996). The ability of the TCR to trigger via a monovalent ligand has again been shown recently with a very detailed study using single molecule tracking (Brameshuber et al., 2018). They also went to great lengths to show that clustering of the TCR was not required for triggering.

One model to explain this discrepancy in the literature is co-receptor heterodimerisation. It postulates that SFKs associated with the co-receptors CD4 and/or CD8 (which bind the same pMHC ligand as the TCR), are brought close to the TCR to initiate triggering (Trautmann & Randriamampita, 2003). While co-receptors are known to aid in immune cell activation they are not required for TCR activation as this has been shown to occur even in the absence of coreceptors in mouse models (Locksley et al., 1993; Schilham et al., 1993). Additionally, this explanation would only apply to TCR activity and not to other NTRs.

Another alternative is the pseudo-dimer model which suggests TCR activation is initiated by two pMHC molecules one presenting an endogenous self-peptide and the other an agonist peptide. Each peptide binds a specific TCR, and the MHC molecules are maintained as a dimer via the co-receptors CD4 or CD8, which can bridge between the two TCR-pMHC interactions leading to activation of both TCRs (Irvine et al., 2002; Krogsgaard et al., 2005). Like the co-receptor heterodimerization model, the pseudo-dimerization model cannot account for coreceptor-independent TCR triggering, as occurs with unconventional T cells and gamma/delta T cells (Groh et al., 1989). While these models are possible in the context of the TCR they do not explain how the wider NTR family functions.

1.3.3. Kinetic segregation

The kinetic segregation model (Davis & van der Merwe, 1996) stems from the observation that, although NTRs have very different sequences, many receptor-ligand pairs have very similar dimensions, which could hold the opposing membranes at 10-20 nm. Furthermore, formation of the close contacts required for NTR engagement would lead to the exclusion from the close contact of proteins containing large extracellular domains, such as the phosphatases CD45 (James & Vale, 2012) and CD148 (Cordoba et al., 2013). In the unbound state, both SFKs and phosphatases would have access to the tyrosine residues in the tails of NTRs and their adaptors (Figure 1.1A). However, upon formation of close contacts the imbalance in the kinase/phosphatase ratio at the close contacts would favour a predominantly phosphorylated environment (Figure 1.1B). Ligand engagement would act to trap the NTR within this close contact zone. Through varying the affinity or avidity of the receptor ligand interaction, the time that the NTR remains within the close contact would change. Therefore, only ligands which can trap the NTR for long enough to allow downstream signalling to commence would lead to full cellular activation (Davis & van der Merwe, 2006).

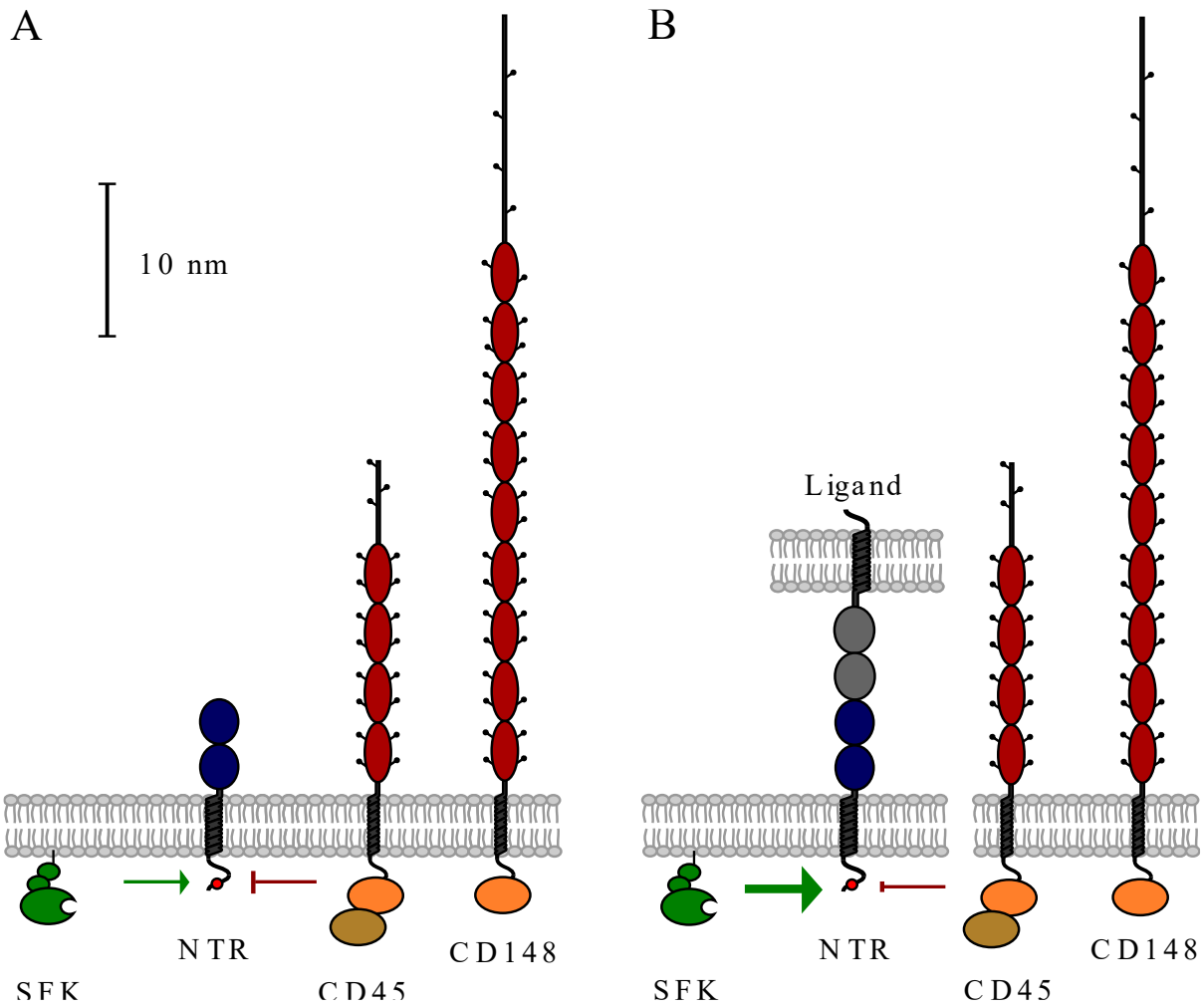


Figure 1.1: Kinetic segregation model diagram

(A) Shows a simplified steady state where a given NTR can be phosphorylated via SFK family kinases and dephosphorylated via the phosphatases CD45 and CD148. **(B)** Once the receptor ligand complex has formed it leads to exclusion of the phosphatases and therefore produces a kinase dominated environment which maintains activation of the receptor and leads to downstream cellular activation.

A key prediction of the KS model is that the phosphatases CD45 and CD148 will be excluded from the close contact site, allowing receptor activation. Indeed, CD45 has been shown to be excluded from the site of TCR activation (Choudhuri et al., 2009; Fernandes et al., 2019; Varma et al., 2006) and Fcγ (Freeman et al., 2016). Additionally, truncation of the extracellular domains of both phosphatases was shown to abrogate immune response activation (measured as IL-2 production) in mouse $CD4^+$ T-cell hybridomas (Cordoba et al., 2013; Irles et al., 2003). The shortened constructs were subsequently seen to co-localise with the TCR using total internal reflection fluorescence (TIRF) microscopy.

The importance of phosphatase exclusion from close contact formation has been highlighted with single molecule tracking, which has allowed for very accurate tracking of the TCR and CD45 in cells supported by lipid bilayers. Not only has it confirmed previous work by (Furlan et al., 2014) showing that CD3 forms micro clusters segregated from CD45, it has also been observed that diffusion of molecules inside micro clusters is slower than that of molecules outside; and that CD45 would very rarely be able to enter TCR micro clusters (Chang et al., 2016; Hui & Vale, 2014; Ito et al., 2017).

Single molecule tracking has also made it possible to show that simply slowing the diffusion of the TCR at the site of membrane close contacts is enough to tigger activation (K. Y. Chen et al., 2021). By adding soluble pMHC to the TCR the diffusion rate was slowed, allowing for TCR activation inside close contacts formed via CD2 binding CD58 on SLBs. Conversely, addition of the extracellular region of CD45RO lead to exclusion of the TCR from the close contact and reduced activation.

A key criticism of the KS model is that CD45 could still enter a close contact if its extracellular domain was flexible enough. However, using variable-angle TIRF microscopy with fluorophores at the ends of the CD45 isoforms it was shown that the molecules were not

lying flat on the supported lipid bilayers but protruding up from the surface (Chang et al., 2016; Junghans et al., 2018).

Another criticism of this model is that knocking out CD45 in mice prevented lymphocyte activation, therefore it was thought that it is not a negative regulator of activation (Trowbridge & Thomas, 1994). However, as discussed in previous sections, it is now thought that CD45 performs a dual role: dephosphorylating SFK family kinases to produce the enzymatically active conformation (positive) but also preventing receptor activation though dephosphorylation of the tyrosine residues on NTRs (negative). This then raises another issue, which is that CD45 molecules must be close to the site of receptor ligand binding to activate the SFKs, giving them enough time to phosphorylate the receptor tails before becoming phosphorylated themselves and inactive again. This issue of how close CD45 is to the receptor has been addressed using modelling and super resolution microscopy to track the TCR and CD45 during activation (Razvag et al., 2018). The results suggest that during initial binding the TCR is contained in micro villi and the CD45 molecules are close enough to perform both functions due to there still being a large enough membrane gap: SFKs are active, but CD45 keeps the NTR tails dephosphorylated. However, if the TCR interaction is strong enough, the contact is maintained, bringing the membranes into a close contact, flattening out the microvilli and therefore segregating the CD45, leaving behind active SFKs to maintain activation.

It has also been possible to test one key aspect of the KS model: the prediction that molecules of different sizes will be segregated from one another during close contact formation. One approach was to test the colocalization of similarly size molecules used fluorescently labelled dextran of different molecular weights added to the surface of YTS cells (Cartwright et al., 2014). The cells were then mixed with Epstein-Barr virus (EBV) transformed B cells to trigger conjugate formation and establish how far the dextran could migrate into the close

contacts that resulted. The larger the dextran the more they were excluded from the contacts, with 10 nm dextran excluded up to 50 % and dextran above 32 nm being almost completely excluded. While dextran was a good test to show generic size exclusion from the close contact, other studies have focused on segregation of specific molecules involved in the immune response. For example, in Jurkat cells presented to SLBs, the TCR and larger adhesion molecule LFA-1 segregate even before a stable close contact had formed (Kaizuka et al., 2007).

Another study used giant unilamellar vesicles (GUVs) and supported lipid bilayers to reconstitute a simplified system that allows for careful control of the number and type of binding or non-binding proteins in the membrane interface (Schmid et al., 2016). An interface between GUVs was formed with single length binding protein (BP) and increasing lengths of non-binding protein added. The longer the non-binding protein added was, the more it segregated away from the binding interface. The lateral footprint of the GUV and binding affinity of the binding protein was also found to affect exclusion of non-binding protein. These experiments, aided by modelling of the membrane interface, found that just a 4.5 nm increase in size above that of the of the binding protein was enough for significant segregation. This was also found using another system which tracked different sized quantum dots entering and leaving close contacts (Kulenkampff et al., 2020). This is interesting because the predicted close contact between the TCR and its pMHC ligand is approximately 13-15 nm (Chang et al., 2016; Choudhuri et al., 2005). The predicted lengths of the extracellular domain of CD45 isoforms were initially found to be 28-53 nm using low resolution electron microscopy (McCall et al., 1992), but this has been refined more recently, with the shortest isoform (CD45RO) found to be 21.6 nm and all other isoforms predicted to be larger. Therefore, the difference in the predicted sizes of the molecules match very well to the segregation limit calculated by (Schmid et al., 2016).

Similar results were seen using GUVs and SLBs with an inducible receptor ligand interaction between FKBP and FRB, which relied on addition of rapamycin for contact formation (Carbone et al., 2017). This system was used to compare the segregation of the two major isoforms of CD45 (CD45 RO and CD45 RABC) on the same membrane. While both were segregated from the FKBP clusters, the larger CD45 RABC isoform was segregated threefold faster. However, the final exclusion of both isoforms was similar. The same trend was observed for a reconstituted TCR using the 2B4 alpha and beta chains, which can bind to peptide loaded IE^k MHC. Finally, the addition of PD-1 and PD-L1 confirmed that when bound, PD-1 would co-localise with the TCR and become segregated from CD45. The GUVs based systems have also shown that CD45 is excluded from the site of TCR-pMHC binding, which was found to colocalize with the similarly sized CD2-CD58 interaction (Jenkins et al., 2019). This study also found ZAP-70 and Lck concentrated in the close contact zone, highlighting that that is the site of receptor activation.

Overall, the prediction that molecules with large extracellular domains can be excluded from areas of close contacts is very convincing due to the number of different cellular and reconstituted systems it has been observed in. Unlike the other models discussed, the power of the KS model is that by its nature it is applicable to all NTRs, irrespective of their sequence diversity. It can also explain why CD45 and CD148 have such large extracellular domains when compared with NTR family. In the next section, I review further experiments within the framework of the KS model, specifically looking at the impact of receptor-ligand dimensions on immune cell activation when compared with other members of the NTR family.

1.4. Studies on the impact of receptor-ligand dimensions on the immune response

The majority of the receptor ligand complexes responsible for immune cell activation, such as the TCR, are relatively small compared to the much larger glycocalyx that surround them (Dushek et al., 2012). Therefore, when immune cells interact with antigen presenting cells to form an immunological synapse (IS) these large proteins are thought to be excluded. There are over one hundred receptors that are predicted to be sensitive to receptor ligand dimensions. Interestingly this sensitivity to receptor ligand dimensions has been shown with both activatory and inhibitory receptors (Köhler et al., 2010). Studying why the receptor ligand dimensions are important in this very crowded environment has been challenging but may be key for making effective immunotherapeutic products which take advantage of immune receptors.

1.4.1. Close contact formation and adhesion molecules

The first suggestions that receptor ligand interactions could depend on size was found through studying adhesion molecules on leucocytes. The main adhesion molecules important for T cell activation are the integrin (LFA)-1, which binds (ICAM)-1, and CD2, which binds CD48 in mice and CD58 in humans. Early work showed that interactions between CD2 and CD58 produced multiple small close contact points between the interacting membranes, surrounded by the larger integrin interactions and glycocalyx (Springer, 1990). This was followed by evidence that the length of the CD2 interaction was functionally important because artificially increasing the length of CD58 showed increased adhesion to T lymphocytes (Chan & Springer, 1992). Digestion of the glycocalyx also increased the adhesion, likely due to a reduction in the charge repulsion between cells and reduced steric hindrance.

While there was some evidence that increasing the size of a receptor ligand pair could improve binding, it did not address what impact this would have on receptor activation or other receptor interactions. This was addressed by producing different length variants of CD48 and looking at changes in TCR activation (Wild et al., 1999). Increasing the size of CD48 lead to a dramatic reduction in TCR activation measured by reduced cytokine release and TCR down-modulation. This was shown to be independent of CD2 signalling, as truncating the cytoplasmic domain did not alter this effect.

Following the resolution of the crystal structure of the TCR-pMHC complex, the interaction was found to be approximately 15 nm in length (Garboczi et al., 1996; Garcia et al., 1996). Therefore, the size of the CD2-CD48 interaction was predicted to have very similar dimensions, so that it would hold the membranes together at the correct distance to allow the TCR to engage its ligand (Van Der Merwe et al., 1995). Conversely, increasing the length of CD2-CD48 would hold the membranes too far apart to stabilise the TCR-pMHC interaction leading to the reduced activation seen by (Wild et al., 1999). This may explain why so many NTRs protrude from the surface of cells to the same extent, for example PD-1, NKG2D, and TREM-1 (Figure 1.2). A conserved length of the receptor-ligand complex would facilitate receptor ligand engagements to occur within sites of opposing membrane close contact without requiring large unfavourable undulations in the plasma membrane (Davis & van der Merwe, 1996). This hypothesis would also predict that molecules with larger extracellular domains should be excluded from the site of close contact formation, for example LFA-1, CD45, CD148, CD44 and CD43 (Figure 1.2). This was observed using the CD2-CD48 axis which was found to segregate from LFA-1-ICAM-1 interactions (Dustin et al., 1998). To rule out the effect of CD2 signalling, its cytoplasmic domain was removed. While this did reduce CD2 clustering compared to the WT, the mutant CD2 still segregated away from LFA-1, highlighting that the difference in size must be key.

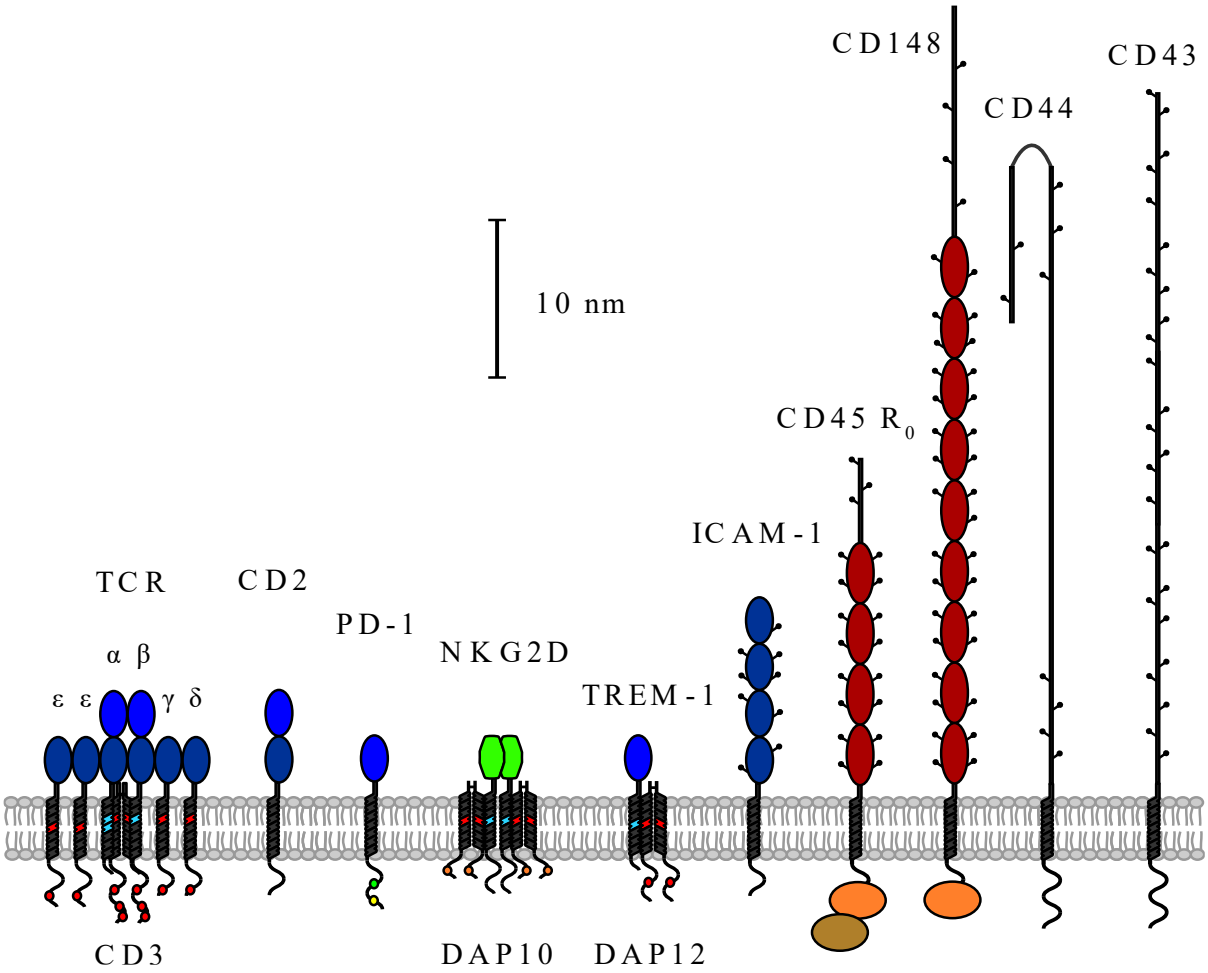


Figure 1.2: Relative size of common leucocyte surface proteins

This diagram highlights the striking difference in the size of different extracellular proteins on leucocytes (Dushek et al., 2012). Most receptors in the NTR family share similar small extracellular dimensions in contrast to the much larger glycocalyxs which include the CD45 and CD148 phosphatases.

A subsequent study again used extended forms of CD48, here attached to SLBs, where mouse T cell blasts were allowed to settle onto the bilayer (Milstein et al., 2008). The contact area was measured using interference reflection microscopy and the adhesion efficiency was seen to decrease by up to 10-fold with an increase in ligand length. The extension of CD48 was suggested to increase the volume it must explore before binding reducing its on rate. The reduction in adhesion seen is in contrast to previous work (Chan & Springer, 1992; Springer, 1990) however, this may be compensated for in a cell-cell system with glycocalyx present on both membranes adding a crowding effect. Interestingly, when two ligands which differed in length by 2-3 Ig domains were added together, they formed separate adhesion domains, whereas ligands that differed in length by one Ig domain could colocalize (Milstein et al., 2008). This shows that molecules of similar size naturally cluster together when the membranes are constrained by receptor ligand binding.

1.4.2. The effect of receptor ligand size on TCR activation

The TCR is the most well studied member of the NTR family due to its importance in the adaptive immune system. Evidence that the dimensions of the TCR-pMHC complex are key to its activation was shown using a single chain trimer (SCT) containing the mouse MHC class I H-2Kβ with an ovalbumin-derived peptide (Choudhuri et al., 2005). The SCT was used to rule out the possibility that elongation could affect peptide loading. This pMHC mimic was placed at the end of various spacers of increasing length using CD2, CD22 and CD4. T-cells exposed to increasing ligand length showed reduced IL-2 release for the same cell-cell conjugation. However, this system had the disadvantage of requiring CD8 interaction to get activation of the TCR. Therefore, a second system was produced presenting a human SCT that was unable to bind CD8 containing a peptide derived from HIV (Choudhuri et al., 2009). This time the T cell clone G10, which does not require CD8 binding to be activated, was challenged with either the membrane proximal or the CD4 ligand spacer.

Like before, elongation prevented activation (as measured by IFNγ release). Imaging showed that while increasing the ligand length had no impact on CD3ζ clustering, it did reduce recruitment of Zap70. This suggests that an elongated ligand leads to tyrosine residues on the CD3ζ not being phosphorylated as efficiently, which prevents Zap70 recruitment. This same effect was found using the membrane proximal ligand in combination with PP2 a SFK family inhibitor, which also prevents Zap70 recruitment by preventing CD3ζ phosphorylation.

A recent study used a different approach to incrementally activate the TCR (Chen et al., 2017). Their system comprises of a large panel of six different ligand lengths, each with three different scFv's against the CD3 chain of the TCR. This allowed for both the length and affinity of the interaction with the CD3 chain to be varied. The intermembrane distance of each ligand was measured using electron microscopy and the range of their panel was found to be from 10-40 nm. Jurkat T cell activation was measured using competition assays with soluble antibody and cytokine release. In general, the results showed that the longer the ligand, the weaker the activation, which is consistent with previous work. However, the affinity of the receptor ligand interaction was also shown to have an important role in activation. The highest affinity OKT3 scFv, (OKT3 K_D of 0.5 nM) caused no reduction to activation when increasing the ligand length. However, a reduction in activation with increased receptor ligand length was again apparent with the BC3 scFv (K_D 8 nM) and very clear with 2C11 (K_D 70 nM) (Chen et al., 2017). The limitations of this study are that the authors do not show data with the elongated OKT3 scFv at low ligand density, perhaps because ligand density is difficult to control in their system. Also, the OKT3 scFv has an affinity roughly three orders of magnitude greater than a typical physiological receptor, which would be close to a K_D of 1 μM (Spear et al., 2013). It is likely that at such high affinities the OKT3 scFv can cluster the TCR/CD3 complexes. While unphysiological, TCR clustering can stimulate TCR triggering. Taken together this may explain why the authors see

no difference when the ligand length is increased with the OTK3 scFv. Therefore, this result may be explained by the affinity of the receptor ligand complex being increased to such an extent that the normal cellular mechanism for activation breaks down. This may be similar to TCR triggering induced by soluble multivalent ligands such as antibodies or pMHC-tetramers, which can lead to cellular activation without a membrane presented ligand (Knobloch et al., 1991).

1.4.3. The effect of receptor ligand size on other activatory NTR members

While the TCR is the best characterised member of the NTR family, it is important to understand if receptor ligand dimension sensitivity also applies to the triggering of other NTRs. Many well studied NTR family members (e.g. CD28, CTLA-4 and PD-1) share small receptor ligand dimensions, use similar tyrosine motifs to the TCR, and are deactivated by phosphatases (Dushek et al., 2012). Therefore, after the TCR the most obvious candidate to look at is CD28, which is the major costimulatory receptor for the TCR. Progressive elongation of one of its ligands (CD80) was shown to reduce stimulation of CD4 and CD8 naive primary T-cells to produce IL-2 (Lim et al., 2015). Importantly the TCR and CD28 ligands were presented on separate antigen presenting cells. This would prevent size mismatching, which otherwise could affect TCR binding as was seen when CD48 was elongated (Wild et al., 1999). This study also found that the longer the ligand, the less CD45 was segregated from CD80, thereby facilitating CD28 dephosphorylation.

The Fc family of receptors is also encompassed by the NTR classification. These receptors work by binding the Fc region of an antibody which has bound to a target on an opposing membrane. Considering the requirement to fit a molecule as large as an antibody into the close contact site, it may seem counterintuitive that the activation of these receptors could be affected by receptor ligand dimensions. However, recent work shows that FcγRIIa and FcεRI are very sensitive to the distance of an epitope from the surface of the membrane (Bakalar et

al., 2018; Felce et al., 2018). In a carefully controlled system using RAW 264.7 macrophage cells interacting with supported lipid bilayers presenting different ligand lengths, it was shown that, independently of any cytoskeletal effects, epitopes that are more than 10 nm away from the surface prevent phagocytosis due to the size of the close contact allowing access to CD45 (Figure 1.3A and B) (Bakalar et al., 2018). Furthermore, the crystal structures of several Fc receptors in complex with antibody fragments revealed that the antibody actually binds upside down to the receptor (J. Lu et al., 2015; Oganesyan et al., 2015; Ramsland et al., 2011). This mode of binding was puzzling when the structures were resolved, as the antibody must form a very compact conformation by folding its binding arms back on itself. However, it can be explained if the activation of Fc receptors is through the kinetic-segregation mechanism, as it allows the intermembrane distance to be small enough to exclude CD45 (Figure 1.3B).

Another example comes from natural killer cells, which contain the NTR NKG2D. This receptor binds its ligand MICA, which is produced by cells as a stress response (Groh et al., 1998). This interaction also produces a close contact similar in size to that of the TCR-pMHC interaction (P. Li et al., 2001). To test if the size of the interaction was significant, MICA was presented on the natural killer tumour cell line NKL at the end of increasing spacer lengths and production of INFγ was used as a readout of activation (Köhler et al., 2010). Following the same pattern as for previous NTRs, the relative levels of INFγ produced decreased with increases in ligand length, with the largest ligand producing no response. Other readouts such as induction of CD107a, an activation marker and target cell lysis, were also length sensitive. To show that the increase in length was not affecting binding to the receptor, beads coated in NKG2D showed comparable binding to all ligand variants. To further control for this a conjugate assay showed similar levels of conjugate formation for each ligand (Köhler et al., 2010).

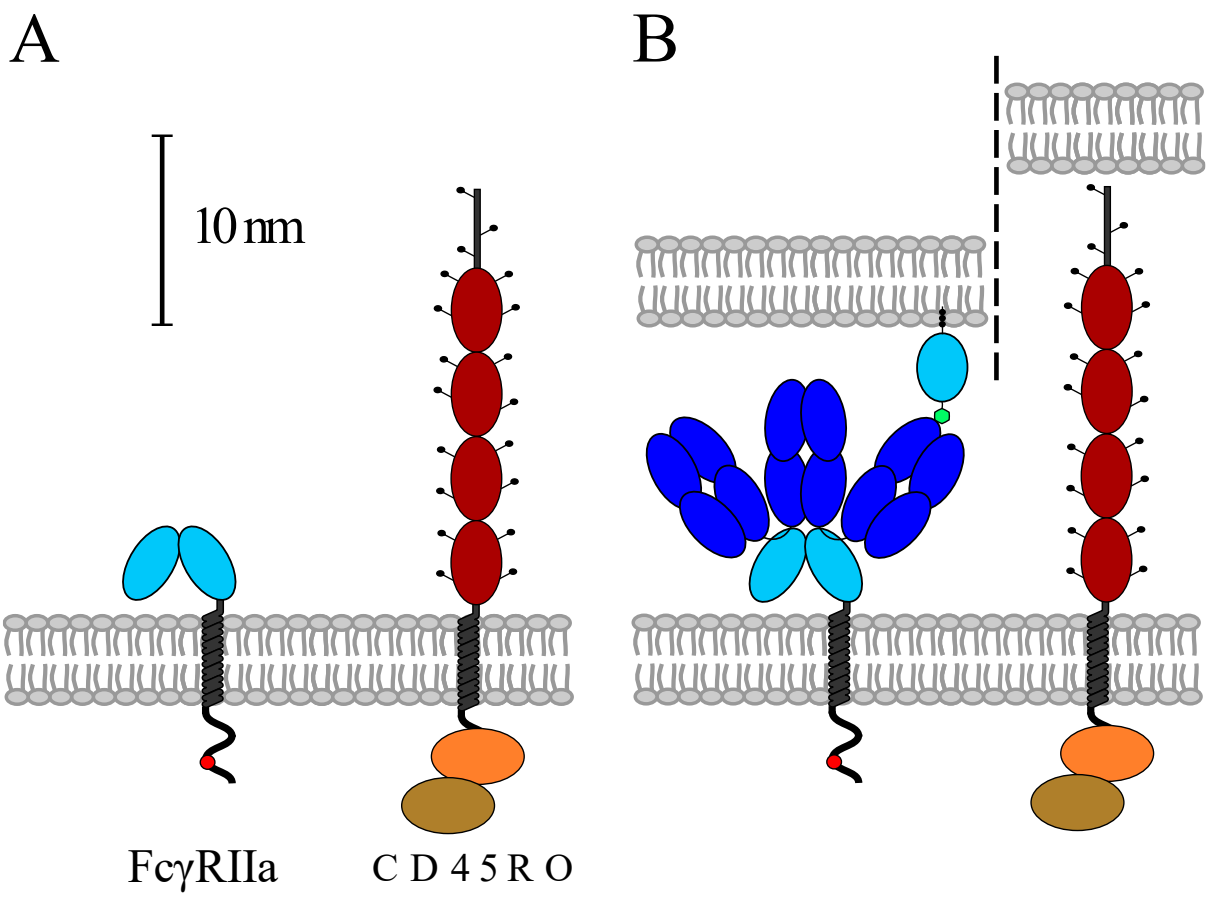


Figure 1.3: Antibody binding to its epitope and an Fc receptor simultaneously

(A) Shows the resting state with the FcγRIIa and CD45 free to move on the membrane of a RAW 264.7 macrophage cell (Bakalar et al., 2018). **(B)** Antibody binding to biotin presented on a supported lipid bilayer while also biding to the FcγRIIa receptor. For this interaction to occur the antibody must bend back on itself, thereby reducing its size in the close contact leading to the exclusion of the CD45 phosphatase.

1.4.4. The effect of receptor ligand size on inhibitory NTR members

Inhibitory NTRs are structurally very similar to the activatory receptors although they differ in the tyrosine motifs present in their cytoplasmic tails (see previous sections). Several studies have looked at the effect of elongation on the triggering of these receptors and their ability to co-localize with activatory receptors.

For example, the YTS natural killer tumour cell line was used with the inhibitory receptor KIR2DL1, which can bind its ligand HLA-Cw6. A stimulatory signal was provided by the activatory receptor NKG2D binding to MICA (Figure 1.4A) (Köhler et al., 2010). Elongation of the HLA-Cw6 ligand reduced inhibition of the KIR2DL1 cells in a lysis assay (Figure 1.4B). It was also shown that extending the HLA-Cw6 ligand did not reduce KIR2DL1 binding in a conjugate assay. Extending both ligands at the same time restored the inhibitory effect resulting in reduced cell lysis but not back to WT levels. This is most likely due to reduced activation of both receptors due to their increased length (Figure 1.4C). Imaging studies confirmed that colocalization of the activatory and inhibitory receptor ligands required them to be the same size. This highlights that for this inhibitory receptor to regulate the activatory receptor it needs to be the same size to allow co-localization. This was confirmed with work on another NK cell inhibitory receptor, Ly45A, which can also co-localize with NKG2D (Tomaz et al., 2018). Here, FRET was used to track the proximity of the two receptors and show that increasing the size of either that Ly45A or NKG2D ligand reduced co-localization. Unfortunately, this study did not show whether extension of both ligands together could rescue co-localization, as reported by (Köhler et al., 2010).

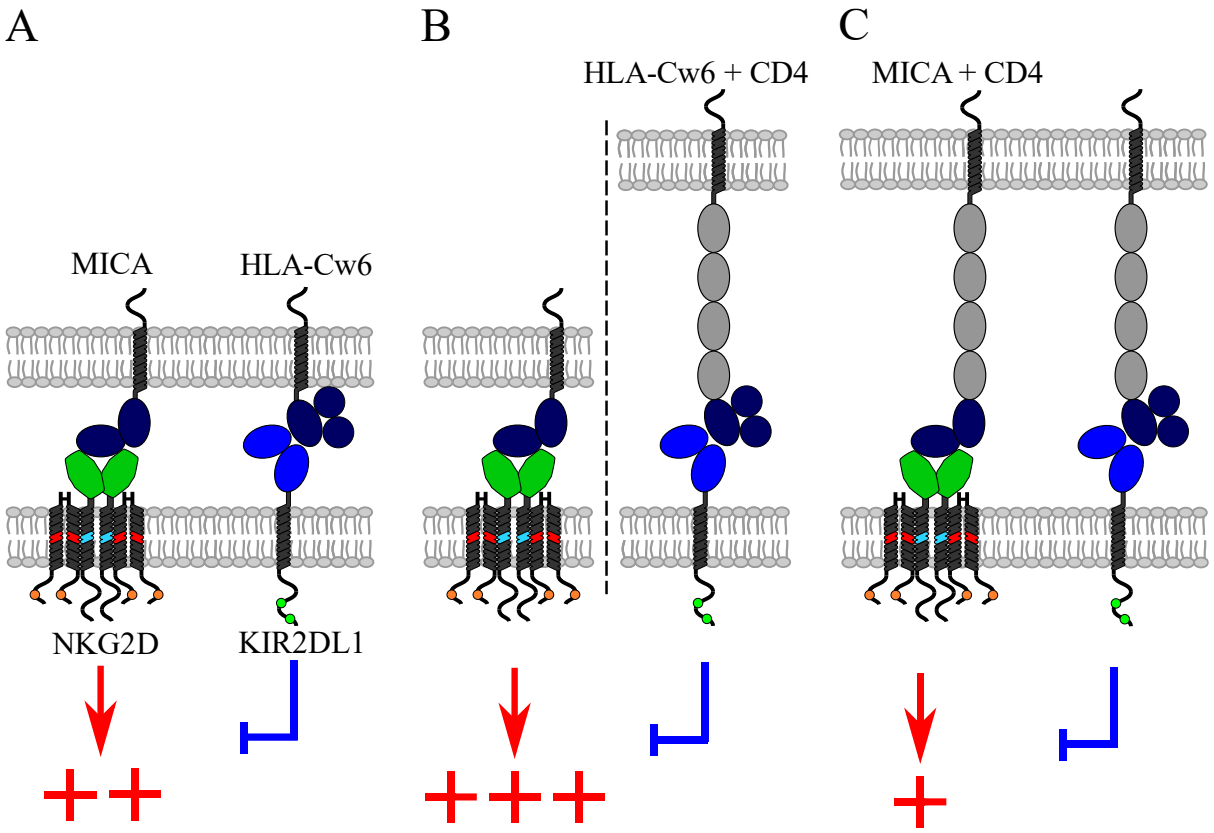


Figure 1.4: Effect of elongation on the activation of the inhibitory receptor KIR2DL1

(A) Shows the WT proteins interacting with their ligands. Both interactions form a similarly small receptor ligand interaction allowing the inhibitory effect of KIR2DL1 to control NKG2D activation. **(B)** Extension of the KIR2DL1 ligand with the addition of CD4 prevents co-localisation of the receptors and prevents the inhibitory effect, thereby leading to increased activation of NKG2D. **(C)** Extension of both ligands allows the two receptors to again co-localise restoring the inhibitory effect.

Similar results have been found with the inhibitory receptor CTLA-4, which competes for the same ligands (CD80/CD86) as TCR co-stimulator CD28 (Yokosuka et al., 2010). It was shown that increasing the size of the ectodomain of CTLA-4 led to its inability to enter micro clusters containing the TCR and CD28 therefore, abrogating its inhibitory functions.

Finally, this sensitivity has also been observed with work on PD-1, another inhibitory NTR which binds its ligand PD-L1/PD-L2 and negatively regulates T-cell activation. The size of the receptor ligand complex for the TCR, CD28 and PD1 is closely matched allowing for all three to co-localize within the site of TCR binding. When PD-1 is activated it leads to the recruitment of the SHP2 phosphatase, which acts to dephosphorylate tyrosine residues on both the TCR and CD28 (Hui et al., 2017; Mizuno et al., 2019). PD-1 is of particular interest to immunotherapy, and it has been reported that T cells that had more CD28 responded better to PD-1 antibody blockade (Kamphorst et al., 2017). This fits the idea that PD-1 can co-localize with CD28 at the site of close contact formation and thereby inhibit CD28 activity. While increasing the size of the PD-1 ectodomain by either two or four Ig domains did not change its ability to bind PD-L1, it did lead to a dramatic decrease in its ability to co-localize with the TCR/CD28 (Yokosuka et al., 2012). This abrogated its suppression of T cell activation. To show that this was not due to reduced signalling by PD-1, they then fused SHP1 or SHP2 to the intracellular tail of PD-1 (to reconstitute a "constitutively signalling" PD-1) and confirmed that elongation abrogated the inhibitory effect of the PD-1-SHP1/2 fusion proteins.

1.4.5. The effect of receptor ligand size on non-NTR cell surface molecules

Taking a step back, the effect of receptor-ligand dimensions on signalling could be relevant not just for immunology but other fields too. Notch signalling is crucially important for cell-cell communication during development (Artavanis-Tsakonas et al., 1999). It is apparent that regulation of this molecule is controlled through ligand engagement, post-translational

modifications, and mechanical force. However, it has now been suggested that Notch signalling is also sensitive to receptor ligand dimensions (Kwak et al., 2020). Due to its large extracellular domain the Notch molecule is normally spatially segregated from E-cadherin-based adherence junctions (cad-AJs), maintaining it in an inactive state. This large extracellular domain is subsequently cleaved by ADAM10 and γ-secretase to produce the signalling active molecule (Fortini, 2009). Several truncations were made to the Notch extracellular region and the shorter variants were found to infiltrate the cad-AJs and lead to ligand independent activation of the pathway (Kwak et al., 2020). Therefore, spatial segregation is acting as a key step in the activation switch for Notch.

1.5. Therapeutic relevance of receptor ligand dimensions

So far, the focus of this introduction has been on NTRs and the factors that control their activation, in particular basic research looking at the size of receptor ligand interactions. In this section, I wanted to explore how this knowledge can be utilised to produce effective immunotherapies.

1.5.1. Antibodies targeting tumour markers

The use of antibodies as an anti-cancer therapy is not a new concept, for example rituximab (RTX) has been used successfully to treat Non-Hogkins lymphoma (NHL) for over two decades (Molina, 2008). The majority of current therapeutic antibodies in clinical use that target cells for destruction act by binding very small molecules (e.g., CD19, CD20, CD33 and CD52) or the membrane proximal epitopes of larger ones (e.g., HER2). The antibodies can then bind effector cells via Fc receptors, leading to antibody depended cytotoxicity (ADCC) and antibody depended phagocytosis (ADCP) (Chan & Carter, 2010; Cho et al., 2003). Therefore, the location of the antibody binding site in relation to the target cell membrane appears to be important for its function.

One study aimed to answer this question using the successful antibodies RTX and CAMPATH-1H, which bind CD20 and CD52 respectively (Cleary et al., 2017). Five ligand molecules (based on CD137) of varying lengths from 0.3-16 nm were produced, with either the CD20 or CD52 epitope at the membrane distal end (Figure 1.5A). They first looked at whether changing the length of the ligand would affect the complement-dependent cytotoxicity (CDC). Interestingly, having the epitopes further away resulted in dramatically less cell lysis than having them close to the membrane when cells were incubated with human serum. It was argued that this was due to the fact that complement components C2a and C4b would be less stable when bound further away from the membrane and therefore, the formation of the C3 convertase complex would be less efficient (Wallis et al., 2010). Importantly, a similar pattern was seen when cells expressing ligands of varying lengths were mixed with human peripheral blood mononuclear cells (PMBCs), where NK cells are thought to be the main source of ADCC (Beum et al., 2008). As discussed before Fc receptors are very sensitive to the distance of an epitope from the surface of the membrane (Bakalar et al., 2018).

1.5.2. Bispecific T-cell dependent antibodies

One of the early methods to artificially manipulate an immune cell to specifically attack a target cell was using bi-specific T-cell engagers (BiTEs). This method uses two scFv's joined via a linker, one for the CD3 chain of the TCR and the other specific to a cancer or target cell marker (Baeuerle & Reinhardt, 2009). When BiTEs were used to target large or highly glycosylated proteins, for example melanoma chondroitin sulfate proteoglycan (MCSP), it was found that antibodies with epitopes close to the membrane were more effective in killing assays than those with epitopes further from the membrane (Figure 1.5B) (Bluemel et al., 2010). This was then confirmed in the same system with a stepwise increase in the distance of the antigen from the membrane surface.

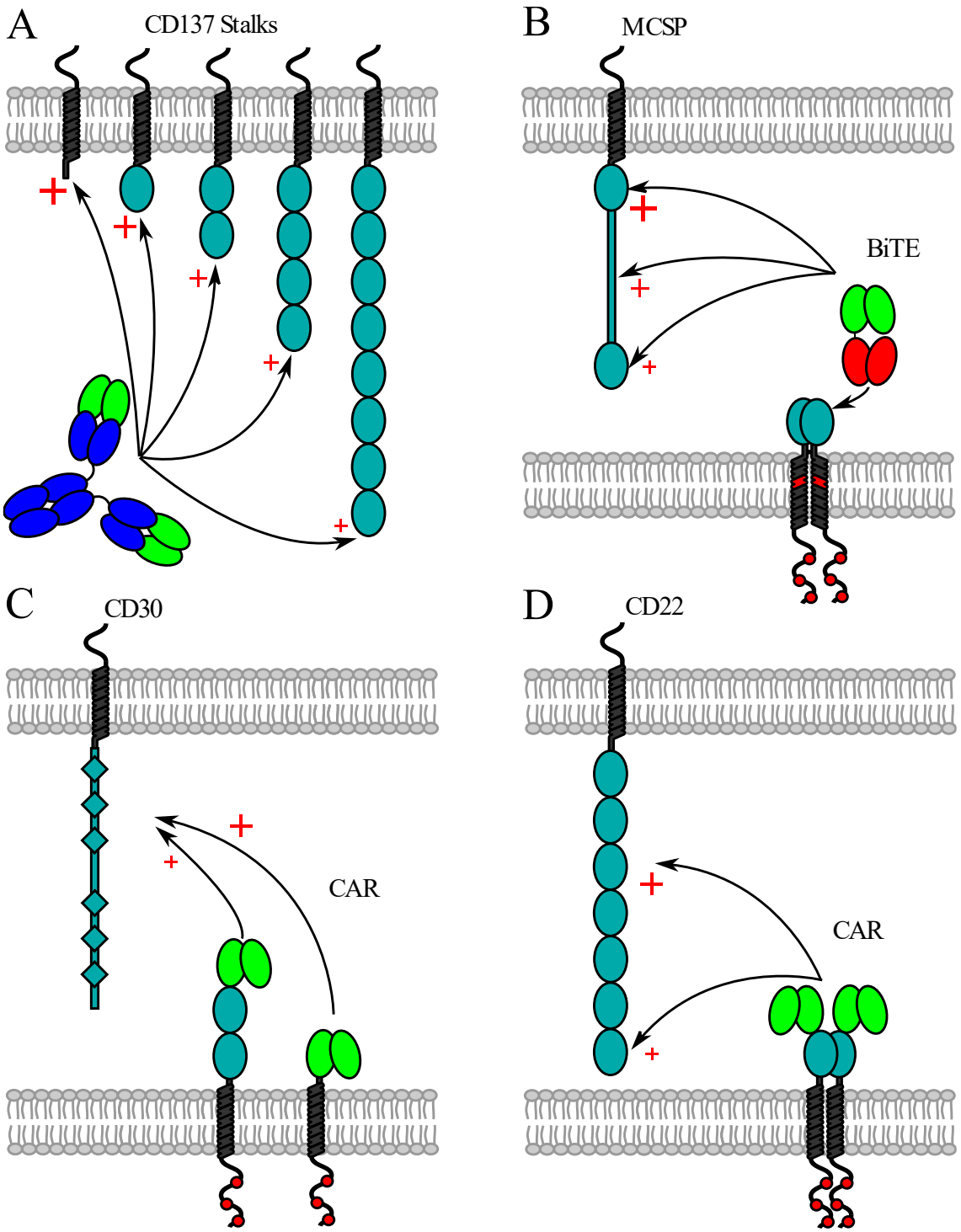


Figure 1.5: Receptor ligand dimensions are key for Immunotherapy

(A) Shows that increasing the epitope distance from the membrane for two therapeutic antibodies, RTX and CAMPATH-1H reduced their potency (Cleary et al., 2017). **(B)** Moving the epitope for a MCSP targeting BiTE away from the target membrane reduced its effectiveness (Bluemel et al., 2010). **(C)** CARs commonly have a linker region between the scFv and the membrane anchor but this can be detrimental to receptor activation (A. Hombach et al., 2000). **(D)** A related CAR system utilises an IgG1 Fc spacer to promote dimerization in the membrane. scFv's specific for two CD22 epitopes showed that targeting membrane proximal epitopes was more potent than targeting membrane distal ones (S. E. James et al., 2008).

Comparable results were found using a similar system: T cell-dependent bispecific antibodies (TDBs), antibodies where one arm that binds CD3, and the other binds the myeloma B cell surface marker FcRH5. Comparing three different TDBs for epitopes spanning the length the length of FcRH5 showed more potent killing for membrane proximal epitopes (J. Li et al., 2017). This study also found that as the epitopes moved closer to the membrane the extent to which CD45 was excluded from the close contact zone was increased. As expected, the opposite effect was seen for Zap70, as the tyrosine residues on the TCR can maintain their phosphotyrosine state longer due to the exclusion of CD45. Further evidence that the size of the FcRH5 itself was playing a role in the efficiency of TDBs binding was shown when truncating the protein lead to increased potency (J. Li et al., 2017). This is important as any large body which can cause steric hindrance during close contact formation can reduce the efficacy of receptor activation.

1.5.3. Chimeric antigen receptors (CARs)

CARs contain a scFv, usually for a cancer marker, joined by a flexible linker to a transmembrane domain and a cytoplasmic signalling domain. This intracellular domain is comprised of combinations of various activatory receptor tails such as CD3, CD28, 4-1BB and OX40 (Sharma & Kranz, 2016). The ability to design and then transduce custom CARs into a patient's own T cells has kick-started an entire field of research. There are a lot of factors to consider when designing a CAR and Srivastava & Riddell, (2015) have reviewed many of them. However, two of the factors with the biggest impact on CAR potency are the distance of the CAR epitope from the target cell membrane and the CAR hinge region (A. A. Hombach et al., 2007; Hudecek et al., 2013, 2015; Krenciute et al., 2016; Rodgers et al., 2016).

The first generation of CARs contained the scFv attached to a hinge, a single pass transmembrane and the CD3ζ chain. However cells expressing this construct were

significantly less potent in terms of proliferation and cytokine production compared to the endogenous TCR (Brocker, 2000). These problems have been partially addressed by the addition of further activatory signalling tail motifs derived from CD28, 4-1BB and OX40 to produce second and third generation CARs (Imai et al., 2004; Khalil et al., 2016; Maher et al., 2002). There have also been additional improvements to try and break into solid tumour environments such as "armoured CARs" produce cytokines such as IL-12 to further enhance the local response (Rafiq et al., 2019; Yeku et al., 2017).

One of the first studies to show that the size of the extracellular region was important designed a CAR against CD30 with either the scFv connected directly to the transmembrane domain or via the CH2CH3 region of an IgG1 as a spacer (Figure 1.5C) (A. Hombach et al., 2000). The results showed that while the addition of the spacer stabilised the CAR expression, it could reduce the efficiency of T-cell activation. The presence of a spacer region was found to be important when the scFv was targeting a membrane proximal epitope. However, a spacer was detrimental when targeting membrane distal epitopes (Guest et al., 1997). This is consistent with an optimal membrane distance for receptor activation inside the close contact.

This optimal distance was also seen using a selection of CARs with scFvs targeting different epitopes of the tumour associated antigen CD22 (Figure 1.5D) (S. E. James et al., 2008). The CARs were transduced into human $CD8^+$ T cells. When these cells were mixed with Daudi CD22 positive B cell lymphoma cells there was a reduction in the level of maximum lysis as the epitopes became more membrane distal. The effect was correlated with a reduction in the degranulation and with diminished INFγ production by the $CD8^+$ T cells. A later study aimed at improving the CD22 CAR confirmed that targeting membrane proximal epitopes was more effective compared to the membrane distal ones (Haso et al., 2013).

1.6. The CD5 and CD6 co-receptors

CD5 and CD6 are somewhat of an enigma amongst other NTRs because of their complex effects on T cell activation. Understanding how both CD5 and CD6 modulate T cell activation may have important therapeutic applications. They are thought to have evolved from a gene duplication event because of their similar structure (Padilla et al., 2000). They both contain three scavenger receptor cysteine rich (SRCR) domains, a single pass transmembrane region and a long unstructured cytoplasmic tail. The tail of CD6 is amongst the longest of any NTR at 244 amino acids and contains 9 tyrosine residues which are thought to recruit positive and negative regulators of T cell activation (Bowen et al., 1997).

It is well established that CD6 binds CD166, a member of the Ig superfamily also known as activated leukocyte cell adhesion molecule (ALCAM) (Hassan et al., 2004). ALCAM contains five Ig domains, and its membrane distal Ig domain binds to the membrane proximal domain of CD6. This interaction is well characterised, and the crystal structure has been solved (Chappell et al., 2015). It has an affinity (K_D 0.4 - 1.0 μM), which is relatively high when compared to other NTR receptor ligand pairs (Bowen et al., 1996; Hassan et al., 2004). CD166 has also been shown by native mass spectrometry to form weak homodimers (Chappell et al., 2015). It is also highly expressed throughout the body but particularly on thymic epithelial cells and in the nervous system (Bowen et al., 1995; Ofori-Acquah & King, 2008). There is also now evidence that CD6 also binds CD318 (Enyindah-Asonye et al., 2017).

Interestingly, ligands for CD5 have been elusive. Several potential ligands have been proposed, including the glucan zymosan on the surface of fungal cells (Vera et al., 2009), but they have never been verified. There is, however, evidence that CD5 forms a homodimer and that this is needed for signalling (Bamberger et al., 2011; Brown & Lacey, 2010). If a ligand

does exist it must be very low affinity as it has never been possible to detect any CD5 dependent differences in adhesion between T cells and APCs (Brossard et al., 2003).

1.6.1. CD5 and CD6 role in T cell development and differentiation

CD5 and CD6 are important for thymocyte development, and their expression is highly regulated (Singer et al., 2002). CD5 is expressed early on in thymocytes, and this increases during development (Azzam et al., 1998). It has been shown to reduce T cell activation during negative selection and thereby fine tune which cells survive (Azzam et al., 2001; Peña-Rossi et al., 1999). This suggests that CD5 acts mainly as a negative regulator of T cell activation preventing negative selection. Indeed, knocking out CD5 in mice resulted in more reactive T cells (Tarakhovsky et al., 1995) and more activation-induced cell death in a model for multiple sclerosis (Axtell et al., 2004). This effect did not require the extracellular domain of CD5, suggesting that it did not require ligand binding (Bhandoola et al., 2002). After negative selection CD5 expression correlates with TCR affinity for self-peptides (Kieper et al., 2004). T cells with high CD5 expression also appear to be more successful at inducing an immune response when challenged (Fulton et al., 2015; Mandl et al., 2013).

Additionally, CD3ζ phosphorylation after TCR engagement with self-peptides has also been linked to increased CD5 expression again highlighting its inhibitory effect (Mandl et al., 2013). This was also found in human T cells where higher CD5 expression reduced cell death in tumour infiltrating T cells (Friedlein et al., 2007). They also looked at blocking CD5 with an antibody, but this result is complicated by the fact no cell surface ligand has been identified for CD5. Therefore, the mode of action of the blocking antibody is not well defined. It may act to down regulate the CD5 which could reduce the inhibitory effect. However, it is still unclear whether CD5 recruits inhibitory molecules which act in conjunction with the TCR signalling machinery or independently.

CD5 and CD6 have been implicated in the regulation of T cell differentiation. For example, CD5 has been shown to reduce the number of Tregs, potentially via inhibiting signalling in the precursor thymocytes (Ordoñez-Rueda et al., 2009). In mature Tregs knocking out CD5 produced cells which were more potent inhibitors of activated responder T cells (Dasu et al., 2008). Conversely, CD5 was also found to promote T cell differentiation into Tregs in the immune periphery (Henderson et al., 2015). This was thought to be due to CD5 having a negative role in mammalian target of rapamycin (mTOR) signalling, thereby protecting Tregs from cytokines. Interestingly, Tregs have low levels of CD6 and so it is likely less important for their development and maintenance (Garcia-Santana et al., 2014).

1.6.2. Role of CD5 and CD6 in disease

Both CD5 and CD6 have been linked to several diseases including autoimmunity and cancer. High CD5 expression is a key marker for malignant lymphocytic leukaemia (Damle et al., 2002; Gary-Gouy et al., 2007). A single nucleotide polymorphism (SNP) in CD5 is also linked to systemic lupus erythematosus, which is an autoimmune disease resulting in the loss of self-tolerance (Cenit et al., 2014). This mutation is in the cytoplasmic tail and leads to increased T cell activity, suggesting that it removes some of the inhibitory effect of CD5. Therefore, its inhibitory role could be targeted for immune modulation (Soldevila et al., 2011).

Genome-wide association studies (GWAS) have linked CD6 to several autoimmune diseases including multiple sclerosis, rheumatoid arthritis, and psoriasis (Alonso-Ramirez et al., 2010; Consuegra-Fernández et al., 2017; De Jager et al., 2009; Y. Li et al., 2017). In the case of multiple sclerosis, these mutations lead to reduced expression of CD6, which increases autoimmunity (Swaminathan et al., 2013). One mutation specific to multiple sclerosis leads to reduced WT CD6 but similar CD6Δd3 expression, which results in reduced ligand binding (Kofler et al., 2011). This increase in the relative number of CD6Δd3 molecules reduces T

cell activation and proliferation. This may lead to more self-reactive T cells surviving negative selection which induces the autoimmunity.

High expression levels of CD166 have also been linked to multiple sclerosis and other neuro inflammatory diseases because it facilitates the passage of CD4+ T cells across the blood-brain barrier (BBB) (Cayrol et al., 2007). Therefore, blocking its interaction with CD6 may be a possible treatment. CD166 can also enhance tumour cell adhesion via its homophilic interaction, which can promote metastasis. For example, tumour mobility was increased when CD166 was truncated (Van Kempen et al., 2004). This overexpression of CD166 on tumour cells could also be used as a target for T cell therapy.

There is currently a CD6 monoclonal antibody (itolizumab) which is being used in the treatment of psoriasis (Krupashankar et al., 2014). This antibody binds domain 1 of CD6 and is thought to act by blocking CD166 binding via steric hinderance, and thereby reduce the co-stimulatory effect of CD6 and subsequently reduce inflammation. A better understanding of CD6 function would allow us to fully understand how these treatments are functioning and potentially improve them in the future.

1.7. SARS-CoV-2

The emergence of severe acute respiratory syndrome coronavirus 2 (SARS-CoV-2) has led to an enormous upheaval of modern life, with the health and economic impacts likely to last for many years to come. However, there has also been a very large scientific response covering all aspects of the virus. This includes the development of new treatments, vaccines and a vast quantity of data generated on basic biology looking at every stage of viral transmission, cell entry and replication.

1.7.1. SARS-CoV-2 structure and cell entry

SARS-CoV-2 is an enveloped virus composed of a single-stranded RNA genome (R. Lu et al., 2020). It shares 79% sequence identity with SARS-CoV-1, which emerged in 2002 and was a deadlier but less transmissible virus. They both bind the same surface expressed receptor angiotensin-converting enzyme 2 (ACE2) to gain cell entry (W. Li et al., 2003). Each SARS-CoV-2 virion is composed of four proteins: the nucleocapsid binds RNA, the membrane and envelope proteins sit in the lipid bilayer, and the spike protein protrudes out from the membrane surface. The spike is a homotrimer where each subunit is itself comprised of an S1 and S2 subunit. These subunits are cleaved during viral assembly by a furin protease in the Golgi apparatus and therefore are associated non-covalently on the surface of the virion (Hoffmann, Kleine-Weber, & Pöhlmann, 2020). The S1 subunit is membrane distal and contains the receptor binding domain (RBD) which binds to ACE2. The S2 subunit is critical for cell entry by mediating fusion between the viral envelope and the cell membrane. When RBD binds ACE2 it exposes a cleavage substrate in the S2 subunit for the transmembrane protease, serine 2 (TMPRSS2) present on the cell surface (Matsuyama et al., 2010). Alternatively, ACE2 binding can induce uptake of the viral particle into an endosomal compartment where cathepsin L performs the cleavage (I. C. Huang et al., 2006; Simmons et al., 2005). In both cases this results in membrane fusion and the release of the viral RNA into the cytoplasm.

The S1 subunit can undergo a conformational change between the ‘up’ and ‘down’ states. In the “up” state the RBD is accessible to ACE2, whereas in the “down” state it is buried against the S2 and other two RBDs. The structure appears to be most stable with a single RBD in the “up” state, however this is not exclusive (Wrapp et al., 2020). After cleavage of the S2 site the last step is for membrane fusion to occur. This cleavage step allows for a series of

conformational changes to occur resulting in the fusion pore formation and entry of the viral RNA into the cytoplasm (Fan et al., 2020; Walls et al., 2017).

ACE2 is required for viral entry into cells and its expression is higher in the upper airways versus the lungs (Hou et al., 2020). This fits the upper airways being the main target of infection during the initial exposure (Sungnak et al., 2020). ACE2 is also expressed at even higher levels in the heart and small intestine (Y. Wang et al., 2020). These tissues have been found to be affected in patients with severe disease (Yuhao Zhang et al., 2020). This may be a clue to understanding part of the vast differences in severity of this disease from person to person.

1.7.2. Immune response

The spike but specifically the RBD is the target of a large percentage of neutralising antibodies (Brouwer et al., 2020). These antibodies block ACE2 binding and thus cell entry (Hansen et al., 2020; Robbiani et al., 2020).

Another factor is the response of immune cells, with large amounts of inflammatory cytokines released in patients with severe disease (Darif et al., 2021). It has also been suggested that this cytokine response can increase the expression of ACE2 in a positive feedback loop thereby aiding further viral entry (Zhuang et al., 2020).

1.7.3. Origins of SARS-CoV-2

It has not been possible to trace the virus back to a single animal reservoir, but it could be a recombinant event between a virus in pangolins and one in bats (X. Li et al., 2020). Pangolin coronaviruses have high sequence homology for SARS-CoV-2, especially in the RBD region (Lam et al., 2020). However, SARS-CoV-2 infection in pangolins lead to severe disease and death, suggesting that significant changes to the virus have occurred (Xiao et al., 2020). The coronaviruses in bats share higher sequence homology to SARS-CoV-2 than those in

pangolins except for the RBD (P. Zhou et al., 2020). An alternative to the recombination hypothesis is that several RBD mutations in the bat coronavirus RBD could have enabled it to jump to pangolins and humans (Boni et al., 2020).

1.8. Aims

- Further develop a generic ligand system to quantify the number of ligands presented by each CHO cell (Chapter 3).
- Test a range of different NTRs for sensitivity to receptor ligand dimensions (Chapter 3).
- Test a range of different NTRs for sensitivity to changes in ligand valency, mobility, and affinity (Chapter 4).
- Use the generic ligand system to explore the relationship between the TCR and CD5/CD6 to better understand their dual role as activatory and inhibitory co-receptors (Chapter 5).
- Develop a surface plasmon resonance binding assay to study the SARS-CoV-2 RBD/ACE2 interaction (Chapter 6).
- Use the SPR assay to test different ACE2 variants which occur in the human population, and different RBD mutations which occur in variants of concern such as Alpha, Beta, Gamma, Delta, and Omicron (Chapter 6).

Chapter 2 - Materials and Methods

2.1. Constructs

Sequences were checked using the sequencing services provided by Eurofins Scientific or Source Bioscience.

2.1.1. Receptors

Canonical receptor sequences for all NTR's expressed were obtained from UniProt (Bateman et al., 2021) and inserted into the modified lentiviral vector pHR-SIN-BX to contain an N-terminal Single Strep-tag II (SAWSHPQFEK) or Twin-Strep-tag II with linker (SAWSHPQFEKGGGSGGGSGGSAWSHPQFEK). The C-terminus contained a FLAG tag for intracellular staining as described by (Denham et al., 2019). Inserting new NTR's was initially completed using restriction enzymes 5' BamHI or XhoI and 3' BsiWI but later constructs were made by linearizing the plasmid with BamHI and inserting the NTR sequence using NEBuilder HiFi DNA Assembly. The pHR-SIN-BX vector containing the α and β chains for the 1G4 TCR with a self-cleaving viral 2A peptide were provided by Eleanor Denham. CD5 and CD6 mutant constructs were made by Marion H Brown.

2.1.2. Adaptors

Canonical adaptor sequences for DAP12, DAP10, FcRy and CD3ζ were obtained from UniProt (Bateman et al., 2021) and their corresponding nucleotide sequence was inserted into pHR-SIN-BX-IRES-EmGFP with a C-terminal Myc tag. Therefore, adaptor expression was linked to GFP production. Subsequently these adaptor sequences were transferred to pHR-SIN-BX without the IRES-EmGFP, and a HA tag was added in place of the N-terminal Strep-tag II tag for checking expression.

2.1.3. Ligand anchor constructs

"Short ligand" – Mouse CD80-SpyTag Sequence

METDTLLLWVLLLWVPGSTGD*YPYDVPDYA*TGGSAHIVMVDAYKPTKGGSGGS*H*

VSEDFTWEKPPEDPPDSKNTLVLFGAGFGAVITVVVIVVIIKCFCKHRSCFRRNEASRETN

NSLTFGPEEALAEQTVFL

"Long ligand" – Mouse CD80-CD4-SpyTag Sequence:

METDTLLLWVLLLWVPGSTGD*YPYDVPDYA*TGGSAHIVMVDAYKPTKGGSGGS*KV*

*VLGKKGDTVELTCTASQKKSIQFHWKNSNQIKILGNQGSFLTKGPSKLND***D***ADSRRSLWD*

QGNFPLIIKNLKIEDSDTYICEVEDQKEEVQLLVFGLTANSDTHLLQGQSLTLTLESPPGSS

PSVQCRSPRGKNIQGGKTLSVSQLELQDSGTWTCTVLQNQKKVEFKIDIVVLAFQKASSIV

YKKEGEQVEFSFPLAFTVEKLTGSGELWWQAERASSSKSWITFDLKNKEVSVKRVTQDPK

LQMGKKLPLHLTLPQALPQYAGSGNLTLALEAKTGKLHQEVNLVVMRATQLQKNLTCEV

WGPTSPKLMLSLKLENKEAKVSKREKAVWVLNPEAGMWQCLLSDSGQVLLESNIKVLPTR

SHVSEDFTWEKPPEDPPDSKNTLVLFGAGFGAVITVVVIVVIIKCFCKHRSCFRRNEASRET

NNSLTFGPEEALAEQTVFL

Bold D marks an R to D point mutation to prevent CD4 binding MHC.

Human LAIR1-SpyTag Sequence

METDTLLLWVLLLWVPGSTGD*YPYDVPDYATGGS*AHIVMVDAYKPTKGGSGGS*AE*

HLYILIGVSVVFLFCLLLLVLFCLHRQNQIKQGPPRSKDEEQKPQQRPDLAVDVLERTADK

ATVNGLPEKDRETDTSALAAGSSQEVTYAQLDHWALTQRTARAVSPQSTKPMAESITYAAV

ARH

Mouse CD43-SpyTag Sequence

METDTLLLWVLLLWVPGSTGD*YPYDVPDYATGGS*AHIVMVDAYKPTKGGSGGS*QE*

SSGMLLVPMLIALVVVLALVALLLLWRQRQKRRTGALTLSGGGKRNGVVDAWAGPARVPD

EEATTTSGAGGNKGSEVLETEGSGQRPTLTTFFSRRKSRQGSLVLEELKPGSGPNLKGEEE PLVGSEDEAVETPTSDGPQAKDEAAPQSL

Human CD52-SpyTag Sequence

METDTLLLWVLLLWVPGSTGD*YPYDVPDYAT*GGSAHIVMVDAYKPTKGGSGGS*DT SQTSSP**S***ASSNISGGIFLFFVANAIIHLFCFS*

For each ligand anchor DNA encoding the Igk leader sequence (highlighted in bold), HA tag (in italics), SpyTag (underlined), and the extracellular hinge-like region, transmembrane and intracellular regions of the indicated protein (in italics and underlined) was inserted into the pEE14 vector. The CD52 anchor is linked to a GPI anchor at the serine residue marked in bold with the remaining sequence removed during expression.

*HLA-A*02 single chain dimer sequence*

MSRSVALAVLAILSLSGLEAIQRTPKIQVYSRHPAENGKSNFLNCYVSGFHPSDIE VDLLKNGERIEKVEHSDLSFSKDWSFYLLYYTEFTPTEKDEYACRVNHVTLSQP KIVKWDRDM*GGGGSGGGGSGGGGS*GSHSMRYFFTSVSRPGRGEPRFIAVGYVDDT QFVRFDSDAASQRMEPRAPWIEQEGPEYWDGETRKVKAHSQTHRVDLGTLRGYYN QSEAGSHTVQRMYGCDVGSDWRFLRGYHQYAYDGKDYIALKEDLRSWTAADMAA QTTKHKWEAAHVAEQLRAYLEGTCVEWLRRYLENGKETLQRTDAPKTHMTHHAV SDHEATLRCWALSFYPAEITLTWQRDGEDQTQDTELVETRPAGDGTFQKWAAVVVP SGQEQRYTCHVQHEGLPKPLTLRWEPGSQPTIPIVGIIAGLVLFGAVITGAVVAAVM WRRKSSDRKGGSYSQAASSDSAQGSDVSLTACKV

DNA encoding human β-2 microglobulin (in bold) and HLA-A*02 (underlined) separated by a GS linker (in italics) was inserted into pDisplay to create the single chain dimer (SCD). This allowed for selection of CHO cells expressing this construct using media containing Geneticin at 1 mg/mL.

2.1.4. SpyCatcher fusion proteins

Streptavidin sequence

MAEAGITGTWYNQLGSTFIVTAGADGALTGTYESAVGNAESRYVLTGRYDSAPATD
GSGTALGWTVAWKNNYRNAHSATTWSGQYVGGAEARINTQWLLTSGTTEANAWK
STLVGHDTFTKVKPSAAS

Strep-Tactin sequence

MAEAGITGTWYNQLGSTFIVTAGADGALTGTYVTARGNAESRYVLTGRYDSAPATD
GSGTALGWTVAWKNNYRNAHSATTWSGQYVGGAEARINTQWLLTSGTTEANAWK
STLVGHDTFTKVKPSAAS

Dead streptavidin sequence

MAEAGITGTWY**A**QLG**D**TFIVTAGADGALTGTYE**A**AVGAESRYVLTGRYDSAPATD
GSGTALGWTVAWKNNYRNAHSATTWSGQYVGGAEARINTQWLLTSGTTEANAWK
STLVGHDTFTKVKPSAAS

Bold amino acids mark substitutions in order to prevent binding to Strep tag II or biotin.

Dead streptavidin with poly aspartate loop sequence

MAEAGITGTWY**A**QLG**D**TFIVTAGADGALTGTYE**A**AVGDDDGDDDGDDDGAESRY
VLTGRYDSAPATDGSGTALGWTVAWKNNYRNAHSATTWSGQYVGGAEARINTQW
LLTSGTTEANAWKSTLVGHDTFTKVKPSAAS

The poly aspartate loop is underlined.

Strep-Tactin SpyCatcher sequence

MAEAGITGTWYNQLGSTFIVTAGADGALTGTYVTARGNAESRYVLTGRYDSAPATD
GSGTALGWTVAWKNNYRNAHSATTWSGQYVGGAEARINTQWLLTSGTTEANAWK
STLVGHDTFTKVKPSAASDDDGDDDGDDDD*SATHIKFSKRDEDGKELAGATMELRDS*

SGKTISTWISDGQVKDFYLYPGKYTFVETAAPDGYEVATAITFTVNEQGQVTVNGKATKGD

AHI

Strep-Tactin is unmarked, poly aspartate sequence is underlined and SpyCatcher is in italics.

Dead Strep-Tactin SpyCatcher sequence

MAEAGITGTWY**A**QLG**D**TFIVTAGADGALTGTYVTARGNAESRYVLTGRYDSAPAT

DGSGTALGWTVAWKNNYRNAHSATTWSGQYVGGAEARINTQWLLTSGTTEANAW

KSTLVGHDTFTKVKPSAASDDDGDDDGDDDD*SATHIKFSKRDEDGKELAGATMELRD*

SSGKTISTWISDGQVKDFYLYPGKYTFVETAAPDGYEVATAITFTVNEQGQVTVNGKATKG

DAHI

Streptavidin SpyCatcher sequence

MAEAGITGTWYNQLGSTFIVTAGADGALTGTYESAVGNAESRYVLTGRYDSAPATD

GSGTALGWTVAWKNNYRNAHSATTWSGQYVGGAEARINTQWLLTSGTTEANAWK

STLVGHDTFTKVKPSAASDDDGDDDGDDDD*SATHIKFSKRDEDGKELAGATMELRDS*

SGKTISTWISDGQVKDFYLYPGKYTFVETAAPDGYEVATAITFTVNEQGQVTVNGKATKGD

AHI

2.1.5. ACE2 and RBD variant constructs

The ACE2 and full-length SARS-CoV-2 spike constructs were kindly provided by Ray Owens at the Oxford Protein Production Facility UK in the pOPINTTGneo expression plasmid. The RBD construct was kindly provided by Florian Krammer at the Icahn School of Medicine at Mount Sinai in the pCAGGS expression plasmid (Amanat et al., 2020). The amino acid sequences can be found in (Barton et al., 2021). ACE2 and RBD point mutations were added using Agilent QuikChange II XL Site-Directed Mutagenesis Kit following the manufactures instructions. The primers were designed using the Agilent QuikChange primer design web program. Constructs with larger numbers of mutations were produced by

ThermoFisher GeneArt gene synthesis service and then cloned into the same expression vector.

2.2. Cell culture

2.2.1. THP-1 cell lines

THP-1 cells were maintained in RPMI-1640 media (Sigma-Aldrich #R8758) supplemented with 10% foetal bovine serum (FBS) and 1 in 100 penicillin/streptomycin (Thermo Fisher Scientific #15140122) at 37 °C in a 5% CO2 containing incubator.

2.2.2. CHO cell lines

Chinese Hamster Ovary (CHO) mock cells were maintained in DMEM (Sigma-Aldrich #D6429) supplemented with 5% FBS and 1 in 100 penicillin/streptomycin. CHO ligand anchor cells ("short" and "long") were maintained in L-Glutamine-free DMEM (Sigma-Aldrich #D6546) supplemented with 10% dialysed FBS (dialysed three times against 10 L PBS), 1 in 100 penicillin/streptomycin, 1x GSEM supplement (Sigma-Aldrich #G9785) and 50 µM L-Methionine sulfoximine (Sigma-Aldrich #M5379).

2.2.3. HEK293F suspension cell culture

Cells were maintained in FreeStyle™ 293 Expression Medium (12338018) in a 37 °C incubator with 8% CO2 on a shaking platform at 130 rpm. Cells were passaged every 2-3 days with the suspension volume always kept below 33.3% of the total flask capacity. The cell density was kept between 0.5 and 2 million per ml.

2.2.4. Transduction of THP-1 or Jurkat cells

HEK293T cells were seeded in 6 well plates with 6 x 10^5 per well one day before transfection. DNA components were mixed at the following ratio per well in serum-free medium: 0.25 µg pRSV (Addgene plasmid #12253), 0.53 µg pGAG (Addgene plasmid #12251), 0.35 µg pVSV (Addgene plasmid #12259) and 0.8 µg pHR-SIN-BX vector

containing the desired receptor or adaptor. This DNA was mixed with 5.8 µL of X-tremeGENE™ HP (Sigma-Aldrich 6366546001) and incubated for 20 minutes at RT. After incubation the mix was added to one well in the 6-well plate and left overnight. The following day the media was exchanged and the plate again left-over night. The virus was harvested by swirling the plate and then filtering the media through a 0.45 µm filter. 5 µg mL^{-1} polybrene was added to each virus preparation before being added to 1 million THP-1 or Jurkat cells. Expression of the desired receptor or adaptor was checked via flow cytometry staining 3 days' post transfection. For double transductions when adding a receptor and an adaptor constructs separate virus transfections were prepared and mixed before adding to THP-1 or Jurkat cells.

2.2.5. Transfection of CHO cells with various ligand anchors

CHO cells were transfected with pEE14 (CHO mock), pEE14-ligand anchor (CHO ligand anchor) or pDISPLAY-SCD (CHO ligand anchor HLA-A*02) using Xtreme-GENE 9™ as per the manufacturer's instructions. Transfected lines were cultured in the appropriate selection media after 48 hours. CHO cells used in this work were a gift from Rachel Paterson and Jesse Goyette.

2.2.6. Transfection of HEK293F suspension cells

Cells were counted to check cell viability was above 95% and the density adjusted to 1.0 million per ml. For 100 ml transfection, 100 µl FreeStyle™ MAX Reagent (16447100) was mixed with 2 ml Opti-MEM (51985034) for 5 minutes. During this incubation 100 µg of expression plasmid was mixed with 2 ml Opti-MEM. For in situ biotinylation of ACE2 90 µg of expression plasmid was mixed with 10 µg of expression plasmid encoding the BirA enzyme. The DNA was then mixed with the MAX Reagent and incubated for 25 minutes before being added to the cell culture. For ACE2 biotinylation biotin was added to the cell

culture at a final concentration of 50 µM. The culture was left for 5 days for protein expression and secretion to take place.

2.3. Flow cytometry

2.3.1. Checking receptor and adaptor expression

Cells were checked for receptor surface expression by flow cytometry using anti-Strep-tag II antibody Oyster 645 or another conjugate (IBA Lifesciences #2-1555-050). Alternatively anti-Strep-tag II antibody (IBA Lifesciences #2-1507-001) and secondary anti-mouse IgG1 antibody Alexa Fluor 647 (Thermo Fisher Scientific #A-21240) (Cytek DxP8). 1G4 TCR expression was checked using PE anti-human TCR Vβ13.1. Introduced adaptor expression was tested via expression of EmGFP encoded on the adaptor lentivector. Later cells expressing the HA tagged adaptors were check using anti-HA antibodies with various conjugated fluorophores. Where needed cells were sorted for matched high expression of receptor plus introduced adaptor by fluorescence-activated cell sorting (FACS) (MoFlo Astrios, Beckman Coulter).

2.3.2. Checking ligand anchor expression

CHO Cells were analysed for ligand anchor surface expression by flow cytometry using anti-HA-Tag antibody Alexa Fluor 647 (6E2; Cell Signalling Technology). Alternatively, cells were coupled with saturating concentration of monovalent Strep-Tactin SpyCatcher. Biotin ATTO 647 was then added at 2 µM for 30 minutes. The cells were washed 3 times in PBS 1 % BSA before they were fixed in PBS 1 % formaldehyde and analysed via flow cytometry. CHO cell SCD expression was check using monoclonal HLA-A2 antibody (clone BB7.2, FITC LS-C188221) (Data not shown).

2.3.3. FACS sorting of ligand anchor expressing CHO cells

CHO cells expressing the SpyTag construct were coupled with a saturating concentration of monovalent Strep-Tactin SpyCatcher. Biotin ATTO 647 (ATTO-TEC #AD 647-71) was added at 2 µM for one hour and the excess washed off with PBS 1 % BSA. The CHO cells were then sorted for high expression of ATTO 647 signal corresponding to the expression level of ligand anchor using FACS (MoFlo Astrios, Beckman Coulter). The "short" and "long" CHO cells were sorted for matched ATTO 647 signal to produce ligand cells with a similar numbers of maximum available binding sites.

2.4. Protein expression and purification

2.4.1. Expression and purification of monovalent, trivalent, and tetravalent Strep-Tactin SpyCatcher and streptavidin SpyCatcher

Individual subunit combinations for the various SpyCatcher fusion proteins used are as follows:

Monovalent Strep-Tactin	1 – Strep-Tactin SpyCatcher	3 – Dead Streptavidin
Trivalent Strep-Tactin	1 – Dead Strep-Tactin SpyCatcher	3 – Strep-Tactin
Tetravalent Strep-Tactin	1 – Strep-Tactin SpyCatcher	3 – Strep-Tactin
Monovalent Streptavidin	1 – Streptavidin SpyCatcher	3 – Dead Streptavidin
Trivalent Streptavidin	1 – Dead Strep-Tactin SpyCatcher	3 – Streptavidin
Tetravalent Streptavidin	1 – Streptavidin SpyCatcher	3 – Streptavidin

Table 2.1 List of different SpyCatcher fusion proteins with the subunits required to make them.

DNA encoding each individual subunit required was transformed into *Escherichia coli* BL21-CodonPlus (DE3)-RIPL cells (Agilent Technologies #230280). A single colony was picked and gown overnight in 10 mL of LB broth culture supplemented with 100 µg mL^{-1} ampicillin

plus 25 µg mL^{-1} chloramphenicol. The next day this was transferred to 1 L LB broth culture and grown to 0.6 at OD600 nm at which point 1 mM IPTG was added to induce protein expression for 4 hours. Cells were harvested washed in BugBuster (Merck Millipore #70921) supplemented with lysozyme, protease inhibitors, DNase I and magnesium sulphate as per the manufacturers' instructions. Inclusion bodies containing the subunits were solubilised with 6 M guanidine pH 1.5. Samples of solubilised subunits were run on SDS-PAGE gel to check for protein expression. Subunits were then mixed at the desired final molar ratio to improve the yield of the required tetramer. The subunits were refolded by rapid dilution in cold PBS and contaminates removed via precipitation using ammonium sulphate before additional ammonium sulphate was added to precipitate the desired tetramer. Precipitated protein was resuspended in 20 mM Tris pH 8.0, filtered (0.22 µm syringe filter), and loaded onto a Mono Q HR 5/5 column (GE Healthcare Life Sciences). Desired tetramers were eluted using a linear gradient of 0-0.5 M NaCl in 20 mM Tris pH 8.0 and distinguished via the charge differences associated with containing one or more poly aspartate sequences. For all SpyCatcher fusion proteins a single poly aspartate sequence was the desired tetramer. Once separated the protein was concentrated, and buffer exchanged into 20 mM MES, 140 mM NaCl pH 6.0 (Denham et al., 2019).

2.4.2. GFP-SpyCatcher

The GFP-SpyCatcher was a gift from Eleanor Denham and was expressed in *Escherichia coli* BL21-CodonPlus (DE3)-RIPL cells. The protocol for its purification can be found in (Denham et al., 2019).

2.4.3. RBD and ACE2 purification from HEK293F suspension cell supernatant

Cells were harvested by centrifugation and the supernatant collected and filtered through a 0.22 µm filter. Imidazole was added to a final concentration of 10 mM and PMSF added to a final concentration of 1 mM. 1 ml of Ni-NTA Agarose (30310) was added per 100 ml of

supernatant and the mix was left on a rolling platform at 4 °C overnight. The supernatant mix was poured through a gravity flow column to collect the Ni-NTA Agarose. The Ni-NTA Agarose was washed 3 times with 25 ml of wash buffer (50 mM NaH2PO4, 300 mM NaCl and 20 mM imidazole at pH 8). The protein was eluted from the Ni-NTA Agarose with elution buffer (50 mM NaH2PO4, 300 mM NaCl and 250 mM imidazole at pH 8). The protein was concentrated, and buffer exchanged into size exclusion buffer (25 mM NaH2PO4, 150 mM NaCl at pH 7.5) using a protein concentrator with a 10,000 molecular weight cut-off. The protein was concentrated down to less than 500 µL before loading onto a Superdex 200 10/300 GL size exclusion column. Fractions corresponding to the desired peak were pooled and frozen at -80 °C. Samples from all observed peaks were analysed on an SDS-PAGE gel.

2.5. Cellular assays

2.5.1. Coupling SpyCatcher fusion proteins to CHO cells

CHO ligand anchor (or CHO mock cells as a control) were incubated with various concentrations of the desired SpyCatcher linked protein in 20 mM MES, 140 mM NaCl, pH 6.0 and 1% BSA (coupling buffer) for 10 minutes at RT. Unbound SpyCatcher protein was removed by washing three times with PBS 1% BSA.

2.5.2. Biotin-4-fluorescein quenching assay

The valency of purified Strep-Tactin or streptavidin SpyCatcher fusion protein was measured using biotin-4-fluorescein (Sigma-Aldrich #B9431-5MG) which when bound to Strep-Tactin or streptavidin becomes quenched. SpyCatcher fusion proteins were incubated with a titration of biotin-4-fluorescein in black opaque plates for 30 minutes at RT in PBS 1% BSA. Fluorescence was measured (λ_{ex} 485 nm, λ_{em} 520 nm) using a plate reader. Fluorescence

values were corrected for background fluorescence before analysis. Negative control (buffer alone) data were fitted with the linear regression. The gradient of the line (M) was extracted.

$$Y = M * X + C$$

Sample data was fitted with a segmental linear regression, equation below, where X is the biotin-4-fluorescein concentration, Y is fluorescence (AU), X0 is the biotin-4-fluorescein concentration at which the line segments intersect. Slope1 was constrained to zero and is the gradient of the first line segment, Slope2 is the gradient of the second line segment. Intercept1 was constrained to zero and is the Y value at which the first line segment intersects the Y axis. Slope2 was constrained to the value of the gradient given by the linear regression of the negative control data above (M).

$$Y1 = Intercept\ 1 + Slope1 * X$$

$$Y\ at\ X0 = Slope1 * X0 + Intercept1$$

$$Y2 = Y\ at\ X0 + Slope2 * (X - X0)$$

$$Y = IF\ (X < X0, Y1, Y2)$$

The X0 value was converted into an estimate of the number of biotin-binding sites per tetramer using the concentration of the SpyCatcher added. For this, we assume complete binding of biotin-4-fluorescein to protein.

2.5.3. Calculating the number of binding sites per coupled CHO ligand cell

CHO cells expressing a SpyTag anchor, or mock transduced (as a negative control) cells (3 x 10^6) were pre-incubated with a single saturating concentration of a specific SpyCatcher fusion protein. The above biotin-4-fluorescein assay was then performed in the same manner but with a known number of cells per well. The X0 term (calculated from the curve fit using equations above) was converted to an estimate of the average number of binding sites per cell

using the equation below, where N is the average number of ligands per cell, X0 is the saturation concentration of biotin-4-fluorescein extracted (M), V is the sample volume (L), N_A is Avogadro's constant and C is the number of cells in the sample.

$$N = \frac{X0 * V * N_A}{C}$$

To measure relative levels of coupled SpyCatcher per cell across a serial dilution, ligand cells were coupled with a SpyCatcher fusion protein or buffer alone (as a negative control) before being incubated with 2 μM biotin ATTO 488 (ATTO-TEC #AD 488-71) pre-mixed with 40 μM biotin for 30 minutes at RT. The presence of biotin minimises the self-quenching activity of ATTO dye we observed when using multivalent SpyCatcher fusion proteins.

Cells were analysed by flow cytometry and the gMFI when cells were incubated with buffer alone was subtracted from all corresponding sample gMFI values. These values were then fitted with the single site binding model, equation below, where Y is the gMFI (AU), Bmax is the maximum specific SpyCatcher binding indicated by gMFI in AU, X is the [SpyCatcher] added (M) and K_D is the [SpyCatcher] that yields 50% maximal binding to CHO cells (M).

$$Y = \frac{Bmax * X}{K_D + X}$$

To convert Y values into the average number of binding sites per ligand cell, the number of binding sites per cell at saturating SpyCatcher fusion protein concentrations calculated in the biotin-4-fluorescein assay was substituted into the equation above as Bmax. Y values were then re-calculated following this adjustment. This method was followed in each independent experiment and then an average value for the K_D and Bmax was used when combining replicates. All error bars represent one standard deviation (SD).

2.5.4. Down-regulation of generic ligand anchors

CHO ligand anchor cells were incubated with 15 µM monovalent Strep-Tactin SpyCatcher (or buffer alone) as described above and incubated at 37 °C to match stimulation assay conditions for the time points indicated. Cells were analysed for generic ligand surface expression at a number of time points using biotin ATTO 488 as above and normalised to the gMFI value at time 0. To calculate the decay, the gMFI values were fitted with the equation below where Y0 is the Y value when X = 0, Plateau is the Y value at which the curve reaches a plateau, X is time in minutes, and K is the rate constant in inverse minutes.

$$Y = (\text{Y0} - \text{Plateau}).e^{-K.X} + \text{Plateau}$$

2.5.5. Measuring the number of 9V-HLA-A*02 per cell

CHO mock or CHO ligand anchor cells expressing the HLA-A*02 (SCD) were incubated with a serial dilution of NY-ESO-1 9V peptide for three hours at 37 °C to match stimulation conditions. Cells were washed three times in PBS 1% BSA and mixed with soluble high affinity c58c61 1G4 TCR labelled with Alexa Flour 647 NHS Ester for one hour at 4 °C (Thermo Fisher Scientific #A37573). The intensity of the 1G4 TCR 647 fluorescent signal was analysed by flow cytometry along with Alexa Fluor 647 fluorescence quantitation beads (Bangs Laboratories #647). Bead MFI values were used to plot a standard curve from which sample value could be interpolated to give an estimate for the number of 9V containing SCD molecules per cell. Alexa Flour 647 labelled the high affinity 1G4 TCR was a gift from Eleanor Denham.

2.5.6. THP-1 cell assays

CHO ligand anchor cells (2 x 10^5) were coupled with the appropriate SpyCatcher fusion protein or buffer alone and mixed with single Strep-tag II tagged receptor and adaptor expressing THP-1 or untransduced THP-1 cells (1 x 10^5) in DMEM 5% FBS, 1 in 100

penicillin/streptomycin, 2 µg mL^{-1} avidin. Cells were incubated in a 37 °C 10% CO2 containing incubator for 20 hours. Supernatants were harvested and assayed for IL-8 by ELISA following manufactures instructions (Thermo Fisher Scientific #88808688).

2.5.7. Jurkat NFκB eGFP and Jurkat cells not harbouring an eGFP reporter assays

CHO ligand anchor HLA-A*02 cells were stained with CellTrace Far Red (Thermo Fisher Scientific #C34564) at a final concentration of 1 µM in PBS at a density of 1 x 10^6 cells per ml. The cells (2 x 10^5) were coupled with the appropriate SpyCatcher fusion protein or buffer alone and mixed with twin Strep-tag II tagged receptor and/or adaptor expressing Jurkat or untransduced Jurkat cells (1 x 10^5) in DMEM 5% FBS, 1 in 100 penicillin/streptomycin, 2 µg mL^{-1} avidin. Cells were incubated in a 37 °C 10% CO2 containing incubator for 20 hours. Cells were harvested and CHO cells excluded from the analysis via gating on CellTrace Far Red negative cells. No TCR Jurkat cells (Yang et al., 2021) were washed twice with PBS 1 % BSA, and resuspended in alexa fluor 488 anti-human CD69 antibody (BioLegend 310916) at a final concentration of 1 µg/ml. The cells were left to incubate for one hour at room temperature, and subsequently washed twice with PBS 1 % BSA. The eGFP reporter cells were analysed for the percentage of cells that were positive for the NFκB eGFP reporter (Ratzinger et al., 2014) or alexa flour 488 (BD Fortessa X20, 640 nm laser, 488 nm laser, BD Biosciences).

2.5.8. Conjugation assays

CHO ligand anchor cells were stained with CellTrace Far Red (Thermo Fisher Scientific #C34564) at a final concentration of 1 µM in PBS at a density of 1 x 10^6 cells per ml. THP-1 receptor cells were stained with CellTrace Violet (Thermo Fisher Scientific #C34557) at a final concentration of 1 µM in PBS for 20 minutes. CHO Ligand cells (4 x 10^5) coupled with the appropriate Strep-Tactin SpyCatcher fusion protein were mixed with (2 x 10^5) THP-1 or Jurkat cells in PBS 1 % BSA on Ice for 1 hour and analysed by flow cytometry. For

conjugation assays at 37 °C receptor and ligand cells were mixed in a water bath for 1 hour before being analysed flow cytometry. The percentage of receptor cells forming conjugates was calculated using the equation below. Where double positive cells refer to events containing both a CellTrace Far Red and CellTrace Violet signal.

$$Percentage\ of\ receptor\ cells\ forming\ conjugates = \frac{Double\ positive\ cells}{(Receptor\ only\ cells + Double\ posative\ cells)} * 100$$

To fit conjugate assay data was then plotted against the concentration of SpyCatcher fusion protein or the average number of binding sites per cell. The data was then fit using the same four parameter dose response equation used for the stimulation assays.

2.5.9. Stimulation assays

For receptor stimulation assays, IL-8 concentrations in negative controls (where CHO cells were pre-incubated with buffer alone instead of a SpyCatcher fusion protein) were subtracted from corresponding sample IL-8 concentrations to account for background levels. Dose-response curves were then fitted with the below equation where Y is the measured cell response (normalised), Bottom and Top are the minimum and maximum cell response respectively, EC50 is the number of binding sites per cell that yields a half maximal response, X is the number of binding sites per cell and Hill slope relates to the steepness of the curve.

$$Y = Bottom + \frac{(X^{Hillslope})(Top - Bottom)}{(X^{Hillslope} + EC50^{Hillslope})}$$

To plot stimulation as a function of conjugation the average number of binding sites on the CHO cells used in the stimulation assay were interpolated from the fit of the conjugation data using the four-parameter dose response equation. The normalised IL-8 values from the stimulation were then plotted against the interpolated values of conjugate formation.

To compare between data sets in the conjugation, stimulation and stimulation versus conjugation an extra sum-of-squares F test was performed. This test compares the EC50 and Top parameters between the data sets and tests if they could be shared or not. The null hypothesis is that the parameters can be shared if this is not possible then a more complex model is required and the confidence for this is expressed as a P value.

2.5.10. Fluorescence recovery after photobleaching (FRAP)

CHO cells (1 x10^5) expressing the four ligand anchors (CD80, LAIR-1, CD43 and CD52) were transferred to a 35 mm glass bottom dish one day before imaging. To prepare cells for imaging each dish was washed 3 times with coupling buffer plus 10 % FBS. SpyCatcher-GFP was then added in excess (approximately 10 µM) and left for 10 minutes. Before washing the cells three times in PBS 1 % BSA 10 % FBS. Cells were transferred to the Olympus FV1200 laser scanning microscope with 37 °C chamber for equilibration. The 60X magnification lens was used to locate cells spread over the glass coverslip. A small area of the cell (approximately 10 %) was selected a few control images were taken before a 20 second bleach performed. A time lapse series of images was then taken to track the recovery of the GFP signal.

Time lapse image series were imported into ImageJ for analysis. For each time lapse the bleach area was selected (bleach) along with a control area which was taken to be the rest of the cell contact with the glass (control area) and a negative control area around the outside of the cell (negative). Firstly, the intensity from the negative area was subtracted from the bleach and control area. The bleach area was then divided by the control area for each time frame and these values were normalised to the control image before the bleach was performed. These values were then plotted against time and the equation below used to find the half time for each ligand anchor. Where Y0 is the value when X (time) is zero, Plateau is the Y value at infinite times and K is the rate constant from which the half time is derived.

$$Y = Y0 + (Plateau - Y0) * (1 - \exp(-K * x))$$

The half time value could then be converted into the diffusion coefficient using the equation below (Soumpasis, 1983). Where 0.224 is a constant for a circular bleach area, r is the radius of the bleach area, and the half time is the derived from fitting the one phase association equation to the bleach recovery above.

$$\text{Diffusion coefficient} = \frac{0.224 * r^2}{Half\ time}$$

2.6. Surface plasmon resonance (SPR)

SARS-CoV-2 receptor binding domain binding to human extracellular ACE2 was analysed on a Biacore T200 instrument (GE Healthcare Life Sciences) at 37°C and a flow rate of 30 µl/min. Running buffer was HBS-EP (BR100669). Streptavidin was coupled to a CM5 sensor chip (29149603) using an amine coupling kit (BR100050) to near saturation, typically 10000-12000 response units (RU). Biotinylated ACE2 WT and variants were injected into the experimental flow cells (FC2–FC4) for different lengths of time to produce desired immobilisation levels (40–800 RU). FC1 was used as a reference and contained streptavidin only. Excess streptavidin was blocked with two 40 s injections of 250 µM biotin (Avidity). Before RBD injections, the chip surface was conditioned with 8 injections of the running buffer. A dilution series of RBD was then injected simultaneously in all FCs. Buffer was injected after every 2 or 3 RBD injections. The lowest RBD concentration was injected at the beginning and at the end of each dilution series to ensure reproducibility. The length of all injections was 30 s, and dissociation was monitored from 180-670 s. Binding measured in FC1 was subtracted from the other three FCs. Additionally, all binding and dissociation data were double referenced using the closest buffer injection (Myszka, 1999). In all experiments, an ACE2-specific antibody (NOVUS Biologicals, AC384) was injected at 5 µg/ml for 10 minutes with the disassociation monitored for 30 minutes.

2.6.1. SPR data fitting

Double referenced binding data was plotted and fit with GraphPad Prism. Two methods were then used to fit a dissociation constant (K_D) to the data, either a calculated K_D or an equilibrium K_D. Firstly, to find the calculated K_D, the dissociation rate (k_{off}) was found using a one-phase exponential decay model below, only fitting data from the dissociation phase of each injection. Depending on the quality of the data the k_{off} from at least four RBD injections was averaged to give a representative value for the k_{off}.

$$Y = (Y0 - NS) * exp(-k_{off} * X) + NS$$

To determine the association rate (k_{on}) it was first necessary to determine the observed-on rate (k_{obs}) which was found using a one-phase association model below, only fitting data from the association phase of each injection.

$$Y = Y0 + (Plateau - Y0) * (1 - exp(-k_{obs} * x))$$

The association rate could then be obtained by plotting the k_{obs} vs the concentration of RBD in each injection. This plot could then be fit with a linier regression with the y-intercept constrained to the k_{off} value found above and the gradient of the line extracted to give the k_{on} using the question below.

$$k_{obs} = k_{on} * [RBD] + k_{off}$$

The calculated K_D can then be found by dividing the average k_{off} by the k_{on}. To find the equilibrium K_D the plateau values from the one-phase association model fit were extracted and plotted against the corresponding concentration of RBD. This plot was then fit with a one-site specific binding model below and the value for the equilibrium K_D extracted.

$$Y = \frac{Bmax * X}{(K_D + X)}$$

To convert K_D values to Delta G (ΔG) the equation below was used. Where R is the gas constant measured in cal mol^{-1} K^{-1}, K_D is the equilibrium constant in M and T is the temperature measured in K.

$$\Delta G = R * T * ln\, K_D$$

A ΔΔG value was calculated for each mutant by subtracting the ΔG of each mutant from the ΔG of the WT. To look at whether the effects of individual RBD mutations were additive the ΔΔG values for the single mutants could be summed and directly compared to the ΔΔG values for the multiple mutants. Similarly, cooperativity between RBD and ACE2 mutations could be determined by subtracting a predicted ΔΔG from the measured ΔΔG to give a ΔΔΔG value. Where the predicted ΔΔG was calculated by adding the measured ΔΔG for variant RBD binding WT ACE2 and WT RBD binding variant ACE2.

When binding was too poor to fit accurately an estimate for the lower limit for the K_D was calculated using the formula below. Where the "Maximum [RBD]" is the highest concentration of RBD flown over the surface, the "Binding at K_D (WT)" is the RU value at the equilibrium K_D for the WT protein on the same chip and the "Binding at maximum [RBD] (variant)" is the maximum RU value for the variant binding RBD at the highest concentration. The estimated K_D lower limit could then be converted into ΔG and then ΔΔG using the same method above.

$$\text{Estimated } K_D \text{ lower limit} = \text{Maximum [RBD]} * \frac{\text{Binding at } K_D \text{ (WT)}}{\text{Binding at maximum [RBD] (variant)}}$$

Chapter 3 - Developing a generic ligand system to study the effect of ligand length on NTR activation

3.1. Introduction

3.1.1. Challenges to studying NTRs

While some key NTRs such as the TCR have been well studied it has not been possible to replicate this with the majority of NTRs due to several constraints. Firstly, the NTR in question must have a defined ligand which can be expressed on a target cell. While this is possible for many NTRs, there can be complications such as controlling for endogenous expression of the ligand. There may also be issues caused by cross reactivity if the target cell is from another species. Controlling the ligand density has been relatively straight forward for the TCR due the ability to pulse ligand cells with peptides that can be loaded onto MHC molecules for presentation. This is however not possible for other NTR family members and so makes generating accurate dose response curves for receptor activation very challenging. Altering ligand density for other NTRs can be done via FACS, inducible expression systems or blocking antibodies. However, each of these are difficult and time consuming to implement and optimise in addition to being limited to studying a single NTR at a time. Other approaches using simplified systems such as ligands immobilised on plastic or SLBs can activate receptors in a dose dependent manner but lack the complexity of cell-cell interactions and so may not reproduce a reliable physiological response. This inability to look at a large range of NTRs in a carefully controlled manner has also made it impossible to validate if a universal mechanism for their activation can be identified.

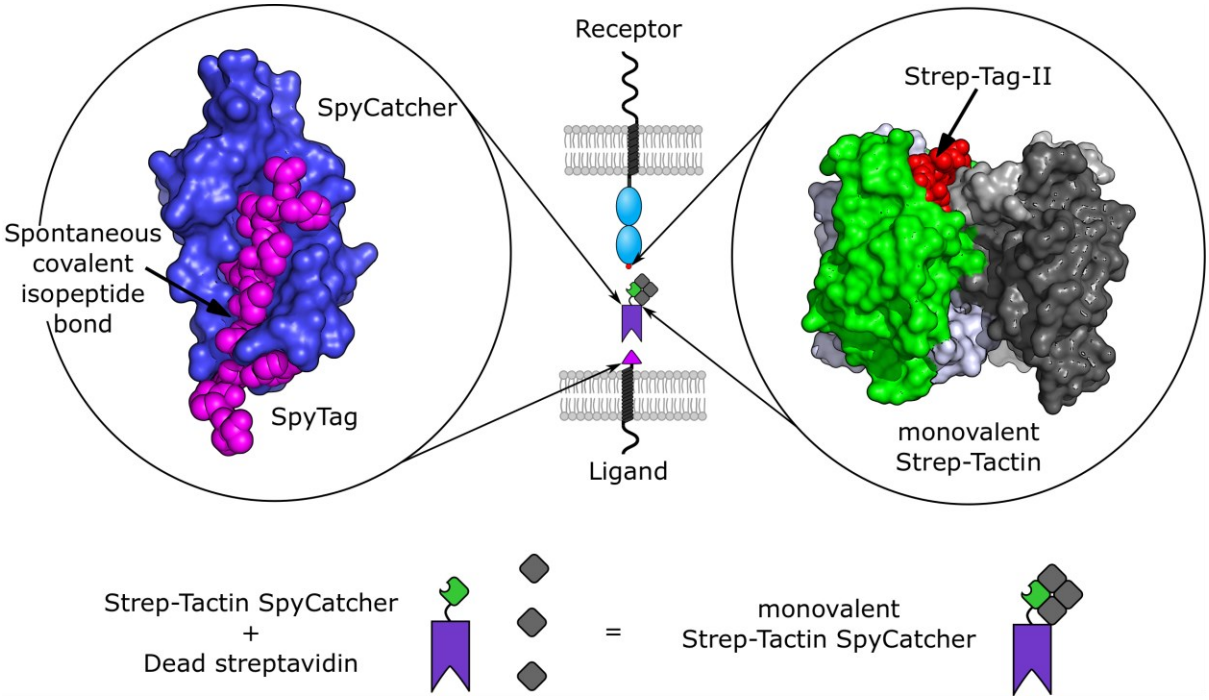


Figure 3.1: Cartoon diagram of the generic ligand system showing the key components

The SpyTag is presented on CHO ligand cells and soluble monovalent Strep-Tactin SpyCatcher molecules added allowing the SpyTag and SpyCatcher to covalently bind. The receptor of choice is modified to contain a Strep-Tag-II tag which can bind the Strep-Tactin. Monovalent Strep-Tactin SpyCatcher is composed of one Strep-Tactin SpyCatcher and three dead streptavidin molecules which are refolded together and purified to produce the final molecule. Figure adapted from Eleanor Denham.

3.1.2. The generic ligand system

In order to solve these issues, we have developed a generic cell surface ligand system for studying cell–cell recognition (Figure 3.1) (Denham et al., 2019). The system had been previously established to take advantage of the SpyTag-SpyCatcher system developed by Zakeri et al., (2012). The short SpyTag peptide can form a spontaneous isopeptide bond when mixed in solution with SpyCatcher. We have exploited this in our system by expressing the SpyTag on CHO cells as a universal anchor protein. SpyCatcher linked to a tetramer of streptavidin or Strep-Tactin can be coupled to the SpyTag, in a dose dependant manner and produce CHO cells presenting different numbers of SpyCatcher fusion proteins which act as ligands. The NTR of choice is then subtly modified to include an N-terminal Strep-Tag-II tag (STII) which can bind the Strep-Tactin with a physiological affinity or streptavidin with a lower affinity to complete receptor ligand biding. Most NTRs bind their ligands via their N-terminal domains therefore this small tag mimics this binding as much as possible while not altering the structure of the receptor.

The great strength of this system is the ability to carefully titrate in the SpyCatcher protein and therefore produce CHO cells with decreasing numbers of available binding sites. The system can present millions of ligands per cell down to a single ligand on average. This titration allows for accurate dose response curves to be produced, something which had been extremely challenging until now. Thus, parameters such as the half maximal response (EC50) of different NTRs under specific conditions can be quantified and compared. The generic ligand system has been designed to be as small as possible to mimic the physiological size of most NTR ligands. The sum of the structures of the SpyCatcher and Strep-Tactin molecules plus the linker lengths is estimated to span 2-3 immunoglobulin domains (Korndörfer & Skerra, 2002; L. Li et al., 2014).

While the system had been tested on several NTRs as a proof of principal by Eleanor Denham this had not been extended to asking specific questions such as what properties of NTRs and their ligands affect their activation. Therefore, I started by asking if ligand length affects NTR activation, and if so how. There had been many reports that ligand length is a key parameter of NTR activation (Bakalar et al., 2018; Choudhuri et al., 2005, 2009; Köhler et al., 2010; Yokosuka et al., 2010), but it was not clear whether this was a universal effect of all NTRs or just the few that had been tested thus far. It is also now possible to make comparisons across many experiments and experimental conditions using a method I developed to quantify the number of available ligands per CHO cell in each experiment.

3.1.3. Selected NTRs for this study

I have focused on NTRs selected from four different families to capture the diversity of NTRs (Dushek et al., 2012). The four chosen NTRs all activate cell signalling through their shared association with the adaptor protein DAP12 (Lanier & Bakker, 2000): signal regulatory protein β1 (**SIRPβ1**), sialic acid-binding immunoglobulin-type lectin 14 (**Siglec 14**), natural killer receptor 44 (**NKp44**) and triggering receptor expressed on myeloid cells 1 (**TREM-1**). Although they have been less widely studied compared to the TCR, they are still of great biological significance (Barclay & Brown, 2006; Ford & McVicar, 2009; Lenza et al., 2020; Moretta et al., 2003). This diversity of NTRs gives us some confidence that differences I see with this group of receptors can be extrapolated across NTRs in general, although a comprehensive study of all NTRs would be needed in the future to confirm this.

SIRPβ1 is highly homologous to the inhibitory receptor and major therapeutic target SIRPα (Kharitonenkov et al., 1997; Weiskopf, 2017). SIRPα is known to bind CD47 and is an important “don’t eat me” signal during neuronal development (Lehrman et al., 2018). The two receptors are thought to be paired receptors which act to balance activation and inhibitory

signals. However, the native ligand of SIRPβ1 is unknown but it is thought to promote phagocytosis in macrophages (Hayashi et al., 2004).

Siglec 14 is part of the larger sialic acid binding family of receptors which act to mediate cell-cell contacts (Crocker et al., 2007). It was found to have very high sequence homology with the inhibitory receptor Siglec 5, making them another example of paired receptors (Angata et al., 2006).

NKp44 is important for the activation and cytotoxic activity of natural killer cells, it is thought to bind the protein proliferating cell nuclear antigen (PCNA) (Rosental et al., 2011) and an isoform of the mixed lineage leukemia-5 (MLL-5) protein (Baychelier et al., 2013).

TREM-1 activates monocytes and although no ligand has been confirmed it has been suggested that it binds peptidoglycan (PGN) recognition protein 1 (PGLYRP1) (Read et al., 2015) and extracellular actin (Fu et al., 2017).

3.1.4. Key findings

In this chapter, I have purified a monovalent Strep-Tactin SpyCatcher ligand and developed a method to quantify the average number of ligands each CHO cell is presenting after coupling of a serial dilution of monovalent Strep-Tactin SpyCatcher. I have used the generic ligand system to study the effect of changing the receptor-ligand dimensions on conjugate formation and cellular activation of four NTRs. The data shows that short ligands formed worse conjugates but produced better cellular activation with the opposite true of long ligands. I was also able to distinguish between NTRs of different lengths with shorter ones acting more potently than longer ones.

3.2. Results

3.2.1. Purification of monovalent Strep-Tactin SpyCatcher

The first task I had was to produce enough high-quality soluble protein needed for the cellular assays. The Strep-Tactin SpyCatcher is a tetramer therefore the production of the final protein requires the refolding of two subunits (Figure 3.1). For monovalent Strep-Tactin SpyCatcher one Strep-Tactin SpyCatcher and three dead streptavidin units are used. This is a stochastic process and so produces a range of different ratios of the two subunits. To separate the desired 1:3 ratio of Strep-Tactin SpyCatcher: dead streptavidin the Strep-Tactin SpyCatcher subunit contains a poly aspartic acid sequence. I can then separate this mixture using anion exchange chromatography. This process is shown in Figure 3.2A with samples from each marked peak run on an SDS-PAGE gel (Figure 3.2B). Here peak 3 is the desired monovalent Strep-Tactin SpyCatcher with smaller peaks corresponding to degradation products and larger peaks corresponding to protein complexes with more than one SpyCatcher subunit. To confirm peak 3 was the correct protein a serial dilution of biotin-4-fluorescein was added to a known concentration of protein from peak 3. Importantly, because the affinity of biotin for streptavidin and Strep-Tactin is so high, binding can be considered essentially irreversible in these assays (Green, 1990). Therefore, the concentration of biotin-4-fluorescein where the inflection occurs in the graph indicated the concentration at which all the biotin binding sites are occupied because upon binding the fluorescein becomes quenched (Figure 3.2C). Therefore, when 50 nM monovalent Strep-Tactin SpyCatcher was used the inflection occurred at 49 nM of biotin-4-fluorescein.

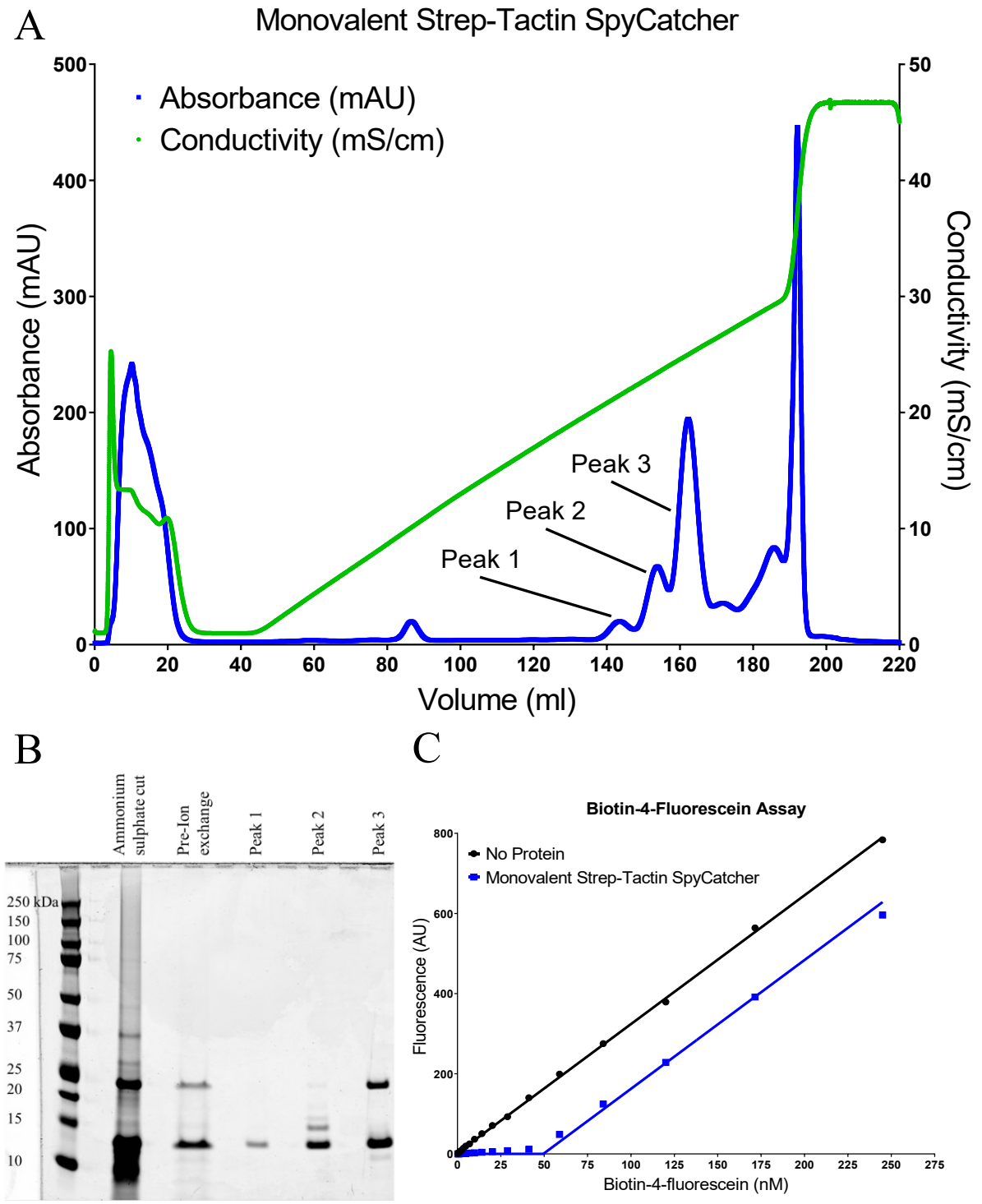


Figure 3.2: Purification of monovalent Strep-Tactin SpyCatcher

(A) Representative anion exchange chromatography run to purify monovalent Strep-Tactin SpyCatcher. **(B)** SDS-PAGE gel, lane 1, a sample after the first ammonium sulphate cut, lane 2, a sample pre anion exchange, lanes 3-5, peaks 1-3 corresponding to the peaks shown in A. Peak 3 corresponds to the purified monovalent Strep-Tactin SpyCatcher. The two major bands represent one molecule of Strep-Tactin SpyCatcher for every three molecules of dead streptavidin (calculated by densitometry). **(C)** Biotin-4-fluorescein assay using 50 nM purified monovalent Strep-Tactin SpyCatcher.

3.2.2. Developing a method to calculate the average number of available generic ligands on CHO ligand cells to study NTR ligand length

To study the effect of ligand length I used two CHO cell lines one expressing the SpyTag close to the membrane (short ligand cells) and one with the SpyTag on the end of a mutated version of CD4 (long ligand cells). This extension produced an approximate size difference of 12 nm assuming 3 nm per Ig domain (H. Wu et al., 1997). This need for two independent CHO cell lines meant that I needed a way of calculating the coupling efficiency of the SpyCatcher to each SpyTag. Simply relying on the concentration of soluble protein added to each cell line would not sufficiently control for all the variables associated with coupling. A serial dilution of monovalent Strep-Tactin SpyCatcher was coupled to CHO ligand cells to show it was possible to calculate a measure of the degree of coupling using a fluorescently labelled biotin molecule. The Strep-Tactin binding site which is needed to bind the single STII tagged receptors can also bind biotin similar to streptavidin with an affinity in the low picomolar to femtomolar range making it essentially irreversible for my assays (Green, 1990). Therefore, I showed that both short and long ligand cells could be coupled with a serial dilution of monovalent Strep-Tactin SpyCatcher. The coupling efficiency was calculated by adding biotin ATTO 488 and measuring the signal via flow cytometry and plotting the geometric mean fluorescence intensity (gMFI) against the concentration of SpyCatcher used for coupling (Figure 3.3A).

Figure 3.3A shows a representative assay where the fluorescence signal decreases as the SpyCatcher concentration decreases due to the decreasing numbers of binding sites available. Figure 3.3B shows the extracted K_D values from the one site specific binding model and is the combined data from six biological replicates. I believe that the reason for the lower K_D when coupling to the long ligand cells is due to the increased accessibility of the SpyTag, which allows more efficient coupling of SpyCatcher proteins compared to the short ligand.

This effect was consistent across all SpyCatcher fusion proteins coupled to short and long ligand cells (see Chapter 4). Knowing the coupling efficiency for monovalent Strep-Tactin SpyCatcher to both short and long ligand cells I could compare subsequent stimulation or conjugation assays fairly. However, I wanted to go one step further and quantify absolute numbers of binding sites per cell. This would in theory allow for universal comparison of any future ligand and SpyCatcher fusion protein combinations (see Chapter 4). I therefore used the biotin-4-fluorescein assay which was previously used to accurately check the valency of each batch of purified Strep-Tactin SpyCatcher fusion proteins.

I adapted this existing assay to work on ligand cells which had been coupled with any SpyCatcher fusion protein. Figure 3.3C shows this biotin-4-fluorescein assay performed on ligand cells which have been coupled with a saturating concentration of monovalent Strep-Tactin SpyCatcher. Importantly the empty ligand cells do not bind the monovalent protein due to the lack of the SpyTag and this leads to a linear increase in the fluorescent signal from the biotin-4-fluorescein. By counting the number of cells prior to the assay I know the number of cells per well. From the inflection points extracted from a segmented linear regression it is possible to calculate an average number of molecules per cell. These values are plotted in Figure 3.3D where the data was combined for six biological replicates. It is possible to see that the long ligand cells express the SpyTag at a slightly lower maximum surface density than the short ligand cells. In parallel, I checked the expression of a HA tag linked to the SpyTag and obtained a similar result (data not shown).

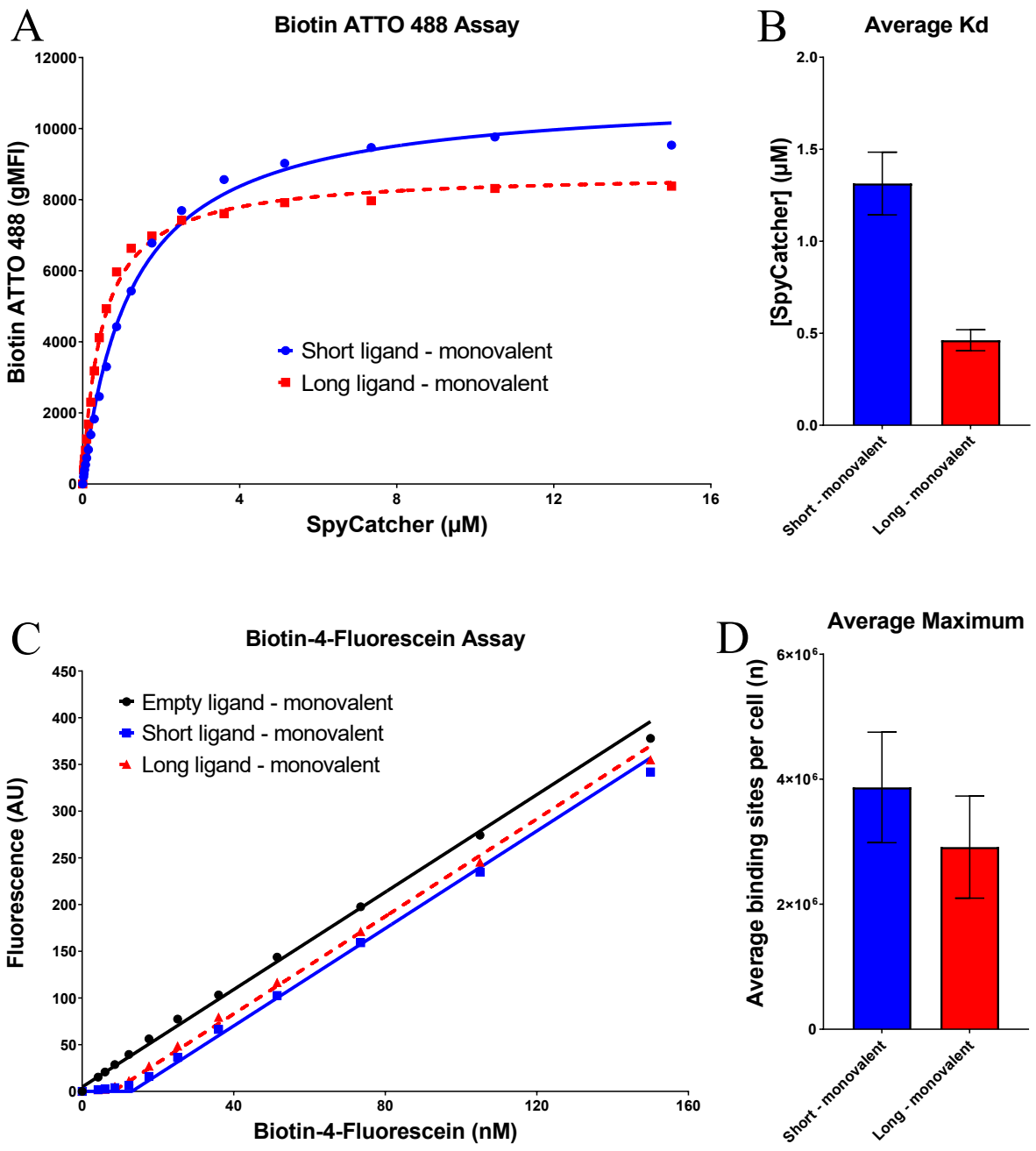


Figure 3.3: Calculating the average number of binding sites per ligand cell, short ligand or long ligand coupled with monovalent Strep-Tactin SpyCatcher

(A) A representative biotin ATTO 488 assay where short ligand or long ligand cells were coupled with a serial dilution of monovalent Strep-Tactin SpyCatcher and mixed with biotin ATTO 488 which was measured by flow cytometry and the geometric mean plotted. The data was fit with a one site specific binding model and the K_D extracted from each curve. **(B)** The K_D values extracted from six independent experiments was plotted. **(C)** A representative biotin-4-fluorescein assay where empty ligand, short ligand and long ligand cells were incubated with a saturating concentration of monovalent (15 µM) Strep-Tactin SpyCatcher. The cells were then mixed with a serial dilution of biotin-4-fluorescein and the remaining florescence measured. **(D)** The average maximum number of binding sites for six independent experiments were plotted, error bars show SD.

In theory it would be possible to use this biotin-4-fluorescein assay to calculate the average number of binding sites at any density of coupled ligand cells. However, as the ligand density decreases the number of cells required for the assay greatly increases as the assay is only sensitive down to approximately 1 nM. After this point it is not possible to measure an inflection point compared to the control. Therefore, I decided to only perform this assay when all the SpyTag ligands on the surface of the ligand cells were saturated. It was then possible to calculate the average number of binding sites per cell for any concentration of SpyCatcher added. This was achieved by combining the K_D value from the biotin ATTO 488 assay and the Bmax from the biotin-4-fluorescence assay. This is shown in the equation below and was used for all the SpyCatcher fusion proteins used in this thesis.

$$Average\ number\ of\ binding\ sites\ per\ cell = \frac{Average\ Bmax\ (Biotin-4-fluorescein\ assay)\ *[SpyCatcher]}{Average\ K_D\ (Biotin\ ATTO\ 488\ assay)+[SpyCatcher]}$$

When plotting the functional cellular assays, I initially wanted to use the individual values of K_D and Bmax from each replicate. However, there was too much variation in the values obtained from each assay from replicate to replicate. This meant that to combine the functional results from multiple replicates I had to calculate an average K_D and Bmax value for monovalent Strep-Tactin SpyCatcher coupled to short and long ligand cells (Figure 3.3B and D). Therefore, I present the functional data plotted against the average binding sites per cell. While this is no longer a true value for the exact number of ligands presented in each replicate it does account for the differences in coupling efficiency of the monovalent Strep-Tactin SpyCatcher to the short and long ligand cells, as well as the differences in expression of the two SpyTag ligand anchors. It is therefore far superior to plotting the stimulation against the concentration of soluble SpyCatcher fusion protein added to the cells.

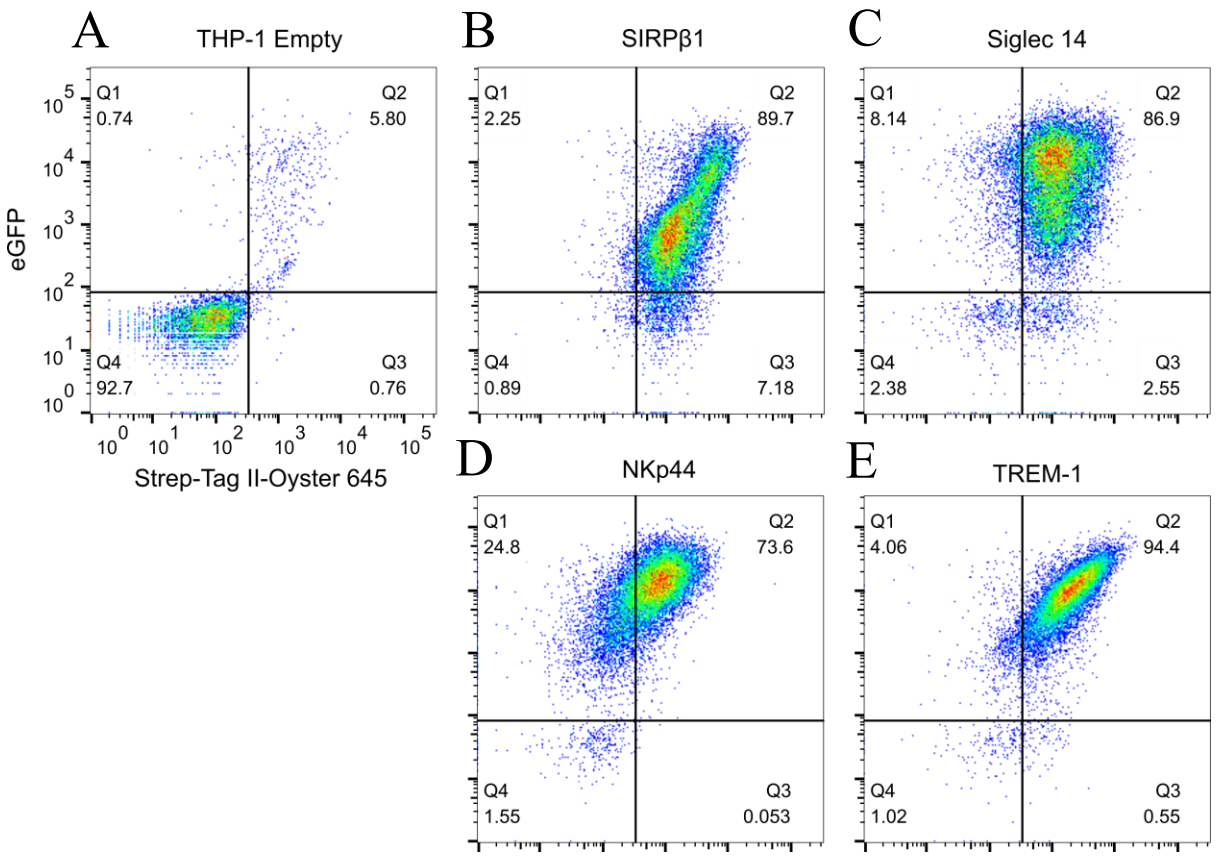


Figure 3.4: Checking expression levels of SIRPβ1, Siglec 14, NKp44 and TREM-1 plus the adaptor DAP12

(A) Staining of THP-1 cells which were transfected with an empty vector containing no receptor or adaptor. (**B-E**) Shows the expression of SIRPβ1, Siglec 14, NKp44 and TREM-1 plus DAP12 in each cell line. The x-axis shows signal from the anti-STII antibody conjugated with Oyster 645 fluorophore. The y-axis shows the signal from the eGFP which is co-expressed with the DAP12 adaptor.

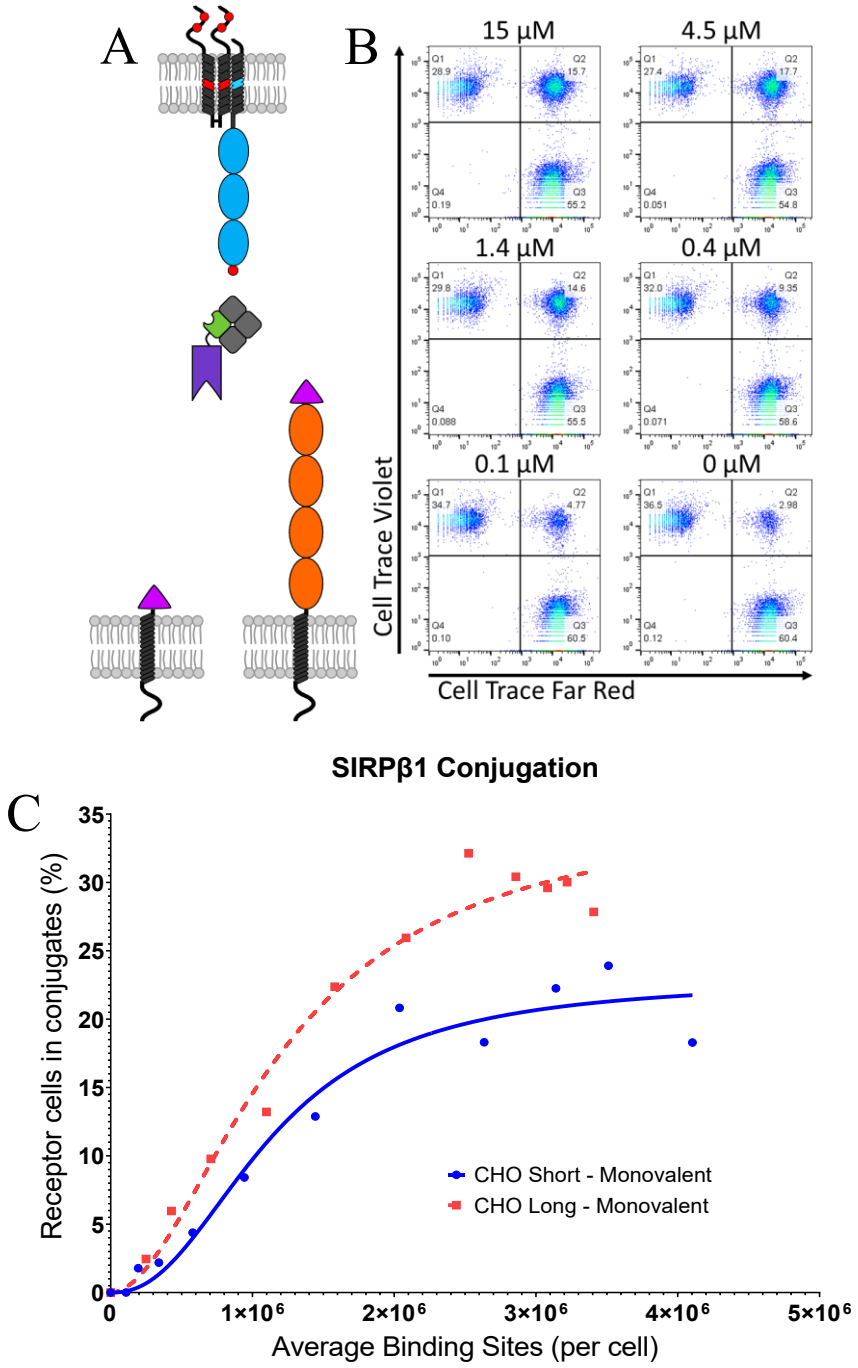


Figure 3.5: Comparison of conjugate formation using monovalent Strep-Tactin SpyCatcher coupled to short and long ligand cells

(A) A schematic diagram of the experimental set up where each receptor cell line is mixed with CHO cells presenting different numbers of a monovalent Strep-Tactin SpyCatcher coupled to either the short or long ligand cells. **(B)** Flow cytometry data of a representative conjugation assay showing short ligand cells coupled with a range of monovalent Strep-Tactin SpyCatcher concentrations. Receptor cells were stained with CellTrace Violet and ligand cells with CellTrace Far Red, therefore the upper right quadrate represents double positive events. **(C)** One representative data set plotting the percentage of double positive events from B for the SIRPβ1 receptor mixed with a series of short or long ligand cells with decreasing numbers of monovalent Strep-Tactin SpyCatcher on their surface.

3.2.3. Long ligands are superior binders in conjugate assays

Before each set of experiments, the expression level of the four receptors and their adaptor in the THP-1 cells was checked (Figure 3.4A-E). The receptor is measured via an antibody to the STII tag shown on the x-axis, and the adaptor is measured via production of eGFP shown on the y-axis. While there is some variation in the expression levels, we do not believe this will influence the conclusions.

With the generic ligand system set up and optimised I then moved to assess the ability of the generic ligand to bind to the different receptors. To do this I optimised a conjugation assay to measure conjugate formation between the receptor and ligand cells via flow cytometry. This method involved dyeing the receptor and ligand cells with two cell trace dyes, coupling the ligand cells with a serial dilution of a SpyCatcher fusion protein and then mixing the two cell types on ice so any conjugation observed is driven by specific receptor-ligand interactions and not induced via signalling.

Figure 3.5A shows the experimental set up with monovalent Strep-Tactin SpyCatcher added to the short and long ligand cells. The SIRPβ1 receptor is shown as an example here as this receptor was extensively used for the optimisation of the work in this thesis before more receptors were tested. The raw conjugation data is shown in Figure 3.5B where the two-dimensional scatter plots show the signal from the CellTrace Far Red on the x-axis (ligand cells) and the signal from the CellTrace Violet on the y-axis (receptor cells). The value above each scatter plot corresponds to the concentration of monovalent Strep-Tactin SpyCatcher added to ligand cells. As this value decreases so do the percentage of cells in the upper right quadrant and therefore the less conjugate formation is occurring. On average the background level of conjugation with no SpyCatcher added was 1-4 % of cells which was then subtracted from all other values. The resulting data was plotted in Figure 3.5C. Interestingly the SIRPβ1 receptor cells show an increase in the percentage of conjugates formed with the long ligand

cells for the same number of available binding sites. I believe this could be due to greater accessibility of the ligand similar to the reason I see an increase in coupling efficiency of monovalent Strep-Tactin SpyCatcher to bind long ligand cells (Figure 3.3B).

I next wanted to take advantage of the ability of our system to present the same ligand cells to multiple receptor cell lines expressing single STII tagged receptors. In Figure 3.6A-D I show the combined conjugation data for three biological replicates with the four receptors above. In three out of the four NTRs an F test comparison between the fit of the short versus long ligand data showed significantly more conjugation with the long ligand cells. The F test is the most useful test here as it checks if the same curve could fit both data sets. This result confirms the idea that in general, the longer ligand is more accessible and therefore binds the receptors more efficiently. Interestingly there is no difference for the Siglec 14 receptor whereas there is a large difference for the SIRPβ1. Considering that these receptors should be the same length at 3 Ig domains each it is strange that they are so different, but it may be due to differences in the orientation of their extracellular domains and therefore, the location and accessibility of the STII. There is also some evidence that Siglec 14 forms a dimer which may have an effect, and this will be discussed later.

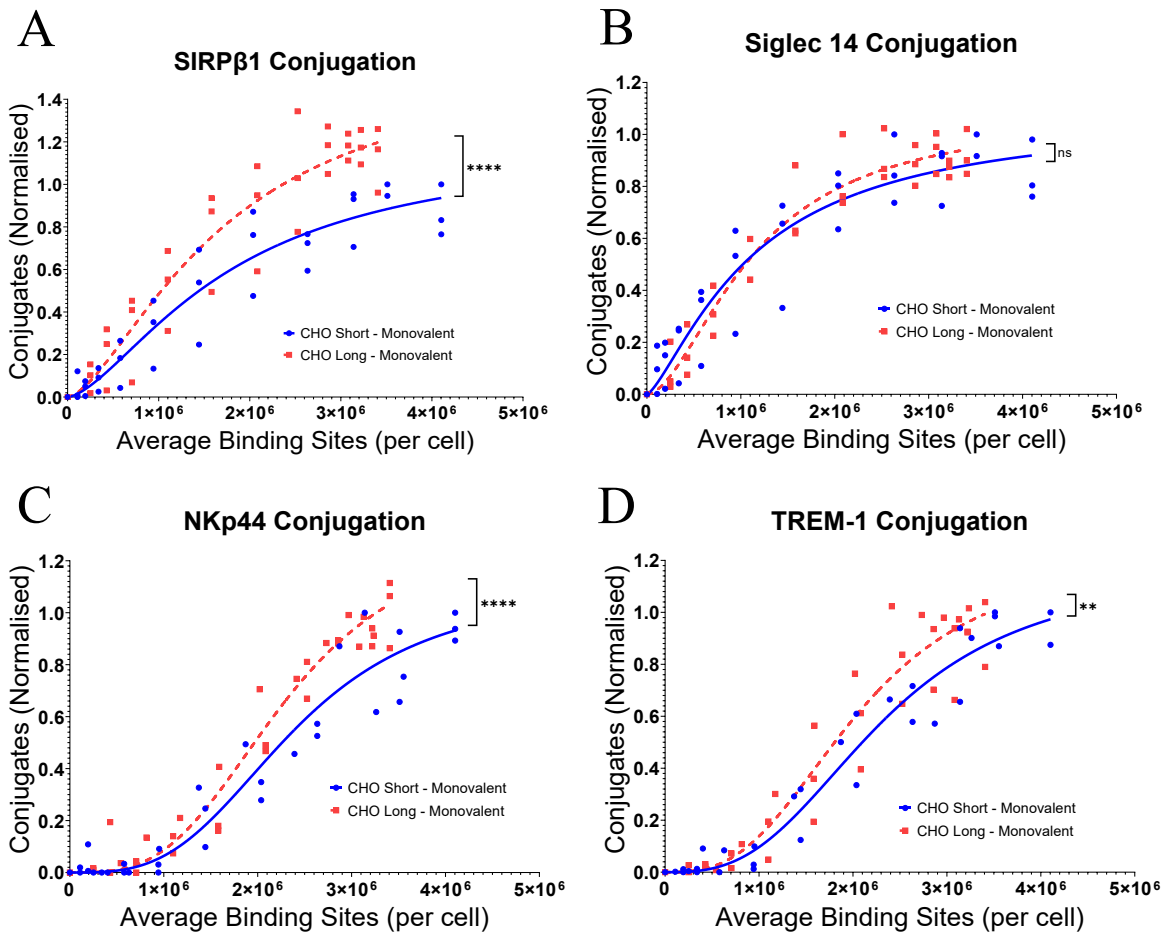


Figure 3.6: Conjugate formation of four receptors with short or long ligand cells coupled with monovalent Strep-Tactin SpyCatcher

(A-D) Conjugation assay comparing short and long ligand cells coupled with monovalent Strep-Tactin SpyCatcher. Four different DAP12 associating receptors (SIRPβ1, Siglec 14, NKp44 and TREM-1) were tested and the combined data from three biological replicates is shown with the data normalised to the maximum of the long ligand cells. An F test was used to compare the curves between the short and long conditions for each receptor (ns = not significant, ** = P <0.01, **** = P <0.0001). Data is combined from three biological replicates.

3.2.4. Despite less efficient conjugation short ligands trigger stronger activation

The conjugation assay showed that all combinations of receptor and ligand cells were forming good conjugates, but the extent of conjugation varied. However, I had intentionally removed the possibility of receptor activation by performing the assay on ice. Next, I wanted to measure the activation of these receptors under the same ligand conditions. To do this I used a twenty-hour stimulation assay at 37 °C. IL-8 release from the receptor cells was measured via ELISA as a read out for how much stimulation had occurred under the different conditions.

The combined data from three biological replicates for each of the same four receptors is shown in Figure 3.7A-D. Again, the x-axis is plotted as the average number of binding sites per cell for an accurate comparison between the short and long ligand conditions. The results in these stimulation experiments show that short ligands are consistently more potent activators for all receptors. While the differences between the short and long ligand are not identical for all NTRs the same pattern is observed where the short ligand leads to better activation of the cells for the same number of available ligands.

This matches previous data from our laboratory and others using alternative receptor-ligand systems (Bakalar et al., 2018; Choudhuri et al., 2005, 2009; Köhler et al., 2010; Wild et al., 1999). This highlights that the activation of NTRs is strongly determined by the dimensions of the receptor ligand complex. Increasing the intermembrane distance for receptor ligand interactions reduced signalling from these receptors. This evidence further supports the kinetic segregation model for receptor activation discussed in Chapter 1.

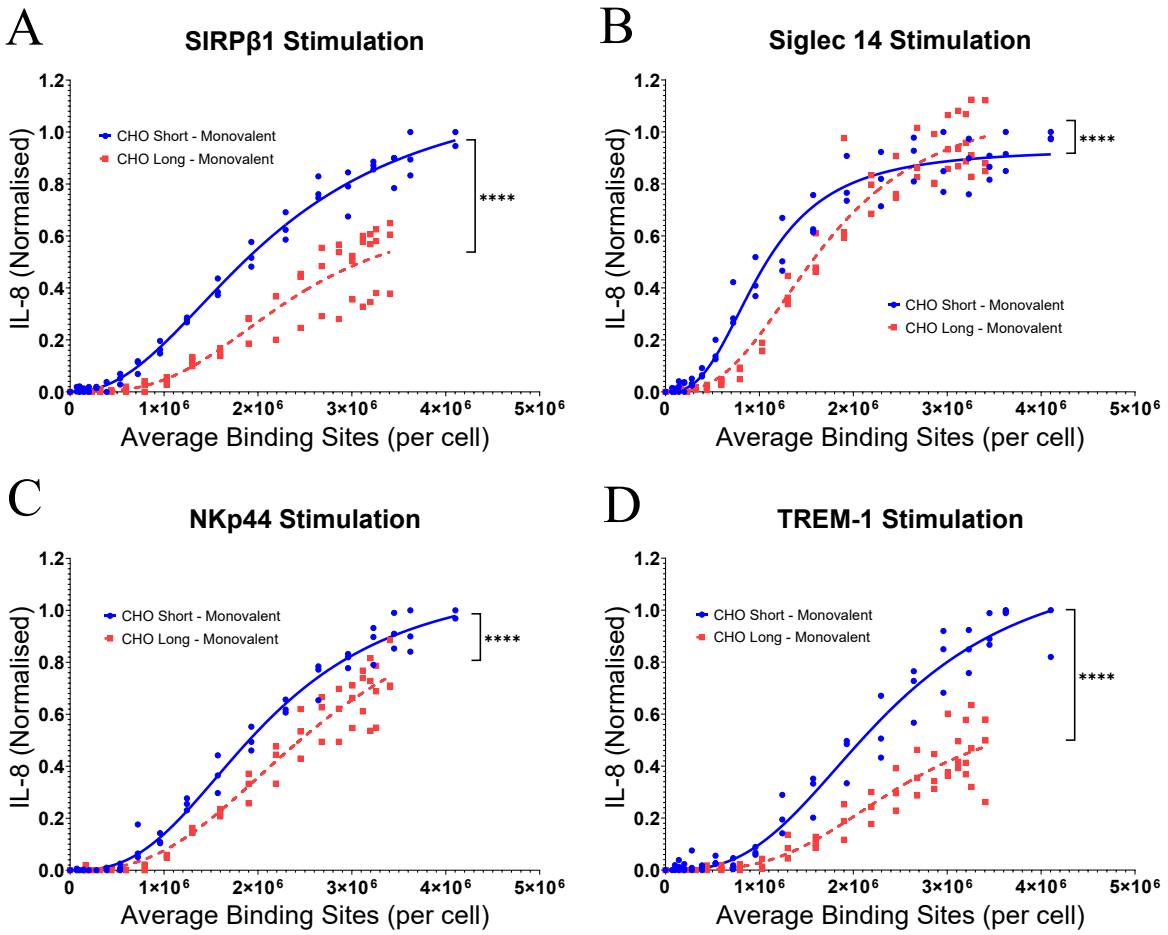


Figure 3.7: Stimulation assay comparison using monovalent Strep-Tactin SpyCatcher coupled to short and long ligand cells

(A-D) Stimulation assay comparing short and long ligand cells coupled with monovalent Strep-Tactin SpyCatcher. Four different DAP12 associating receptors (SIRPβ1, Siglec 14, NKp44 and TREM-1) were tested and the combined data from three biological replicates is shown with the data normalised to the maximum IL-8 release of the short ligand cells. An F test was used to compare the curves between the short and long conditions for each receptor (**** = P <0.0001). Data is combined from three biological replicates.

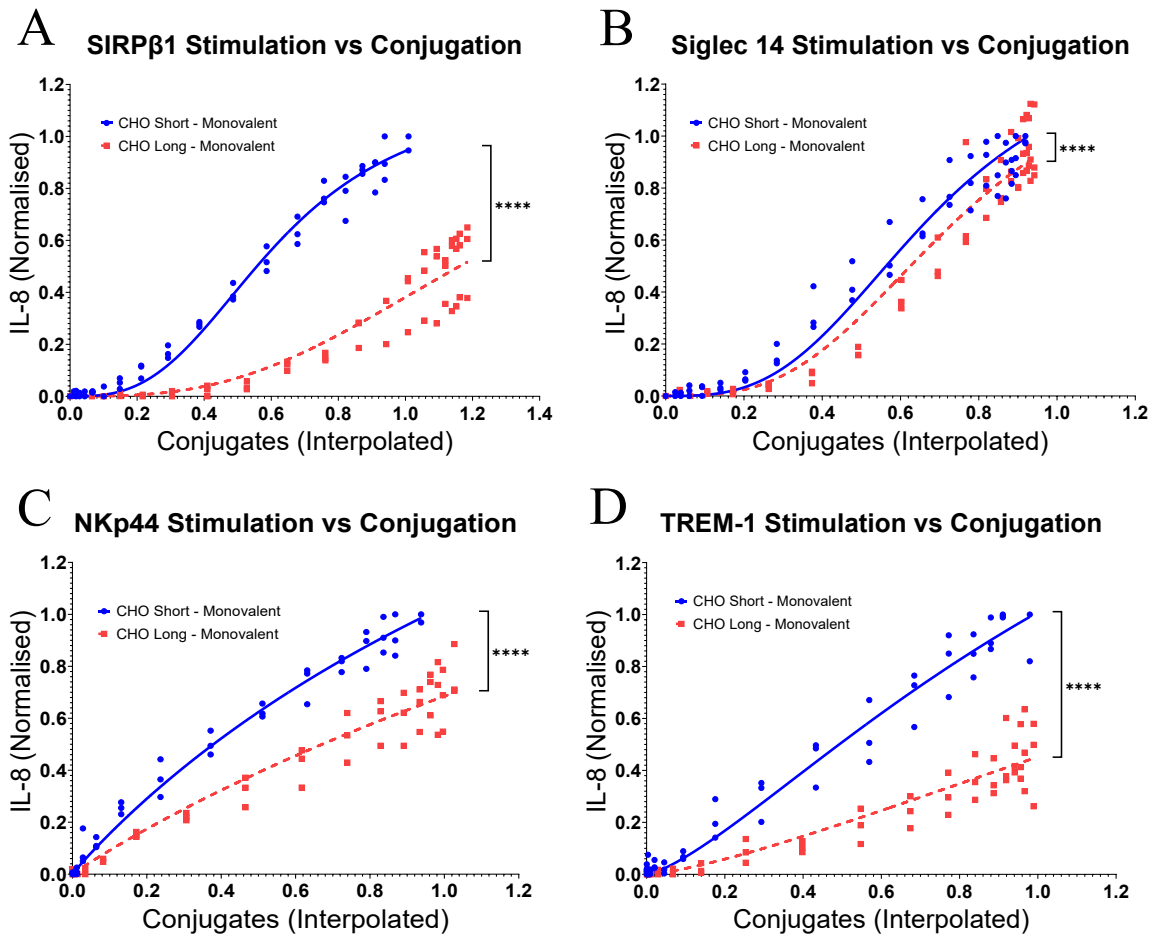


Figure 3.8: Stimulation versus Conjugation assay comparison using monovalent Strep-Tactin SpyCatcher coupled to short and long ligand cells

(A-D) Stimulation assay data plotted against conjugation assay data comparing short versus long ligand cells coupled with monovalent Strep-Tactin SpyCatcher. For four different DAP12 associating receptors (SIRPβ1, Siglec 14, NKp44 and TREM-1). An F test was used to compare the curves between the short and long conditions for each receptor (**** = P <0.0001). Data is combined from three biological replicates.

The effects I see where a shorter ligand induced better cellular activation is further emphasised by adjusting for the lower levels of conjugate formation observed with the short ligand. This is achieved by plotting the IL-8 stimulation data against the degree of conjugation observed at equivalent levels of ligand. These plots are shown for the four receptors used and clearly emphasises the superiority of the short ligand over the long ligand in terms of cellular activation at equivalent receptor ligand engagement (Figure 3.8A-D). This is because the two effects I see are antagonistic. The long ligand leads to superior conjugation but worse stimulation. Whereas the short ligand generates less conjugation but more potent stimulation. This impressive result highlights the need to quantify the amount of ligand binding when altering its length. This effect has been seen before with the TCR but is not something that is routinely checked in the literature when looking at receptor ligand dimensions (Choudhuri et al., 2005).

This comparison required the combination of data generated over separate days and so it was important to validate that the same receptor and ligand cells would behave in a similar manner. To do this I performed the conjugation (Figure 3.9A) and stimulation (Figure 3.9B) assays on the same cells using the SIRPβ1 receptor. As expected, this data and the combined stimulation versus conjugations data generated in Figure 3.9C matched very well to that in Figure 3.8A. This gave me confidence that the system was robust enough to combine data from multiple assays collected over several days.

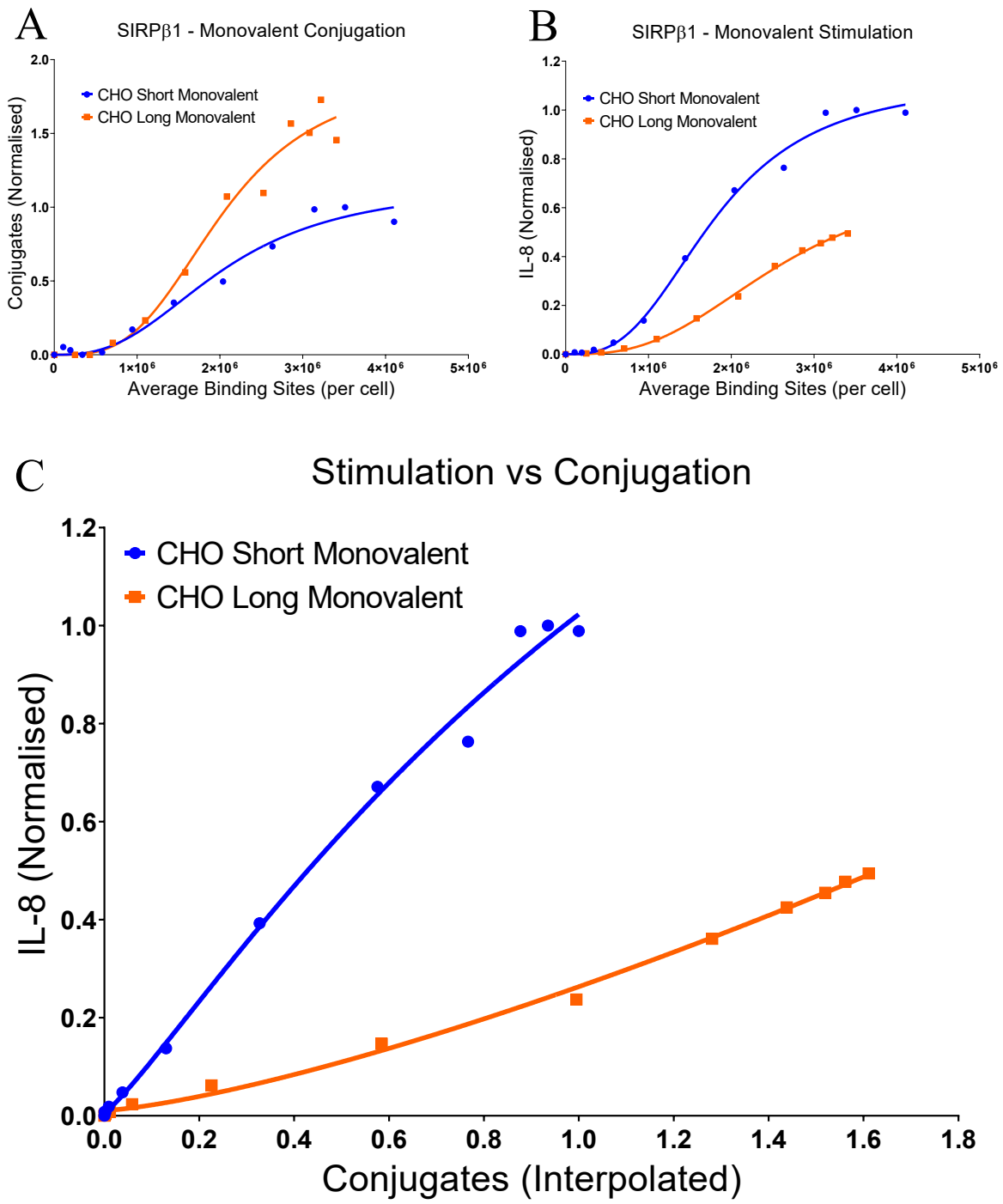


Figure 3.9: Stimulation and conjugation assays using the same receptor and CHO cells within one experiment shows the same result as the combined data from multiple experiments

(A) Conjugation assay measuring the SIRPβ1 receptor cells forming conjugates with the short or long CHO cells coupled with monovalent Strep-Tactin SpyCatcher. **(B)** The same batch of cells from A were used in a stimulation assay measuring the IL-8 release. **(C)** The stimulation and conjugation data from A and B was combined to plot simulation versus conjugation.

The second issue I wanted to address when combining stimulation and conjugation data in this way was the discrepancy in the temperature of the assay conditions. The conjugation assay was performed on ice whereas the stimulation assay was at 37 °C. I therefore set up a conjugation assay to compare the conjugation obtained when the cells were mixed on ice or at 37 °C in a water bath (Figure 3.10A). To prevent signalling affecting the results at 37 °C I added the SFK inhibitor 'A 419259 trihydrochloride' which prevents all signalling from the THP-1 cells (see Chapter 4). The results show that increasing the temperature increases the conjugate formation. This is not unexpected as the increased temperature will increase membrane dynamics and mobility of receptors and ligands in the membrane. However, the superiority of the long ligand was still maintained. Plotting this conjugation data against the stimulation data in Figure 3.7A showed that the temperature of the conjugation assay did not affect the conclusions I have previously made (Figure 3.10B). Taken together I feel these controls show it is fair to combine the conjugation and stimulation data in this way.

3.2.5. Short receptors are more sensitive than long receptors

This system also makes it possible to compare the stimulation and conjugation data between the four different receptors tested so far. The rational for this analysis is that SIRPβ1 and Siglec 14 both contain three extracellular Ig domains whereas NKp44 and TREM-1 contain only one Ig domain. Therefore, if the ligand is kept the same it could be possible to observe differences in their behaviour based on receptor size alone. However, any differences would reflect a relatively small difference of just two Ig domains whereas the previous experiments comparing short and long ligands use a relative difference of four Ig domains. Therefore, any differences between receptors may be modest by comparison. To do this it was necessary to normalise the maxima of each data set to one.

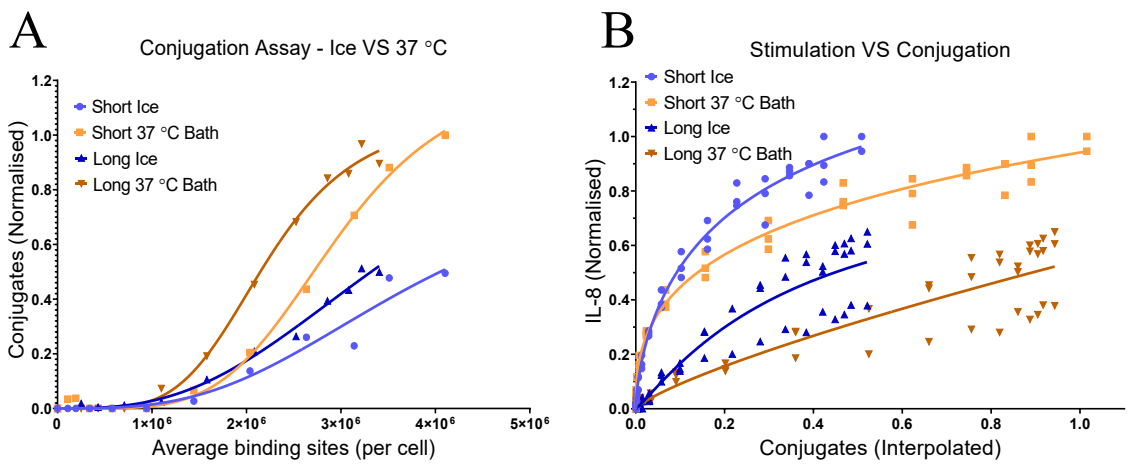


Figure 3.10: Conjugation assays on ice and at 37 °C in a water bath for monovalent Strep-Tactin SpyCatcher coupled to CHO short or long ligand cells shows the same pattern of ligand length sensitivity

(A) Conjugation assays comparing the percentage of cells forming conjugates with either CHO short or long cells coupled with monovalent Strep-Tactin SpyCatcher on ice or in a 37 °C water bath. Data is combined from three biological replicates. The SFK inhibitor 'A 419259 trihydrochloride' was added at a final concentration of 10 µM to prevent signalling. The data is representative of three biological replicates. **(B)** The SIRPβ1 monovalent stimulation data from Figure 3.7A was plotted against the interpolated conjugation values in A using the same method for both the ice and 37 °C water bath conditions.

The conjugation data for each receptor mixed with short ligand cells coupled with monovalent Strep-Tactin SpyCatcher is shown in Figure 3.11A. The data clearly shows the longer receptors SIRPβ1 and Siglec14 forming better conjugates for the same number of binding sites. This reinforces the results in Figure 3.6 where I show that the long ligand cells form better conjugates than the short ligand cells with three out of the four receptors tested. This comparison further emphasises the role of receptor ligand length on binding, which then has an impact on signalling. Surprisingly, when the same comparison was done with the stimulation data in Figure 3.11B, Siglec 14 was a clear outlier. This is strange as I would expect it to behave like SIRPβ1 as they are the same size. However, there is the possibility that Siglec 14 may form a dimer in the plasma membrane as this occurs with other members of the Siglec family. For example, Siglec 5 has very high sequence homology with Siglec 14 (Angata et al., 2006; Freeman et al., 1995). The dimer may act to maintain the receptor ligand interaction for longer thereby enhancing its stimulation. When looking at the stimulation versus conjugation in Figure 3.11C there is a clear trend supporting the idea that shorter receptor ligand interactions are better at converting engagement into signalling. This trend was still observed when comparing the four receptors and the long ligand (Figure 3.11D-E). The same pattern can be observed where short receptors are more potent given the same conjugate formation (Figure 3.11F). This is interesting as it shows that I am still seeing the effects of length differences even with the long ligand. This, therefore, raises the possibility that I would see even more pronounced differences in both conjugation and signalling with receptor ligand dimensions greater than the 4 Ig domains used here.

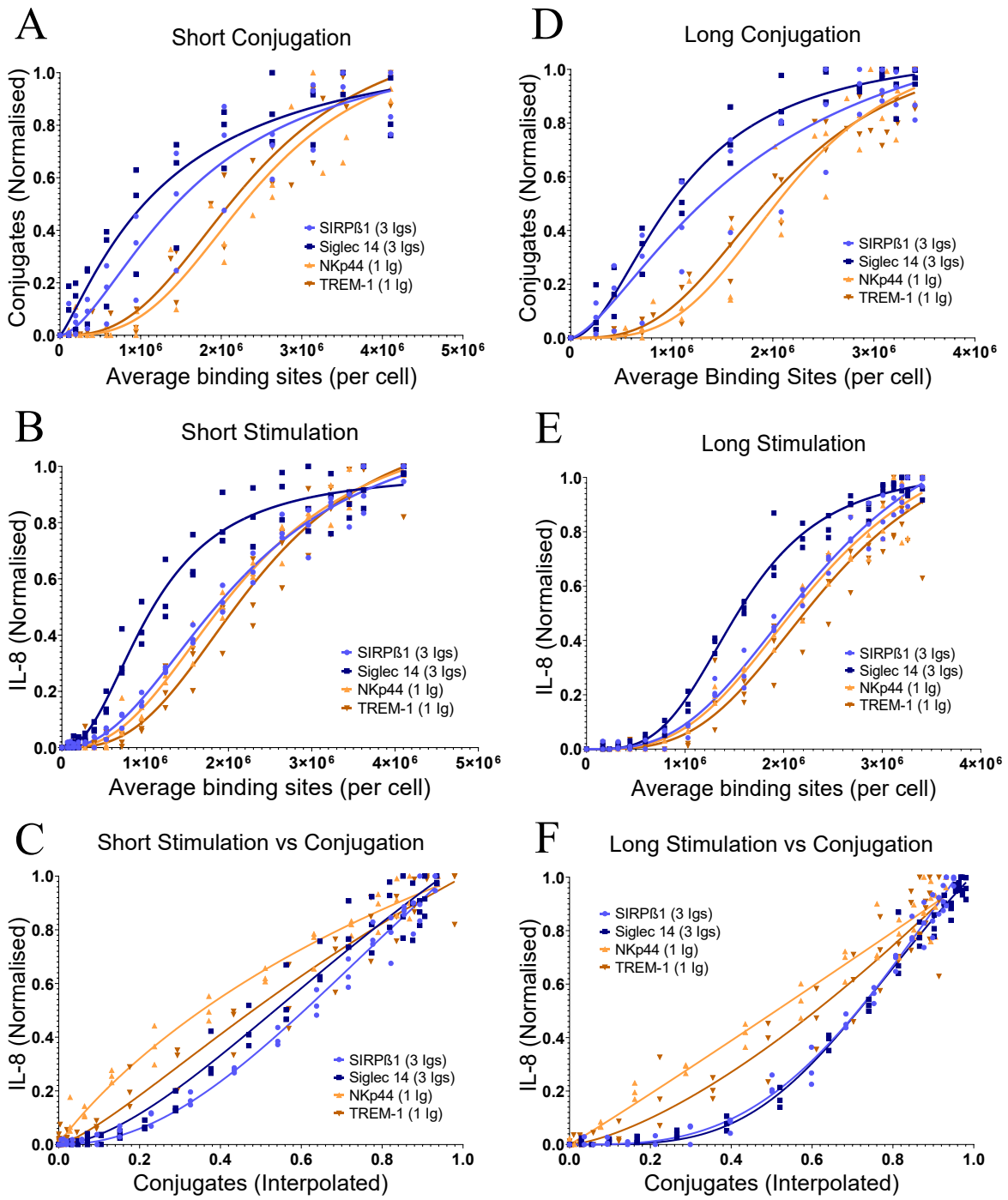


Figure 3.11: Comparison of SIRPβ1, Siglec 14, NKp44 and TREM-1 shows short receptors are more potent in inducing signalling than long receptors

The data from Figure 3.6, 3.7 and 3.8 was reanalysed to compare stimulation and conjugation efficacy between the four receptors for the same ligand stimulus. **(A)** Conjugation assay with short ligand cells coupled with monovalent Strep-Tactin SpyCatcher. **(B)** Stimulation assay measuring IL-8 release with short ligand cells coupled with monovalent Strep-Tactin SpyCatcher. **(C)** The same method used in Figure 3.8 was used to plot the stimulation data against the conjugation data. **(D-F)** Shows the same analysis comparing stimulation, conjugation, and stimulation versus conjugation for the long ligand cells coupled with monovalent Strep-Tactin SpyCatcher. Data is combined from three biological replicates.

3.3. Discussion

The work presented in the chapter consists of the development and optimization of a generic ligand system to study NTR activation. I have showcased its ability to activate multiple NTRs in a carefully controlled manner. This began with the characterisation of how the SpyTag-SpyCatcher interaction performs in this system and the quantification of the number of ligands presented on the surface of the ligand cells.

Clearly, there are many outstanding questions about the nature and function of these receptors, highlighting the potential of an artificial ligand system to address some of these issues. I was therefore able to test four NTRs simultaneously in the system and look at their sensitivity to receptor ligand dimensions. The combination of both conjugation and stimulation assays showed a clear sensitivity to ligand dimensions for all four receptors. The one outlier was Siglec 14; while still sensitive to ligand dimensions its effect was clearly different from the other three. I speculate that this is due to it forming a dimer. This would increase the density of STII tag available and allow it to maintain close contacts for longer which can lead to better activation. This can be seen in the conjugation data in Figure 3.11A where Siglec 14 appears to produce the best conjugate formation. This gives the receptor a greater chance to rebind the ligand when the interaction breaks before the membrane move apart. This is supported by (Chen et al., 2017) that showed that increasing the ligand affinity can reduce the dependence on length. This effect is also like using a multivalent ligand which will be tested and discussed in Chapter 4.

While our system is not unique in its ability to titrate the number of ligands available to a receptor it is the only one to my knowledge where control and measurement of the number of ligands presented is possible. Another system uses the FK506 binding protein (FKBP) expressed at the N-termini of the NTR and FKBP-binding domain (FRB) as the ligand (J. R. James, 2018; James & Vale, 2012). The addition of rapamycin can then induce receptor

ligand binding with physiological affinity in a titratable manner (Banaszynski et al., 2005). However, measuring precise numbers of ligands in this system is not possible and the addition of the FRB and FKBP to the receptors is a larger modification compared to our STII tag.

Switch mediated CAR based systems also allow for some degree of control over receptor ligand binding. CARs can contain Fab fragments which bind a soluble CAR-adaptor which then binds the surface expressed target antigen (Darowski et al., 2019; Minutolo et al., 2019). The related split CAR system uses a membrane ligand anchor which can bind different Fab fragments via a leucine zipper (Cho et al., 2018). While these systems address the issue of controlling the number of ligands available to a receptor, it is not possible to quantify the number of ligands presented and therefore compare to physiological conditions. The receptors in these systems are also heavily modified to allow the systems to function. My aim was to look at other parameters which may affect NTR activation such as ligand valency, mobility and affinity are therefore only feasible in our system.

The lack of a native receptor ligand interaction is the greatest criticism of a generic ligand system like ours or the others discussed, but it is also a strength. For example, if a conformational change was required for receptor activation, then this system would not be appropriate. However it is clear that the system can activate the TCR with a similar potency to the native pMHC ligand as shown in (Denham et al., 2019). It is also well established that CARs which contain scFvs rather than traditional extracellular domains are also capable of triggering though the same signalling machinery used by all NTRs. Taken together this suggests that the need for a native ligand is not as important as other factors such as length, valency, mobility, and affinity which could affect NTR activation. I can test these other characteristics through manipulation of the generic ligand system, and this will be discussed in Chapter 4.

This version of the generic ligands system is only capable of testing activatory receptors however, we have also developed a proof of principle for how inhibitory receptors could be studied (Denham et al., 2019). The problem with studying inhibitory receptors is that the cell needs an activatory signal to integrate the inhibitory signal from different receptors. It is also thought to be important to match the size of the extracellular domain of the activatory and inhibitory receptors for colocalization to take place. This is likely because the signalling molecules inhibitory receptors recruit are cytoplasmic enzymes such as phosphatases that can only perform their function within a small radius of the receptor. For example upon phosphorylation PD-1 recruits SHP-1 and SHP-2 which can act to inhibit TCR activity via dephosphorylating CD3ζ and ZAP70 (Sheppard et al., 2004). Therefore, to address these issues our proposed system uses chimeric receptors with the extracellular domain of the activatory and inhibitory receptors swapped for the LaG17 and LaM8 nanobodies respectively. These nanobodies bind GFP and mCherry which can be expressed as SpyCatcher fusion proteins. This allows careful control of the number of both ligands and therefore a constant activatory ligand can be mixed with a progressive increase in inhibitory ligand. Initial experiments showed good inhibition of the activatory signal provided by the CD3ζ with both inhibitory receptors PD-1 and BTLA.

In the process of optimising the system I also tested several other NTRs including LILRA1, NKp30, and FcγRI. Unfortunately, none of these receptors were activated with the STII tag binding the monovalent ligand. The most likely explanation for this is the fact these receptors use the FcRγ adaptor rather than DAP12 and that the FcRy adaptor is less efficient than DAP12, at least in the THP-1 cells used in this assay. This is supported by the fact we did see good stimulation of NKp30 using the higher affinity twin STII system used in our paper (Denham et al., 2019). Plus, I was able to get stimulation of all three receptors using the tetravalent ligand discussed in Chapter 4.

Finally, these results should be confirmed in primary cells using other readouts. This is all possible with the generic ligand and allows for many potential uses going forward to study other cell types or even other cell surface receptors unrelated to NTRs. The nature of the STII or higher affinity twin STII means it required a very small modification to make the target receptor compatible compared to other systems. The same ligand cells can then be decorated with a large range of different SpyCatcher fusion proteins or combinations of different ligands.

Chapter 4 - Extending the generic ligand system to study the effect of ligand valency, mobility, and affinity on NTR activation

4.1. Introduction

Having validated that the generic ligand system can reproduce previous findings such as the importance of receptor ligand dimensions for NTR activation, the next step was to study if other physical characteristics of receptors and ligands could also influence their binding and receptor activation. Using the versatility of our system it is possible to test how changing the valency, mobility, and affinity of the generic ligand can affect NTR activation.

4.1.1. Ligand valency

Initially, I looked at altering the valency of the ligand to artificially cluster the NTRs together. One of the main mechanisms proposed for NTR activation is through receptor clustering, where signalling requires a specific local concentration of receptor in the membrane at the site of ligand binding to trigger activation (Cooper & Qian, 2008; Pageon et al., 2016). This clustering of receptor tails may aid sequential phosphorylation of their tyrosine motifs by SFKs and lead to receptor triggering. The ability for receptors to trigger via clustering was first proposed due to the ability of soluble crosslinking antibodies to induce NTR activation (Kaye & Janeway, 1984; Woodruff et al., 1967). This is not physiological as NTR ligands are almost exclusively monovalent and presented on cell surfaces (Dushek et al., 2012). However, this does strongly suggest that receptor clustering is an important factor to consider when studying their activation.

While very few NTRs are thought to bind multivalent ligands, there are a few examples that have been suggested to bind ligands which contain repeated subunits. For example, TREM-1

has been shown to bind extracellular actin (Fu et al., 2017). There is also evidence in the context of the TCR that receptor clustering is important for activation (Alarcón et al., 2006; Minguet et al., 2007; Pageon et al., 2016; Schamel & Alarcón, 2013). In addition, several NTR family members are known to form dimers in the plasma membrane, which may improve activation. Therefore, the aim was to understand if receptor clustering would affect NTR activation in a physiological cell-cell interaction. To study the effect of receptor clustering I used multivalent Strep-Tactin SpyCatcher fusion proteins which could bind multiple receptors per ligand molecule.

4.1.2. Ligand mobility

The next parameter I wanted to test was the mobility of the ligand. The complex nature of the plasma membrane leads to much slower diffusion of proteins compared to the same proteins in artificial bilayers (Kusumi et al., 2005). It has been proposed that NTRs cannot freely move throughout the plasma membrane due to a lattice of cortical actin filaments which form close to the inner membrane (Kusumi et al., 2005). This lead to the picket fence model where NTRs are confined to a section of membrane (Jaumouillé & Grinstein, 2011; Nakada et al., 2003). Within these compartments the NTRs can diffuse freely but it is difficult for the molecules to hop from one compartment to another. Recent evidence suggests CD44 can act as a key mediator of the compartments ("picket fence") through interactions with ezrin and ankyrin, which bind to the cytoskeleton (Freeman et al., 2018). Furthermore, the large extracellular domain of CD44 binds hyaluronan, a key component of the extracellular matrix (Aruffo et al., 1990). This may influence the lateral clustering of NTRs during receptor ligand engagement. These observations suggest that the lateral mobility of NTR ligands might affect activation of NTRs.

To test this in the generic ligand system I used four different ligand anchors containing the transmembrane and cytoplasmic regions of CD80, LAIR-1, CD43 and CD52 which could

alter the behaviour or mobility of the ligand. CD80 was originally chosen for the short and long ligands tested in Chapter 3 as it had been used extensively as a membrane anchor for expression of different proteins due to its stability and because it is not thought to form a dimer (Doty & Clark, 1996). In a similar manner, the LAIR-1 anchor should also be a stable monomer in the membrane (Meyaard et al., 1997). It contains an ITIM motif, however, this would not be expected to have any effect when expressed in CHO cells. Therefore, this anchor should behave in a similar way to CD80. Conversely, CD43 interacts with the cytoskeleton though Ezrin/Radixin/Moesin (ERM) proteins which should alter its mobility in the membrane (Cannon et al., 2011; Yonemura et al., 1998). Finally, CD52 is a glycosylphosphatidylinositol (GPI) anchored protein and therefore should have greater mobility in the membrane (Paulick et al., 2007; Treumann et al., 1995). The question was whether these different anchors would lead to functional differences in receptor activation.

4.1.3. Ligand affinity

The final parameter I wanted to study was the affinity of the NTR-ligand interaction. To test this with the generic ligand system I had to produce SpyCatcher fusion proteins which could bind the STII with different affinities. An alternative to Strep-Tactin was to use streptavidin, which has approximately a tenfold lower affinity for the STII tag (Voss & Skerra, 1997). I therefore produced monovalent and tetravalent streptavidin SpyCatcher to test with different NTRs.

The TCR is able to discriminate between high affinity non-self peptides and lower affinity self-peptides (Courtney et al., 2018; Depoil & Dustin, 2014). This is crucial to the function of T cells in the adaptive immune response. This discrimination is thought to depend on kinetic proof-reading in which the duration of the interaction is critical (Mckeithan, 1995). This occurs because once the ligand binds, the NTR must be phosphorylated and then recruit other signalling molecules before downstream signalling can commence (Lever et al., 2014). This

introduces several steps which can be quickly undone by phosphatases if the interaction between receptor and ligand is not maintained for long enough. While other NTRs do not need to be sensitive to different affinity ligands in the same way as the TCR it would help to define a common mechanism for activation if they were found to be. Therefore, I wanted to find out how the other NTRs would function when presented to ligands of different affinity and whether increased valency could act in a similar way.

4.1.4. Key findings

In this chapter I show that multivalent ligands lead to superior conjugation formation, which in turn leads to better stimulation responses compared to monovalent ligands. However, when controlling for the level of conjugation, multivalent ligands are less potent than monovalent ligands. I also show that while multivalent ligands produce much stronger stimulation, they are still sensitive to changes in receptor-ligand dimensions. I then look at altering the ligand anchor and mobility of the ligand and find that this does not influence NTR activation or conjugate formation. Finally, I show that NTR responses can discriminate between ligands of differing affinity, and that increased valency can act in a similar manner to increased affinity.

4.2. Results

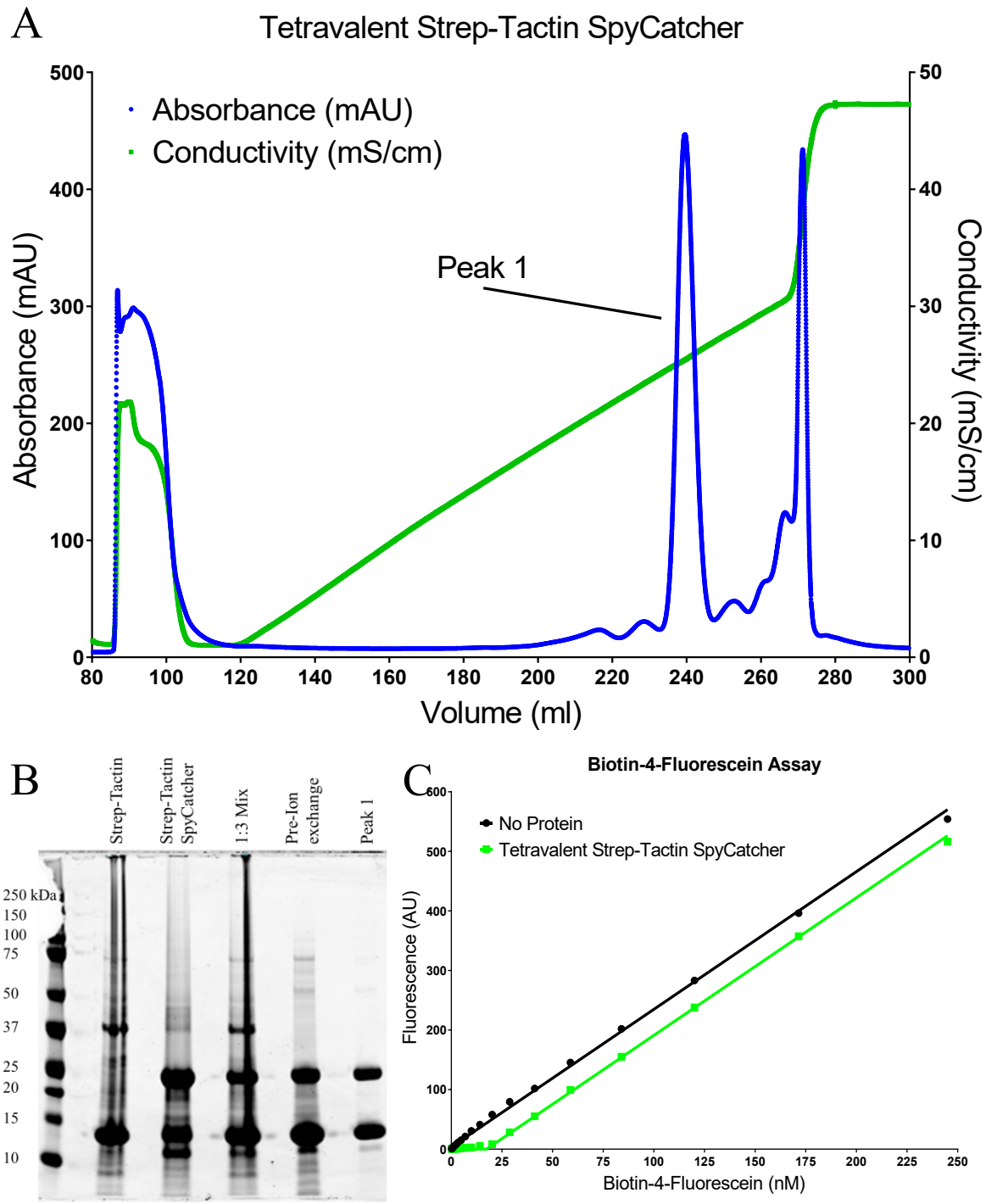


Figure 4.1: Purification of tetravalent Strep-Tactin SpyCatcher

(A) Representative anion exchange chromatography run to purify tetravalent Strep-Tactin SpyCatcher. **(B)** SDS-PAGE gel, lane 1, solubilised Strep-Tactin, Lane 2, solubilised Strep-Tactin SpyCatcher, Lane 3, a 1:3 molar ratio of Strep-Tactin SpyCatcher mixed with Strep-Tactin, Lane 4, pre- anion exchange and lane 5, Peak 1 corresponding to the purified tetravalent Strep-Tactin SpyCatcher. The two major bands represent one molecule of Strep-Tactin SpyCatcher for every three molecules of Strep-Tactin (calculated by densitometry). **(C)** Biotin-4-fluorescein assay using 5 nM purified tetravalent Strep-Tactin SpyCatcher.

4.2.1. Measuring the average number of monovalent and tetravalent ligands presented on ligand cells

To test the effect of valency, I produced a tetravalent Strep-Tactin SpyCatcher protein composed of the same active monovalent Strep-Tactin SpyCatcher unit in the monovalent protein but mixed with three active Strep-Tactin units to make up four total active binding sites per molecule. This could then be purified in the same way as the monovalent Strep-Tactin SpyCatcher protein using anion exchange chromatography. This allows for molecules with a single SpyCatcher to be purified based on the charge from the poly aspartic acid sequence (Figure 4.1A). Samples from pre- and post- anion exchange were run on an SDS-PAGE gel, with the desired protein (marked as 'peak 1') showing the two bands for the Strep-Tactin and larger Strep-Tactin SpyCatcher units (Figure 4.1B). To check the protein was indeed tetravalent and contained four functional binding sites per molecules the biotin-4-fluorescein assay was used. The inflection point was measured at 17 nM, which is close to the predicted value of 20 nM based on four binding sites per tetravalent Strep-Tactin molecule (Figure 4.1C).

I then coupled either the monovalent or a tetravalent Strep-Tactin SpyCatcher to the short ligand cells. To compare accurately the number of available binding sites on the cells coupled with the two SpyCatcher fusion proteins. I used the same method described in Chapter 3 to calculate the average number of binding sites per cell (Figure 4.2). Without this method it would have been impossible to compare the numbers of available binding sites due to quenching of the biotin ATTO 488 when bound to tetravalent protein. This process is not well understood but fluorophores in tight proximity (as is the case when four are bound to a single Strep-Tactin molecule) have significantly reduced intensity compared with the expected value. This can be seen in Figure 4.2A where the maximum florescence from the

tetravalent is in fact lower than the monovalent even though there are four-fold more binding sites as measured by biotin-4-fluoroscein binding (Figure 4.2C and D).

Interestingly, the tetravalent Strep-Tactin SpyCatcher coupled to SpyTag ligand cells with a significantly lower K_D, as measured by the biotin ATTO 488 assay Figure 4.2A and B). This is likely a consequence of the lower isoelectric point of the monovalent versus the tetravalent Strep-Tactin SpyCatcher protein (pI 5.03 vs 5.64 respectively). This would make the monovalent Strep-Tactin SpyCatcher more negatively charged in the coupling buffer, increasing its repulsion from the negatively charged cell surface. The observation of differing coupling efficiency between the SpyCatcher fusion proteins will be addressed in the discussion of this chapter.

When calculating the average number of binding sites per cell for short ligand cells coupled with tetravalent protein there are a maximum of four available biotin binding sites per molecule. This can be seen in Figure 4.2C and D where the average maximum number of binding sites is approximately 1.5 $x10^7$ molecules per cell. Dividing this number by four converts this value to the number of tetravalent Strep-Tactin SpyCatcher molecules coupled per cell, which matches well to the average number of binding sites per cell when monovalent Strep-Tactin SpyCatcher is coupled. This acts as an internal control and indicates that the activity for binding biotin between the two SpyCatcher fusion proteins is the same; giving me confidence that the number of ligands I measure is accurate. Therefore, any differences observed between the functional ability of monovalent or tetravalent to bind and activate the STII tagged receptors is due to the valency alone. While the tetravalent molecule in theory could bind up to four NTRs tagged with STII tags I do not expect this to be very favourable due to steric hinderance. Instead, each tetravalent molecule will likely bind three NTRs at most.

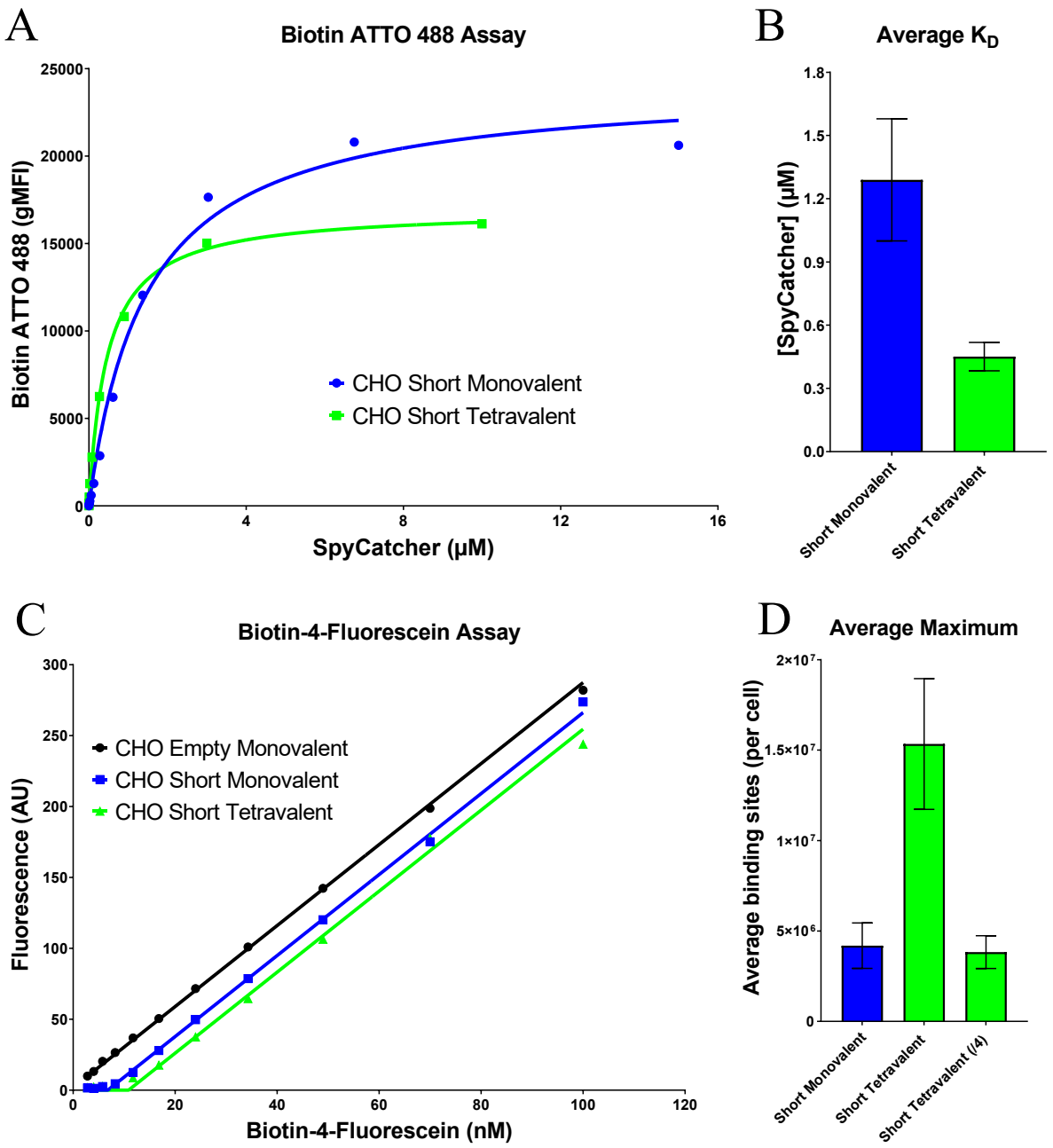


Figure 4.2: Calculating the average number of binding sites per short ligand cell coupled with monovalent or tetravalent Strep-Tactin SpyCatcher

(A) A representative biotin ATTO 488 assay where CHO short cells were coupled with a serial dilution of monovalent or tetravalent Strep-Tactin SpyCatcher and mixed with biotin ATTO 488 which was measured by flow cytometry and the geometric mean plotted. The data was fit with a one site specific binding model and the K_D extracted from each curve. **(B)** The K_D values extracted from eight independent experiments were plotted. **(C)** A representative of a biotin-4-fluorescein assay where CHO empty and short cells were incubated with a saturating concentration of monovalent (15 µM) or tetravalent (10 µM) Strep-Tactin SpyCatcher. **(D)** The average maximum number of binding sites for five independent experiments was plotted. For comparison to monovalent the tetravalent values were divided by four and re-plotted. Error bars show SD.

4.2.2. Tetravalent ligands are superior binders in conjugate formation assays

The conjugation assay described in the previous chapter showed how I could quantify the dependence of cell-cell interactions on the length of the ligands presented on cells. Here I will use the same assay to examine the effect of valency on cell-cell interactions. To compare any differences between monovalent and tetravalent it is critical to consider the difference in the number of available binding sites. In Figure 4.3A-D I show the ability of the four NTRs to form conjugates when plotted against the average number of binding sites.

The data clearly shows that the tetravalent ligand is far superior to the monovalent both in terms of an increase in the maximum level of conjugate formation but also a decrease in the EC50. Thus, increasing the valency of the ligand substantially increased cell-cell interactions.

Note that the plots in Figure 4.3 assume that all four binding sites on each tetravalent protein are available to bind a receptor, but as explained above due to steric hindrance it is more likely that only two or three receptors are bound simultaneously. This means the EC50 shift is likely to be an underestimate of the true shift. A comparison of trivalent and tetravalent ligands is discussed later in this chapter.

This stark difference between monovalent and tetravalent conjugation shows that increasing the valency of the ligand increases receptor binding at cell-cell interfaces. Presumably once one receptor binds a tetravalent molecule it facilitates binding of subsequent receptors. Furthermore, if multiple receptors are bound to a tetravalent ligand, when one receptor unbinds other receptors remain bound. This ensures that the membranes are still held together at the optimum distance increasing the chances that the same or another receptor will bind the vacant site on the ligand.

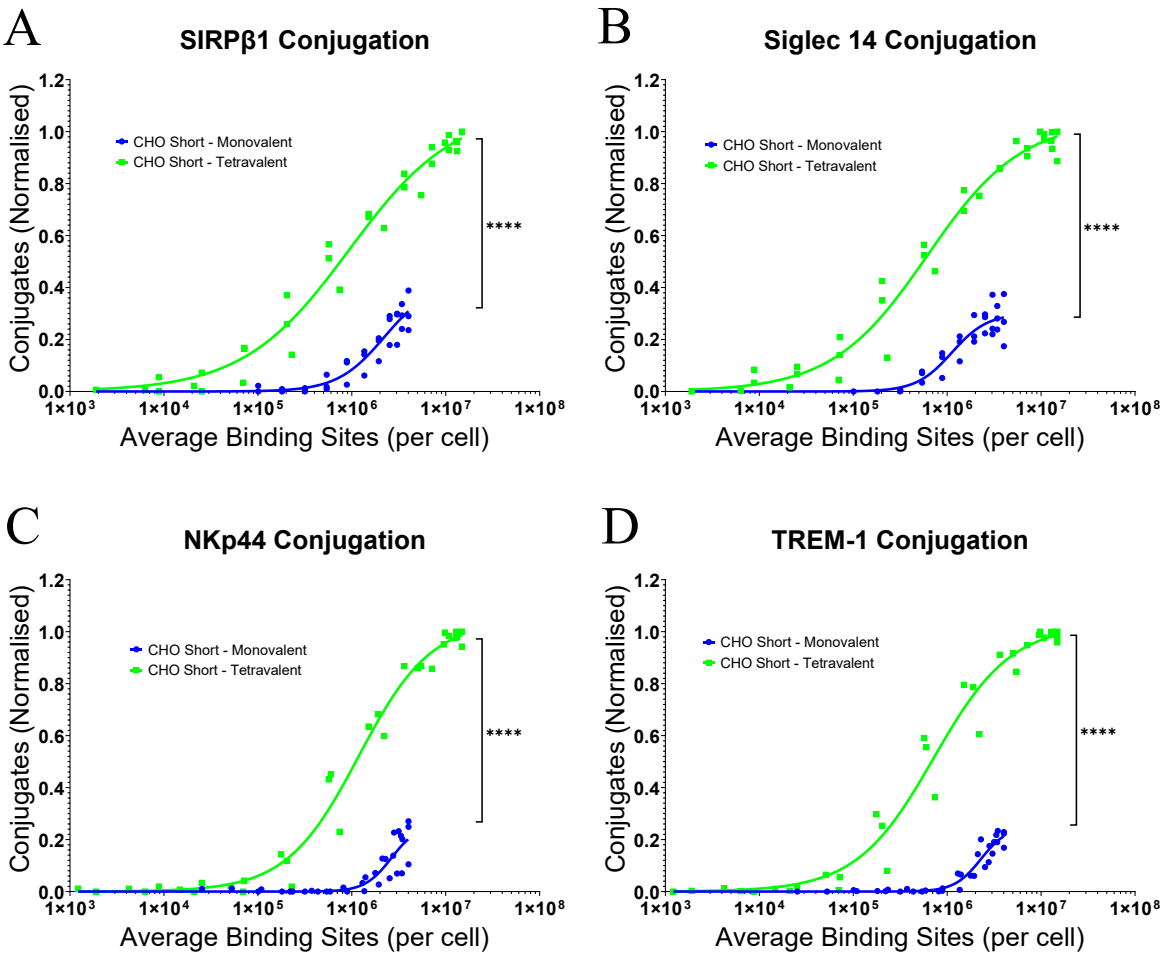


Figure 4.3: Conjugate formation of four receptors with short ligand cells coupled with monovalent or tetravalent Strep-Tactin SpyCatcher

(A-D) Conjugation assay comparing short ligand cells coupled with monovalent or tetravalent Strep-Tactin SpyCatcher. Four different DAP12 associating receptors (SIRPβ1, Siglec 14, NKp44 and TREM-1) were tested and the combined data from three biological replicates is shown with the data normalised to the maximum of the tetravalent coupled short ligand cells. An F test was used to compare the curves between the monovalent and tetravalent conditions for each receptor (**** = P <0.0001).

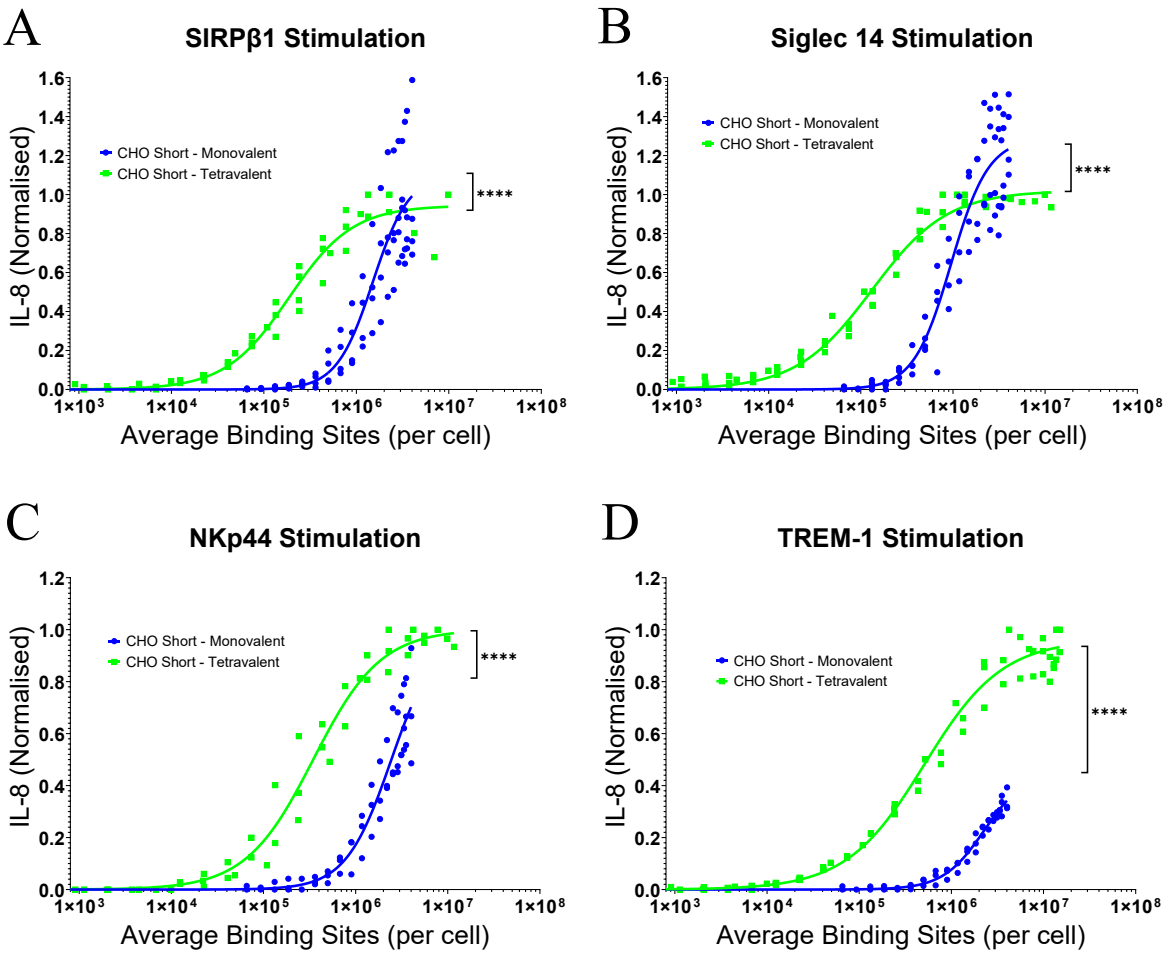


Figure 4.4: Stimulation assay comparison using monovalent or tetravalent Strep-Tactin SpyCatcher coupled to short ligand cells

(A-D) Stimulation assay comparing short ligand cells coupled with monovalent or tetravalent Strep-Tactin SpyCatcher. Four different DAP12 associating receptors (SIRPβ1, Siglec 14, NKp44 and TREM-1) were tested and the combined data from three (NKp44 and TREM-1) or four (SIRPβ1, Siglec 14) biological replicates is shown with the data normalised to the maximum IL-8 release of the tetravalent coupled ligand cells. An F test was used to compare the curves between the monovalent and tetravalent conditions for each receptor (**** = P <0.0001).

4.2.3. Despite less efficient conjugation, monovalent ligands trigger equal or stronger activation

With the observation that the tetravalent ligand led to significantly more conjugate formation compared to the monovalent ligand, I next performed stimulation experiments to see if this increased conjugation would lead to increased signalling. Figure 4.4A-D shows the production of IL-8 by THP-1 cells expressing four NTRs from Chapter 3 when cultured with short ligand cells coupled with either monovalent or tetravalent Strep-Tactin SpyCatcher. Again, there is a large decrease in the EC50 for the tetravalent ligand in the stimulation assay measuring IL-8 production.

Interestingly though, when comparing the maximum IL-8 response there is more variation between the different NTRs. Siglec 14 and SIRPβ1 show higher maximum stimulation with the monovalent ligand compared to the tetravalent. I believe this is due to significant downregulation of the receptor which, as shown in the next section, only occurs when engaging the tetravalent ligand. This produced a bell-shaped curve at the highest levels of stimulation. I then excluded the data points where significant downregulation had occurred to fit a maximum level of activation to the tetravalent data. I predict this downregulation occurs less with NKp44 and is almost non-existent with TREM-1. I would therefore expect the cells to reach the same maximum response for all four receptors with both monovalent and tetravalent ligands if there was no receptor downregulation.

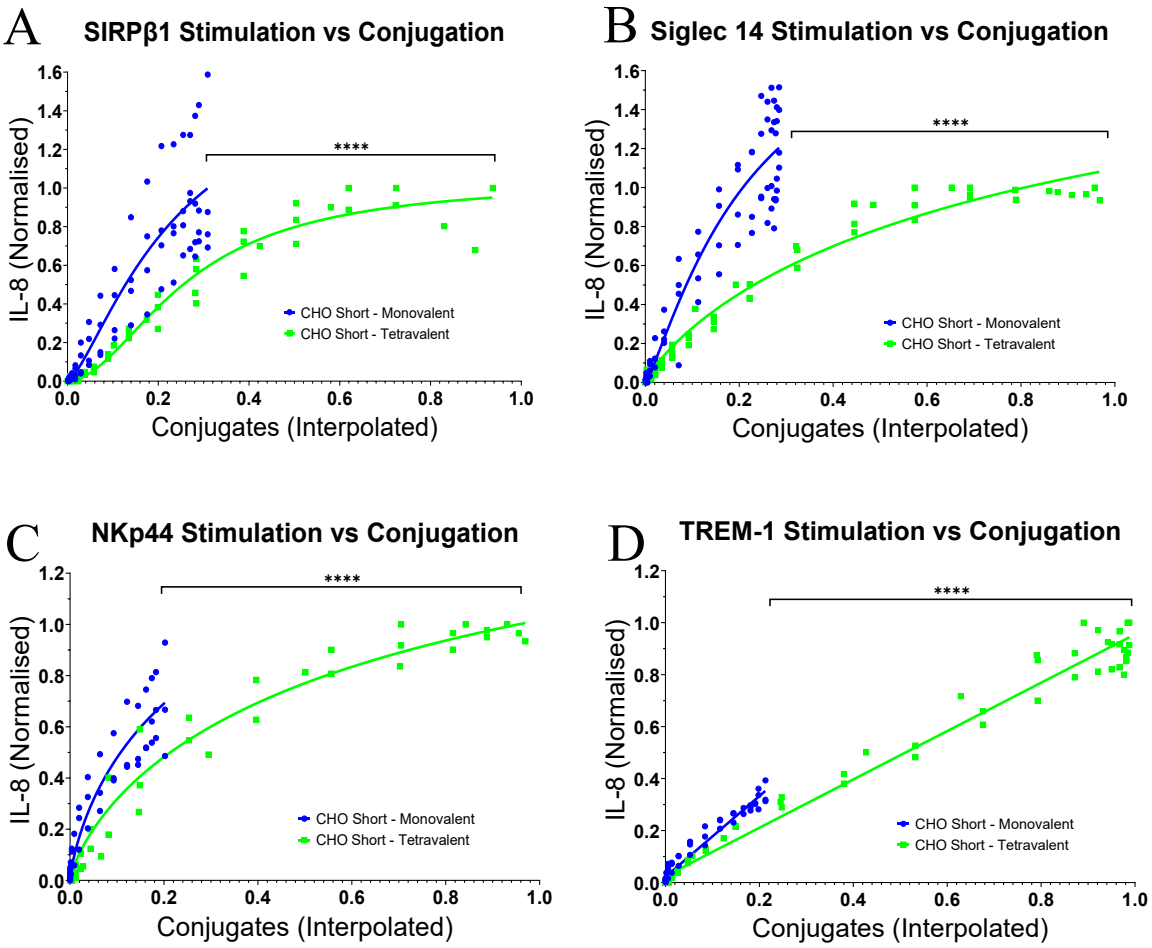


Figure 4.5: Stimulation versus Conjugation assay comparison using monovalent or tetravalent Strep-Tactin SpyCatcher coupled to short ligand cells

(A-D) Stimulation assay data plotted against conjugation assay data from comparing short ligand cells coupled with monovalent or tetravalent Strep-Tactin SpyCatcher. Four different DAP12 associating receptors are shown (SIRPβ1, Siglec 14, NKp44 and TREM-1). An F test was used to compare the curves between the monovalent and tetravalent conditions for each receptor (**** = P <0.0001). Data is combined from three biological replicates.

To understand the relationship between conjugation efficiency and stimulation for monovalent versus tetravalent Strep-Tactin SpyCatcher, I used the same method used in Chapter 3 to plot the stimulation data against the conjugation data. The results in Figure 4.5A-D are striking as they clearly show that, at equivalent levels of conjugate formation, the monovalent stimulation is in fact equal or superior to the tetravalent. There are again differences when comparing the four NTRs: SIRPβ1 and Siglec 14 show the biggest improvement when stimulating with a monovalent ligand, possibly due to the increased downregulation of these NTRs when stimulated with the tetravalent ligand. This is because it is likely that some down regulation is still occurring even at lower ligand density. This would explain why the NKp44 and TREM-1 NTRs show significant but less improvement with the monovalent ligand.

Similar to the short versus long ligand comparison in Chapter 3, I wanted to make sure that it was fair to combine the conjugation and stimulation data in this way. This is because the assays are performed under different conditions which may cause artifacts when combining the data. I therefore repeated the conjugation assay with the monovalent and tetravalent Strep-Tactin SpyCatcher on ice and at 37 °C in a water bath with SIRPβ1 (Figure 4.6A). The monovalent conjugation is indistinguishable whereas the tetravalent conjugation is slightly better when performed at 37 °C. I would expect to see slightly better conjugation at 37 °C due to increased membrane dynamics at higher temperatures. Again, the SFK inhibitor (A-419259 trihydrochloride) was added to prevent any signalling which may induce further cell-cell adhesion. This conjugation data was then plotted against the SIRPβ1 stimulation data (Figure 4.6B). This confirms the key result I show in Figure 4.4A where the monovalent stimulation is equivalent or better than the tetravalent for the same conjugation efficiency.

Taken together, these results show that increasing the valency of the ligand enhances NTR binding, as measured by conjugate formation. However, when controlling for conjugate

formation, monovalent ligands are as or more stimulatory than tetravalent ligands. This finding argues strongly against a critical role for clustering in triggering of NTRs.

4.2.4. Increasing ligand valency results in NTR downregulation

In the process of stimulating NTRs with tetravalent ligands I noticed that with SIRPβ1 and Siglec 14, stimulation could decrease at the highest numbers of binding sites per cell (Figure 4.7). This would lead to a bell-shaped curve and so these points were excluded to fit dose response curves. To investigate whether this effect was due to receptor downregulation I set up a stimulation assay with monovalent and tetravalent Strep-Tactin SpyCatcher and measured both the IL-8 response and NTR expression after the stimulation. It was clear that at higher levels of tetravalent ligand there was downregulation of both SIRPB1 and Siglec14 receptors, and this downregulation coincided with lower levels of IL-8 secretion (Figure 4.7A-D). These results confirm that the apparently lower stimulation by tetravalent ligand is result of enhanced NTR downregulation. In order to see if the downregulation was due to signalling or not, I performed the stimulation assay with and without the SFK inhibitor (A-419259 trihydrochloride). Interestingly, NTR downregulation still occurs in the presence of the SFK inhibitor suggesting that receptor ligand binding is sufficient to induce downregulation.

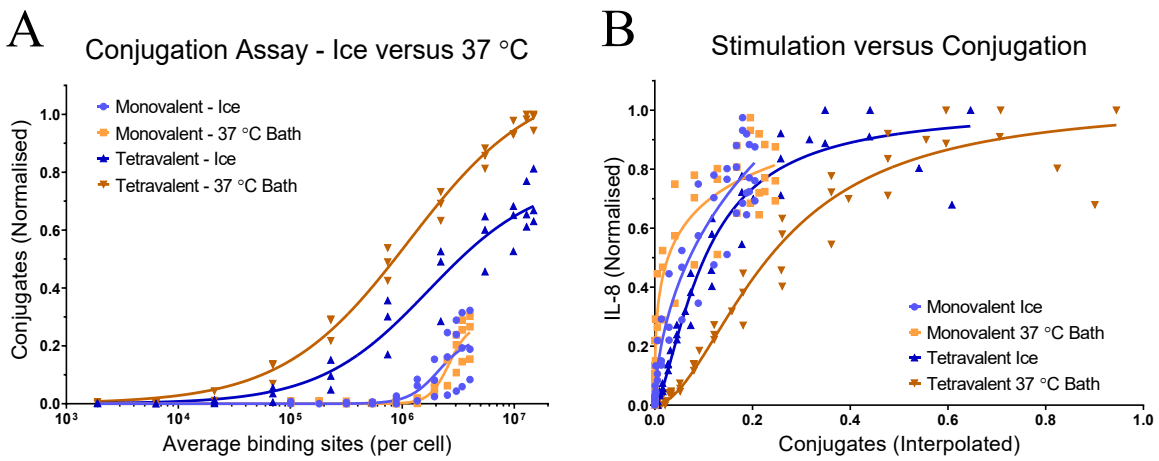


Figure 4.6: Conjugation assay on ice and at 37 °C in a water bath for monovalent versus tetravalent Strep-Tactin SpyCatcher highlights that the monovalent stimulation is still equal to or superior at equivalent conjugate formation

(A) Conjugation assay using the SIRPβ1 receptor and CHO short cells to compare the percentage of cells forming conjugates with either monovalent or tetravalent Strep-Tactin SpyCatcher on ice or at 37 °C in a water bath. The SFK inhibitor (A-419259 trihydrochloride) was added to all experimental conditions at a final concentration of 10 µM to prevent signalling. **(B)** The SIRPβ1 monovalent and tetravalent stimulation data from Figure 4.4A was plotted against the level of conjugation for both the ice and 37 °C water bath conditions. Data is combined from three biological replicates.

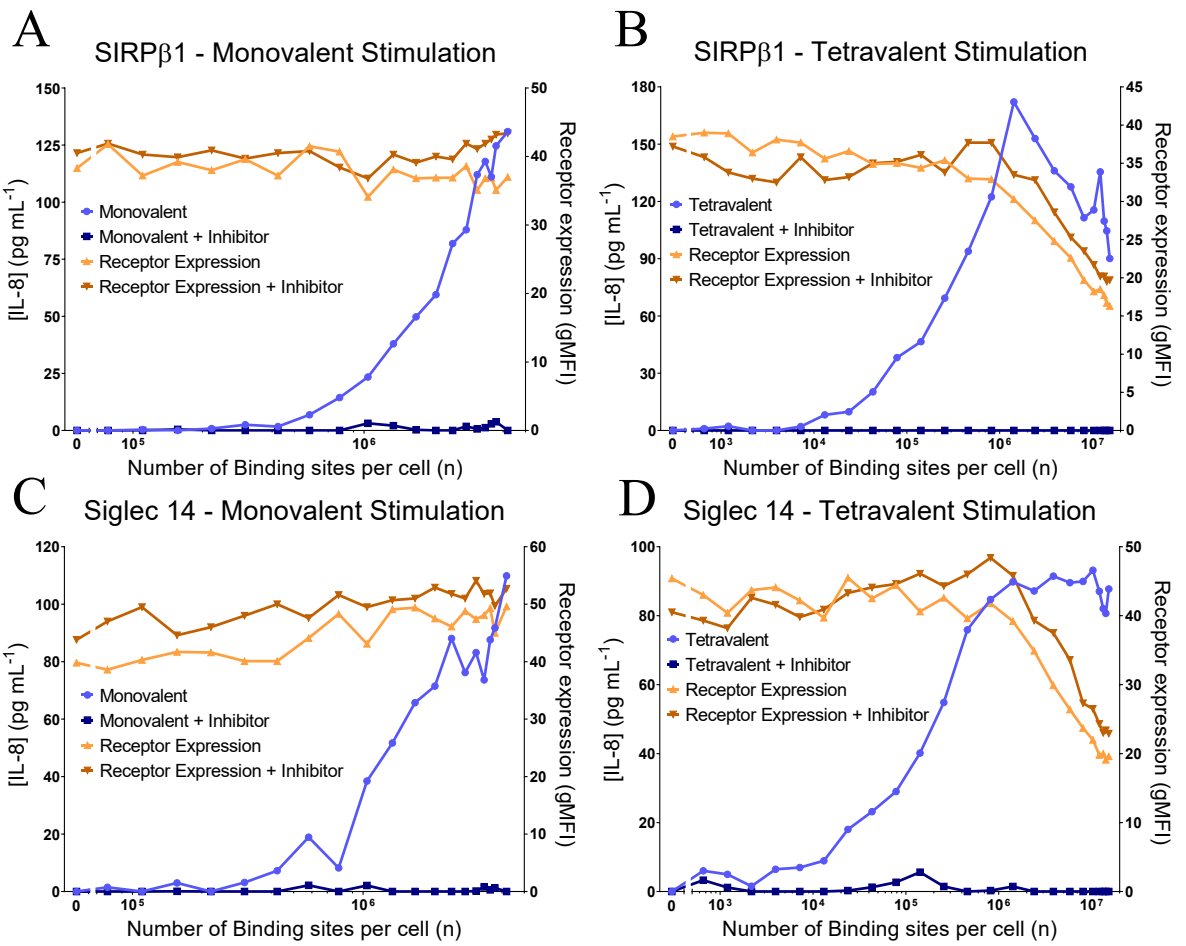


Figure 4.7: The SFK inhibitor (A-419259 trihydrochloride) prevents signalling from THP-1 cells but does not prevent receptor-ligand engagement measured by receptor downregulation

(A) THP-1 cells expressing the SIRPβ1 receptor were mixed with short ligand cells presenting monovalent Strep-Tactin SpyCatcher or in **(B)** tetravalent Strep-Tactin SpyCatcher either with or without the SFK inhibitor. Receptor expression was measured after the stimulation by staining the cells with an anti STII antibody, measured by flow cytometry. **(C and D)** Shows the same experiment with Siglec 14.

4.2.5. Trivalent Strep-Tactin is equivalent to tetravalent Strep-Tactin

Increasing the valency from monovalent to tetravalent produced a very strong increase in potency driven by increased conjugation. However, I had doubts as to whether four NTRs on the receptor cell surface could simultaneously bind tetravalent Strep-Tactin SpyCatcher presented on a ligand cell. To investigate this, I examined the effects of trivalent Strep-Tactin SpyCatcher produced by Eleanor Denham (Denham et al., 2019). I first compared the coupling of monovalent and trivalent Strep-Tactin SpyCatcher to short ligand cells (Figure 4.8A and B). As observed with tetravalent Strep-Tactin SpyCatcher, the average K_D measured for trivalent Strep-Tactin SpyCatcher was significantly lower than for monovalent Strep-Tactin SpyCatcher. This makes sense as the trivalent and tetravalent proteins are very similar and therefore have similar properties in terms of their isoelectric point. As seen with tetravalent Strep-Tactin SpyCatcher, and presumably because of quenching, the maximum fluorescence from the trivalent Strep-Tactin SpyCatcher was significantly lower than that of the monovalent. Therefore, the biotin-4-fluorescein assay was also used to calculate the average maximum number of binding sites per cell (Figure 4.8C). The maximum for the monovalent was the same as before and as expected the trivalent had approximately three times this number. This is shown in Figure 4.8D were dividing the trivalent values by three matches the monovalent maximum.

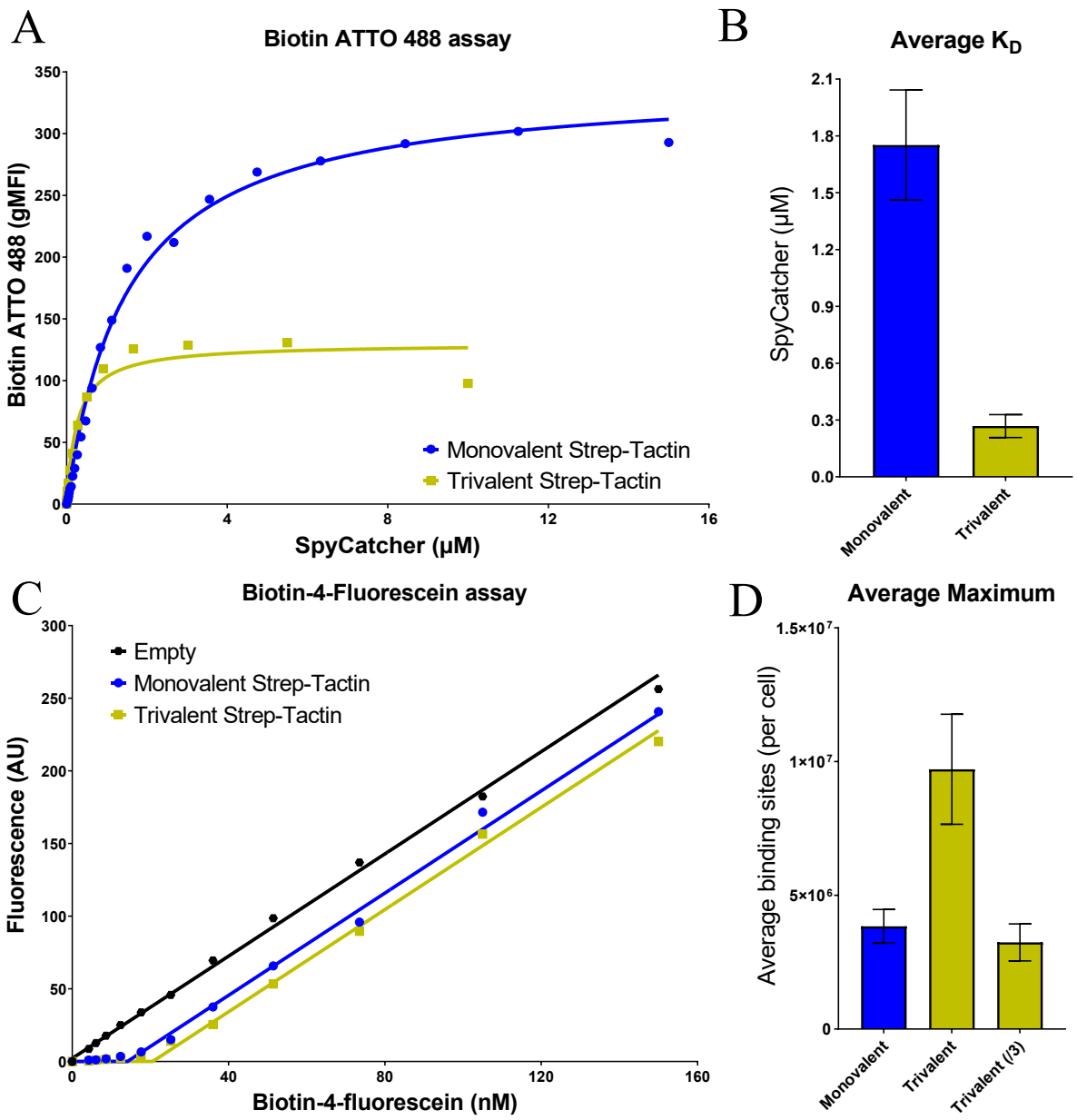


Figure 4.8: Calculating the average number of binding sites per short ligand cell coupled with monovalent or trivalent Strep-Tactin SpyCatcher

(A) A representative of a biotin ATTO 488 assay where CHO short cells were coupled with a serial dilution of monovalent or tetravalent Strep-Tactin SpyCatcher and mixed with biotin ATTO 488 which was measured by flow cytometry and the geometric mean plotted. The data was fit with a one site specific binding model and the K_D extracted from each curve. **(B)** The K_D values extracted from three independent experiments were plotted. **(C)** A representative of a biotin-4-fluorescein assay where CHO empty and short cells were incubated with a saturating concentration of monovalent (15 μM) or trivalent (10 μM) Strep-Tactin SpyCatcher. **(D)** The average maximum number of binding sites for three independent experiments was plotted. For comparison to monovalent the trivalent values were divided by three and re-plotted. Error bars show SD.

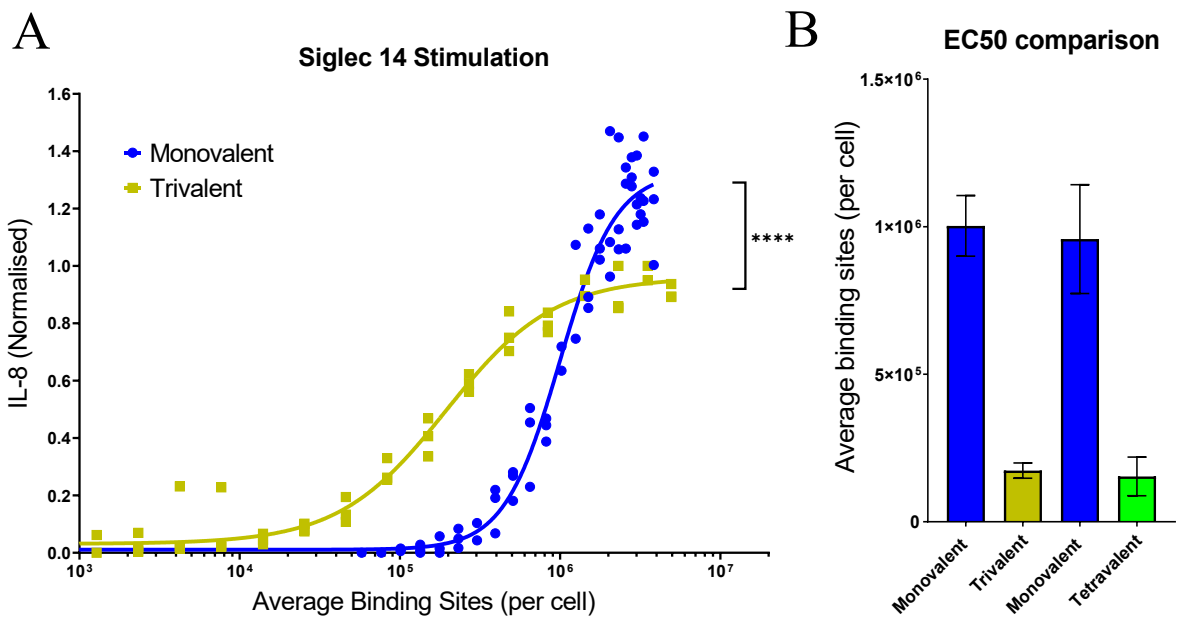


Figure 4.9: Stimulation assay comparison using monovalent or trivalent Strep-Tactin SpyCatcher coupled to short ligand cells

(A) Stimulation assay comparing Siglec 14 binding to short ligand cells coupled with monovalent or trivalent Strep-Tactin SpyCatcher, three biological replicates are shown with the data normalised to the maximum IL-8 release of the trivalent coupled ligand cells. An F test was used to compare the curves between the monovalent and trivalent conditions (**** = P <0.0001). **(B)** Comparison of the monovalent, trivalent, and tetravalent EC50 values for each biological replicate. The first two columns represent the data in A, the second two represent the data in Figure 4.4B.

The next step was to look at the functional effect of the trivalent Strep-Tactin. To reduce the complexity of the experiment I only performed the stimulation assay with the Siglec 14 receptor (Figure 4.9A). Like the tetravalent, the trivalent also produced a very potent response with a large shift in the EC50. Although the three repeats of trivalent and monovalent stimulations were performed on separate days to those for the tetravalent-monovalent stimulations, the data is highly reproducible. Importantly, the shift in EC50 observed with the trivalent Strep-Tactin was indistinguishable from the shift in EC50 previously observed with the tetravalent Strep-Tactin (Figure 4.9B). This strongly suggests that steric hinderance prevents all four binding sites of the tetravalent molecule from being occupied. While it would be informative to also analyse a divalent form of Strep-Tactin, we are not able to produce a divalent SpyCatcher fusion protein due to the need for additional purification steps

4.2.6. NTR activation is still sensitive to changes in ligand length even with multivalent ligands

So far, I have shown that making an NTR ligand multivalent enhances conjugation, presumably by enhancing binding. In Chapter 3 I showed that NTR activation was decreased by increasing ligand length, which points towards the KS mechanism playing a key role. It has been found that high affinity TCR ligands presented on an opposing membrane can cause triggering even with elongated ligands (Chen et al., 2017). This points towards a mechanism where lateral crowding of the NTRs in the receptor cell can lead to activation independent of receptor ligand dimensions. I therefore used the generic ligand system to test this lateral crowding effect by examining the effect of elongation on the tetravalent ligand.

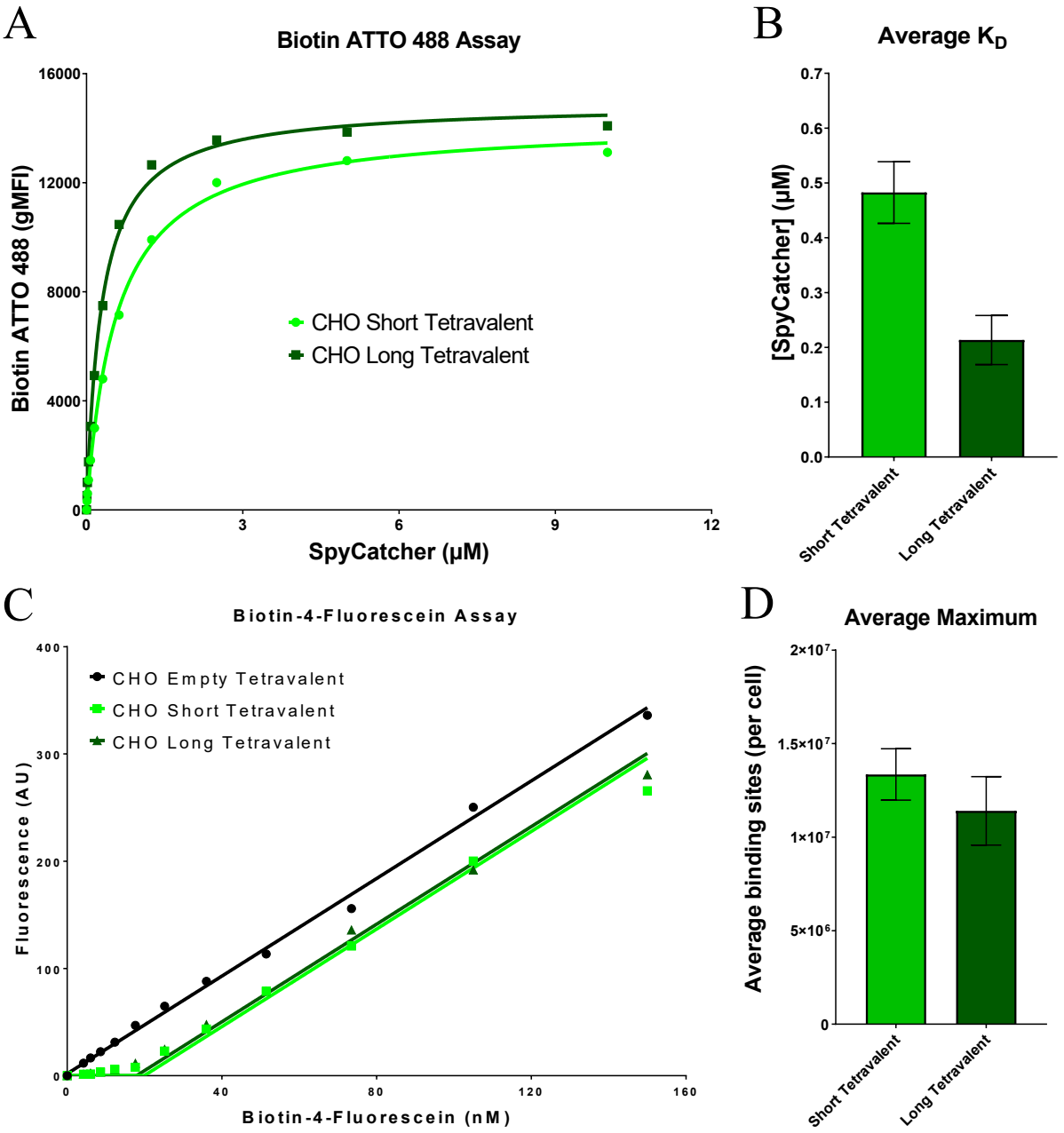


Figure 4.10: Calculating the average number of binding sites per ligand cell, short ligand or long ligand coupled with tetravalent Strep-Tactin SpyCatcher

(A) A representative biotin ATTO 488 assay where short ligand or long ligand cells coupled with a serial dilution of tetravalent Strep-Tactin SpyCatcher were mixed with biotin ATTO 488 which was measured by flow cytometry and the geometric mean plotted. The data was fit with a one site specific binding model and the K_D extracted from each curve. **(B)** The K_D values extracted from six independent experiments was plotted. **(C)** A representative of a biotin-4-fluorescein assay where empty ligand, short ligand and long ligand cells were incubated with a saturating concentration of tetravalent (10 μM) Strep-Tactin SpyCatcher. The cells were then mixed with a serial dilution of biotin-4-fluorescein and the remaining florescence measured. **(D)** The average maximum number of binding sites for six independent experiments were plotted. Error bars show SD.

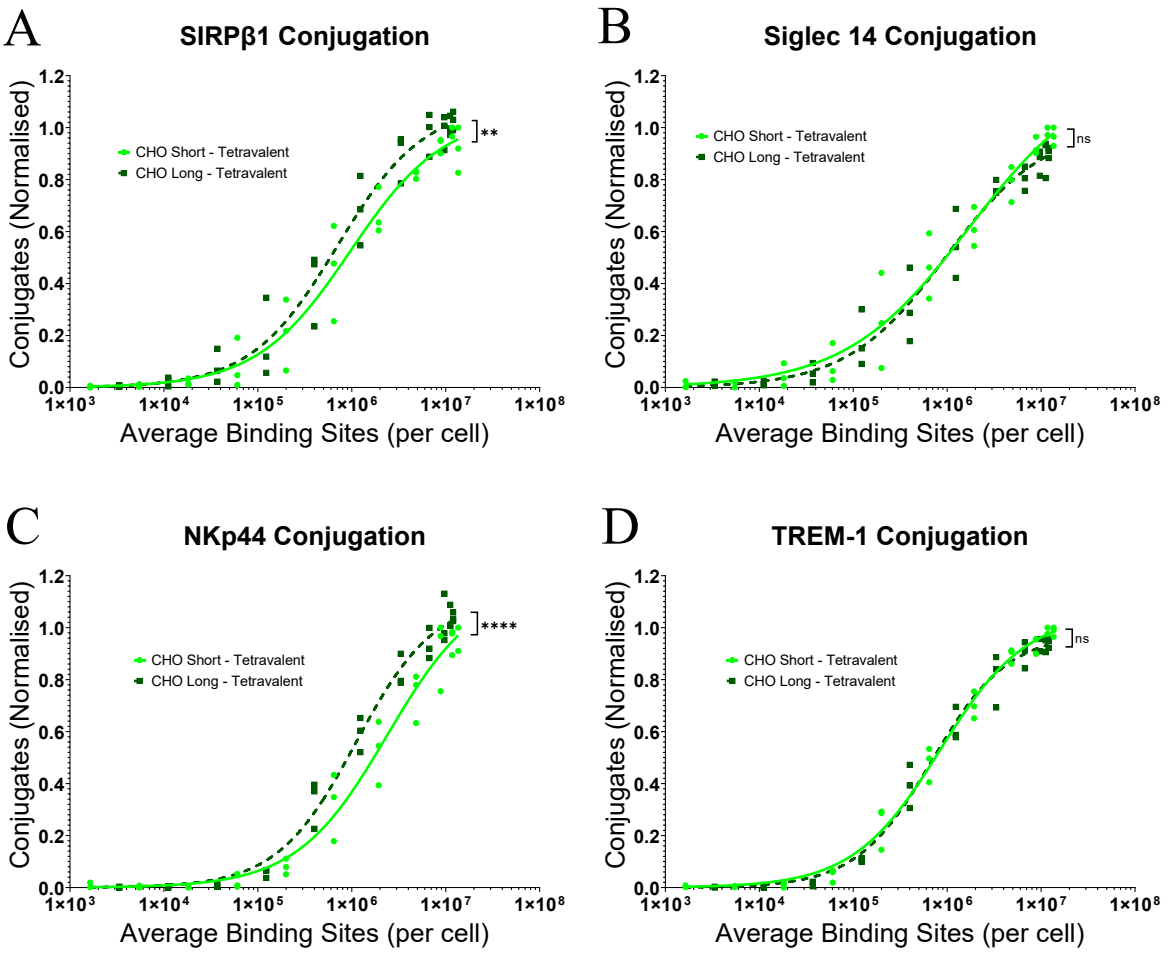


Figure 4.11: Conjugate formation of four receptors with short or long ligand cells coupled with tetravalent Strep-Tactin SpyCatcher

(A-D) Conjugation assay comparing short and long ligand cells coupled with tetravalent Strep-Tactin SpyCatcher. Four different DAP12 associating receptors (SIRPβ1, Siglec 14, NKp44 and TREM-1) were tested and the combined data from three biological replicates is shown with the data normalised to the maximum of the long ligand cells. An F test was used to compare the curves between the short and long conditions for each receptor (ns = not significant, ** = P <0.01, **** = P <0.0001).

In Figure 4.10 I quantify the average number of binding sites per short or long ligand cell coupled with tetravalent Strep-Tactin SpyCatcher. Again, I found that the coupling efficiency of the SpyCatcher was better with the long ligand cells (Figure 4.10A and B). Perhaps due to the greater accessibility of the SpyTag on the long ligand cells to couple the SpyCatcher. The maximum number of available binding sites at saturation calculated using the biotin-4-fluorescein assay was similar (Figure 4.10C and D).

Interestingly, Figure 4.11A-D shows that all four receptors tested showed very similar levels of conjugate formation with either the short or long ligand. For two of the receptors (SIRPβ1 and NKp44) there was still a small but significant improvement in conjugate formation with the long ligand compared to the short. This is again presumed to be due to better accessibility of the long ligand to bind the receptors. However, there was no significant difference between short and long ligands with Siglec 14 and TREM-1. This suggests that the stability of the cell-cell contact with tetravalent conjugation is such that ligand length becomes a much less significant factor in determining conjugation efficiency.

However, while there were no large differences in the levels of conjugate formation, there was still a clear improvement in IL-8 production when using short ligands in the stimulation assay. In Figure 4.12A-D the difference between the short and long tetravalent ligands is very clear for SIRPβ1, NKp44 and TREM-1, while for Siglec 14 it is not statistically different. Overall, this suggests that although the tetravalent SpyCatcher on the long ligand can hold the cells together very effectively, there is still a cost in terms of the ability of this ligand to stimulate the cells. This is consistent with the KS mechanism which requires short intermembrane distances to exclude tyrosine phosphatases with large ectodomain, such as CD45 and CD148. In this experiment although the cells are held together for a longer time, there is still room for the phosphates to move more freely in the contact, and this likely reduces the level of activation obtained. The exception of Siglec 14 could be due to this

receptor forming a dimer, as I hypothesised previously. Again, I see clear differences in the effect between the similarly sized SIRPβ1 and Siglec 14 NTRs, and the EC50 for Siglec 14 stimulation is shifted to the left of the other NTRs. In theory a multivalent receptor and ligand will lead to the formation of large densely packed aggregates through a zipper-like effect. This would make signalling less dependent on receptor ligand dimensions due to strong exclusion of phosphatases by lateral crowding. Plotting the stimulation data against conjugation in Figure 4.13A-D further highlights the clear superiority of short ligands versus long ligands with three out of the four receptors tested.

4.2.7. Initial characterisation of ligand anchors of different mobility and stability at the membrane

All experiments using the generic ligand thus far have used the short or long ligand which both contain the CD80 transmembrane region and cytoplasmic tail. It has been reported that the CD80 cytoplasmic tail influences its distribution within the immunological synapse (Doty & Clark, 1996; Tseng et al., 2005). Therefore, I wanted to firstly confirm my previous results looking at ligand valency and receptor clustering with a different ligand anchor. Secondly, I wanted to alter the mobility of the ligand and look to see if this would have any effect on receptor activation. Three new alternative SpyTag ligand anchors, which had been cloned and expressed in CHO cells by Jesse Goyette were tested experimentally. These anchors are based on the transmembrane and cytoplasmic regions of human LAIR-1, mouse CD43 and human CD52.

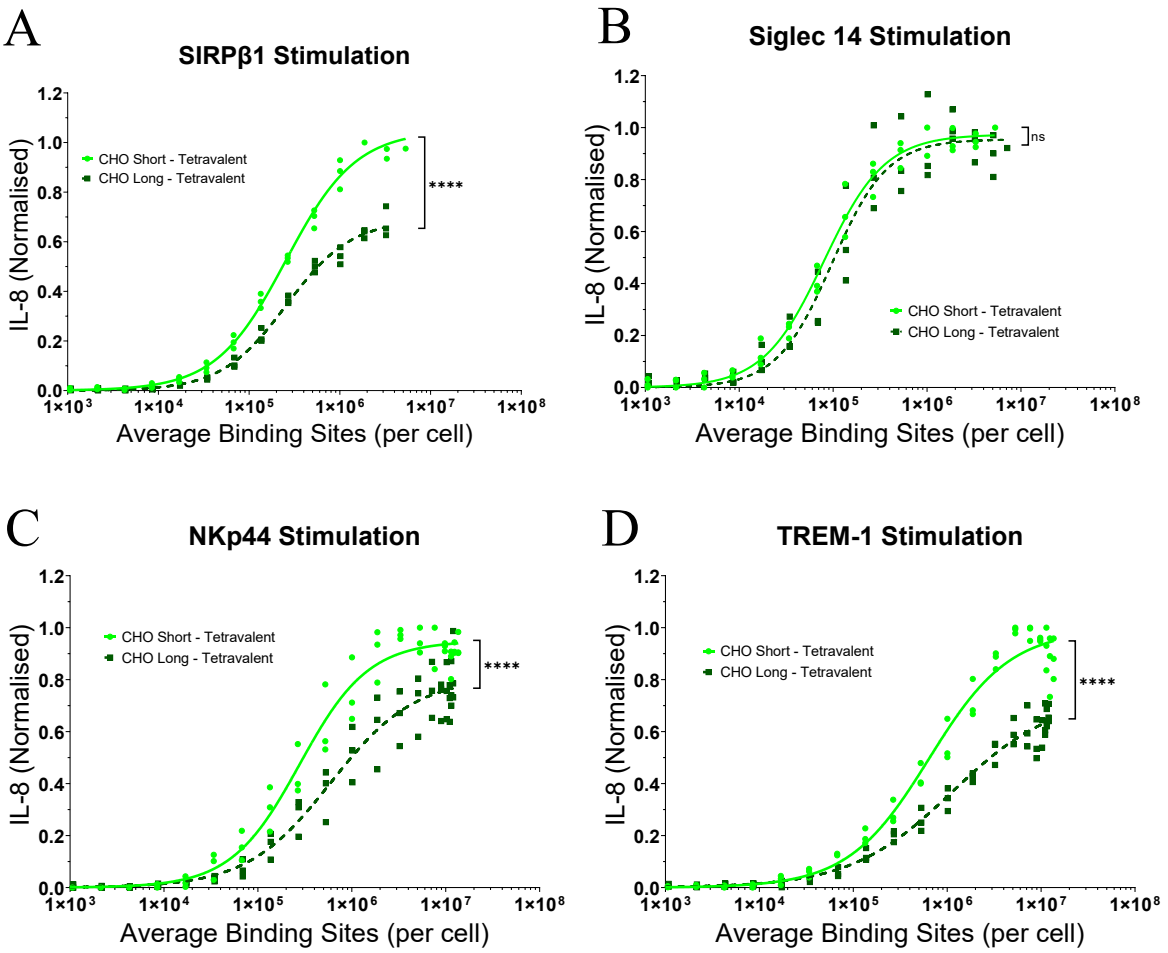


Figure 4.12: Stimulation assay comparison using tetravalent Strep-Tactin SpyCatcher coupled to short and long ligand cells

(A-D) Stimulation assay comparing short and long ligand cells coupled with tetravalent Strep-Tactin SpyCatcher. Four different DAP12 associating receptors (SIRPβ1, Siglec 14, NKp44 and TREM-1) were tested and the combined data from three biological replicates is shown with the data normalised to the maximum IL-8 release of the short ligand cells. An F test was used to compare the curves between the short and long conditions for each receptor (ns = not significant, **** = P <0.0001).

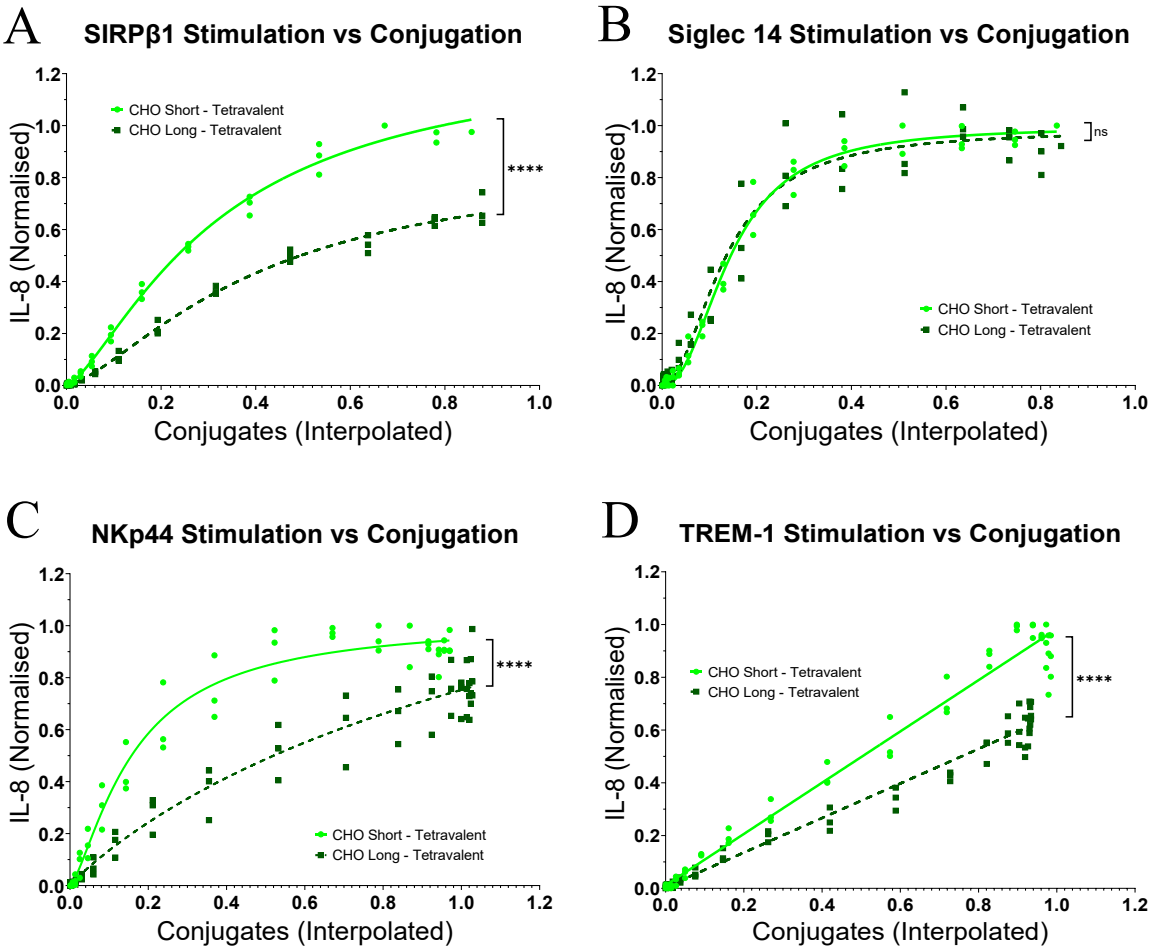


Figure 4.13: Stimulation versus conjugation assay comparison using tetravalent Strep-Tactin SpyCatcher coupled to short and long ligand cells

(A-D) Stimulation assay data plotted against conjugation assay data when comparing short and long ligand cells coupled with tetravalent Strep-Tactin SpyCatcher. For four different DAP12 associating receptors (SIRPβ1, Siglec 14, NKp44 and TREM-1). An F test was used to compare the curves between the short and long conditions for each receptor (ns = not significant, **** = P <0.0001). Data is combined from three biological replicates.

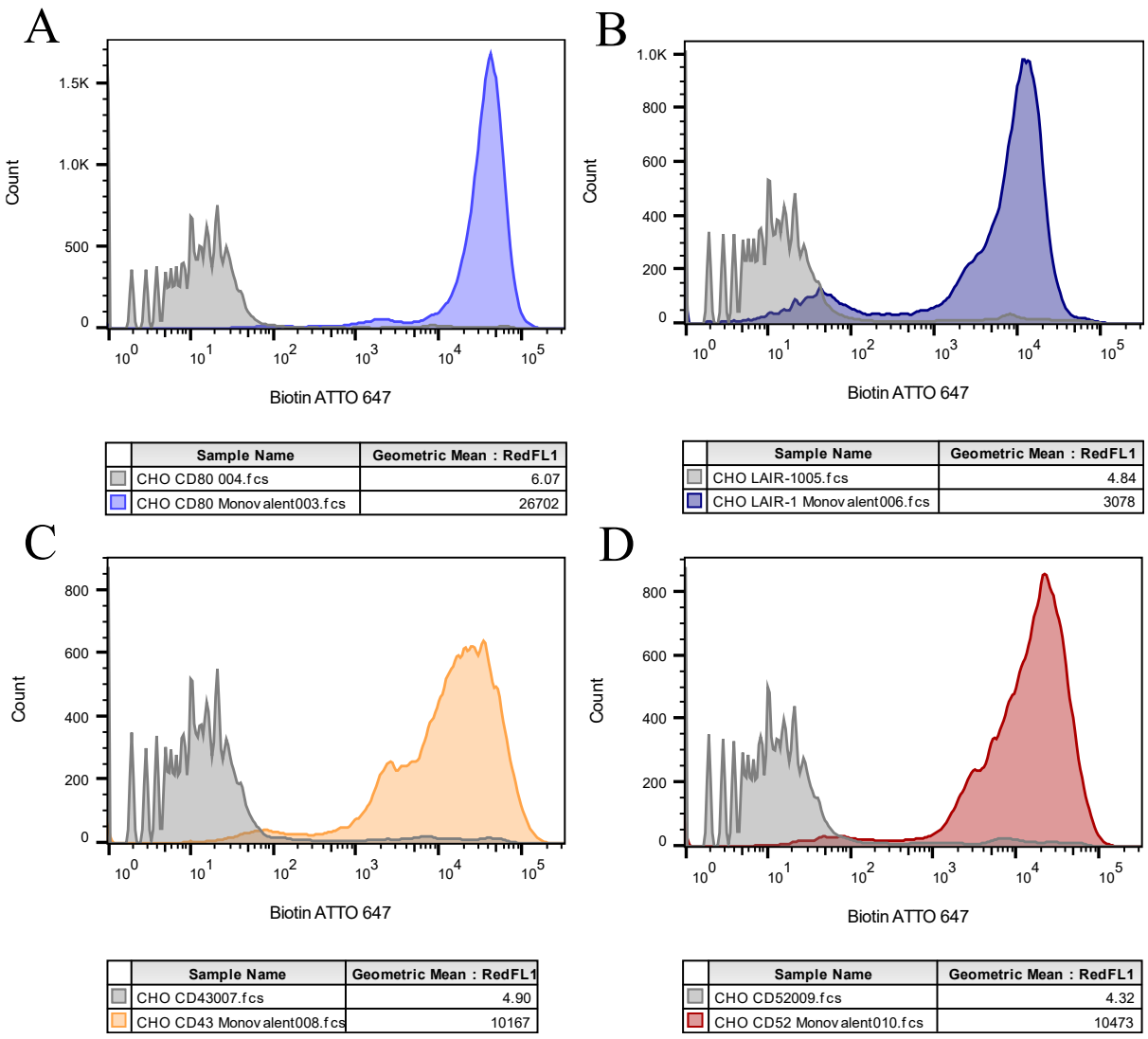


Figure 4.14: Expression levels of the four ligand anchors, CD80, LAIR-1, CD43 and CD52

(A-D) The expression level was checked by coupling CHO cells expressing the different ligand anchors with a saturating level (15 µM) of monovalent Strep-Tactin SpyCatcher. Biotin ATTO 647 was then used to assess the relative expression level of functional SpyTag on the surface using flow cytometry. Each panel has a negative peak (grey) which represents cells which were mixed with Biotin ATTO 647 but had not been coupled with monovalent Strep-Tactin SpyCatcher. Legend shows the geometric mean of each peak for comparison.

Initially, I coupled monovalent Strep-Tactin SpyCatcher to the four ligand anchors, added biotin ATTO 488 and used FACS to select for the highest expressing cells. Unfortunately, I was not able to get matching levels for all four ligand anchors and the original CD80 has a higher surface expression compared to the other three (Figure 4.14A-D). However, I decided to move forward and use my method to calculate the number of available ligands to normalise results between the different anchors.

I then coupled either monovalent or tetravalent Strep-Tactin SpyCatcher to the four ligand anchors and performed the biotin ATTO 488 assay to find the K_D (Figure 4.15A and B). The results reproduced the clear reduction in the K_D measured when coupling tetravalent Strep-Tactin SpyCatcher versus monovalent to short ligand cells. This difference is conserved for all four ligand anchors, which suggests that the anchor type is not causing this effect. This is consistent with the suggestion that this is the result of the greater negative charge of the monovalent Strep-Tactin SpyCatcher. The next step was to measure the average maximum number of binding sites per cell using the biotin-4-fluorescein assay with a saturating concentration of either monovalent or tetravalent protein coupled to short ligand cells. The results clearly show the difference in expression level of each ligand anchor: CD80 is expressed with the highest average number of available ligands per cell at 4.7×10^6 and LAIR-1 has the lowest average at 7.1×10^5 (Figure 4.15C). As before the maximum number of Strep-Tactin SpyCatcher proteins coupled to each anchor was the same for monovalent and tetravalent forms, as shown by dividing the average number of binding sites for the tetravalent by four and comparing it to the monovalent value.

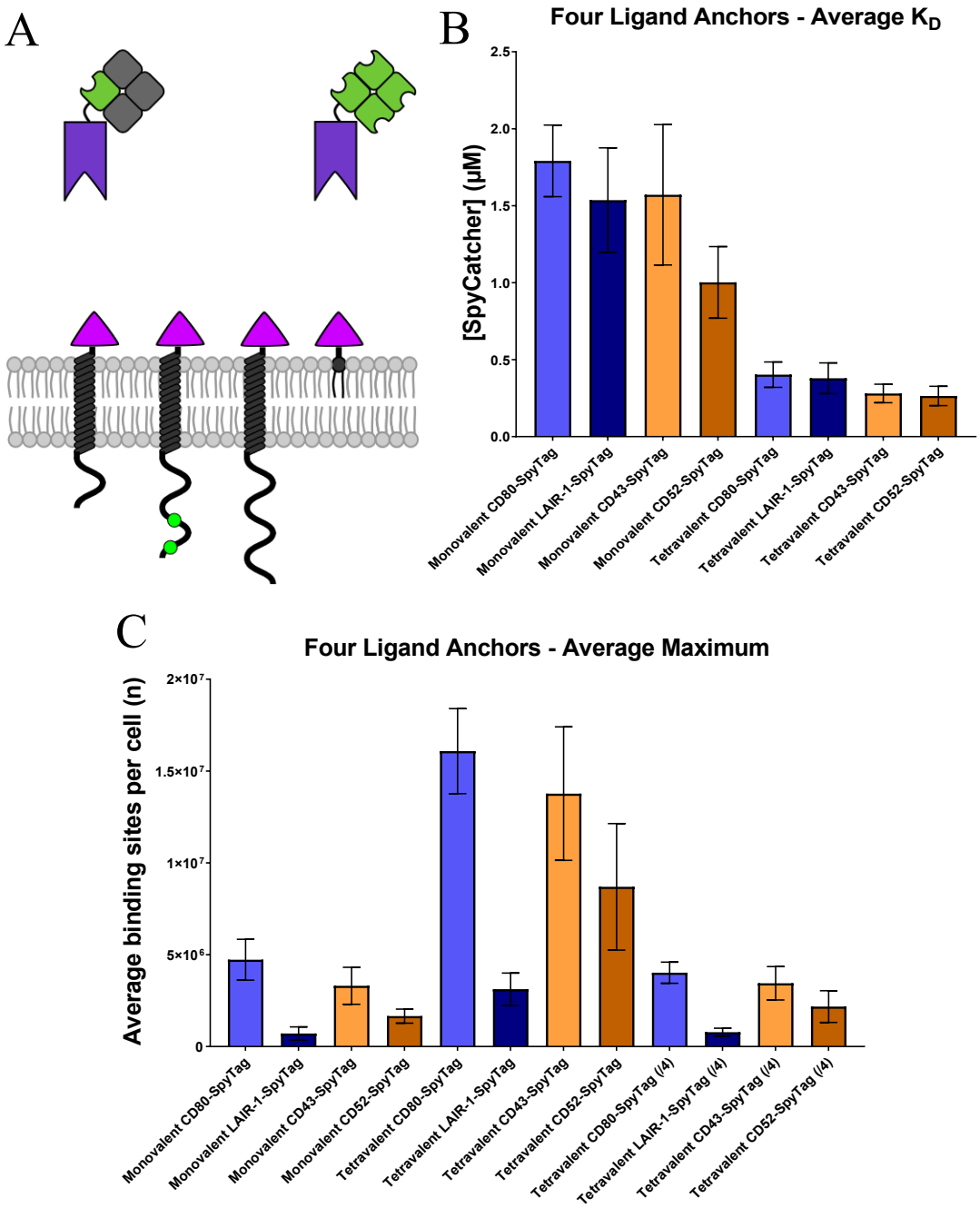


Figure 4.15: Calculating the number of biding sites per ligand cell, Short (CD80-SpyTag), LAIR-1-SpyTag, CD43-SpyTag and CD52-SpyTag coupled with monovalent or tetravalent Strep-Tactin SpyCatcher

(A) Schematic diagram of the four ligand anchors presenting the SpyTag, left to right: CD80-SpyTag, LAIR-1-SpyTag, CD43-SpyTag and CD52-SpyTag. All have trans membrane and cytoplasmic tails except CD52, which has a GPI lipid anchor. Each of the ligand anchors was coupled with either monovalent or tetravalent Strep-Tactin SpyCatcher. **(B)** The K_D values from nine independent biotin ATTO 488 assay experiments are plotted. **(C)** The average maximum number of binding sites from six independent biotin-4-fluorescein assay experiments. For comparison to monovalent the tetravalent values were divided by four and re-plotted (4 columns on the right).

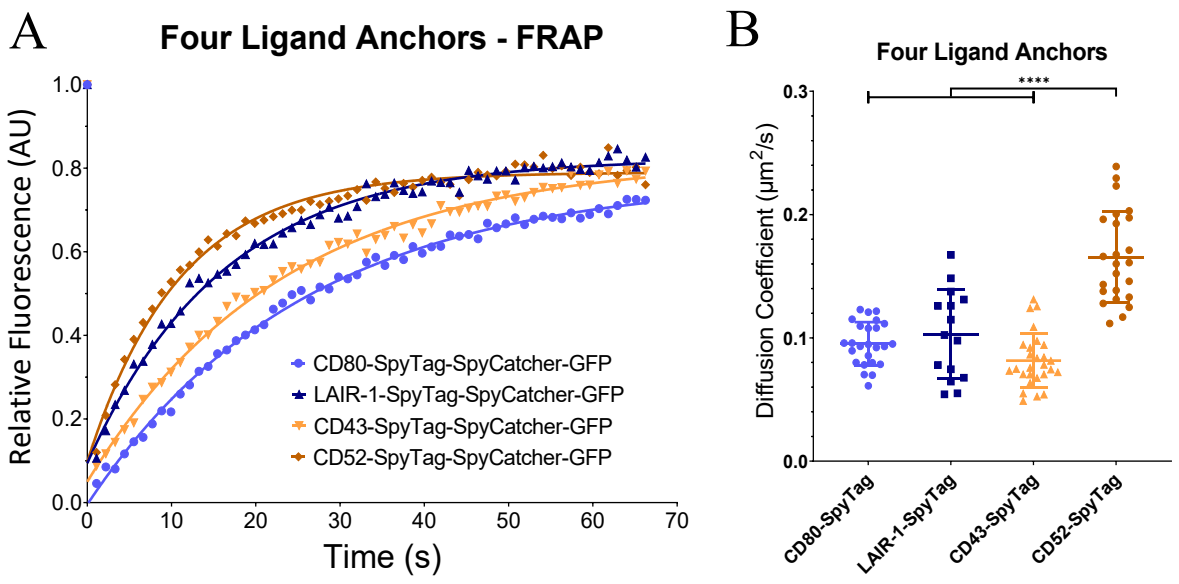


Figure 4.16: Measuring the mobility of four ligand anchors presenting the SpyTag

(A) One representative data set for each of the ligand anchors coupled with SpyCatcher-GFP measuring fluorescence recovery after photobleaching (FRAP). The data was fit with a one-phase association model and the half-life extracted from each curve. **(B)** Each data point represents the half-life for the fluorescence recovery of a single cell and was converted to a diffusion coefficient for comparison (see methods), error bars show SD. A one-way ANOVA was used and then Tukey's multiple comparison test to compare the diffusion coefficient between ligand anchors (**** = P <0.0001).

Next, I measured whether different ligand anchors had different mobility in the membrane. To do this I turned to a fluorescence recovery after photobleaching (FRAP) assay using SpyCatcher-GFP to couple to and specifically label the ligand anchors. Representative data for the recovery after photobleaching for each ligand anchor is shown in Figure 4.16A with the data normalised to the fluorescence before the bleach was performed. It was possible to bleach the fluorescence down to approximately 10 % of the pre- bleach intensity and the intensity would then recover to approximately 80 % of the pre- bleach intensity. To calculate the diffusion coefficient a one-phase association model was fit to each FRAP data set and the half-life extracted. This could then be converted to the diffusion coefficient (see methods) (Figure 4.16B).

The results show that only CD52 had a statistically different diffusion coefficient. CD52 has a GPI anchor, and so it was expected to have the highest mobility of all anchors on the surface of the membrane. As expected, the LAIR-1 anchor was very similar to that of CD80. However, it was disappointing that I did not see any distinguishable difference for CD43, which I had hoped would have a slower diffusion coefficient. This is likely due to the lack of cross reactivity between the mouse CD43 tail and hamster ERM proteins in the CHO cells. Nevertheless, as will be discussed in the following section, retaining the CD43 anchor in my assay was still informative.

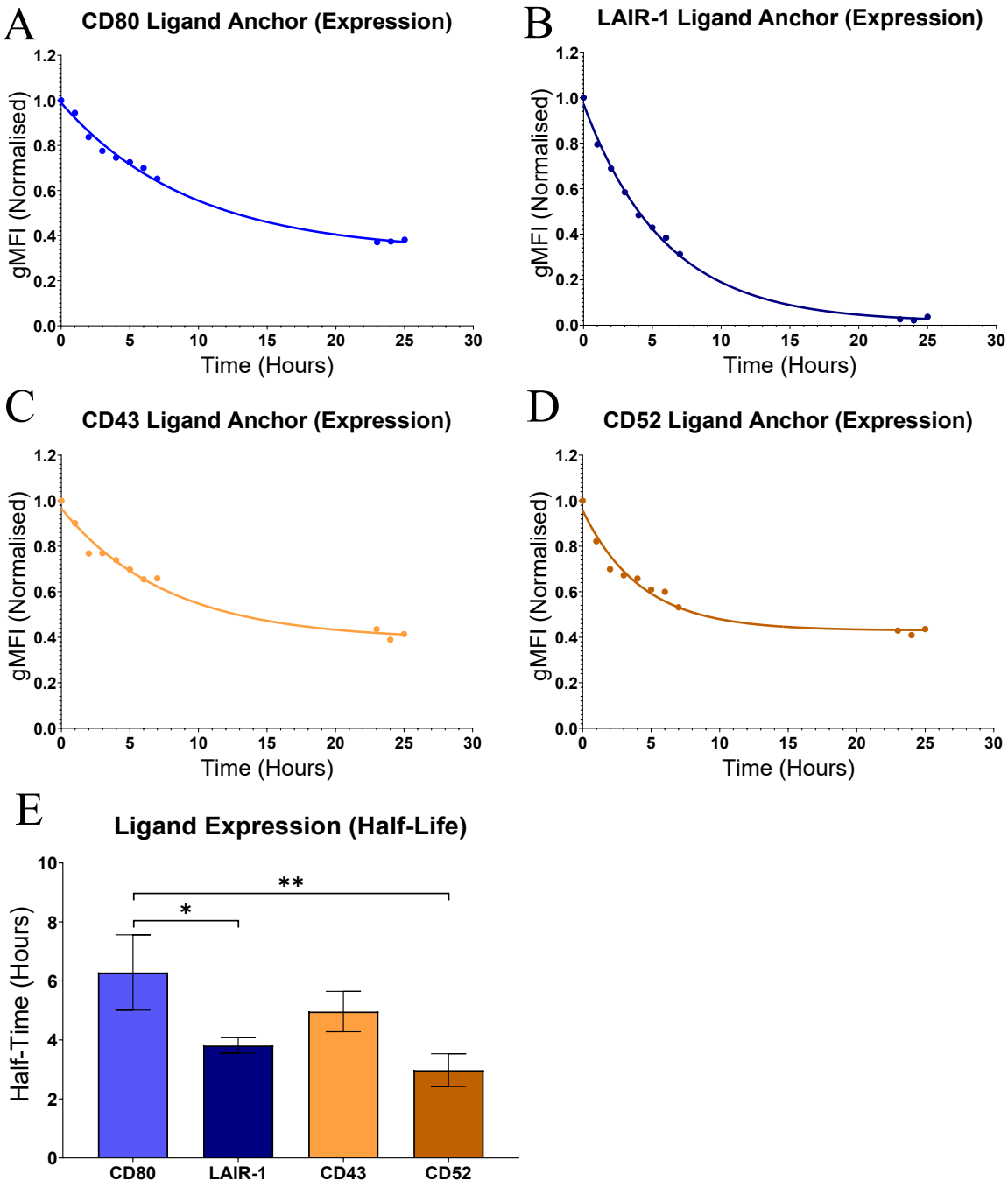


Figure 4.17: Time course assay showing the ligand anchor half-life on the plasma membrane

(A-D) CHO cells expressing the four ligand anchors, CD80, LAIR-1, CD43 and CD52 coupled with monovalent Strep-Tactin SpyCatcher. A sample of cells was taken each hour and stained with biotin ATTO 488 to assess the remaining ligand expression on the cell surface. The graphs show the relative level of ligand expression with the maximum normalised to time point zero. The data is a representative of three biological replicates and was fit with an exponential one phase decay model. **(E)** Combined half-life data for the three biological replicates. A one-way ANOVA was used and then Tukey's multiple comparison test to compare the diffusion coefficient (* = P <0.05). (** = P <0.01).

The next parameter I wanted to compare was the stability of each ligand anchor on the cell surface. This was achieved by coupling ligand cells with monovalent Strep-Tactin SpyCatcher and then incubating them at 37 °C. A sample of cells was taken at regular intervals and the remaining ligand expression assessed using the biotin ATTO 488 assay (see methods). Figure 4.17A-D shows the gradual loss of available ligand for each ligand anchor over a 25-hour period. The data was fit with an exponential one-phase decay model and the half-life extracted. Interestingly, three of the ligand anchor levels decreased over time but plateaued at a similar level of 40 % of the initial expression. However, LAIR-1 decreased down to undetectable levels during the same time. In Figure 4.17E half-life measurements extracted from three biological replicates are compared showing that the CD80 is the most stable anchor followed by CD43. These differences need to be considered when comparing any functional difference found with the stimulation assays as they are performed over the same time frame.

4.2.8. Altering ligand anchors has no clear impact on NTR activation

Moving on to look at the functional differences of altering the anchor mobility I focused on the monovalent Strep-Tactin SpyCatcher. This is because increasing the ligand valency could also influence the mobility once bound and complicate the results. Figure 4.18A shows the conjugation assay data with the four ligand anchors coupled with monovalent Strep-Tactin SpyCatcher binding to the SIRPβ1 receptor. As predicted, the different expression levels of the ligand anchors lead to changes in the maximum conjugate formation, but all four ligand anchors lead to similar levels of conjugate formation when normalised for the number of available binding sites.

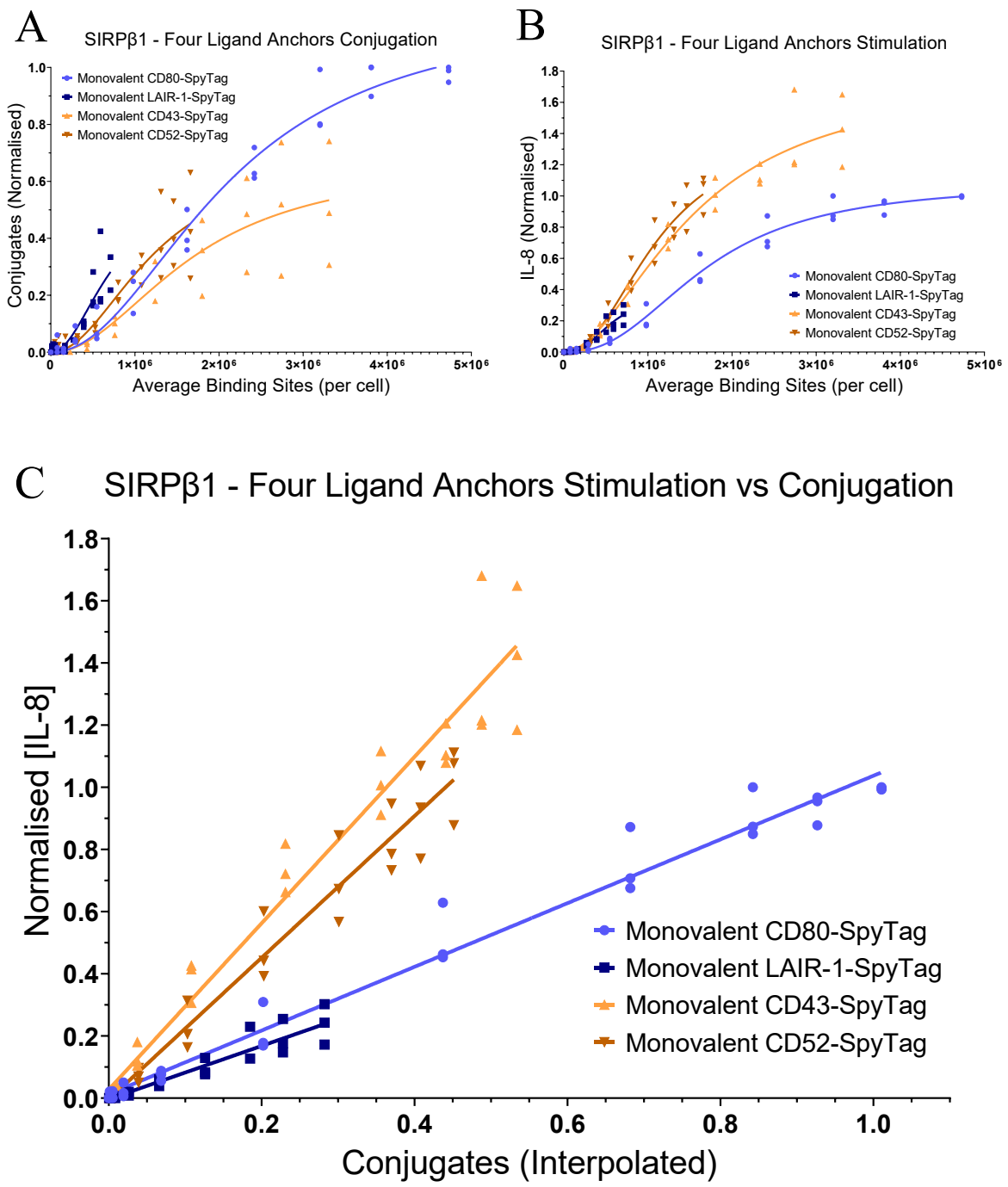


Figure 4.18: Comparison of the ability for four ligand anchors to form conjugates and stimulate the SIRPβ1 receptor with monovalent Strep-Tactin SpyCatcher

(A) Conjugation assay comparing CD80-SpyTag, LAIR-1-SpyTag, CD43-SpyTag and CD52-SpyTag ligand anchors coupled with monovalent Strep-Tactin SpyCatcher binding to cells expressing SIRPβ1. The combined data from three biological replicates is shown with the data normalised to the maximum of the CD80-SpyTag anchor cells. **(B)** Stimulation assay data compared in the same way as in A. **(C)** Combined data from A and B using the same method as previously described to show stimulation versus conjugation.

I next looked at stimulation assay data for the SIRPβ1 receptor and found very similar results except for the CD80 anchor, which had noticeable less IL-8 production for the same number of available ligands (Figure 4.18B). This observation of the CD80 anchor leading to less activation is therefore also apparent when the stimulation is plotted against levels of conjugation (Figure 4.18C). One possible explanation for this is that the increased stability of the CD80 on the surface leads to some receptor cells becoming exhausted more quickly thereby reducing the overall IL-8 response. An alternative explanation is that the CD80 anchor affects the distribution of the generic ligand within the immunological synapse (Doty & Clark, 1996; Tseng et al., 2005). The LAIR-1 anchor also displays low levels of stimulation but in this case, it is likely due to the instability of the anchor on the surface seen in Figure 4.17B, which leads to reduced signalling in the stimulation assay as the ligand is removed from the surface.

Importantly, monovalent Strep-Tactin SpyCatcher presented on CD43 and CD52 anchors both show a similar level of stimulation (Figure 4.18B and C). Both proteins are expressed to equivalent levels and show similar stability on the surface but have different mobility. This leads to almost identical levels of conjugate formation and stimulation seen in Figure 4.18A and B. This suggests that in this system the mobility of the ligand anchor does not influence receptor activation.

4.2.9. Confirmation that the CD80 ligand anchor does not influence receptor clustering

The second motivation for altering the ligand anchor was to confirm the key result I observed using the CD80 ligand anchor that despite less efficient conjugation, monovalent ligands trigger equal or stronger activation than trivalent and tetravalent ligands. There is evidence that the native CD80 protein, upon binding its receptor CD28, is then trafficked to a site in the immunological synapse distinct from the TCR (Tseng et al., 2005). This was found to be dependent on the CD80 cytoplasmic tail as truncating it allowed it to colocalise with the

TCR. This raised the question as to whether the unexpected finding that monovalent Strep-Tactin was as potent as tetravalent Strep-Tactin in stimulating through NTRs (Section 4.2.3) was a result of a special property of the CD80 anchor. Therefore, it was important to confirm these results with a ligand anchor other than CD80.

To do this I used the same four ligand anchors described above and coupled either monovalent or tetravalent Strep-Tactin SpyCatcher. I then performed conjugation assay experiments using the SIRPβ1 receptor and each of the ligand anchors (Figure 4.19A-D). I then performed the same comparison with stimulation assay experiments with each of the ligand anchors (Figure 4.19E-H). For both conjugation and stimulation assays there is visually very little difference in the profile of the CD80 and those of the other three ligand anchors. I also completed stimulation assays using the other three receptors (Siglec 14, NKp44 and TREM-1) and observed similar differences between monovalent and tetravalent stimuli (Figure 4.20A-D). For the SIRPβ1 receptor the stimulation data is plotted against the conjugation data in Figure 4.19I-L.

The CD52 anchor closely reproduces the observation with CD80 anchor in that monovalent stimulation is more potent than tetravalent stimulation for the same level of conjugation. The CD43 ligand anchor shows no statistical difference between the monovalent and tetravalent stimulus. The LAIR-1 anchor appears to favour the tetravalent but, given the limited overlap in the data due to the lower expression of this anchor on the cell surface, these data are not reliable.

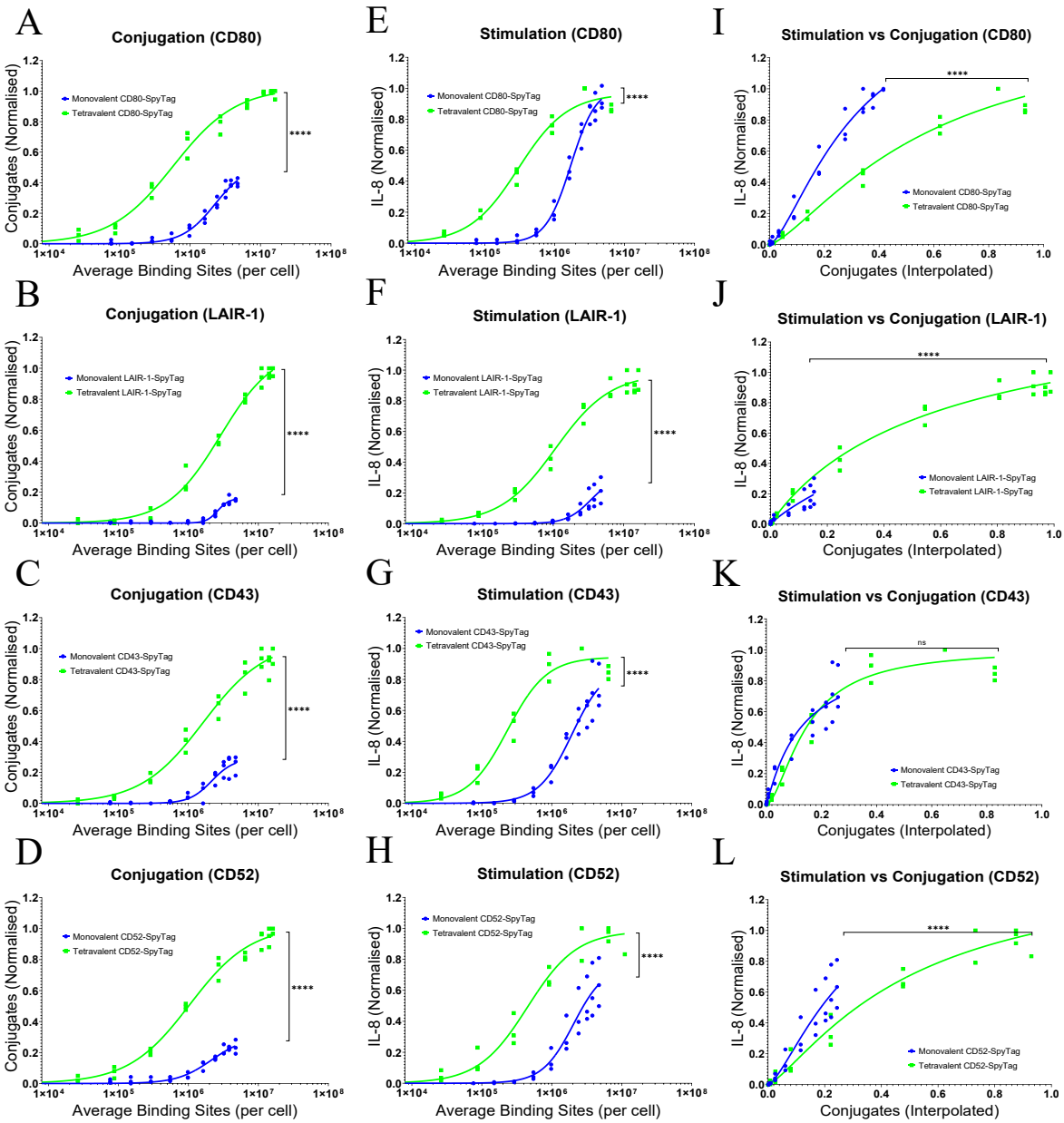


Figure 4.19: Conjugation, stimulation, and stimulation versus conjugation assay comparison for CD80-SpyTag, LAIR-1-SpyTag, CD43-SpyTag and CD52-SpyTag ligand anchors coupled with monovalent or tetravalent Strep-Tactin SpyCatcher interacting with cells expressing SIRPβ1 receptor

(A-D) Conjugation assay, **(E-H)** Stimulation assay and **(I-J)** Stimulation versus conjugation assay comparing the four ligand anchors coupled with monovalent or tetravalent Strep-Tactin SpyCatcher. Each data set combines three biological replicates. An F test was used to compare the curves between the monovalent and tetravalent conditions for each ligand anchor (ns = not significant, **** = P <0.0001).

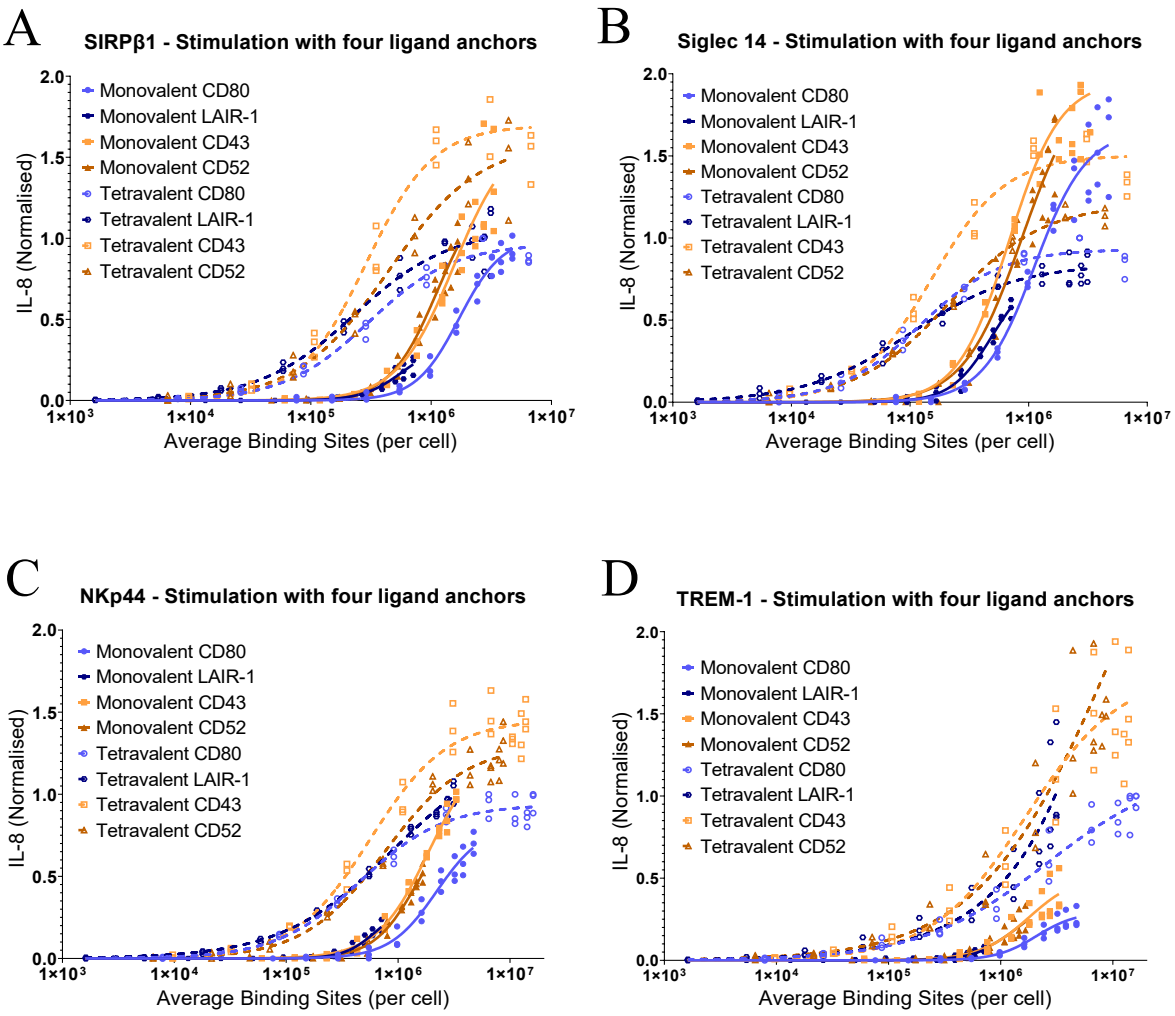


Figure 4.20: Stimulation comparison of SIRPβ1, Siglec 14, NKp44 and TREM-1 with ligand cells expressing CD80-SpyTag, LAIR-1-SpyTag, CD43-SpyTag and CD52-SpyTag coupled with either monovalent or tetravalent Strep-Tactin SpyCatcher

(A-D) Stimulation assay showing the combined data from three biological replicates is shown with the data normalised to the maximum IL-8 release of the CD80-Spy ligand cells coupled with tetravalent Strep-Tactin SpyCatcher.

Overall, it can be concluded that the monovalent stimulation is either equivalent to or better than the tetravalent using different ligand anchors other than CD80. This is evidence against clustering being a key mechanism for SIRPβ1 activation. However, receptor-ligand engagements that can utilise multivalent interactions will result in strong responses at lower numbers of receptor ligand complexes. This effect could be exploited when producing therapeutic receptors for immunotherapy.

4.2.10. Altering the affinity of the ligand shows evidence that kinetic proof reading is important for NTR activation

Finally, to test the ability of our NTRs to discriminate against antigens of different affinity I produced two more SpyCatcher fusion proteins using streptavidin instead of Strep-Tactin for the active STII binding sites. Firstly, I produced monovalent streptavidin SpyCatcher which comprises of an active streptavidin SpyCatcher subunit combined with three dead streptavidin units. An example anion exchange chromatography run is shown in Figure 4.21A. The individual subunits and peaks 1-3 were then run on an SDS-PAGE gel. Figure 4.21B shows the large number of contaminating proteins which are removed through anion exchange. The pure protein is contained within ‘peak 3’, with ‘peak 2’ corresponding to a degradation product most likely consisting of a degraded streptavidin SpyCatcher subunit. Close peaks like this are difficult to separate as there is a significant amount of overlap under the curve. However, it was possible to remove most of this contaminating protein and the pure protein was then tested for activity using the biotin-4-fluorescein assay (Figure 4.21C). Here the inflection point is at 35 nM when it would be predicted to be at 20 nM. This is likely the result of experimental or fitting errors. It is notable that the titration data do not fall on a straight line.

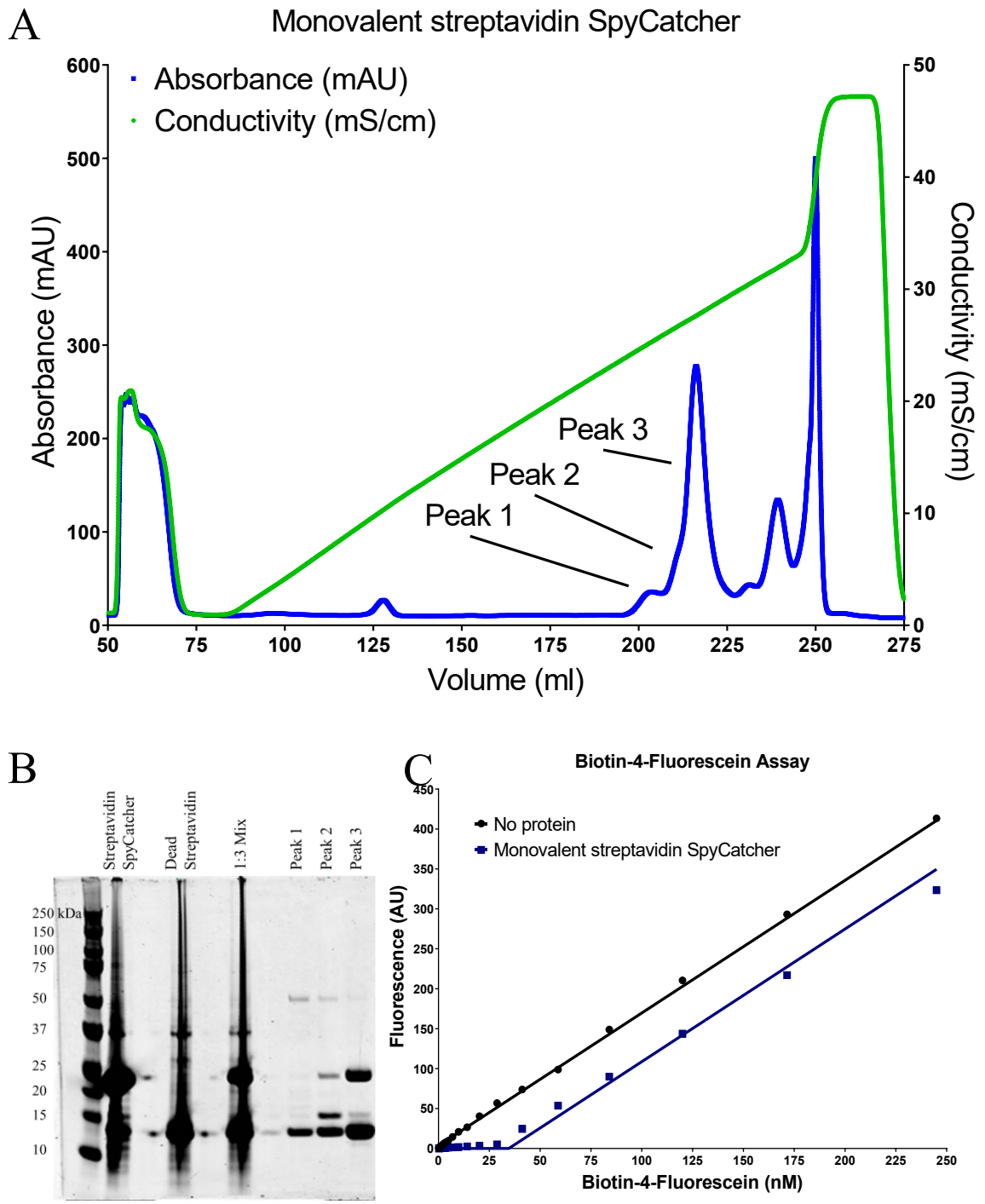


Figure 4.21: Purification of monovalent streptavidin SpyCatcher

(A) Representative anion exchange chromatography run to purify monovalent streptavidin SpyCatcher. **(B)** SDS-PAGE gel, lane 1, solubilised streptavidin SpyCatcher, Lane 2, solubilised dead streptavidin, Lane 3, a 1:3 molar ratio of streptavidin SpyCatcher mixed with dead streptavidin, Lanes 4-6, peaks 1-3 corresponding to the peaks shown in A. Peak 3 corresponds to the purified monovalent streptavidin SpyCatcher. The two bands represent one molecule of streptavidin SpyCatcher for every three molecules of dead streptavidin (calculated by densitometry). **(C)** Biotin-4-fluorescein assay using 20 nM purified monovalent streptavidin SpyCatcher.

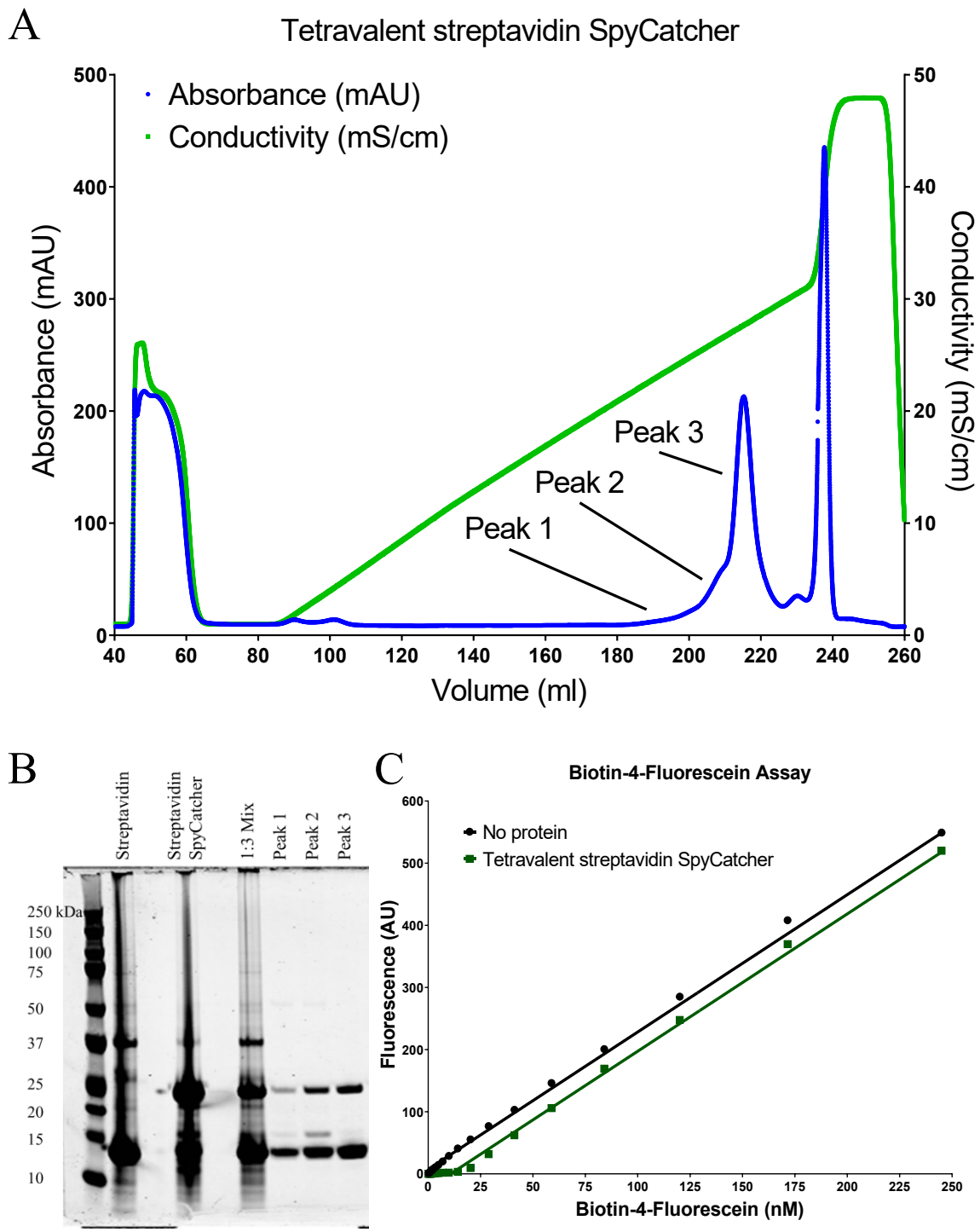


Figure 4.22: Purification of tetravalent streptavidin SpyCatcher

(A) Representative anion exchange chromatography run to purify tetravalent streptavidin SpyCatcher. **(B)** SDS-PAGE gel, lane 1, solubilised streptavidin, Lane 2, solubilised streptavidin SpyCatcher, Lane 3, a 1:3 molar ratio of streptavidin SpyCatcher mixed with streptavidin, Lanes 4-6, peaks 1-3 corresponding to the peaks shown in A. Peak 3 corresponds to the purified tetravalent streptavidin SpyCatcher. The two bands represent one molecule of streptavidin SpyCatcher for every three molecules of streptavidin (calculated by densitometry). **(C)** Biotin-4-fluorescein assay using 5 nM purified tetravalent streptavidin SpyCatcher.

Based on my work showing that increasing the valency of the Strep-Tactin ligand greatly increased its potency by enhancing conjugation, I also produced a tetravalent streptavidin SpyCatcher to confirm this result with a lower affinity ligand. Its purification is shown in Figure 4.22A and B and follows the same pattern as the monovalent streptavidin. Here the biotin-4-fluorescein assay measured an inflection at 11 nM which considering experimental error, is again close to the predicted value of 20 nM due to there being 4 binding sites per molecule (Figure 4.22C).

Streptavidin has approximately ten fold lower affinity for STII compared to Strep-Tactin (Voss & Skerra, 1997). To test the functional effect of such a change in affinity I designed a number for experiments which were carried out by Katy Lillie, a medical student working in our lab under my supervision. Firstly, I wanted to check that we could couple these new SpyCatcher fusion proteins to the ligand cells and measure the average binding sites per cell. This was done in the same way as has been described in previous sections, using the biotin ATTO 488 and biotin-4-fluorescein assays. In these experiments we compared the four different SpyCatcher fusion proteins containing Strep-Tactin or streptavidin in either monovalent or tetravalent form (Figure 4.23A). The biotin ATTO 488 assay reproduced comparable K_D values for Strep-Tactin SpyCatcher binding to short ligand cells, with the average K_D value for the streptavidin SpyCatcher fusion protein falling in between (Figure 4.23B). The biotin-4-fluorescein assay also matched the expected maximum number of binding sites for the monovalent and tetravalent Strep-Tactin. The monovalent streptavidin had a similar maximum, but the tetravalent streptavidin maximum was approximately one third lower than expected Figure 4.23C and D). This may be due to several factors, such as the quality of the protein and its stability. Fortunately, there is still a very large number of available ligands for the receptors to bind and these differences can be accounted for using my method to calculate the average binding sites per cell.

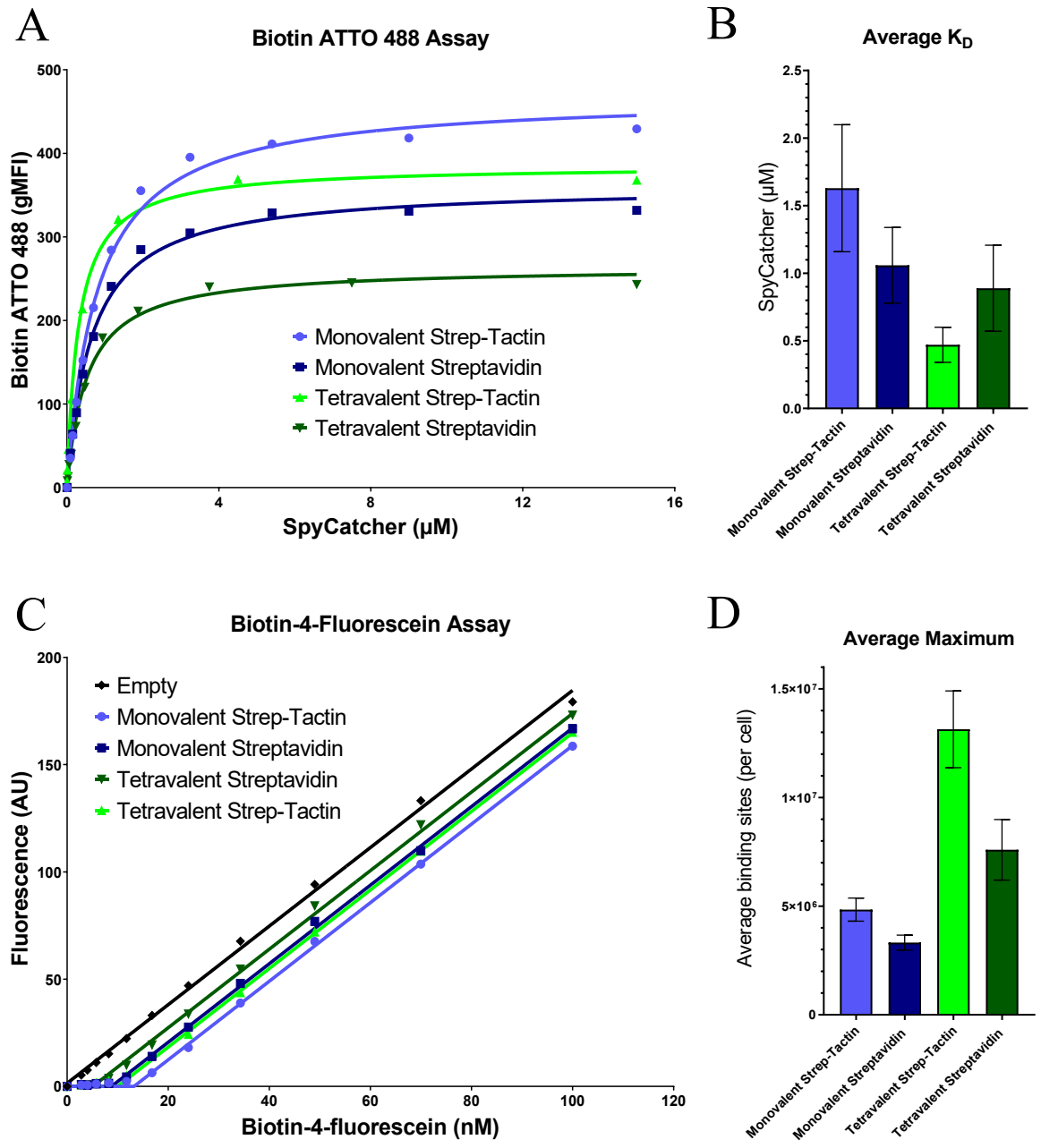


Figure 4.23: Calculating the average number of binding sites per ligand cell, short ligand coupled with monovalent or tetravalent Strep-Tactin or streptavidin SpyCatcher

(A) A representative biotin ATTO 488 assay where short ligand cells coupled with a serial dilution of monovalent Strep-Tactin, monovalent streptavidin, tetravalent Strep-Tactin or tetravalent streptavidin SpyCatcher are mixed with biotin ATTO 488 which was measured by flow cytometry and the geometric mean plotted. The data was fit with a one site specific binding model and the K_D extracted from each curve. **(B)** The K_D values extracted from five independent experiments was plotted. **(C)** A representative of a biotin-4-fluorescein assay where short ligand cells were incubated with a saturating concentration of monovalent Strep-Tactin, monovalent streptavidin, tetravalent Strep-Tactin or tetravalent streptavidin SpyCatcher (15 μM). The cells were then mixed with a serial dilution of biotin-4-fluorescein and the remaining florescence measured. **(D)** The average maximum number of binding sites for three independent experiments were plotted. Data generated by Katy Lillie.

To reduce the complexity when testing the new SpyCatcher fusion proteins we decided to focus on just two receptors: SIRPβ1 and Siglec 14. The results from conjugation assays again showed significantly better conjugation with the tetravalent Strep-Tactin compared the monovalent (Figure 4.24A and B). Interestingly, the monovalent streptavidin did not produce any measurable conjugates with SIRPβ1 and only very low levels with Siglec 14. Conversely, tetravalent streptavidin produced a level of conjugation comparable to that of monovalent Strep-Tactin. This highlights the ability of the multivalent ligands to greatly shift the potency of the conjugation response.

The data from the stimulation assay for all four SpyCatcher fusion proteins followed a similar pattern highlighting that conjugation level is a good indicator of stimulation potential (Figure 4.24C and D). SIRPβ1 did not show any response to monovalent streptavidin. Siglec 14 is more sensitive and did show a small amount of activation and conjugate formation at the highest number of available ligands. However, due to this low level of response monovalent streptavidin was excluded from further analysis.

When we plotted the stimulation against conjugation the responses from all three SpyCatcher fusion proteins collapsed down on top of each other (Figure 4.24E and F). Therefore, the level of stimulation can be fully accounted for by the level of conjugation. However, to produce the same conjugate formation with the monovalent Strep-Tactin and tetravalent streptavidin there needs to be many more individual binding events over a given time period with the tetravalent streptavidin. This large discrepancy in the number of receptor ligand binding events still leads to the same degree of signalling. This means the higher affinity interaction of the Strep-Tactin is more productive in initiating signalling per binding event. These results show that an increase in valency can compensate for a decrease in affinity.

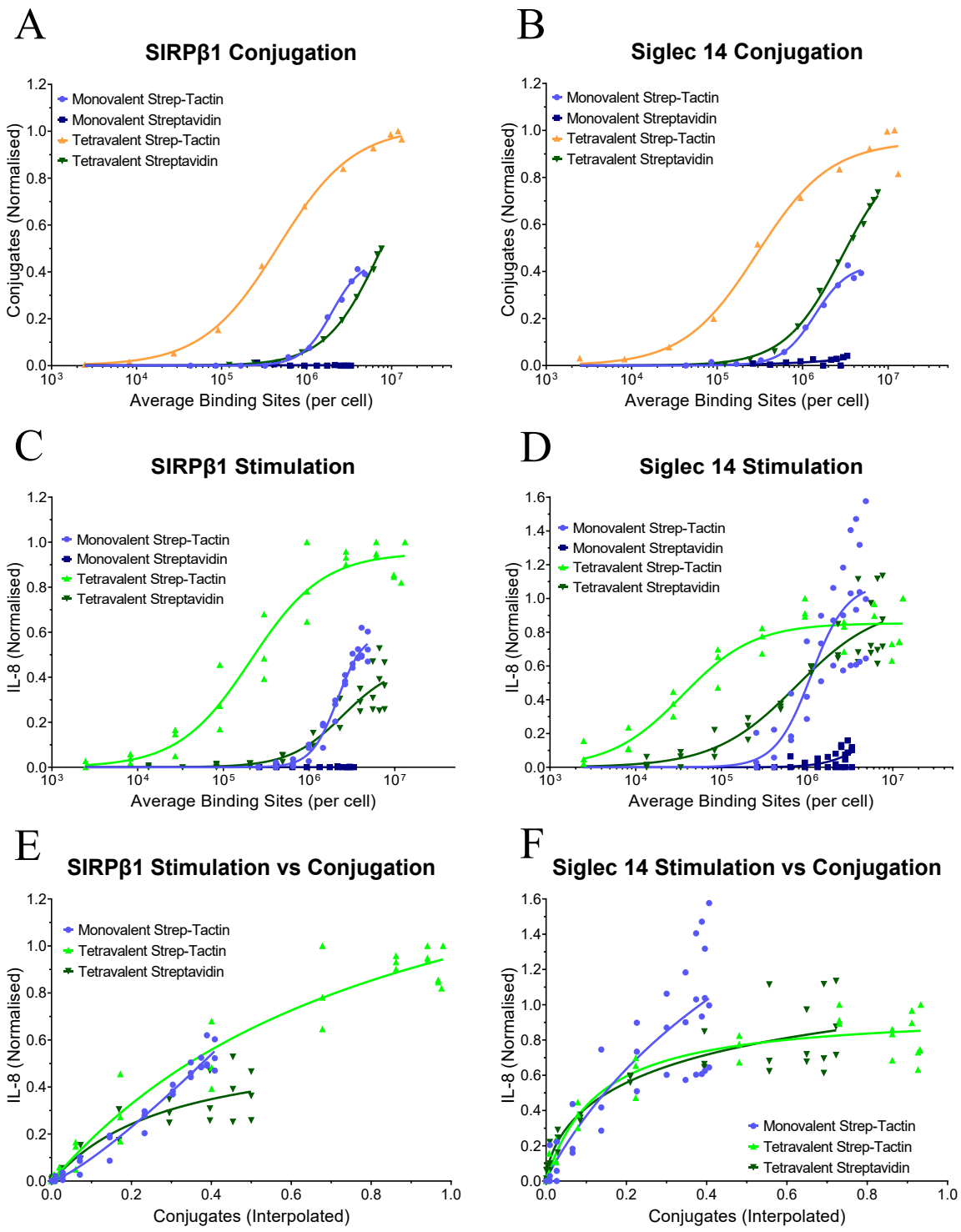


Figure 4.24: Comparison of SIRPβ1 and Siglec 14 behaviour when engaged with monovalent or tetravalent Strep-Tactin or streptavidin

(A and B) SIRPβ1 and Siglec 14 conjugation assay with short ligand cells coupled with monovalent or tetravalent Strep-Tactin or streptavidin SpyCatcher. **(C and D)** Stimulation assay measuring IL-8 release with short ligand cells coupled with monovalent or tetravalent Strep-Tactin or streptavidin SpyCatcher. **(E and F)** The same method as described before was used to plot the stimulation data against the conjugation data. Data is combined from three biological replicates. Data generated by Katy Lillie.

It is also interesting to compare the tetravalent Strep-Tactin and tetravalent streptavidin response because there is a very large shift in the potency. This is due to the approximate ten-fold decrease in affinity of streptavidin versus Strep-Tactin showing that these NTRs are sensitive to altering the receptor ligand affinity. In principle it is possible to determine the discriminatory power of cell surface receptors by measuring the change in EC50 when the affinity is changed. Unfortunately, because monovalent streptavidin produced no stimulation, it was not possible to estimate the discriminatory power using monovalent ligands (Pettmann et al., 2021). There was a 12-fold and 22-fold difference in EC50 for SIRPβ1 and Siglec 14 stimulation respectively between the tetravalent Strep-Tactin and streptavidin ligands. This is similar to the approximate 10-fold different in K_D, suggesting that these NTRs have a discriminatory power of approximately one. This is typical of cell-surface receptors but significantly lower than the discriminatory power of the TCR which has been found to be two (Pettmann et al., 2021), which would represent a 100-fold change between the K_D and the EC50 for the stimulation.

Taken together this data shows that the duration of the binding event is key to its functional effect. The tetravalent Strep-Tactin can form very stable long-lived contacts which translate into strong cellular activation. However, the monovalent Strep-Tactin can still achieve the same functional response when conjugation is taken into account. The lower affinity tetravalent streptavidin also shows the same functional response but requires the increased valency to create many interactions each of which is less productive to maintain cell-cell contact.

4.3. Discussion

In this chapter I have shown that NTRs are sensitive to changes in the valency and affinity of their ligands but not to their mobility. I found that increases in the valency of the ligand substantially increased conjugation, presumably through avidity effects. A striking finding

was that, when controlling for enhanced cell-cell conjugation, multivalent ligands were no better or worse at stimulating through NTRs. This argues against a critical role for NTR clustering during receptor triggering, which is consistent with the fact that the vast majority of NTR ligands are monovalent (Dushek et al., 2012).

To generate receptor clustering this system requires the use of multivalent ligands rather than modifying the receptor. However, the majority of NTR ligands are monovalent. While I assume that this is equivalent to directly clustering the receptors it may not be. Therefore, it may be useful to confirm the results in this chapter using an inducible system such as the rapamycin system (Hui & Vale, 2014). However, this would require the modification of the NTR tail to incorporate the FKBP and a second construct with the same NTR expressing its partner the FRB. The addition of rapamycin would then link the two receptors together and induce clustering. However, this would be technically very challenging with multiple receptors. It may also be possible to use such a system to cluster receptor tails which do not have an extracellular ligand binding domain. This may allow for decoupling of the effect of improved signalling via improved conjugation and improved signalling via simply clustering the receptor tails. However, these experiments would require a significant modification to the tail of the receptors which may alter their function and it would not be possible to easily scale this up to test multiple NTRs. Therefore, I feel the current approach is the best of both worlds in terms of its ability to be both high throughput and require minimal receptor modification.

It would also be interesting to confirm how a divalent ligand would perform in this system. The data so far shows that trivalent and tetravalent ligands are equivalent. This is likely due to steric hindrance which prevents the fourth binding site being occupied. So, the question would be whether the divalent ligand was like the monovalent or multivalent ligands. I would predict the multivalent ligands are working to stabilise the interaction therefore, I would argue that a divalent ligand would have a very similar effect. This is because the divalent

ligand would allow for the same stabilisation effect that trivalent and tetravalent ligands offer which can prolong the interaction and it allows for rapid rebinding to occur when one receptor dissociates.

Receptor downregulation is another area which would be interesting to explore further. It is not immediately clear why different NTRs would exhibit different rates of downregulation but identifying a mechanism behind this could help inform CAR design. The fact I only see strong downregulation of receptors when stimulating with high levels of the tetravalent ligand suggests it not a very sensitive effect. It is known that for other types of receptors such as epidermal growth factor (EGFR) that the process of downregulation occurs via endosomes which are then trafficked to the lysosome for breakdown (Katzmann et al., 2002). However, in terms of immune receptors it is less well defined, and downregulation is normally thought of as a sign of exhaustion. Patients with chronic inflammation show downregulation of the CD3ζ chain which is thought to be due to sustained exposure to antigen (Baniyash, 2004). The mechanism that triggers downregulation is not well understood. However, it is likely to be a negative feedback loop with the aim of preventing over activation of immune cells. The fact I still see downregulation even when signalling is inhibited is interesting as it suggests there is a mechanical component involved where the pulling on the membrane from receptor ligand binding induced the downregulation. There was slightly more downregulation with signalling present which could suggest signalling is also important for the effect. It may also be due to up regulation of intergrins upon activation which could improve cell-cell contact and therefore lead to further receptor ligand interactions and increased downregulation (Yanbo Zhang & Wang, 2012). However, the extent to which there is cross reactivity for integrin interactions between the THP-1 and the CHO cells is not known.

While there are differences in the response of the four NTRs tested with multivalent ligands the Siglec 14 is noticeable in its divergence from the others. I have suggested this is due to it

forming a dimer based on the fact it is thought to have evolved as a paired receptor to Siglec 5 which is known to form a dimer (Ali et al., 2014; Cornish et al., 1998). Therefore, when Siglec 14 binds a multivalent ligand, it could produce a "zipper" like effect to create a very large cluster of receptor ligand interactions. My data shows that it clearly leads to very strong conjugation and activation of the receptor. Under these conditions, receptor ligand properties such as length are less effective at altering the response. This is similar to the way an antibody can crosslink large numbers of receptors together. This allows for lateral exclusion of phosphatases from the contact site and receptor triggering even without the need for a ligand on an opposing membrane. To test this further I could make chimeric receptors with the disulphide bond forming region of the Siglec 14 is swapped with another NTR which is known to me monomeric. In principle the CTLA-4/CD80 interaction could also form a zipper as both are divalent due to their extracellular domains (Collins et al., 2002). Therefore, quantitative comparisons of this interaction and monovalent interactions may clarify this.

While the lack of a clear effect from altering the mobility of the ligand is disappointing it does act as a clear control for the use of CD80 as the main ligand anchor used for all other experiments. There were unfortunately also issues with the expression of the different anchors which did make comparisons more challenging. This was possible to overcome thanks to the ability to calculate the average number of biding sites per cell. However, for example with the LAIR-1 anchor the maximum binding sites at saturation was less than one million which was significantly less than the others. This study is also using the mouse sequence of CD43, therefore the level of cross reactivity with ERM proteins in the CHO cells has not been determined. Finally, the GPI anchor of the CD52 did improve the mobility of the ligand but it was only a modest 1.5-2 fold improvement over a full transmembrane domain which is consistent with the literature (F. Zhang et al., 1991). Therefore, altering the mobility significantly more may still affect receptor activation but would not be physiological.

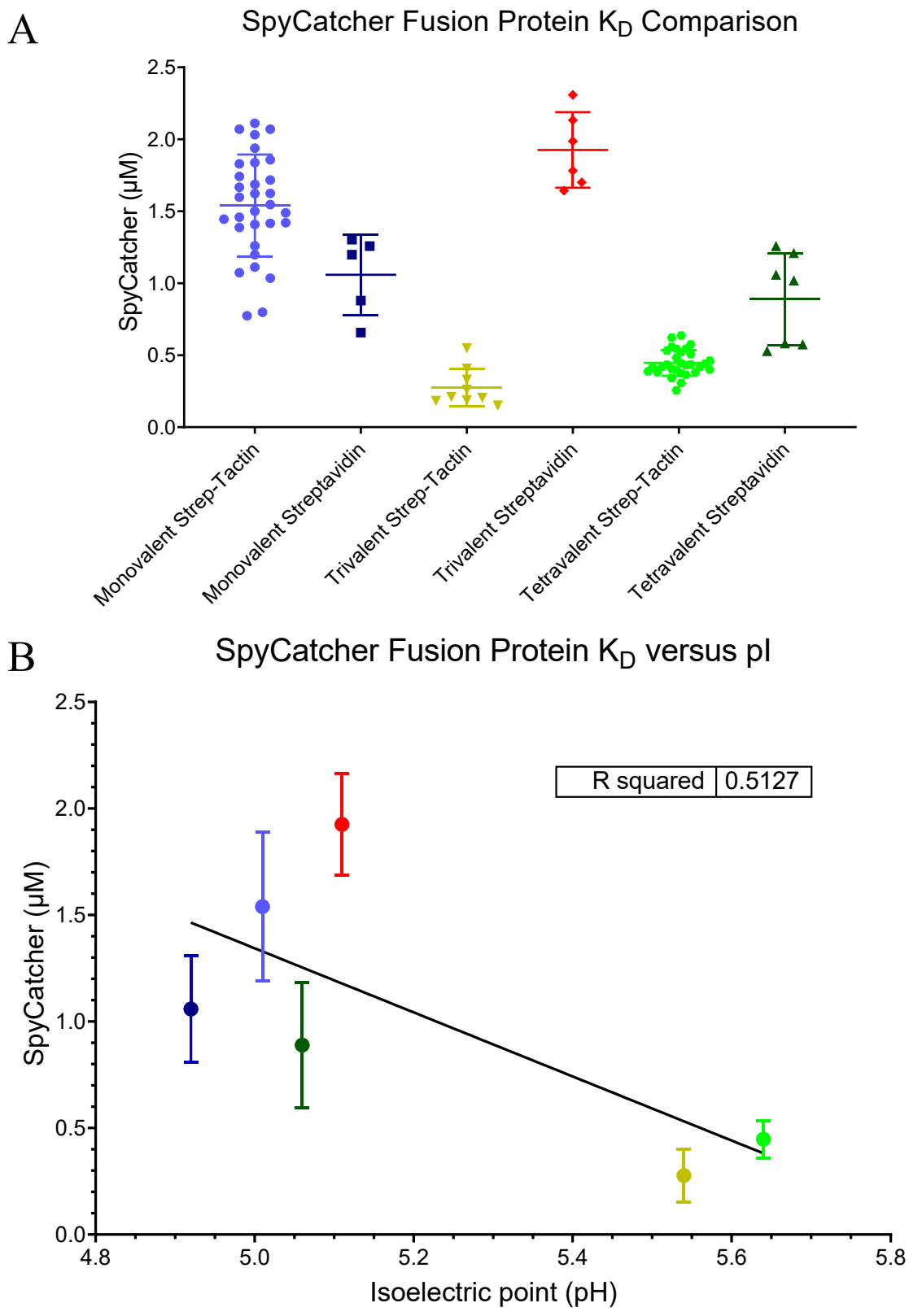


Figure 4.25: SpyCatcher fusion protein coupling efficiency comparison

(A) Comparison of the K_D values extracted from the biotin ATTO 488 assay coupling six different SpyCatcher fusion proteins to short ligand cells. **(B)** plotting the K_D values against the isoelectric point of each SpyCatcher fusion protein based on its amino acid sequence.

The combined comparison of both valency and affinity using the monovalent and tetravalent Strep-Tactin and streptavidin suggest to me that both effects are governed by a similar kinetic proof-reading mechanism. This is because increasing the valency or affinity leads to very similar improvements in receptor activation. However, from a mechanical viewpoint of receptor ligand binding the effects should be very different. This is because an increase in affinity will maintain a single receptor ligand interaction for longer, whereas going from a monovalent to a multivalent ligand will lead to an increase in the total number of interactions due to receptor rebinding. Both effects lead to improved signalling but are distinctly different. The fact that these two effects are shown to be equivalent when activation is normalised to the conjugation efficiency suggests a common mechanism which is not based on the force on the receptor or the number of binding events but the cumulative time which it is engaged. This would need to be explored further by generating a range of streptavidin mutations to produce a panel of different affinities. These could then be tested as monovalent and multivalent ligands.

I have suggested the differences in K_D I measure for the monovalent and tetravalent Strep-Tactin binding to the short ligand cells were due to differences in the charge of the proteins. However, I could not say for sure without more SpyCatcher fusion proteins to compare. This is now possible by combining the data I have generated with the streptavidin binding data from Katy Lillie, and the trivalent Strep-Tactin and streptavidin binding data generated by Eleanor Denham (Figure 4.25A). The K_D values for each of the six SpyCatcher fusion proteins were plotted against the isoelectric point, calculated using the amino acid sequence, while this may not reflect the true surface charge of the folded protein (Figure 4.25B). This analysis shows a clear trend that proteins with higher isoelectric points bind the ligand cells better. This supports the theory by which the proteins with less negative charge are not as repelled from the negative cell surface as those with lower isoelectric points, and therefore

couple more efficiently. Importantly, there is no corelation between affinity and valency or streptavidin/Strep-Tactin. These subtle differences are taken into account when calculating the average number of binding sites per cell.

Chapter 5 - Applying the generic ligand system to better understand the behaviour of CD5 and CD6

5.1. Introduction

While the focus when studying T cell activation is often the TCR several NTRs offer co-stimulatory or inhibitory roles to carefully control activation. Two NTRs that fall into this category are the structurally similar CD5 and CD6 (Gonçalves et al., 2018). They are found on the surface of thymocytes and T cells and are known to be upregulated upon cellular activation (Aruffo et al., 1991; Brown & Lacey, 2010; Gimferrer et al., 2004). They are thought to tune T cell activation by the recruitment of activatory or inhibitory molecules to the site of TCR engagement, which is crucial during T cell development to distinguish between self and non-self peptides (Gaud et al., 2018).

CD5 and CD6 contain similar extracellular domains consisting of three SRCR domains attached to a membrane stalk (Aruffo et al., 1991; Chappell et al., 2015). Despite a great deal of effort no ligand has been confirmed for CD5, although there is evidence that it can bind itself via homophilic interactions involving SRCR domain 1 (Brown & Lacey, 2010). CD6 however, is known to bind CD166, also known as ALCAM, which is found on activated leukocytes but also more broadly in the thymus and nervous system (Bowen et al., 1995). The membrane proximal domain 3 of CD6 binds the most membrane distal domain of CD166 and the crystal structure of this interaction has been solved (Chappell et al., 2015).

There is a lot of evidence that CD5 acts predominantly as a negative regulator of T cell activation, although the exact mechanism is not well understood (Burgess et al., 1992; Peña-Rossi et al., 1999; Voisinne et al., 2018). Conversely, initial work on CD6 using crosslinking antibodies suggested that it was acting as an activatory receptor (Bott et al., 1993; Gangemi et al., 1989; Osorio et al., 1994; Zimmerman et al., 2006). However, it has also been shown that

expression of CD6 could reduce the responsiveness of T cells (Hassan et al., 2006). Later work has confirmed this and shown a clear inhibitory role for CD6 without ligand engagement (Oliveira et al., 2012). The dule role of CD6 has again been shown recently with the recruitment of positive (SLP-76, ZAP70, VAV1) and negative (UBASH3A/STS-2) signalling molecules during TCR activation (Mori et al., 2021).

A key difference between CD5 and CD6 is the cytoplasmic tail. The tail of CD6 is one of the longest of all NTRs and contains nine tyrosine residues, although none can be defined as canonical activatory or inhibitory signalling motifs. However, many of these tyrosine residues have been shown to be phosphorylated upon T-cell activation (Kobarg et al., 1997; Wee et al., 1993). This has led to suggestions that the tail acts as a scaffold similar to LAT, allowing it to recruit and maintain a complex signalosome (Mori et al., 2021; Roncagalli et al., 2014). For example, like LAT, CD6 has been shown to recruit the activatory molecules SLP-76 and GADS, which bind specifically to tyrosine residues Y662 and Y629 respectively (Breuning & Brown, 2017). When this C-terminal section of the CD6 tail was added to a second generation CAR containing the CD3ζ and 4-1BB it was shown to enhance cytotoxicity and cytokine release (Breuning et al., 2019). The only evidence linking a specific tyrosine residue to the inhibitory effect comes from the mutation of Y489 (Hassan et al., 2006). However, this data is not very strong, and they were not able to show what this residue may be recruiting when phosphorylated.

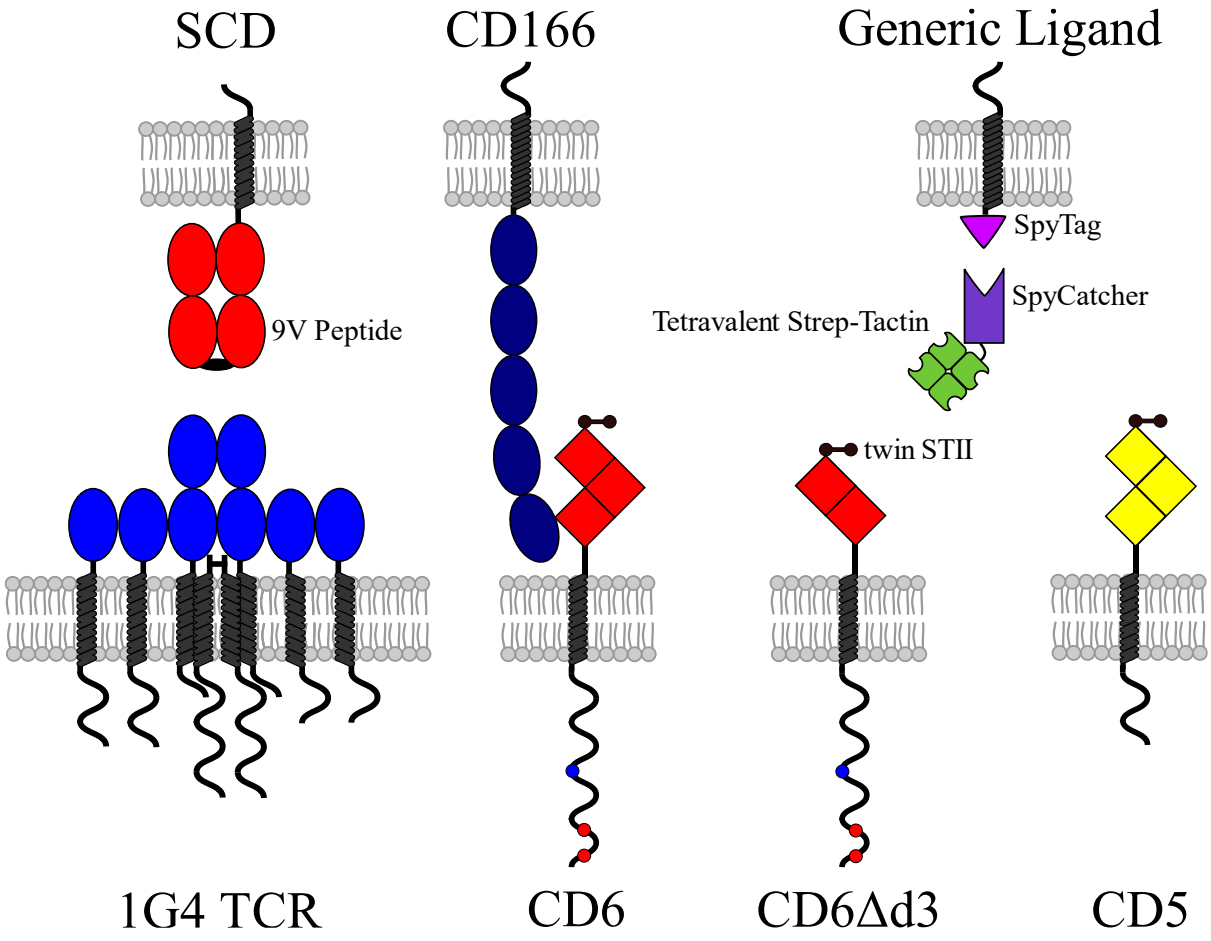


Figure 5.1: Cartoon representing the experimental set up to engage the TCR in combination with CD5 and CD6

The 1G4 TCR plus either CD5 or CD6 was expressed in Jurkat NFκB reporter cells. The TCR was activated using 9V peptide loaded on the HLA-A*02 SCD. The CD6-CD166 is shown where CD166 binds CD6 domain three. The CD5 and CD6 receptors were engaged with the generic ligand system using a twin STII tag on the receptor to bind the tetravalent Strep-Tactin SpyCatcher ligand. The blue dot in cytoplasmic tail of CD6 represents the Y489 tyrosine residue and the red dots represent residues Y662 and Y629.

This dual function of CD6 seems to depend on the environment in which the receptor is being studied. Factors such as the expression level of the molecule, ligand engagement and the degree of activation from other receptors such as the TCR combine to produce a very complex picture. It is therefore difficult to untangle all these confounding effects to define whether this receptor is predominantly activatory or inhibitory. This has caused a large degree of uncertainty as to the true role of CD6 in the immune system.

Through applying the generic ligand system to this problem, I can carefully control the level of engagement of both the TCR and CD5 or CD6, allowing me to dissect out the activatory and inhibitory effects attributed thus far to these molecules. The different receptor ligand interactions for these experiments are highlighted in Figure 5.1. The complex behaviour of CD6 requires it to be studied in the context of TCR activation. This is because it is thought to tune cellular activation, so I need to have an activatory signal to be modulated by CD6. These experiments were carried out using Jurkat cells transduced with the 1G4 TCR. This TCR can be activated by a large range of different affinity peptides, but I chose to use only the 9V peptide loaded on an SCD, as this has a physiological affinity (5.5 μM) for the TCR (Aleksic et al., 2010; J.-L. Chen et al., 2010). As a read-out for activation these cells contain an eGFP sequence under the control of an NFκB promoter (Jutz et al., 2017). NFκB is a key transcription factor which is important for many signalling pathways and induces downstream cellular activation upon TCR triggering (Matsumoto et al., 2002).

5.1.1. Key findings

In this chapter, I show that expression of CD6 without any ligand engagement is sufficient to reduce T cell activation via the TCR. This inhibitory behaviour is dependent on its cytoplasmic tail, and this is largely mediated by the Y489 tyrosine. I then show that engagement of CD6 in the absence of TCR ligand leads to weak cellular activation, this was found to be the result of CD6 tail mediated co-stimulation and adhesion which caused ligand

independent TCR triggering, as both effects were abolished in experiments using cells with no TCR. I also found that I cannot confirm previous reports that CD6 can perform an activatory role using the Y662 and Y629 tyrosine residues. However, the use of a CD5/CD6 Tail chimera confirmed the CD6 tail is strongly co-stimulatory. Finally, CD5 appears to have both activatory and inhibitory roles. The co-stimulatory effect is dependent on the extracellular domain but does not require ligand engagement. Conversely, the inhibitory effect is dependent on the cytoplasmic tail, and it is masked by the co-stimulatory effect in the original Jurkat reporter cells, but it can be detected when comparing WT CD5 to a CD5 No tail mutant construct and when WT CD5 is expressed in the No TCR Jurkat cell line.

5.2. Results

5.2.1. CD6 cross-reacts with hamster CD166 on CHO cells

Based on previous work by Marion H Brown, it was predicted that there may be problems using the CHO ligand system due to the possibility of human WT CD6 binding the endogenously expressed hamster CD166. As a control I used the CD6Δd3 natural splice variant of CD6 which does not contain domain 3 and therefore cannot bind to its ligand CD166 (Castro et al., 2007). To establish if this cross-reactivity was occurring, I first expressed the WT CD6 and CD6Δd3 in the Jurkat reporter cells expressing the 1G4 TCR. Stimulating these cells with a serial dilution of 9V peptide showed strong activation when only the 1G4 TCR was expressed (Figure 5.2A). 1G4 TCR + WT CD6 cells produced a similar maximum response but had very high background activation, with approximately 50 % of cells positive for eGFP. Conversely, 1G4 TCR + CD6Δd3 showed a similar background stimulation to 1G4 TCR-only cells but a clear reduction in maximum activation compared with 1G4 TCR-only cells. Subtracting the background stimulation shows that WT CD6 and CD6Δd3 do have a similar inhibitory effect by reducing cellular activation (Figure 5.2B). This was the first confirmation in my system that expression of CD6 alone could alter the

activation of the TCR in Jurkat cells (Oliveira et al., 2012). The large difference between the stimulation of cells expressing WT CD6 and CD6Δd3 at low levels of TCR activation suggested that CD6 was potentially interacting with CD166 on the CHO cells. This also suggests CD6 can be activatory when engaged by its ligand.

Engagement of these cells with tetravalent Strep-Tactin SpyCatcher only confirmed the strange behaviour of WT CD6 (Figure 5.2C). The use of a twin STII tag increases the affinity for the ligand by approximately six-fold over the single STII used for the other NTRs in the first two results chapters (Denham et al., 2019). This was to better match the physiological CD6-CD166 affinity, which is significantly higher than would be achieved using the single STII. In this case, the engagement of WT CD6 via the generic ligand reduced activation compared with CD6Δd3, which increased activation upon engagement as expected. Removing the background activation shows that only cells expressing the CD6Δd3 were capable of showing the specific contribution of generic ligand stimulation (Figure 5.2A). Engagement of WT CD6 with the generic ligand paradoxically inhibited stimulation. This behaviour suggested that WT CD6 was binding an endogenous ligand on the CHO cells and the background stimulatory effect of this engagement was inhibited by generic ligand.

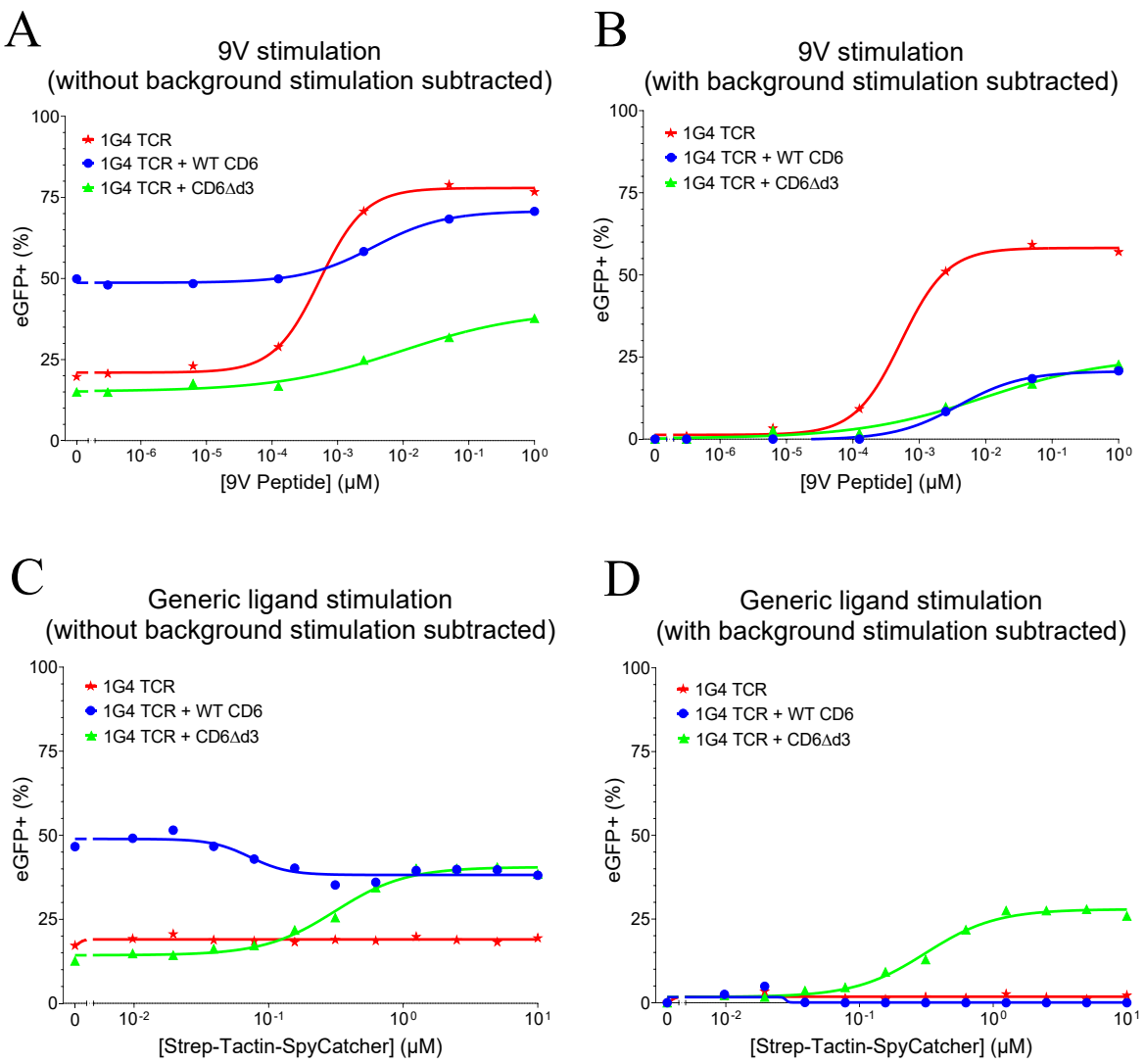


Figure 5.2: Cross-reactivity between WT CD6 and endogenously expressed hamster CD166

Stimulation of Jurkat reporter cells expressing the 1G4 TCR, 1G4 TCR + WT CD6 and 1G4 TCR + CD6Δd3. **(A and B)** Dose-response curves showing the percentage of eGFP+ reporter cells after stimulation with short ligand cells presenting 9V peptide only, A before subtracting background stimulation and B after subtracting background stimulation. **(C and D)** Dose-response curves showing the percentage of eGFP+ reporter cells after stimulation with short ligand cells coupled with tetravalent Strep-Tactin SpyCatcher only, C before subtracting background stimulation and D after subtracting background stimulation.

To confirm if WT CD6 could bind hamster CD166 on the CHO cells I used the anti-CD6 domain three antibody OX124 which can block ligand binding (Santos et al., 2019). As a control I used an unrelated OX21 antibody which binds the C3b component of the complement system (Hsiung et al., 1982). Mixing the Jurkat reporter cells with the two antibodies showed very weak activation of the cells with OX124 and no response from OX21 (Figure 5.3A). This is likely due to cross linking of CD6 receptors leading to some weak cellular activation. This is not unexpected and has been observed before when crosslinking CD6 in this way (Bott et al., 1993; Gangemi et al., 1989; Osorio et al., 1994; Zimmerman et al., 2006). In Figure 5.3B when Jurkat cells were mixed with control antibody and CHO short ligand cells without SpyCatcher or 9V peptide, there was high background activation, similar to Figure 5.2A (*left*) and C (*left*). The addition of the OX124 blocking antibody significantly reduced this background activation even at low concentrations of antibody (Figure 5.3B).

This suggests that WT CD6 can bind hamster CD166 on the CHO cells. This leads to complicated effects when engaging via the generic ligand as I cannot control the level of WT CD6 engagement (Figure 5.2C). I therefore used the CD6Δd3 for all future experiments to avoid this issue.

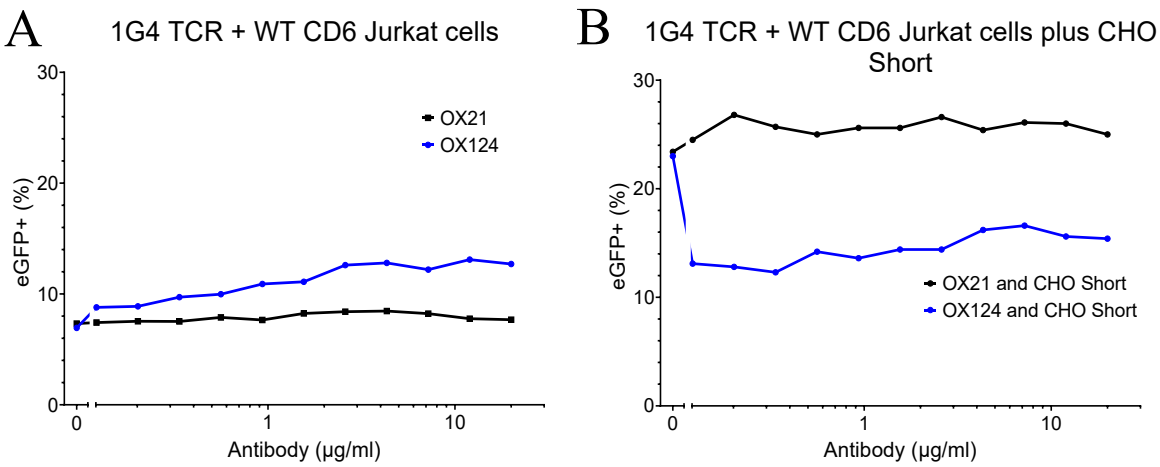


Figure 5.3: Blocking WT CD6 prevents cross reactivity with hamster CD166 on CHO cells

(A) Reporter Jurkat cells with 1G4 TCR and WT CD6 were mixed with a serial dilution of either control antibody (OX21) or anti CD6 domain three antibody (OX124). **(B)** Jurkat cells were pre- incubated with either OX21 or OX124 and then mixed with CHO short cells.

5.2.2. CD5 and CD6 are not canonical activatory receptors and they differ in their sensitivity to ligand length

So far, all the NTRs I have tested have been sensitive to receptor ligand dimensions. I therefore wanted to see if this was also true of WT CD5 and CD6Δd3. I used tetravalent Strep-Tactin SpyCatcher coupled to short and long ligand cells to stimulate Jurkat reporter cells expressing the 1G4 TCR and either CD6Δd3 or WT CD5. Figure 5.4A and B shows that both the short and long ligand can activate the Jurkat cells to a similar degree. It should be noted that, overall, the maximum percentage of cells stimulated with CD5 and CD6Δd3 was 10-20 %, whereas stimulation via the TCR alone could reach up to 80 %. Additionally, although CD5 does not have any confirmed ligand I show that it can also weakly stimulate cells when engaged with either short or long ligand cells (Figure 5.4B). However, it is significantly weaker when compared to the stimulation of CD6. There are two explanations for this: stimulation via the CD5 receptor causes less activation than the CD6 because it has a larger extracellular domain (under the kinetic segregation model, this would lead to less activation for the same levels of conjugation), or there is a difference in their tails that causes less activation/more inhibition when the CD5 is engaged. This point will be further explored in this chapter.

I next performed conjugation assays and found that, as expected, due to the higher affinity interaction of the STII tag on the CD5 and CD6, the cells formed very good conjugates with both short and long ligand cells (Figure 5.4C and D). This is further evidence that increasing the affinity of the receptor ligand interaction (using the twin STII tag instead of single STII tag) reduces the sensitivity of this interaction to ligand length. This is similar to what I have shown when altering the avidity in Chapter 4 with the lack of effect on conjugation assays when elongating the tetravalent ligand (Figure 4.11), compared to the monovalent ligand (Figure 3.5). Finally, plotting the stimulation data against the conjugation data as described

before showed a small but statistically significant difference in overall activation levels between the two ligands. Interestingly, the CD6Δd3-presenting cells were slightly more activated with the long ligand, whereas the CD5-presenting cells had higher activation with the short ligand (Figure 5.4E and F). This suggests the CD6 receptor is not behaving in the same way to the others tested in previous chapters. This is likely due to CD5 and CD6 not being canonical activatory receptors, which can induce strong cellular activation on their own, but receptors with more complex effects on TCR co-stimulation.

This suggests that CD5 and CD6 alone cannot induce the same kind of activation seen from the TCR. A possible explanation for this low-level activation could be that adhesion driven by CD5 or CD6 could drive ligand-independent activation of the TCR on the Jurkat cells. However, the fact that CD5 produced lower stimulation for the same level of conjugation suggests it is acting in an inhibitory manner. This will be explored again later in this chapter when activating CD5 and CD6 in TCR negative cells.

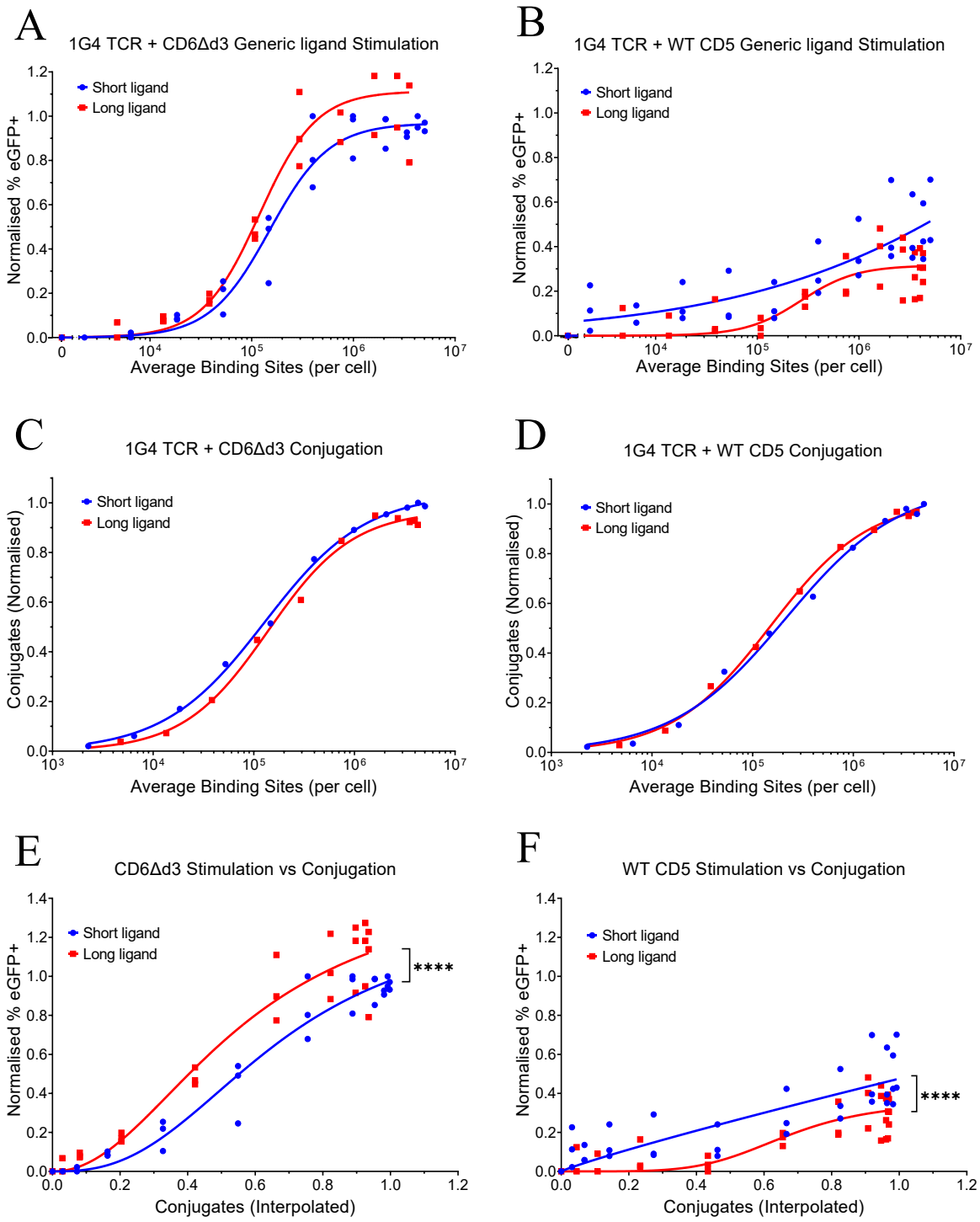


Figure 5.4: WT CD5 and CD6Δd3 show different dependences on ligand length

(A and B) Stimulation assay with Jurkat reporter cells expressing 1G4 TCR and either CD6Δd3 or WT CD5 with short and long ligand cells presenting tetravalent Strep-Tactin SpyCatcher. **(C and D)** Conjugation assay using the same cell lines and tetravalent Strep-Tactin SpyCatcher. **(E and F)** Stimulation versus conjugation assay combining the data in A-D. All data has been normalised to the CD6Δd3 with the short ligand. An F test was used to compare the curves between the short and long ligand conditions (**** = P <0.0001). Data is combined from three biological replicates.

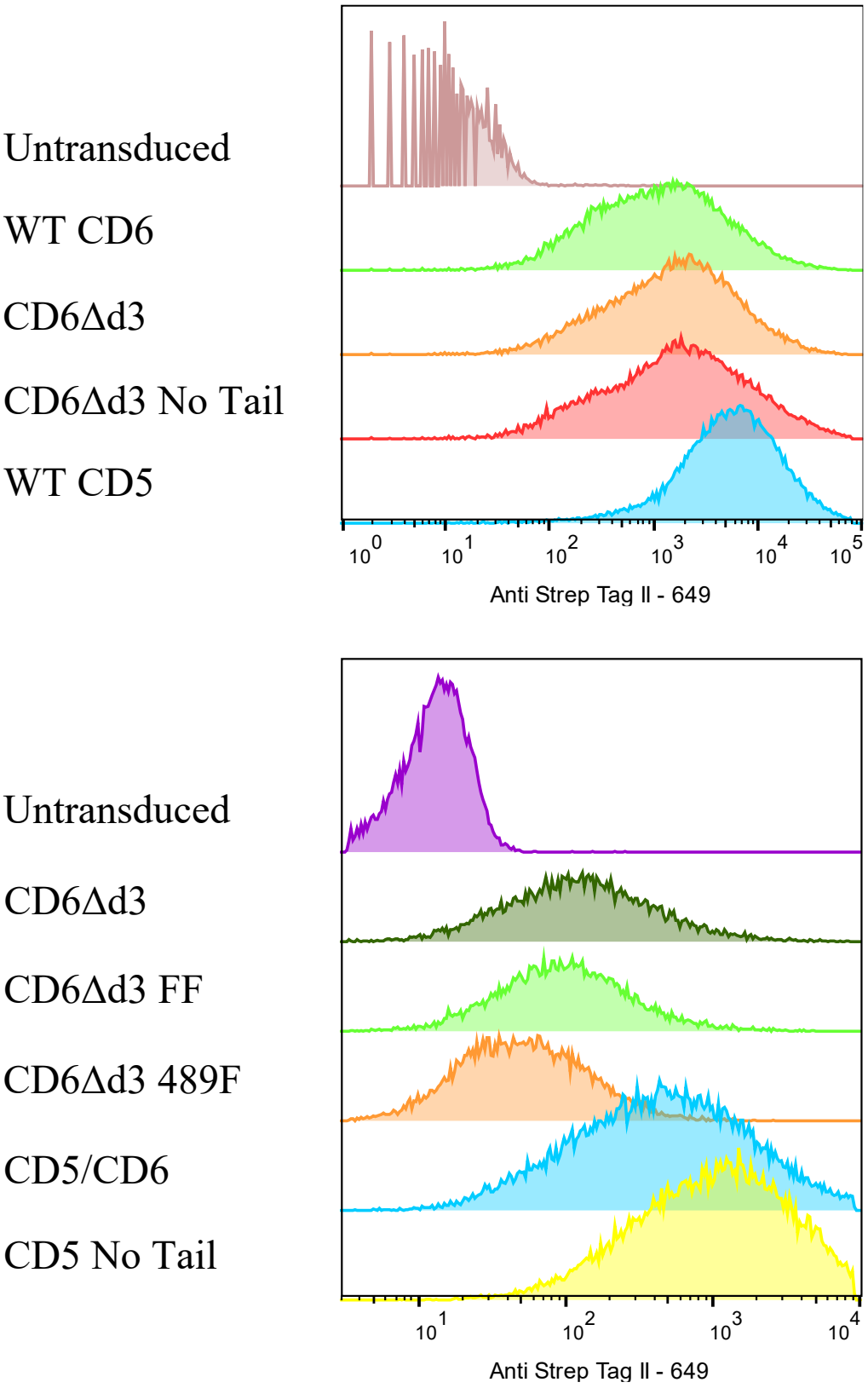


Figure 5.5: Expression check for NFkB reporter Jurkat cells expressing the 1G4 TCR

Cells expressing the WT and mutant constructs of CD6 and CD5 receptors used in the stimulation assays. Cells were stained using an anti STII tag antibody conjugated to a DY649 fluorophore. Panels show expression checks on different days with different constructs.

5.2.3. Expression of CD6 in Jurkat cells inhibits TCR activation in a ligand independent manner

Next, I wanted to further investigate the inhibitory and stimulatory effect seen in Figure 5.2A and C. To do this I compared stimulation with Jurkat reporter cells expressing the 1G4 TCR plus CD6Δd3 or WT CD5 (Figure 5.5). However, I also added two additional cell lines with key tyrosine residues in the CD6 tail mutated to phenylalanine (Figure 5.1). Firstly, CD6Δd3 FF, where the Y662 and Y629 tyrosine residues had been mutated, and secondly CD6Δd3 489F, with a single mutation at tyrosine residue Y489. Figure 5.6A shows the 9V-mediated TCR stimulation of these five cell lines when the different CD5 and CD6 receptors are not being engaged by a ligand. Again, expression of the CD6Δd3 in these cells had a ligand-independent inhibitory effect on cellular activation (compare *black* and *red* lines). The WT CD5 (*grey* line) had no clear inhibitory effect, which is surprising as this is thought to be predominantly an inhibitory receptor (Burgess et al., 1992; Peña-Rossi et al., 1999; Voisinne et al., 2018). The CD6 tail mutations appear to modulate the inhibitory effect which will be assessed in detail later in this chapter.

Activation of the same five cell lines via only engaging the CD5 and CD6 receptors with the generic ligand produced similar small levels of activation as seen in Figure 5.2 and Figure 5.4 (note the difference in y-axis scale between Figure 5.6A and B). It is possible that this activation is not directly mediated by the CD5 and CD6 receptors, but that because generic ligand binding to CD5 and CD6 leads to increased conjugation, and this leads to ligand independent activation of the TCR, which is investigated in the next section. Again, the CD6 tail mutations seem to alter the level of stimulation, but this could also be due to differences in expression level, which could lead to different levels of ligand independent TCR activation. For example, the CD6Δd3 489F showed the least inhibition and activation, but is also expressed at a lower level than the other two CD6Δd3 constructs (Figure 5.5).

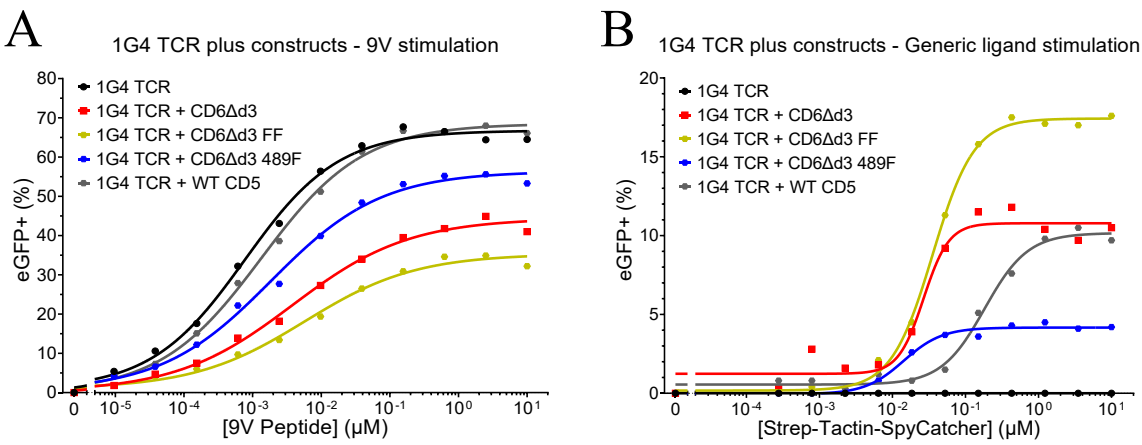


Figure 5.6: Mutations in CD6 tail tyrosine residues modify its behaviour

Stimulation of Jurkat reporter cells expressing the 1G4 TCR, 1G4 TCR + CD6Δd3, 1G4 TCR + CD6Δd3 FF, 1G4 TCR + CD6Δd3 489F and 1G4 TCR + WT CD5. **(A)** Dose-response curves showing the percentage of eGFP+ reporter cells after stimulation with short ligand cells presenting 9V peptide only. **(B)** Dose-response curves showing the percentage of eGFP+ reporter cells after stimulation with short ligand cells presenting tetravalent Strep-Tactin SpyCatcher only.

Strikingly, there is an EC50 shift in activation for the WT CD5 cells compared to those with the CD6Δd3 constructs (Figure 5.6B). This cannot be explained by differences in levels of receptor expression as CD5 is more highly expressed than the CD6Δd3 constructs (Figure 5.5). If WT CD5 was just driving indirect cell activation by binding to the ligand cells, higher levels of receptor should lead to more conjugation and higher activation. It is true that under the KS model and based on the conclusions from Chapter 3, the larger extracellular domain of CD5 could lead to lower activation than if it were smaller like that of CD6Δd3. However, this assumes that the observation that smaller receptors trigger higher levels of activation from Chapter 3 applies in this scenario. As seen when comparing the short and long ligand these receptors do not appear to be very sensitive to ligand length. One possibility is that this apparent shift is due to co-stimulatory signalling via the different CD6Δd3 receptors when they become engaged adding to the overall cellular activation observed. An alternative explanation is that CD5 is truly an inhibitory receptor, but its inhibitory effect in these experiments is only noticeable when it becomes engaged by the generic ligand and the overall activation of the cells is low (i.e. conditions in Figure 5.4B, F and Figure 5.6B, but not Figure 5.6A).

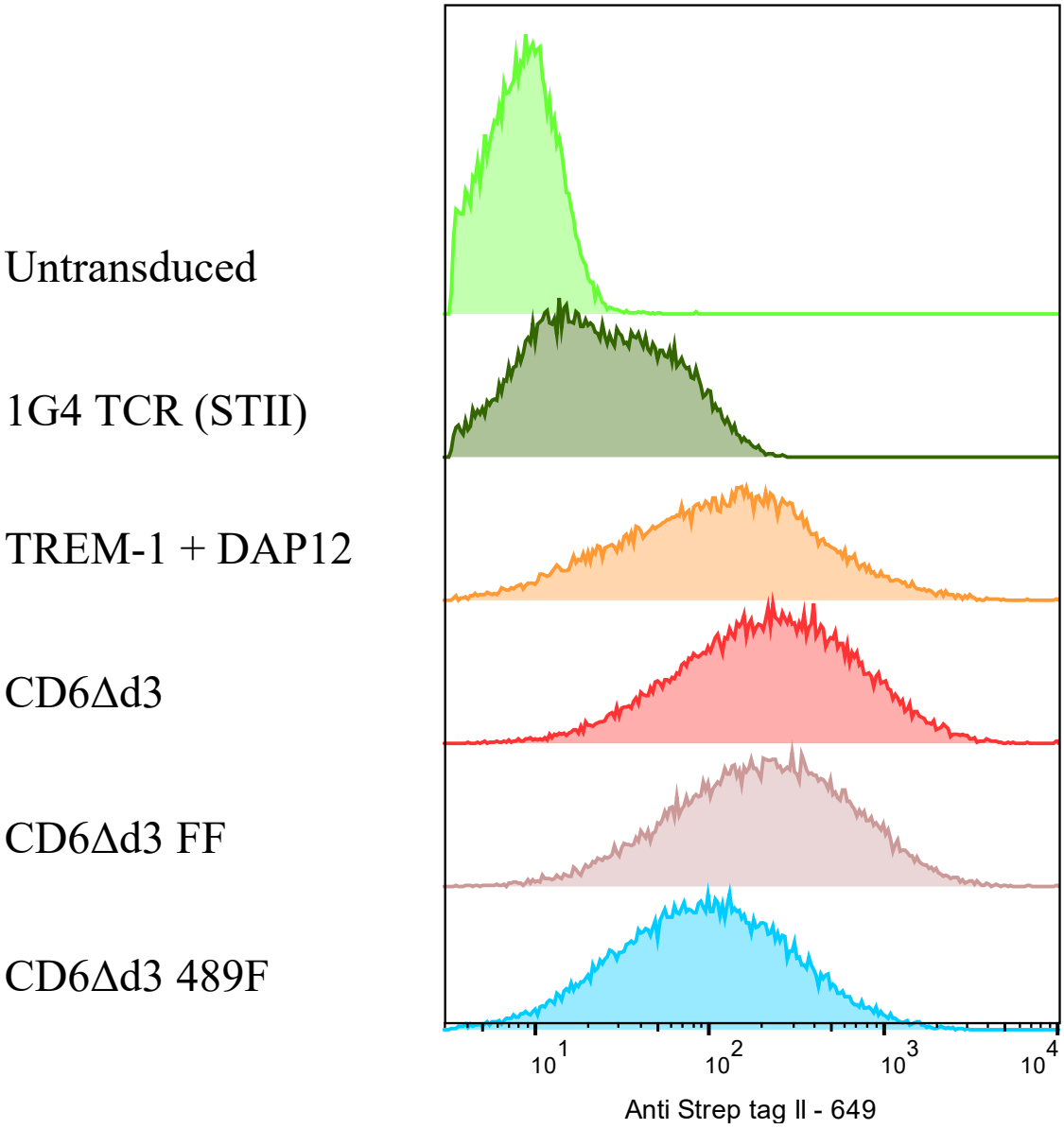


Figure 5.7: Expression check for No TCR Jurkat cells

Cells expressing the 1G4 TCR (STII), TREM-1 + DAP12, CD6Δd3, CD6Δd3 FF and CD6Δd3 489F. Cells were stained using an anti STII tag antibody conjugated to a 649 fluorophore.

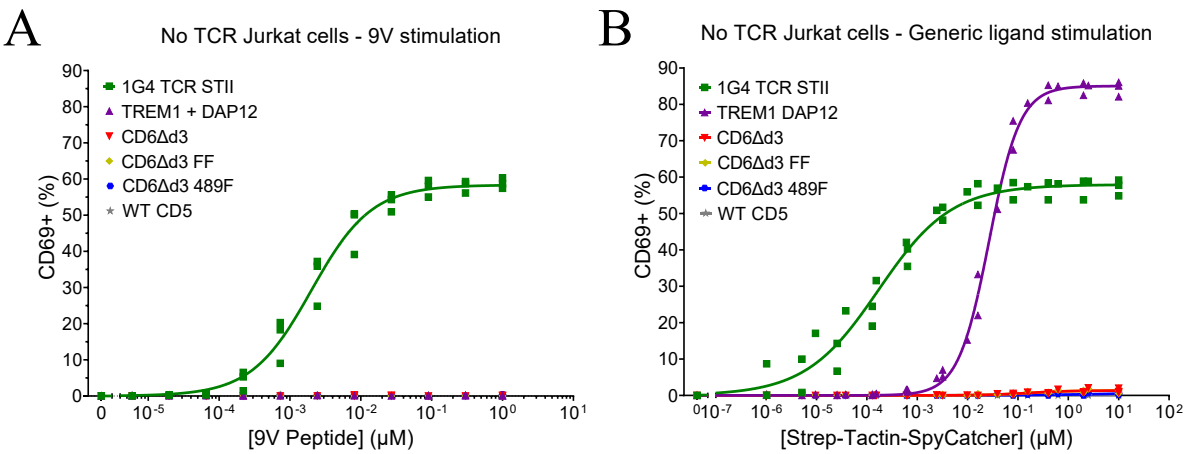


Figure 5.8: CD5 and CD6 constructs cannot stimulate without the TCR

Stimulation assay with the No TCR Jurkat cells expressing the 1G4 TCR STII, TREM1 + DAP12, CD6Δd3, CD6Δd3 FF, CD6Δd3 489F and WT CD5. **(A)** Dose-response curves showing the percentage of CD69+ cells after stimulation with short ligand cells presenting 9V peptide only. **(B)** Dose-response curves showing the percentage of CD69+ cells after stimulation with short ligand cells presenting tetravalent Strep-Tactin SpyCatcher only. Data is combined from three biological replicates.

5.2.4. Jurkat activation by CD5 and CD6 engagement requires TCR expression.

Previous studies have shown that engagement of T cell receptors, such as CD2 and CD58, can activate T cells indirectly by triggering the TCR in the absence of pMHC. This is known as ligand-independent TCR activation (Chang et al., 2016; Kaizuka et al., 2009). I therefore wanted to check whether the activation I observed upon engagement of the CD5 and CD6 receptors in the absence of direct TCR stimulation with 9V peptide was dependent on the TCR. To do this, I expressed CD5 and CD6 receptor constructs in a Jurkat cell line lacking a TCR (No TCR cells) (Figure 5.7). This cell line also lacked the eGFP reporter, and so the percentage of cells positive for CD69 after the stimulation assay was measured instead (Cibrián & Sánchez-Madrid, 2017). I have found that CD69 expression matches eGFP expression in the reporter Jurkat cells, which allows me to compare the two as an equivalent readout for cellular activation (data not shown).

When No TCR Jurkat cells expressing the CD5 or CD6 receptor constructs were cultured with short ligand cells presenting 9V peptide, as expected no activation was observed (Figure 5.8A). As a positive control, the 1G4 TCR with a twin STII tag at the N-terminus was expressed in the No TCR cells. This cell line produced very strong activation measured by CD69 expression. More importantly, no activation was observed when No TCR cells expressing CD5 or CD6 receptor constructs were cultured with short ligand cells coupled with tetravalent Strep-Tactin SpyCatcher (Figure 5.8B). Again, the TCR positive control showed strong activation confirming previous findings that the generic ligand system can reproduce TCR activation with its native peptide ligand (Denham et al., 2019). Additionally, the TREM-1 NTR was also found to strongly activate the No TCR cells although it is significantly less sensitive than the TCR. These findings suggest that activation of the 1G4 TCR reporter cells by CD5 and CD6 engagement with generic ligand in the absence of 9V peptide (Figure 5.2, Figure 5.4 and Figure 5.6B) was in fact mediated by TCR activation.

This is likely an effect mediated by CD5 or CD6 binding leading to ligand-independent TCR triggering, an effect predicted by the kinetic-segregation model (Chang et al., 2016; Kaizuka et al., 2009).

I had been surprised to observe no inhibition of TCR activation after stimulation with 9V peptide in cells expressing WT CD5 (Figure 5.6A). I wanted to confirm that this result was not due to the Jurkat reporter cell line used in the previous section. I, therefore, reconstituted the 1G4 TCR without the STII in the No TCR cells (Figure 5.9A). This parental cell line was sorted to have high levels of 1G4 TCR expression and then twin STII tagged receptors CD6Δd3, CD6Δd3 FF, CD6Δd3 489F or WT CD5 were added (Figure 5.9B). I then repeated with these new cell lines the experiments using only 9V peptide or the generic ligand for stimulation. Overall, the results agreed with my previous observations (compare Figure 5.6A and Figure 5.10A, and Figure 5.6B and Figure 5.10B), confirming that activation following CD5 and CD6 engagement is mediated by the TCR. Again, I observed that CD6 has an inhibitory effect when the TCR is activated, and a modest net activatory effect when only the generic ligand was used. The pattern between different CD6 mutant constructs was generally the same, although there are some differences which could be due to variation in expression level (Figure 5.9B).

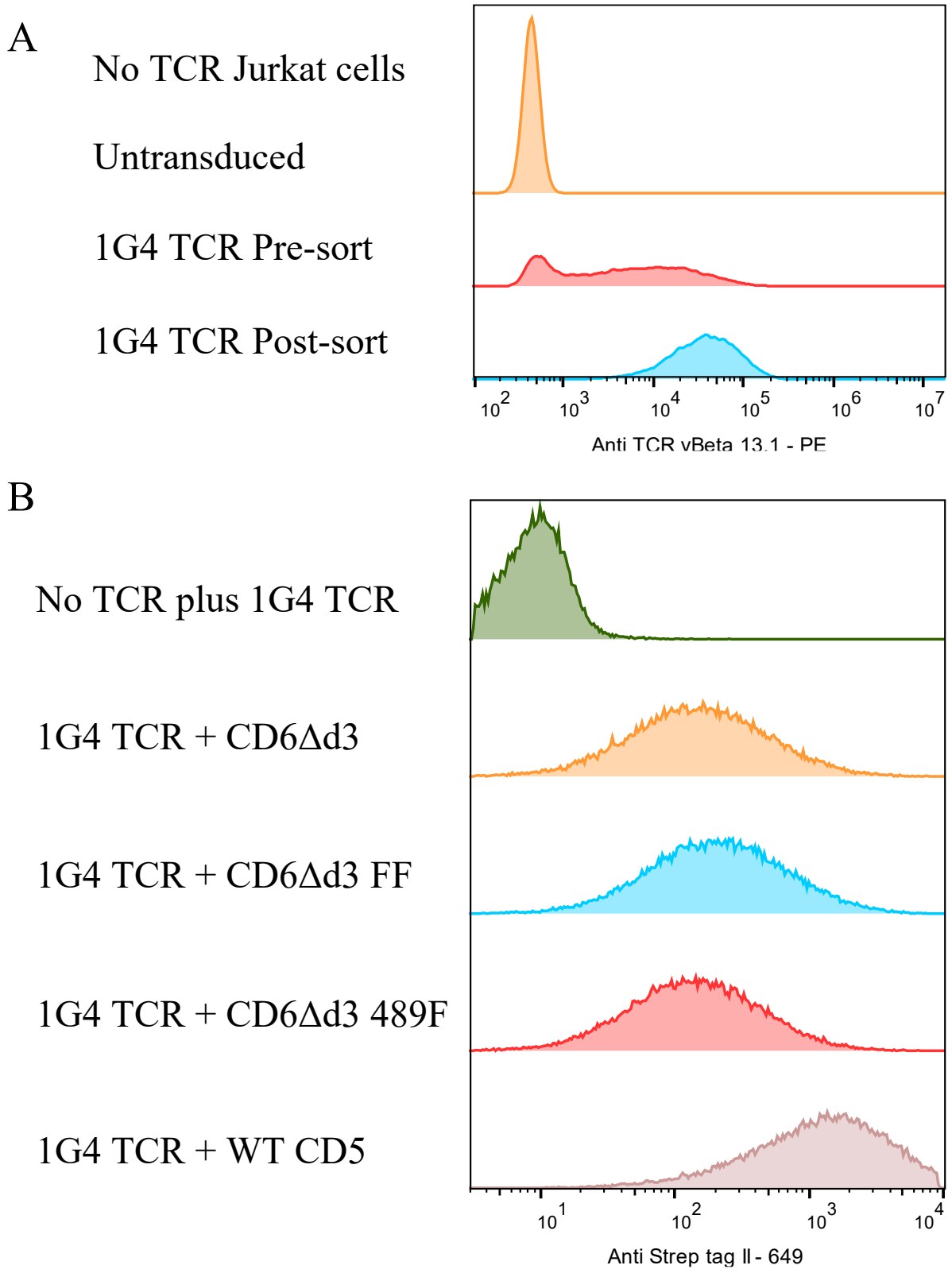


Figure 5.9: Producing No TCR Jurkat cells reconstituted with the 1G4 TCR

(A) Addition of the 1G4 TCR to the No TCR Jurkat cells showing the before and after FACS sorting. **(B)** Addition of CD6 constructs plus CD5 WT to the No TCR plus 1G4 TCR cells. Cells were stained using an anti STII tag antibody conjugated to a 649 fluorophore.

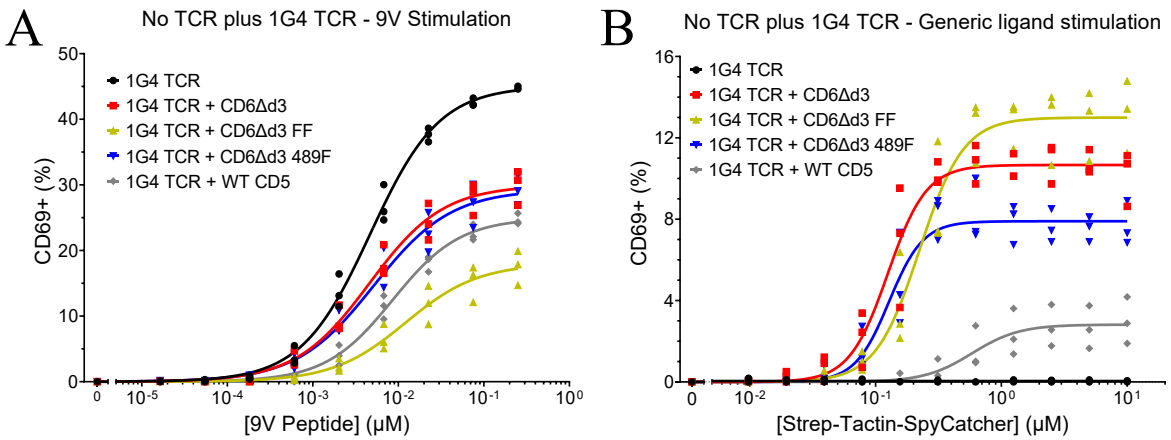


Figure 5.10: Reconstituting No TCR cells with 1G4 TCR plus CD5 and CD6 constructs rescues the stimulatory effect

Stimulation assay with reconstituted No TCR Jurkat cells expressing the 1G4 TCR plus, CD6Δd3, CD6Δd3 FF, CD6Δd3 489F or WT CD5. **(A)** Dose-response curves showing the percentage of CD69+ cells after stimulation with short ligand cells presenting 9V peptide only. **(B)** Dose-response curves showing the percentage of CD69+ cells after stimulation with short ligand cells presenting tetravalent Strep-Tactin SpyCatcher only. Data is combined from three biological replicates.

5.2.5. Both CD5 and CD6 receptors have an inhibitory effect on TCR activation.

There is however one key difference between both sets of experiments, which is the effect of CD5. In the stimulation experiment with only 9V peptide and the reconstituted No TCR Jurkat cells, CD5 was also found to have a clear inhibitory effect, like CD6Δd3 (Figure 5.10A). In the stimulation with generic ligand, the activation observed with CD5 is also much lower (Figure 5.10B). This supports previous reports that CD5 is an inhibitory receptor (Burgess et al., 1992; Peña-Rossi et al., 1999; Voisinne et al., 2018). One possible explanation for this difference between experiments is that CD5 is a ligand-independent inhibitor, but expression of CD5 in the original reporter Jurkat cells has an additional, TCR-dependent co-stimulatory effect which masks this inhibition, so overall CD5 appears to have little net effect (Figure 5.6A). However, in low activation conditions (without 9V stimulation), inhibition by CD5 is more noticeable (Figure 5.6B and Figure 5.10B). Whatever factor would cause this additional co-stimulatory effect was not present in the No TCR Jurkat cells (at least not to the same level), so in the experiments using the remade cell lines this masking of the inhibitory effect is reduced and CD5-mediated inhibition is more readily detectable (Figure 5.10A and B). This may be explained by the higher expression of endogenous CD5 found in the No TCR cells, and this enhances the inhibitory effect of CD5 (Figure 5.11A and B).

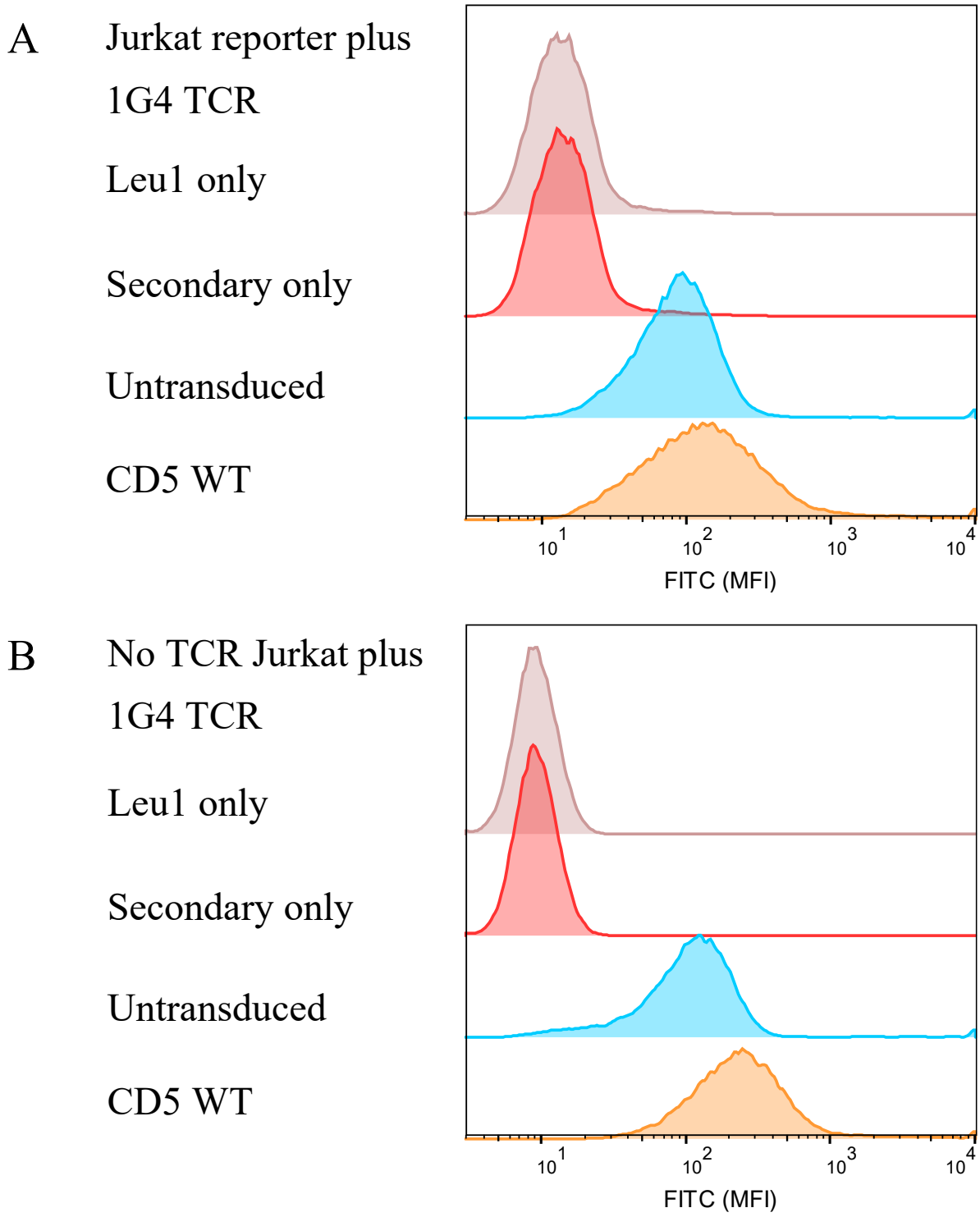


Figure 5.11: Expression test for endogenous CD5 in the Jurkat reporter and No TCR Jurkat cells.

(A) Staining of the Jurkat reporter plus CD5 WT cells with the anti CD5 (Leu1) antibody and FITC secondary showed a 9.6-fold shift in gMFI from the controls. **(B)** Staining of the No TCR plus 1G4 TCR and CD5 WT Jurkat cells in the same way showed a 26.5-fold shift in gMFI from the controls.

5.2.6. Factorial stimulation assays confirm dual behaviour of CD6.

To further dissect the dual behaviours of CD6 observed so far, I designed a factorial stimulation assay where different combinations of ligands (9V peptide and generic ligand) could be presented on the CHO cells to engage the TCR and CD6 simultaneously. While I completed the initial stimulation assays, the COVID-19 pandemic prevented me from doing replicates. Therefore, the experiments presented here were carried out by Elena Perticucci, a medical student I supervised in our laboratory. The 1G4 TCR only control cell line was incubated with short ligand cells presenting a serial dilution of 9V peptide (

Figure 5.12A and B, *red* dose response curve). The cell line expressing both 1G4 TCR and CD6Δd3 was also incubated with short ligand cells presenting a serial dilution of 9V peptide in addition to being coupled with specific concentrations of tetravalent Strep-Tactin SpyCatcher (Figure 5.12A and B). The dose response curves corresponding to the different conditions were fit and the minimum (Figure 5.12C) and maximum (Figure 5.12D) and values extracted (*multicoloured* curves, with the *black* response curve corresponding to 1G4 TCR + CD6Δd3 cells stimulated without generic ligand).

At low 9V peptide concentrations there was an increase in the cellular activation as CD6Δd3 engagement increased compared to the 1G4 TCR only control (Figure 5.12A, *left* of the graph, Figure 5.12C). This again suggests that CD6Δd3 engagement can enhance cellular activation, but as I have shown this effect is dependent on TCR expression. At high 9V peptide concentrations expression of CD6Δd3 reduced cellular activation as I have shown before (Figure 5.12A, *right* of the graph, Figure 5.12B and D). The raw data in Figure 5.12A appears to show engagement of CD6Δd3 removing the inhibitory effect. However, by subtracting the "background activation" attributed to CD6Δd3 engagement in the presence of no peptide it is possible to see that the curves collapse down on top of each other shown in Figure 5.12B and summarised in Figure 5.12D. There is no statistically significant difference

between maximum response in highly engaged CD6Δd3 compared to no/low levels of CD6Δd3 engagement once CD6Δd3 activation is subtracted (Figure 5.12B and D). This indicates that irrespective of engagement status, CD6Δd3 has a strong inhibitory effect, but there is a co-stimulatory component to CD6Δd3 engagement that enhances TCR activation. This could be explained by a combination of CD6Δd3 signalling and adhesion causing TCR ligand independent activation. I have therefore presented the data for all factorial stimulation assays in this way to highlight the effect on cellular activation with and without CD5/6 engagement.

5.2.7. The CD5 and CD6 cytoplasmic tails mediate their inhibitory functions, but their contributions to co-stimulatory functions are more challenging to characterise.

I then proceeded to use the factorial stimulation assay to study the importance of the CD6 cytoplasmic tail for its function. Removal of the tail (CD6Δd3 No Tail construct) did not prevent activation of the cells in conditions with low levels of 9V peptide but high levels of generic ligand, indicating the tail is not absolutely necessary for activation, consistent with CD6 engagement activating T cells indirectly by TCR triggering (Figure 5.13A, *left side* and C, Summary Figure 5.19A). However, the generic ligand-mediated stimulation appeared slightly weaker (compare Figure 5.12C and Figure 5.13C). This would suggest that the CD6Δd3 signalling has been stopped due to the loss of the tail however, there may still be an adhesion effect which can cause some ligand independent triggering of the TCR. Crucially, at high concentrations of 9V peptide, the inhibitory effect of CD6 was completely eliminated by the loss of the CD6 tail (Figure 5.13A, *right side;* and B, D, Summary Figure 5.19B). There is a slight decrease in the levels of activation achieved between engaged and non-engaged CD6Δd3 No Tail conditions, but this difference is not statistically significant. This clearly shows the cytoplasmic tail is absolutely required for the inhibitory effect.

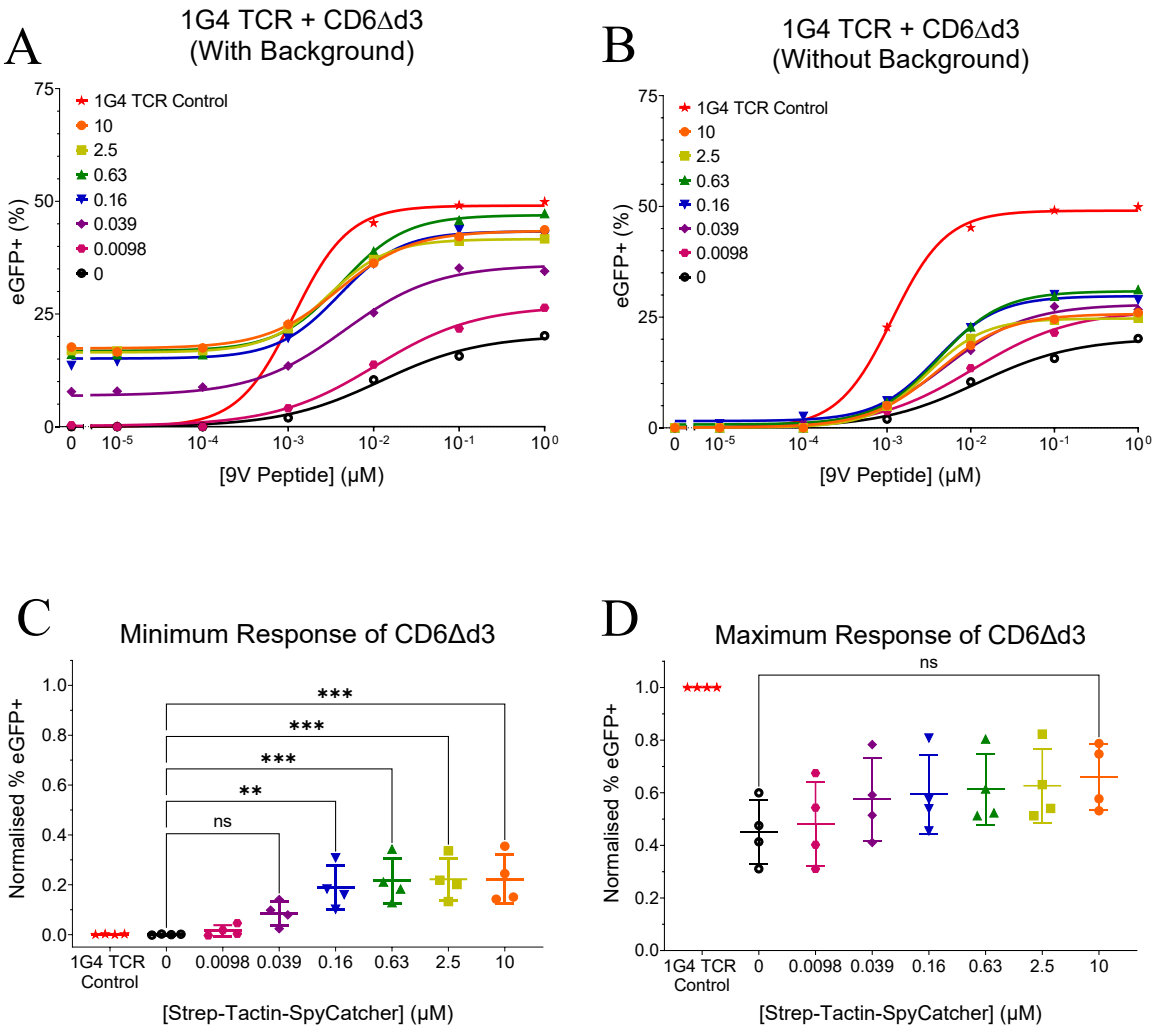


Figure 5.12: CD6Δd3 is both stimulatory and inhibitory in the context of TCR activation

(A) Representative dose response curves for CD6Δd3 cell line activation with a serial dilution of 9V peptide plus the indicated fixed concentrations of tetravalent Strep-Tactin SpyCatcher, measured by the percentage of reporter cells that are eGFP+. **(B)** The same data set without background stimulation by subtracting generic ligand only stimulation. **(C)** Percentage of eGFP+ cells at the minimum extracted from each curve in A. **(D)** Percentage of eGFP+ cells at the maximum extracted from each curve in B. Data is normalised to the 1G4 TCR control and is combined for 4 biological replicates. A one-way ANOVA was used and then Tukey's multiple comparison test to compare tetravalent Strep-Tactin SpyCatcher concentrations (ns = not significant), (** = P <0.01) (*** = P <0.001). Data generated by Elena Perticucci.

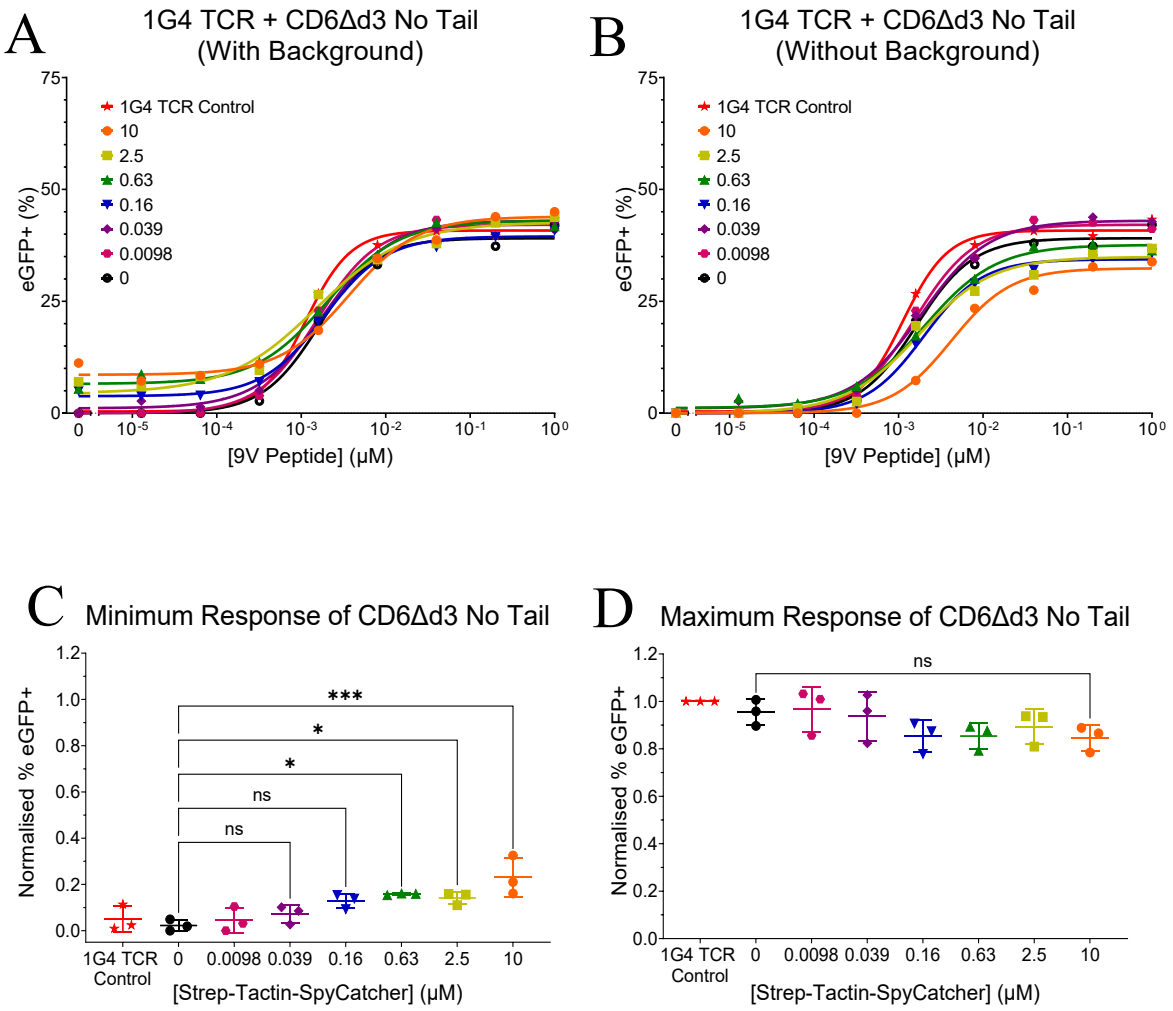


Figure 5.13: Removing the cytoplasmic tail of CD6Δd3 abolishes the inhibitory effect

(A) Representative dose response curves showing CD6Δd3 No Tail cell line activation with a serial dilution of 9V peptide plus the indicated fixed concentrations of Strep-Tactin SpyCatcher, measured by the percentage of reporter cells that are eGFP+. **(B)** The same data set without background stimulation by subtracting generic ligand only stimulation. **(C)** Percentage of eGFP+ cells at the minimum extracted from each curve in A. **(D)** Percentage of eGFP+ cells at the maximum extracted from each curve in B. Data is normalised to the 1G4 TCR control and is combined for 3 biological replicates. A one-way ANOVA was used and then Tukey's multiple comparison test to compare tetravalent Strep-Tactin SpyCatcher concentrations (ns = not significant), (* = P <0.05) (*** = P <0.001). Data generated by Elena Perticucci.

To further explore the apparent differences between the activatory and inhibitory effects of CD5 versus CD6 (Figure 5.6 and Figure 5.10). I next carried out a complementary experiment using a construct that combined the CD5 extracellular and transmembrane domains with the CD6 tail. Similar to other constructs containing the CD5 extracellular domain, the CD5/CD6 Tail chimeric construct was expressed well in the Jurkat cells (Figure 5.5). At low concentrations of 9V peptide, engagement of CD5/CD6 Tail led to strong cellular activation (Figure 5.14A, *left* and C). This confirms the importance of the CD6 tail as a key component of the stimulatory effect mediated through the TCR (Summary Figure 5.19A). Based on this and the previous evidence with short and long ligand it is unlikely that the size difference between CD5 and CD6 extracellular domain has any noticeable effect. However, the higher expression level of this construct could improve the maximum response. In a similar manner to Figure 5.12B, at high levels of 9V peptide the inhibitory effect was still present but again the CD6 tail is inducing strong co-stimulation though the TCR (Figure 5.14A and B). Unlike in Figure 5.12D, the data in Figure 5.14D shows a statistically significant increase when comparing the conditions with high levels of generic ligand (blue, green, yellow and orange curves) to the no generic ligand control (black curve). This may be evidence that the extracellular domain of CD5 is enhancing TCR activation in a ligand independent manner and in a way that the extracellular domain of CD6 cannot. This is further evidence that the extracellular domain of CD5 could be co-stimulatory.

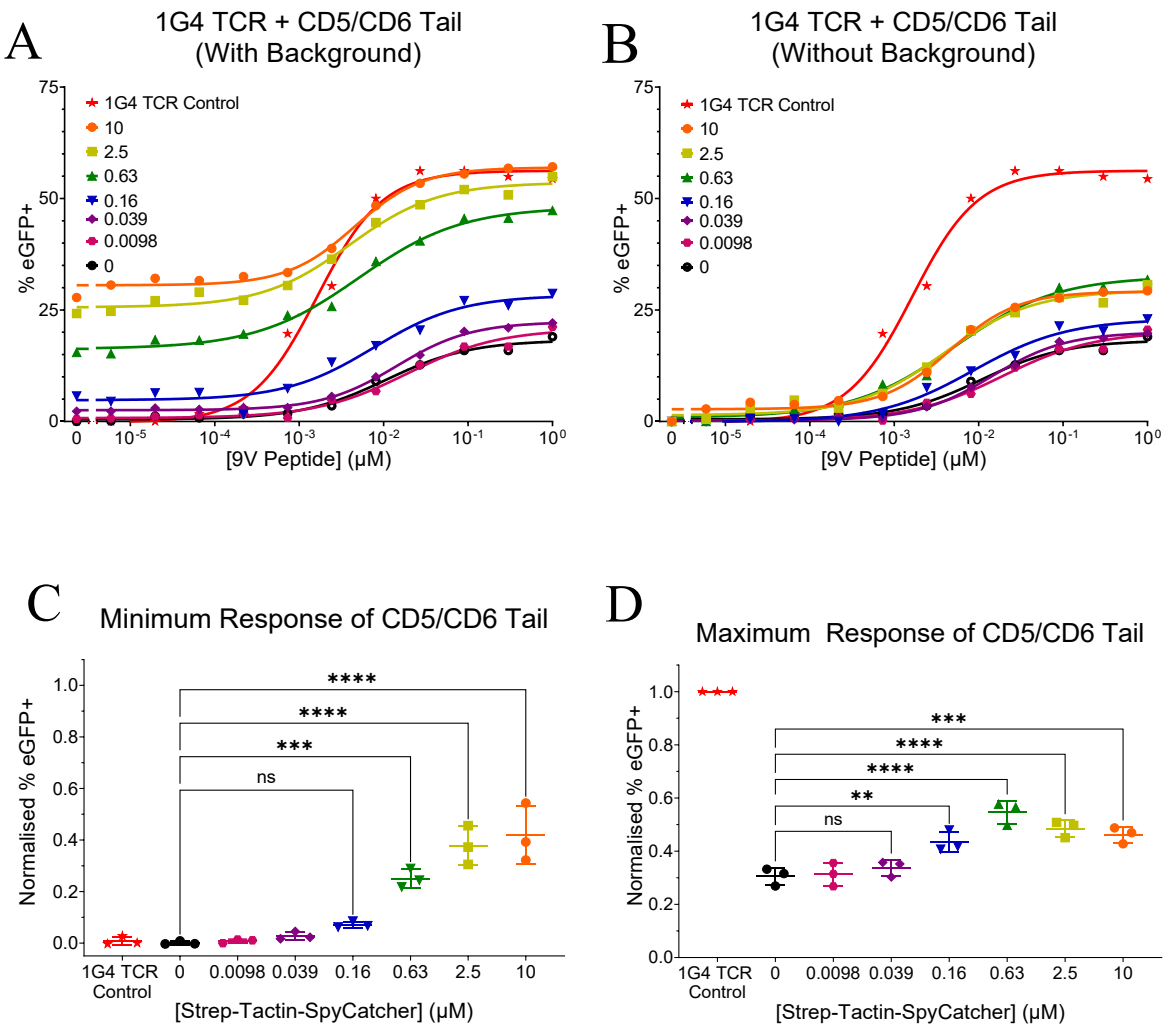


Figure 5.14: The effect of CD6Δd3 can be mimicked by the three-domain chimeric receptor CD5/CD6 Tail

(A) Representative dose response curves showing CD5/CD6 Tail cell line activation with a serial dilution of 9V peptide plus the indicated fixed concentrations of Strep-Tactin SpyCatcher, measured by the percentage of reporter cells that are eGFP+. **(B)** The same data set without background stimulation by subtracting generic ligand only stimulation. **(C)** Percentage of eGFP+ cells at the minimum extracted from each curve in A. **(D)** Percentage of eGFP+ cells at the maximum extracted from each curve in B. Data is normalised to the 1G4 TCR control and is combined for 3 biological replicates. A one-way ANOVA was used and then Tukey's multiple comparison test to compare tetravalent Strep-Tactin SpyCatcher concentrations (ns = not significant), (** = P <0.01) (*** = P <0.001) (**** = P <0.0001). Data generated by Elena Perticucci.

To explore the role of the CD5 cytoplasmic domain, a WT CD5 and a CD5 construct with the tail removed (CD5 No Tail) were tested with the same factorial stimulation assay (Figure 5.15 and Figure 5.16). For the CD5 No Tail, at low 9V peptide there is no significant co-stimulation at all (Figure 5.16A and C). This highlight two points. Firstly, compared to the CD5/CD6 chimera, it confirms the CD6 tail can induce stimulation through the TCR. I will return to this point at the end of this subsection.

Secondly, unlike for CD6 engagement, the CD5 extracellular domain is not capable of inducing any ligand independent activation of the TCR. When the factorial stimulation assay was used with WT CD5 under conditions of no 9V peptide but strong generic ligand stimulation, it led to a small but significant activation of the cells compared to no generic ligand (Figure 5.15A and C). However, this stimulation is very low and when compared to the CD5 No Tail the activation is not significantly different (Summary Figure 5.19A).

Additionally, for the CD5 No Tail at high levels of 9V peptide and generic ligand stimulation the maximum response was above that of the 1G4 TCR Control (Figure 5.16B and D). The CD5 No Tail is the only construct for which this has been observed. This again suggests that the CD5 tail is inhibitory but that this effect is masked by the CD5 extracellular domain being co-stimulatory (compare WT CD5 and CD5 No Tail when no generic ligand is added (Summary Figure 5.19B). Interestingly, this co-stimulation induced by CD5 is not dependent on generic ligand engagement, suggesting an alternative mechanism to the adhesion effect seen with CD6.

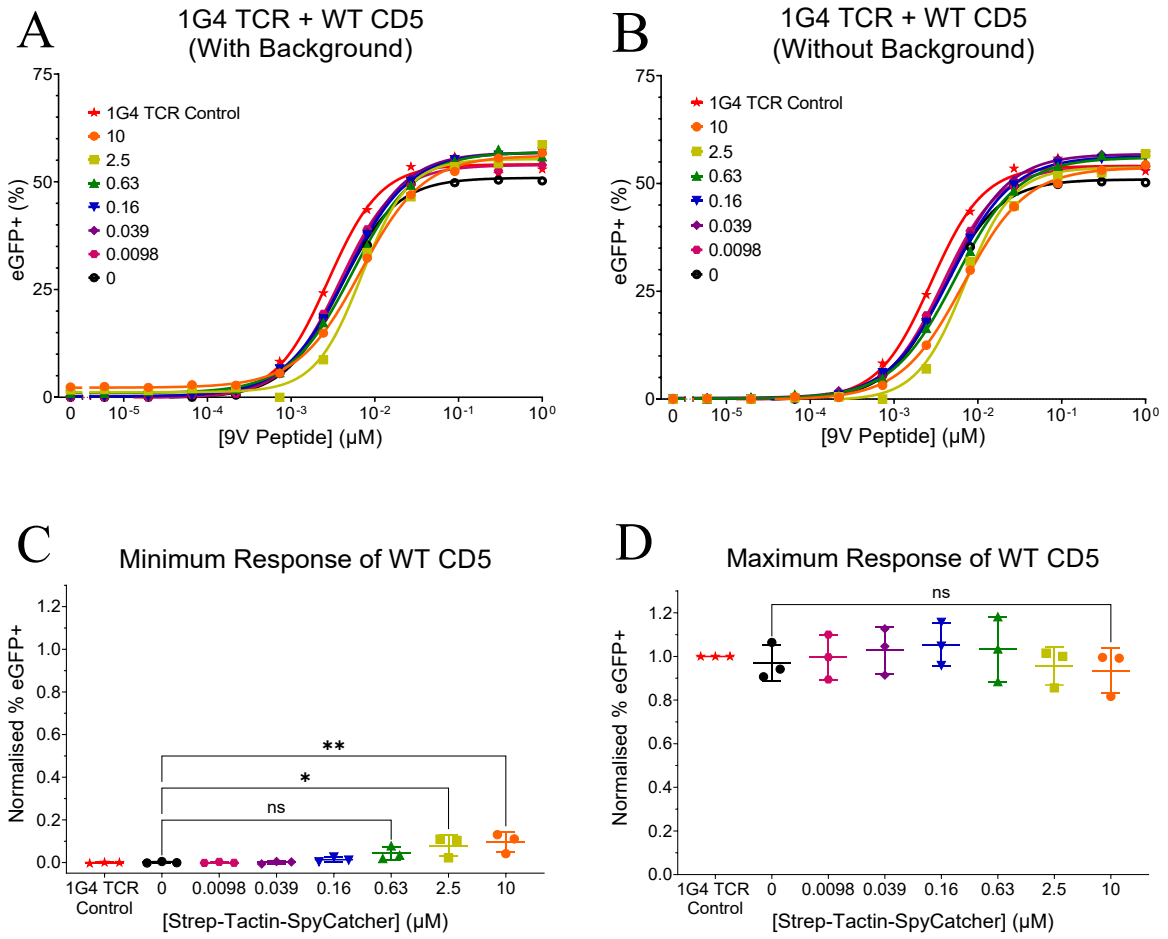


Figure 5.15: Activation of WT CD5 shows only minor effects as activatory, and inhibitory roles mask each other

(A) Representative dose response curves showing WT CD5 cell line activation with a serial dilution of 9V peptide plus the indicated fixed concentrations of Strep-Tactin SpyCatcher, measured by the percentage of reporter cells that are eGFP+. **(B)** The same data set without background stimulation by subtracting generic ligand only stimulation. **(C)** Percentage of eGFP+ cells at the minimum extracted from each curve in A. **(D)** Percentage of eGFP+ cells at the maximum extracted from each curve in B. Data is normalised to the 1G4 TCR control and is combined for 3 biological replicates. A one-way ANOVA was used and then Tukey's multiple comparison test to compare tetravalent Strep-Tactin SpyCatcher concentrations (ns = not significant), (* = P <0.05) (** = P <0.01). Data generated by Elena Perticucci.

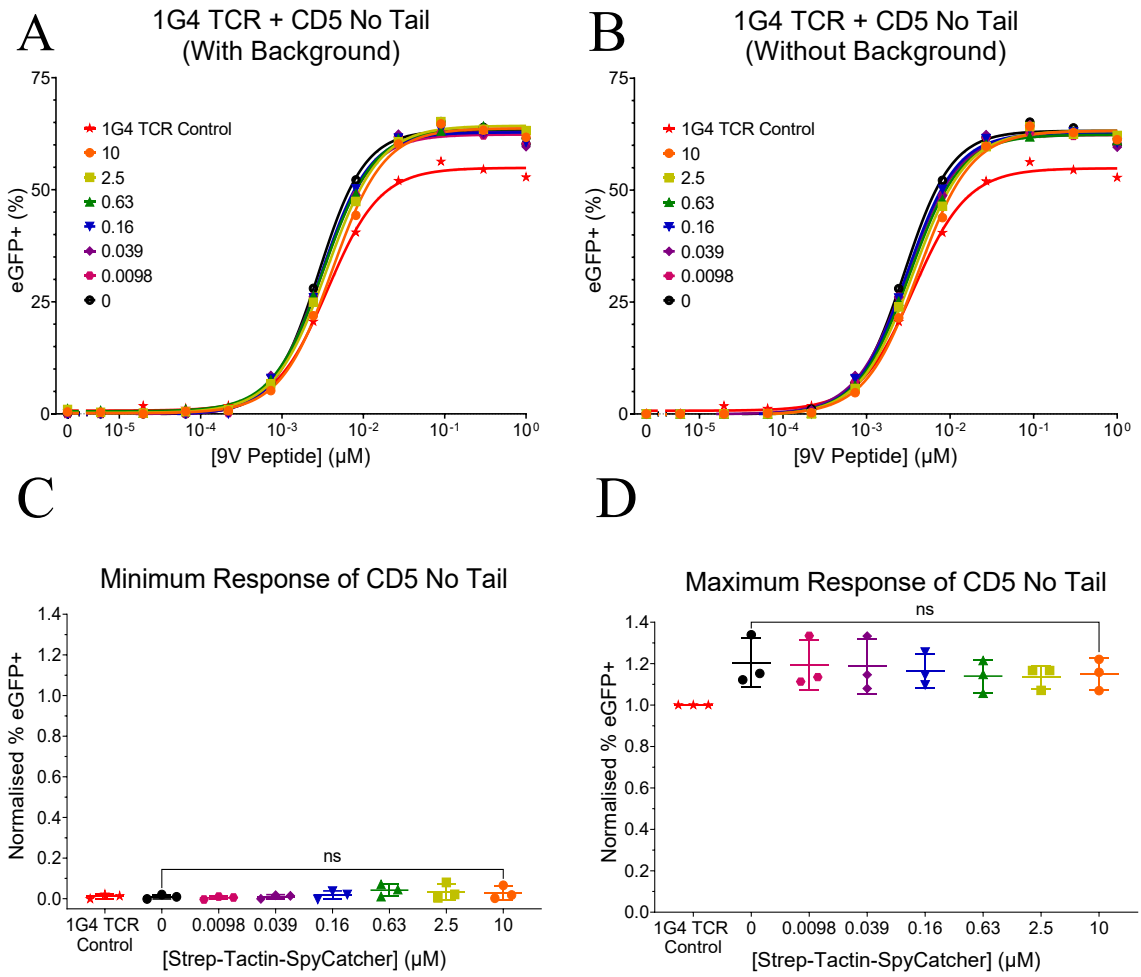


Figure 5.16: Activation of CD5 No Tail shows the inhibitory role of the CD5 tail

(A) Representative dose response curves showing CD5 No Tail cell line activation with a serial dilution of 9V peptide plus the indicated fixed concentrations of Strep-Tactin SpyCatcher, measured by the percentage of reporter cells that are eGFP+. **(B)** The same data set without background stimulation by subtracting generic ligand only stimulation. **(C)** Percentage of eGFP+ cells at the minimum extracted from each curve in A. **(D)** Percentage of eGFP+ cells at the maximum extracted from each curve in B. Data is normalised to the 1G4 TCR control and is combined for 3 biological replicates. A one-way ANOVA was used and then Tukey's multiple comparison test to compare tetravalent Strep-Tactin SpyCatcher concentrations (ns = not significant). Data generated by Elena Perticucci.

Importantly, the extracellular CD5 domain seems to only have a co-stimulatory role at high levels of TCR engagement. Losing CD5-mediated inhibition in the CD5 No Tail cells does not reveal CD6-like ligand-dependent activation at low levels of 9V peptide, unlike that seen with the CD5/CD6 Tail chimera. Again, this supports the idea that the CD6 tail does play a significant role in TCR co-stimulation, although it is not necessary for it.

Therefore, the comparison between WT CD5 and CD5 No Tail expression supports the explanation that CD5-mediated inhibition was masked in the experiments using the Jurkat reporter cells by an additional stimulatory effect which is (a) not mediated by the CD5 tail (Figure 5.16A and B) (b) generic ligand independent (Figure 5.16D), and (c) different from the engagement-dependent, CD6-mediated co-stimulation observed at low levels of 9V peptide (Figure 5.14C and Figure 5.16C). In the case of CD5 and CD5 No Tail, this masking stimulation requires the TCR to be activated by high concentrations of 9V peptide, whereas there is no stimulation at low levels of 9V peptide.

In summary, the factorial stimulation assays confirm that CD5 and CD6 are ligand independent inhibitors of TCR stimulation, and that this inhibition requires their cytoplasmic tails. They also reveal that both receptors can promote TCR-mediated co-stimulation in different ways. In the case of CD5, this is caused by the extracellular domain but does not involve its cytoplasmic tail, whereas for CD6, the tail produces the main co-stimulatory effect, but it is aided by an adhesion effect.

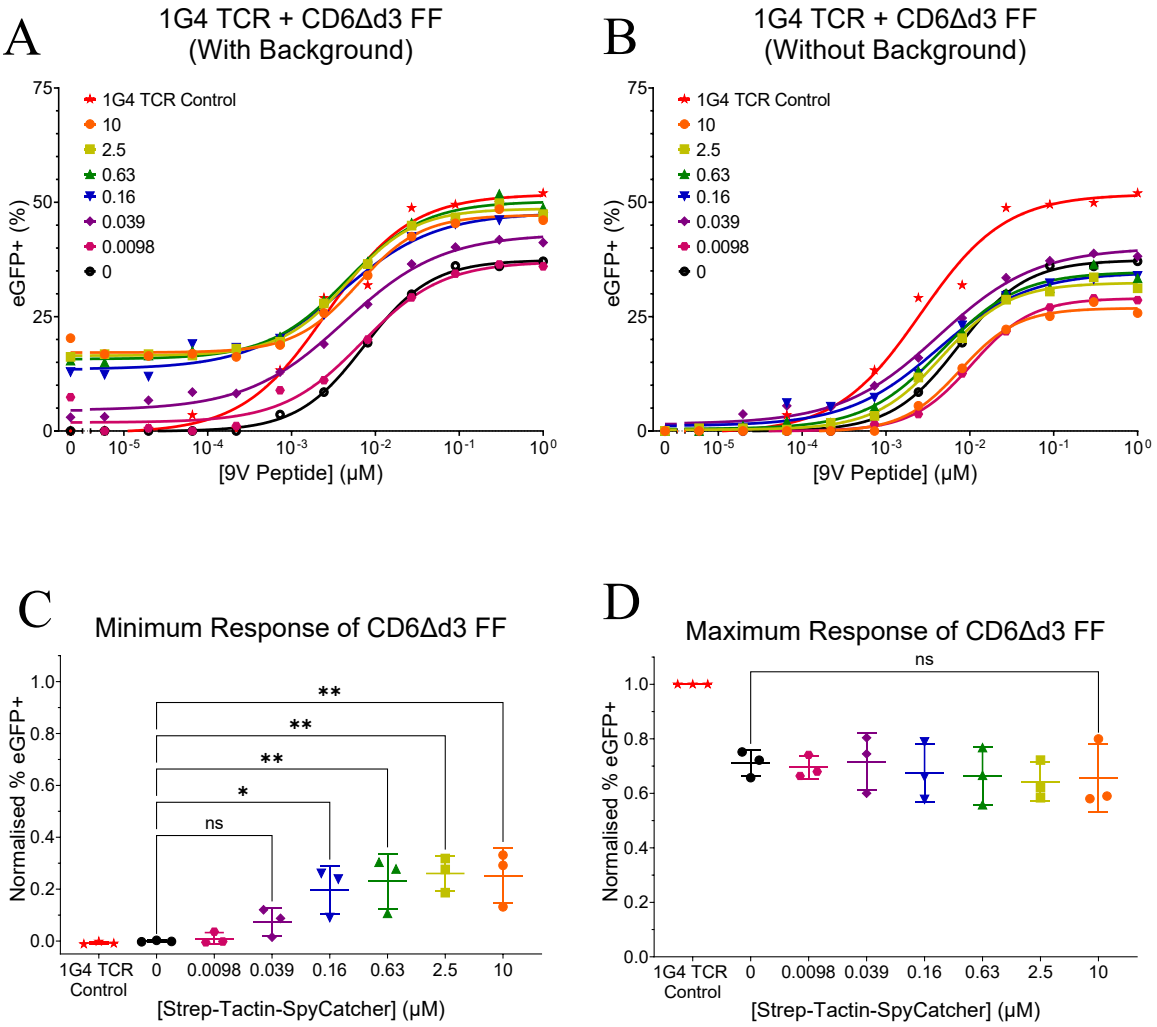


Figure 5.17: Mutating the CD6 tail tyrosine residues Y629 and Y662 does not strongly influence activation

(A) Representative dose response curves showing CD6Δd3 FF (Y629F and Y662F) cell line activation with a serial dilution of 9V peptide plus the indicated fixed concentrations of Strep-Tactin SpyCatcher, measured by the percentage of reporter cells that are eGFP+. **(B)** The same data set without background stimulation by subtracting generic ligand only stimulation. **(C)** Percentage of eGFP+ cells at the minimum extracted from each curve in A. **(D)** Percentage of eGFP+ cells at the maximum extracted from each curve in B. Data is normalised to the 1G4 TCR control and is combined for 3 biological replicates. A one-way ANOVA was used and then Tukey's multiple comparison test to compare tetravalent Strep-Tactin SpyCatcher concentrations (ns = not significant), (* = P <0.05) (** = P <0.01). Data generated by Elena Perticucci.

5.2.8. The Y629 and Y662 residues in the CD6 cytoplasmic tail may be important in localising stimulatory molecules to the TCR.

I next wanted to narrow down the activatory and inhibitory effects associated with the CD6 tail to specific tyrosine residues. Two of the most studied residues in the CD6 cytoplasmic tail are Y629 and Y662 (Alonso-Ramirez et al., 2010; Breuning et al., 2019; Breuning & Brown, 2017; Hassan et al., 2006). To investigate this the CD6Δd3 FF receptor was tested in the factorial stimulation assay (Figure 5.17A-D). At low concentrations of 9V peptide, the assay revealed no clear difference between the CD6Δd3 and the CD6Δd3 FF (Figure 5.12A and C, Figure 5.17A and C, Summary Figure 5.19A). This indicates that it is unlikely that phosphorylation of these two tyrosine residues is directly involved in the CD6 stimulatory effect mediated by the TCR. Therefore, another aspect of the CD6 tail is required in combination with the adhesive properties of the receptor ligand interactions. This is unexpected as these residues have been shown to recruit activatory molecules such as SLP-76 and GADS when phosphorylated. However, I might have seen a stronger effect if these mutations were tested in the CD5/CD6 Tail chimera where I see a stronger stimulatory effect from the CD6 tail.

At high concentrations of 9V peptide a significant proportion of the inhibitory effect on TCR activation was removed (Figure 5.12B and D, Figure 5.17B and D, Summary Figure 5.19B). This suggests that phosphorylation of these residues contributes to the inhibitory effect of CD6. This could be explained if these residues were recruiting inhibitory molecules, but there is no evidence of this. An alternative explanation is that there is competition between the CD6 and LAT recruitment of signalling molecules. With the Y629 and Y662 residues mutated, LAT could recruit more of the cells signalling apparatus towards itself following TCR triggering, thereby reducing overall inhibition.

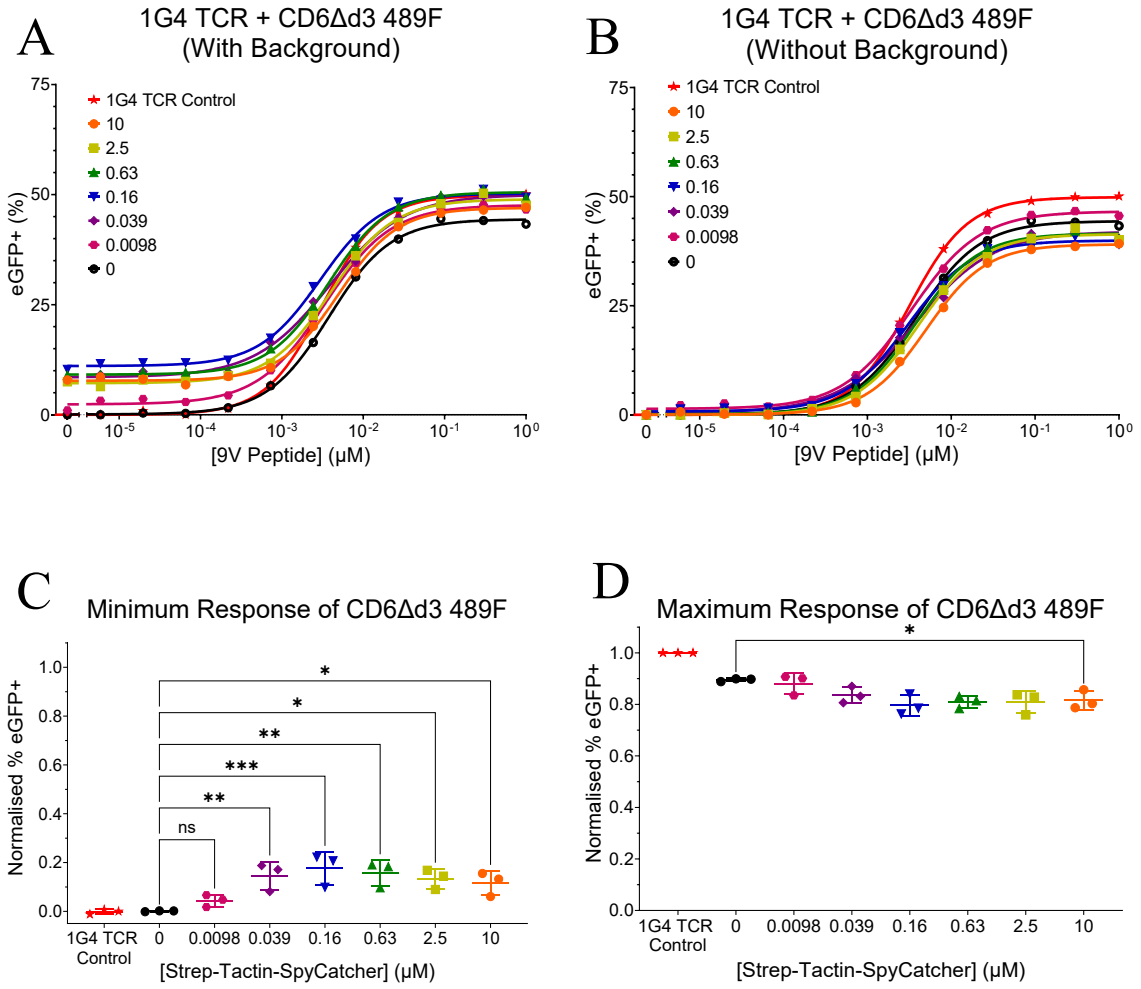
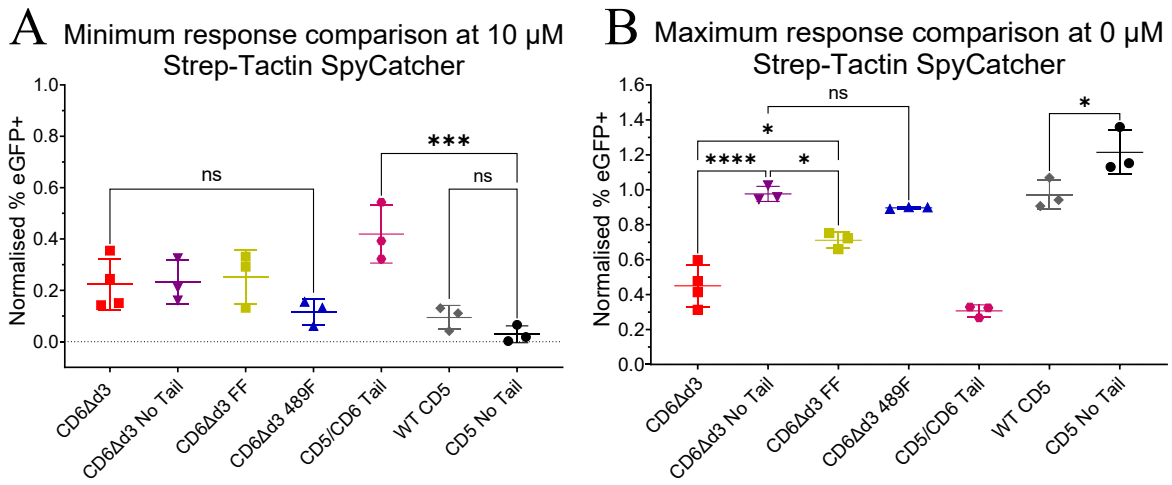


Figure 5.18: Mutating the CD6 tail tyrosine residue Y489 mimics the CD6Δd3 No tail

(A) Representative dose response curves showing CD6Δd3 489F cell line activation with a serial dilution of 9V peptide plus the indicated fixed concentrations of Strep-Tactin SpyCatcher, measured by the percentage of reporter cells that are eGFP+. **(B)** The same data set without background stimulation by subtracting generic ligand only stimulation. **(C)** Percentage of eGFP+ cells at the minimum extracted from each curve in A. **(D)** Percentage of eGFP+ cells at the maximum extracted from each curve in B. Data is normalised to the 1G4 TCR control and is combined for 3 biological replicates. A one-way ANOVA was used and then Tukey's multiple comparison test to compare tetravalent Strep-Tactin SpyCatcher concentrations (ns = not significant), (* = P <0.05) (** = P <0.01) (*** = P <0.001). Data generated by Elena Perticucci.

5.2.9. The Y489 residue in the CD6 cytoplasmic tail is responsible for much of the inhibitory effect observed

There are seven other tyrosine residues in the CD6 cytoplasmic tail, but little is known about their function. One other documented residue is Y489, which has been suggested to recruit negative downstream regulators of T cell activation (Hassan et al., 2006). To test whether phosphorylation of this residue plays a role in the observed inhibitory activity of the CD6 cytoplasmic tail, factorial stimulation assays using a CD6Δd3 receptor with a Y489F mutation (CD6Δd3 489F) were performed (Figure 5.18A-D). At low concentrations of 9V peptide, the level of stimulation was the same as that observed with CD6Δd3 cells (Figure 5.12A and C, Figure 5.18A and C, Summary Figure 5.19A). indicating that this residue is not important for CD6 co-stimulation of the TCR. Crucially, at high levels of 9V peptide, this mutation mimicked the loss of CD6 tail, with almost complete loss of the inhibitory effect on cellular activation (Figure 5.18B and D, Summary Figure 5.19B). Overall, this suggests that phosphorylation of Y489 is critical for the negative regulatory effects of CD6, consistent with previous evidence that it may recruit inhibitory downstream regulators (Hassan et al., 2006).



Summary Figure 5.19: Comparison of the effect of CD5 and CD6 constructs on the minimum and maximum response in reporter Jurkat cells expressing the 1G4 TCR

(A) Combined data for the minimum response at low 9V peptide concentrations and a high concentration of 10 µM tetravalent Strep-Tactin SpyCatcher is presented. **(B)** Combined data for the maximum response to high 9V peptide concentration and no tetravalent Strep-Tactin SpyCatcher is present. A one-way ANOVA was used and then Tukey's multiple comparison test to compare cell lines (ns = not significant), (* = P <0.05), (*** = P <0.001), (**** = P <0.0001).

5.3. Discussion

In this chapter, I present further evidence that CD6 has both stimulatory and inhibitory roles (Breuning & Brown, 2017; Mori et al., 2021). Using a natural splice variant of CD6 (CD6Δd3), I show that CD6 expression alone attenuates TCR mediated T cell activation. CD6-mediated inhibition is ligand independent, as the level of cellular activation is unchanged as binding to the generic ligand increases (once normalised by subtracting background, ligand-dependent CD6-mediated co-stimulation). By using a CD6Δd3 construct lacking a cytoplasmic tail, and a CD5 construct containing the CD6 cytoplasmic tail, I show that the CD6 cytoplasmic tail is necessary and sufficient to explain this inhibitory effect (Figure 5.20). In contrast, I find that in the presence of little or no 9V peptide, engagement of CD6 can activate T cells. This stimulatory effect is dependent on TCR expression and is a combined effect of CD6 signalling and adhesion which causes ligand independent TCR triggering. These effects were reproduced when using the CD5/CD6 Tail chimeric receptor.

The results suggest that the stimulatory effect of CD6 engagement occurs in two different ways. The first is the TCR-dependent, CD6 tail-independent ability of CD6 to form close intermembrane contacts when engaging its ligand. It is well established that CD2, another small T cell molecule that forms close membrane contacts, greatly enhances TCR mediated activation when it engages its ligand, CD58 (Kaizuka et al., 2009; Siller-Farfán & Dushek, 2018; Wild et al., 1999). In the case of CD2, this is thought to be mediated by a combination of positioning the T cell and APC membranes at the optimal distance apart for TCR engagement of the pMHC, which aids the exclusion of larger inhibitory phosphatase molecules, notably CD45, from the vicinity of the TCR (Chang et al., 2016; Davis & van der Merwe, 2006; Kaizuka et al., 2009). Our finding that the stimulatory effect of CD6 engagement is dependent on TCR expression and can occur in the absence of the CD6 cytoplasmic tail, supports an adhesive role for CD6 in the formation of close contacts at the

immunological synapse. This raises the questions as to whether engagement of CD6 with its native ligand CD166 has a similar stimulatory effect. Our findings suggesting that hamster CD166 can activate T cells expressing full length CD6 supports this, but it needs to be directly confirmed, as it is unclear whether the lengths of the CD6/CD166 and the CD6Δd3/generic ligand complexes are similar (Chappell et al., 2015; Denham et al., 2019). Thus, the differences in close-contact formation mediated by CD6 binding CD166 versus the generic ligand would need to be explored by measuring the dimensions of these interactions and testing whether changing these dimensions affects CD6 mediated T cell activation. However, my finding that activation through CD5 and CD6 is only modestly affected by generic ligand length suggests that length differences are unlikely to have a major impact, although it has not been tested in the context of combined TCR and CD6 activation.

The second mechanism mediating the stimulatory effect of CD6 is likely positive signalling through the cytoplasmic tail mediated by the TCR. The activation I see with CD6Δd3 is not significantly reduced when switching to the CD6Δd3 No tail equivalent (Summary Figure 5.19A). However, significantly less generic ligand is needed to detect an activatory response from CD6Δd3 compared with CD6Δd3 No tail. This suggests a role for CD6 tail signalling to also contribute to co-stimulation of the TCR. This was supported by the very strong activation of cells when the CD5/CD6 Tail chimera is engaged in the same way versus its equivalent CD5 No tail construct, which produced almost no stimulation (Summary Figure 5.19A). This result was unexpected and may be due to several factors including the use of the extracellular domain of CD5, higher expression level and difference in the localisation of the CD5 and CD6 transmembrane domain in the membrane. One or more of these factors may allow the CD6 tail to better produce the co-stimulatory effect mediated by the TCR.

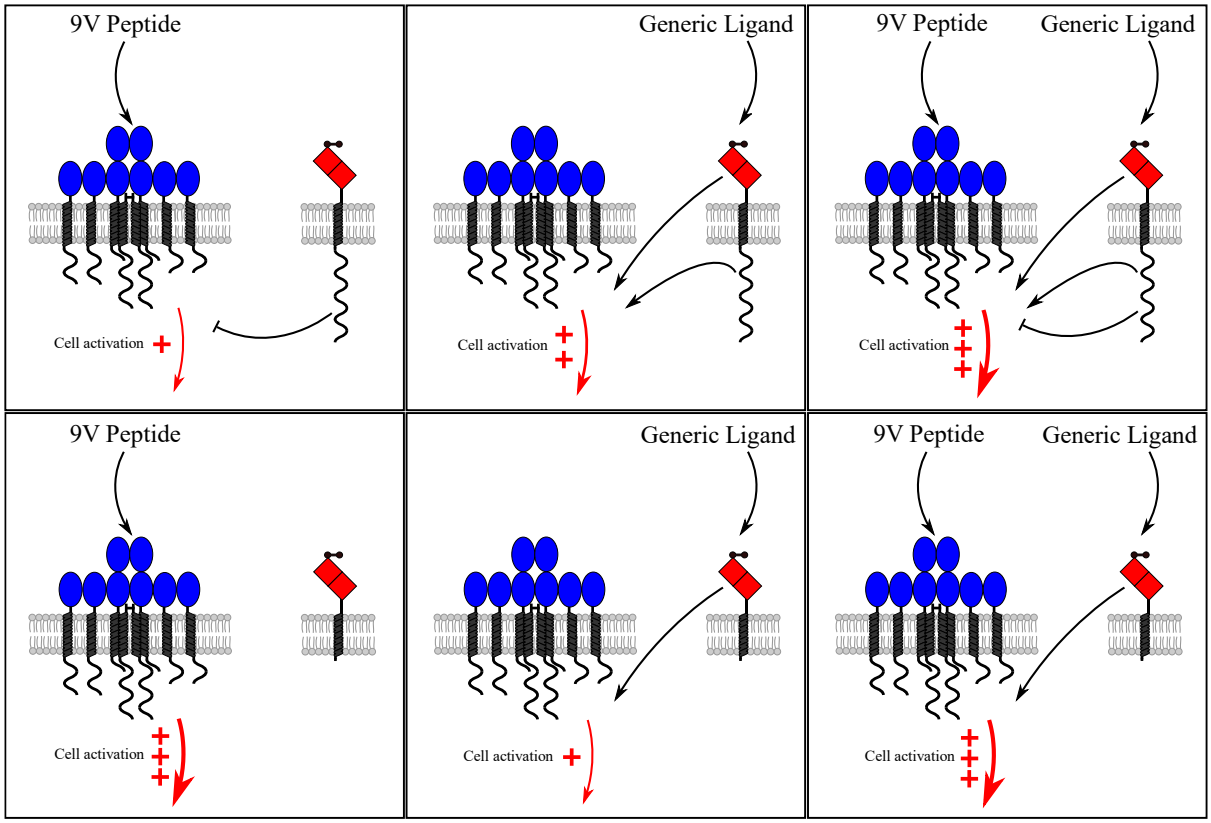


Figure 5.20: Summary diagram for CD6Δd3 and CD6Δd3 No Tail effects on TCR activation

The top three panels depict CD6Δd3 activation via high levels of 9V peptide, generic ligand, and both. The bottom three panels show the same experimental conditions for the CD6Δd3 No Tail. The size of the red arrow and number of pluses indicates the strength of the T cell response under the various conditions.

The CD6 cytoplasmic tail has been previously shown to recruit the adaptors SLP-76 and GADS to the phosphorylated Y662 and Y629 residues respectively, and it has been suggested that the GADS/SLP-76 complex helps to recruit downstream enzymes such as PLC-γ1 and ITK (Breuning & Brown, 2017). Given the GADS/SLP-76 complex is regulated by CD6 binding with CD166, it is possible that this complex contributes to the stimulatory effect of CD6 engagement in the absence of 9V peptide. This fits with the idea that CD6 can act (similarly to Lat) as a signalling scaffold for both positive and negative regulators to bind (Roncagalli et al., 2014). However, in this system I did not detect any contribution of Y662 and Y629 phosphorylation to the activatory effect of CD6. This was a surprising result given the reports in the literature (Breuning et al., 2019; Breuning & Brown, 2017) and it may be explained by the effect CD6 tail co-stimulation has in the CD6Δd3 background compared with the CD5/CD6 Tail where the co-stimulatory effect is stronger. Therefore, testing the Y662F and Y629F in the CD5/CD6 Tail construct may better show the contribution of these residues. These results need to be confirmed with WT CD6 engaging its native ligand CD166. It would be possible to produce soluble CD166 with a SpyTag and then couple this to cells expressing the SpyCatcher protein. However, this would need to be done using another ligand cell or with CHO cells after removing the native hamster CD166 expression.

The observation that mutating Y489 removes the majority of the CD6 inhibitory effect has not been previously reported. Until now there was only a single mention of this residue in the literature suggesting it could recruit inhibitory molecules (Hassan et al., 2006). The inhibitory effect was also shown to be independent of CD6 binding the generic ligand. However, CD6 binding induces co-stimulation through the TCR which results in a recovery of stimulation similar to that of the 1G4 TCR only control.

The fact the signalling of CD6 is completely dependent on the TCR suggests that the localisation of the TCR and CD6 is key to their combined function. The observation that

ligand binding to CD6 improves TCR activation strongly suggests that these molecules need to be in proximity to each other. To investigate this, I would need to do imaging experiments to better understand the location and proximity of the TCR, CD6 and other proximal signalling molecules such as LAT, SLP-76, and GADS during activation. This would involve performing similar experiments using a combination of 9V and generic ligand binding to complement the data presented here. Our collaborator Jesse Goyette at the University of New South Wales has agreed to do these experiments as they are experts in single molecule tracking in TIRF microscopy.

The initial finding that expression of CD5 in Jurkat reporter cells had no inhibitory effect when high concentrations of 9V peptide were stimulating the TCR contrasts with extensive reports on the inhibitory role of CD5 (Burgess et al., 1992; Voisinne et al., 2018). However, this experiment did show that engagement of CD5 via the generic ligand was significantly less stimulatory versus CD6. Subsequently expression of CD5 in the reconstituted No TCR cells showed a similar ligand independent inhibitory effect as CD6 plus showed very weak stimulation via generic ligand engagement. Differences in the CD5 effect between the two cell lines may be explained by higher endogenous levels of CD5 in the No TCR cells which leads to greater inhibition.

Removal of the CD5 tail was a key step to unlocking this complex effect. It revealed a costimulatory effect of the CD5 extracellular and transmembrane domain, which was not seen for any other receptor. This suggests that the CD5 cytoplasmic tail has an inhibitory effect which is masked by an activatory effect of the rest of the CD5 molecule (Figure 5.21). Crucially this activatory effect is not dependent on ligand binding unlike CD6. This would fit the fact that a ligand for CD5 has never been confirmed. A possible experiment to follow this effect would be to express the CD5 tail fused to the extracellular and transmembrane domains of a different receptor, such as CD6 (CD6/CD5), to confirm it is in fact responsible for the

inhibition. The effect may also be due to localisation of the TCR and CD5. However again this would require detailed imaging experiments to elucidate further.

These findings add to a growing body of evidence that CD6 can have both inhibitory and stimulatory effects. Its effect on T cell activation is likely to rely upon the wider context within which T cells function, including the availability of its native ligand as well as the level of TCR stimulus. The fact that CD166 is expressed widely on professional APCs suggests that the function of CD6 may be tightly fine-tuned by ligand engagement during antigen presentation (Bowen et al., 1995). Therefore, given its potential role in autoimmune diseases (Consuegra-Fernández et al., 2017; De Jager et al., 2009; Y. Li et al., 2017), and its potential as a therapeutic target (Krupashankar et al., 2014), it is important that we further explore how this accessory receptor behaves.

This data further highlights the complex role CD5 and CD6 play in the immune system. The fact that these molecules can be both activatory and inhibitory and that their effects are mediated via the TCR explains why defining their function in the literature has been so challenging. The generic ligand system offers a unique way of studying these interactions by carefully controlling the combination of ligands presented. This study has highlighted small changes in expression level of different components can alter the balance of signals and even differences between Jurkat cell lines can influence the effect of these receptors, further complicating matters. This also highlights the need to confirm the results found using cell lines with experiments performed in primary cells. However, the same generic ligand system can be used for these experiments.

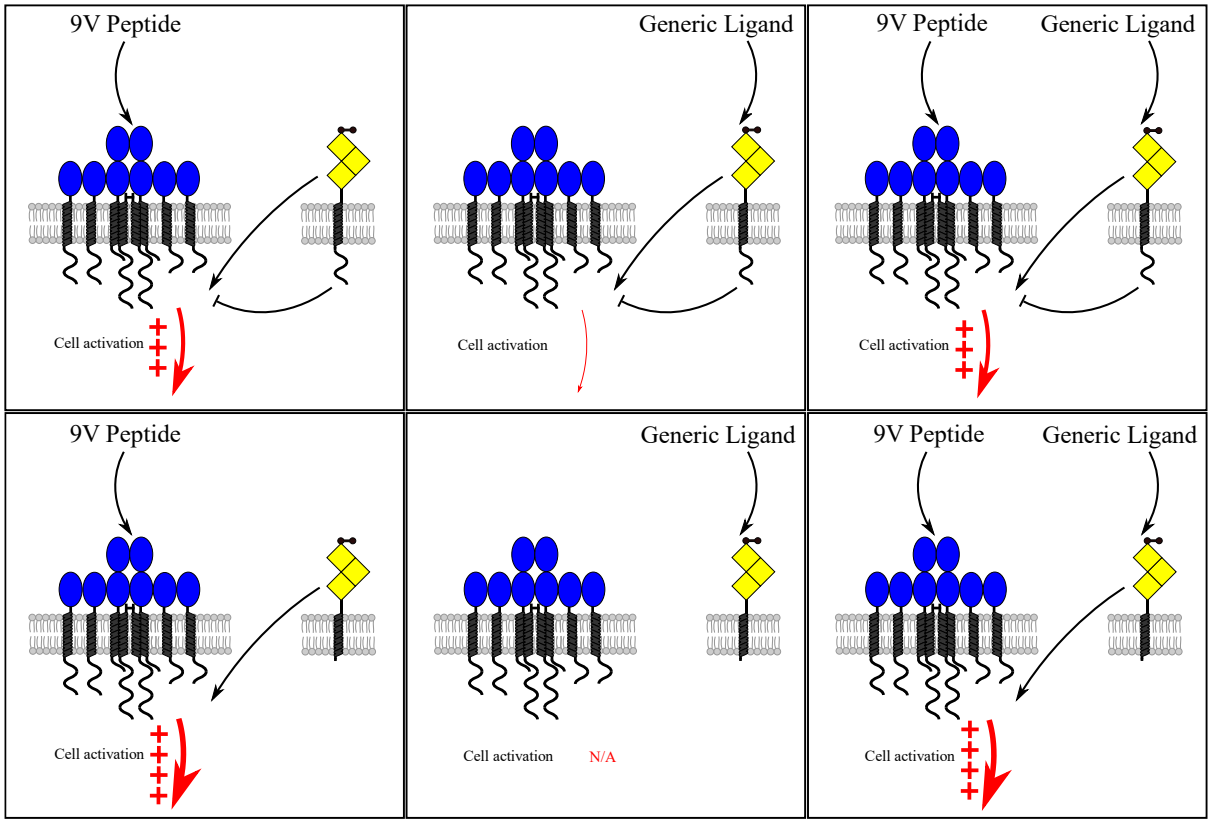


Figure 5.21: Summary diagram for WT CD5 and CD5 No Tail effects on TCR activation

The top three panels depict WT CD5 activation via high levels of 9V peptide, generic ligand, and both. The bottom three panels show the same experimental conditions for the CD5 No Tail. The size of the red arrow and number of pluses indicates the strength of the T cell response under the various conditions.

Chapter 6 - How variants in SARS-CoV-2 RBD domain and its ligand ACE2 change the binding affinity and kinetics

6.1. Introduction

The emergence of severe acute respiratory syndrome coronavirus 2 (SARS-CoV-2) in 2019 and the subsequent pandemic that followed has been the greatest medical challenge the modern world has ever faced. While most people infected with the virus can clear the infection in a couple of weeks, a minority will experience severe disease and even death (P. Zhou et al., 2020). Certain factors such as age and comorbidities significantly increase a person's risk of severe disease (Guan et al., 2020; Verity et al., 2020). However, what is unknown is to what extent genetic factors influence this risk (Cao et al., 2020). Therefore, being able to identify which genetic variants in a population give rise to more risk is of clear benefit to shaping care and potentially priority for booster vaccines.

While research is ongoing at all levels of viral infection from initial infection, viral replication, transmission, and immune response (Kumar et al., 2020) I have focused on the initial first contact between the virus and our cells. This interaction is mediated via the spike protein on the virus binding to human angiotensin-converting enzyme 2 (ACE2) (Hoffmann, Kleine-Weber, Schroeder, et al., 2020; P. Zhou et al., 2020). ACE2s main function is complex but it is thought to regulate heart function (Keidar et al., 2007; Oudit et al., 2003). The same ACE2 receptor was the target of the previous SARS-CoV-1 epidemic in 2002 and there is therefore a large body of research to build from (Hoffmann, Kleine-Weber, Schroeder, et al., 2020; Li et al., 2005; Wan et al., 2020). The spike protein interacts with ACE2 via is receptor binding domain (RBD) and the crystal structure of both viruses share a very similar binding interface (Li et al., 2005; Shang et al., 2020). Work on SARS-CoV-1 has

also highlighted the link between spike binding affinity to ACE2 and infectivity. This may be crucial as SARS-CoV-2 has at least fivefold increased affinity for ACE2 (Shang et al., 2020).

This work started as a collaboration to validate a bioinformatic approach to predicting RBD binding to all possible missense variants in ACE2 (Macgowan et al., 2022). This prediction method has the potential to firstly identify variants that would offer strong or complete protection from SARS-CoV-2 entry into cells via ACE2. Alternatively, it could predict variants that would strongly increase the affinity for ACE2 binding RBD, which might result in an increased risk factor to individuals with those variants, but this is unclear at the current time. An alternative benefit to identifying increased affinity ACE2 variants could be to purify them and then use it as a soluble protein therapy to soak up virus particles in patients with acute symptoms (Monteil et al., 2020).

There are hundreds of ACE2 variants across the human population, a subset of which are specifically located in the RBD-ACE2 binding interface (Macgowan et al., 2022). The known variants have been identified by using the Genome Aggregation Consortium Database (gnomAD) and then mCSM-PPI2 mutation effect predictor used to estimate their RBD affinity *in silico* (Karczewski et al., 2020; Rodrigues et al., 2019). Detailed experimental characterisation of each variant would be extremely time consuming and costly therefore, being able to predict to what extent each variant alters RBD affinity would be greatly beneficial. To assess the validity of the prediction, I purified WT and ten ACE2 missense variants and subsequently characterised their RBD affinity using surface plasmon resonance (SPR). While I do not find the predicted affinity for the variants accurately represents my measurements, it is a starting point which can be refined using the SPR measurements I have produced. Importantly, I can confirm that common ACE2 variants significantly alter RBD affinity. This is particularly true for the two most common ACE2 variants K26R and S19P. They were predicted *in silico* to have very little effect on ACE2 affinity, but with SPR I have

shown that both significantly increase affinity for RBD. Therefore, they could represent an important risk factor for those individuals that have them.

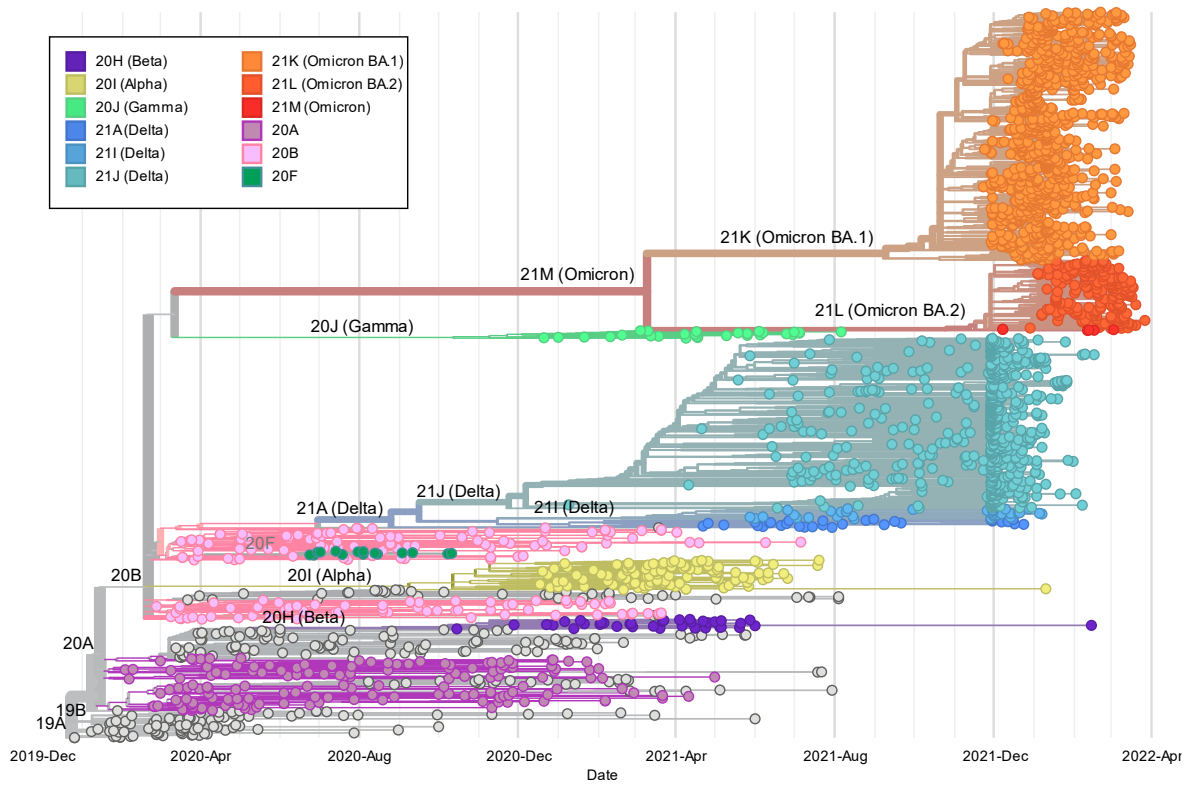
The second wave of the virus, which gripped the world during the winter of 2020-2021, has been predominantly driven by the emergence of new variants with the potential to increase transmissibility and/or disease severity (Davies et al., 2021; Korber et al., 2020; Washington et al., 2021). On a more worrying note, there is the potential for new variants to infect individuals with previous immunity and diminish vaccine protection (Dejnirattisai et al., 2021; Madhi et al., 2021; Mahase, 2021). The first variant of note (D614G in the spike protein) occurred in mid-2020 and quickly became dominant. It is thought that the furin-cleavage site was a key factor in allowing the virus to transfer to humans (Hoffmann, Kleine-Weber, & Pöhlmann, 2020). However, this leads to the S1 and S2 subunits of the spike protein being linked by non-covalent intermolecular forces and causes S1 shedding. This reduced the viral infectivity and so it quickly adapted to incorporate the D614G mutation. This acts to stabilise the spike protein and reduce S1 shedding thereby increasing infectivity (Zhang et al., 2020, 2021).

The rapid growth of the virus means mutations are constantly occurring and therefore new viral variants are emerging quickly. During the autumn of 2020 a number of other mutations occurred directly in the RBD-ACE2 binding interface that strongly increased affinity for ACE2 (Starr et al., 2020; Supasa et al., 2021). This can be seen in Figure 6.1 with the phylogenetic tree where each dot represents a new variant. This plot also shows how the growth of the second wave of infections over the winter of 2020-2021 led to the number of new variants also increasing rapidly (Rambaut et al., 2020). Of note among these new variants were several key mutations in the RBD-ACE2 interface. Mutations at this site are of particular importance not only for modulating the affinity but many antibody responses target the spike protein and particularly this region of the RBD (Chen et al., 2021).

The Alpha variant, which has the RBD mutation N501Y was first identified in the UK and rapidly spread throughout the country and then around the world. The E484K mutation was also identified at the same time and E484K and N501Y were found in both the Beta and the Gamma variants along with another RBD-ACE2 interface mutation K417N/T. An additional variant I also looked at was S477N, which was found early on in Australia and quickly out competed the WT before it was brought under control though tough lockdowns. It has subsequently emerged in New York and Europe (H. Zhou et al., 2021).

What makes S477N, E484K and N501Y variants so important is the fact they have all appeared independently multiple times around the world and are all located in the RBD-ACE2 interface (Figure 6.1B). It was therefore likely that these mutations could alter the binding kinetics to improve infectivity. These mutations were also identified independently following random mutagenesis of the RBD and then selecting mutants which exhibited enhanced affinity for ACE2 (Zahradník et al., 2021). After making and characterising the first round of ten RBD variants which we published (Barton et al., 2021) the virus continued to mutate over the spring of 2021 and I decided to make a further 6 RBD mutations that had emerged with the primary focus being the new Delta variant. This superseded almost all previous variants in both infectivity and clinical severity (Mishra et al., 2021; Teyssou et al., 2021) and is now being replaced by Omicron (Figure 6.1A) (Nishiura et al., 2022). Even more concerning is the reduction in vaccine effectiveness against new variants which poses major challenges to current vaccine programs and the potential need for further booster shots in the future (Bernal et al., 2021).

A



B

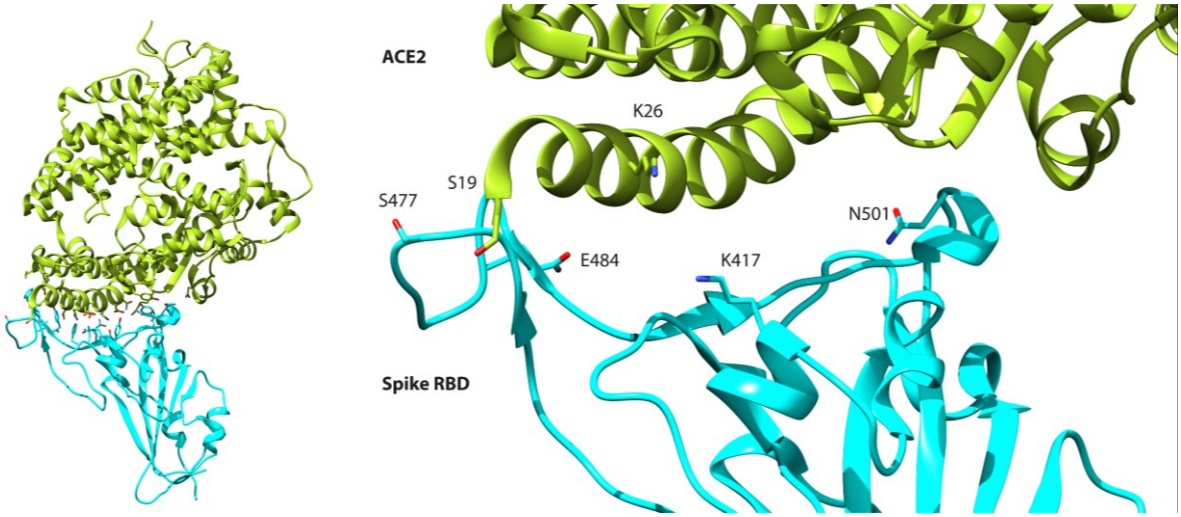


Figure 6.1: SARS-CoV-2 RBD variants

(A) Phylogenetic tree of SARS-CoV-2 from Nextstrain Global, sequences from the GISAID database (Accessed April 2022, N = 4,017). **(B)** The structure of SARS-CoV-2 Spike RBD (cyan) in complex with human ACE2 (green) with key residues marked (PDB ID: 6m0j) (Figure made by Stuart MacGowan).

The current issue facing the literature is the lack of well controlled binding data showing the affinity and binding kinetics for the ACE2-RBD interaction for the different variants (Shang et al., 2020; Supasa et al., 2021). Without precise measurements it is difficult to determine the effect of each RBD variant on the biology of the virus, and whether they were selected based on altering the binding affinity, immune evasion, or both.

6.1.1. SPR is the gold standard to quantify protein binding affinity and kinetics

This project relied on SPR which is a label free method to quantify protein/protein interactions and allows for very accurate measurement of affinity and kinetics (Myszka, 1997). One protein is immobilised in a flow cell of the sensor chip (ligand) with the second protein injected continuously over the surface in solution (analyte). The association of the analyte to the ligand results in a refractive index change that is detected at the sensor surface. The analyte injection is stopped, and buffer run over the surface to allow the dissociation to take place. A reference flow cell with no ligand is used to subtract refractive index changes unrelated to protein binding. Additionally double referencing using additional buffer injections further removes artifacts in the binding trace such as instrument noise and baseline drift (Myszka, 1999). The main competitor to SPR is bio-layer interferometry (BLI) which is less sensitive but allows for much higher throughput (Abdiche et al., 2008). While significantly cheaper the technique cannot measure very accurate rate constants due to the lack of continuous analyte flow over the ligand. This leads to artifacts such as slower rate constants due to rebinding events. This has been observed in several papers reporting binding data for RBD-ACE2 interactions (Supasa et al., 2021; Wrapp et al., 2020; Zhang et al., 2021).

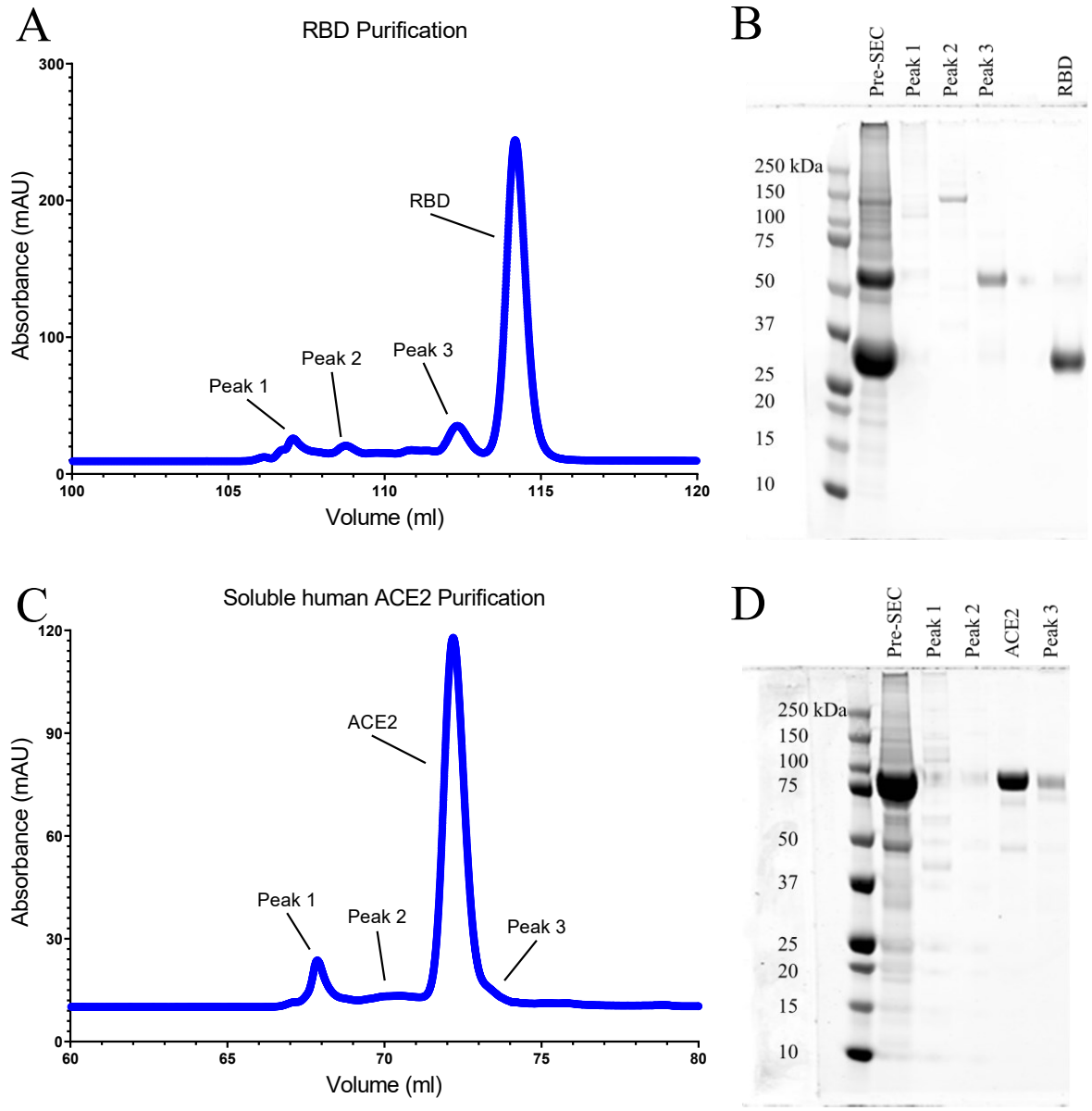


Figure 6.2: Purification of SARS-CoV-2 receptor binding domain and soluble human ACE2

(A) Size exclusion chromatography of RBD. Contaminating peaks are labelled peak 1-3 with the large peak corresponding to pure RBD. **(B)** SDS-PAGE gel, lane 1 contains a protein ladder, lane 2 contains the material after His tag purification, lanes 3-5 contain contaminating proteins removed by SEC and lane 7 contains the purified RBD. **(C)** Size exclusion chromatography of soluble human ACE2. Contaminating peaks are labelled peak 1-3 with large peak corresponding to pure ACE2. **(D)** SDS-PAGE gel, lane 1 contains a protein ladder, lane 2 contains the material after His tag purification, lanes 3, 4 and 6 contain contaminating proteins removed by SEC and lane 5 contains the purified ACE2.

6.1.2. Key findings

In this chapter I produce recombinant RBD and ACE2 in mammalian cells and optimise an SPR assay to measure RBD-ACE2 affinity. I then assess binding of ten ACE2 variants to WT RBD and show that the predicted values do not match my measurements. However, it appears that this is predominantly due to a systematic error with the prediction algorithm. I then focus on obtaining detailed affinity and kinetic measurements for the RBD WT and variants binding ACE2 WT and the two most common variants K26R and S19P. To do this I have optimised the assay to work at very low ACE2 immobilization levels in order to reduce artifacts such as rebinding events and mass transport limitations (Myszka, 1997). I test how different mutations affect RBD affinity for ACE2. The mutations S477N, E484K and N501Y resulted in increased affinity, which suggests why these variants were selected for. While the Beta and Gamma variants also both increase the affinity, it was dampened by the mutations K417N and K417T respectively, both of which significantly decrease the affinity. The subsequent Epsilon (L452R) and Kappa (T478K/E484Q) RBD variants had very little effect on RBD affinity. However, the Delta (L452R/T478K) and Omicron (BA.2) variants did still show a clear increase in affinity for ACE2. This highlights that all successful variants have been selected for on the basis of increased transmissibility via improving the affinity, but other factors such as improved spike protein cleavage and immune evasion have also been selected for.

6.2. Results

6.2.1. Production of SARS-CoV-2 receptor binding domain (RBD)

I began by purifying the SARS-CoV-2 RBD and soluble human ACE2 because they were the minimum requirements needed to set up the SPR assay. This was done using HEK293F suspension cells to maintain the correct posttranslational modifications. The size exclusion chromatography (SEC) of this preparation is shown in Figure 6.2A where you can see three

small contaminating peaks before the large peak corresponding to pure RBD. Each of these peaks was run on an SDS-PAGE gel shown in Figure 6.2B. The Pre-SEC material shows that many contaminating proteins are pulled down during the His tag purification along with RBD. The RBD has a molecular weight of 25.9 kDa which is smaller than the strongest band in the Pre-SEC lane. However, the RBD is expected to be glycosylated which would account for this size discrepancy. After SEC, most of these contaminating proteins have been successfully removed, leaving a relatively pure sample of RBD.

6.2.2. Production of soluble human ACE2

ACE2 production incorporated the biotinylation of the protein during the expression phase which is considerably more efficient than biotinylating the protein after purification. The biotinylation allows for capture of the ACE2 via streptavidin on the chip surface in SPR. The SEC of this preparation shows three small contaminating peaks either side of a single large peak corresponding to pure ACE2 (Figure 6.2C). A sample of material from each peak and a Pre-SEC sample were run on an SDS-PAGE gel shown in Figure 6.2D. The soluble ACE2 has a molecular weight of 71.8 kDa which is again slightly smaller than the ACE2 band on the gel, but this difference can also be accounted for due to glycosylation of the protein. The gel shows the various contaminating bands have been removed leaving a relatively pure sample of ACE2.

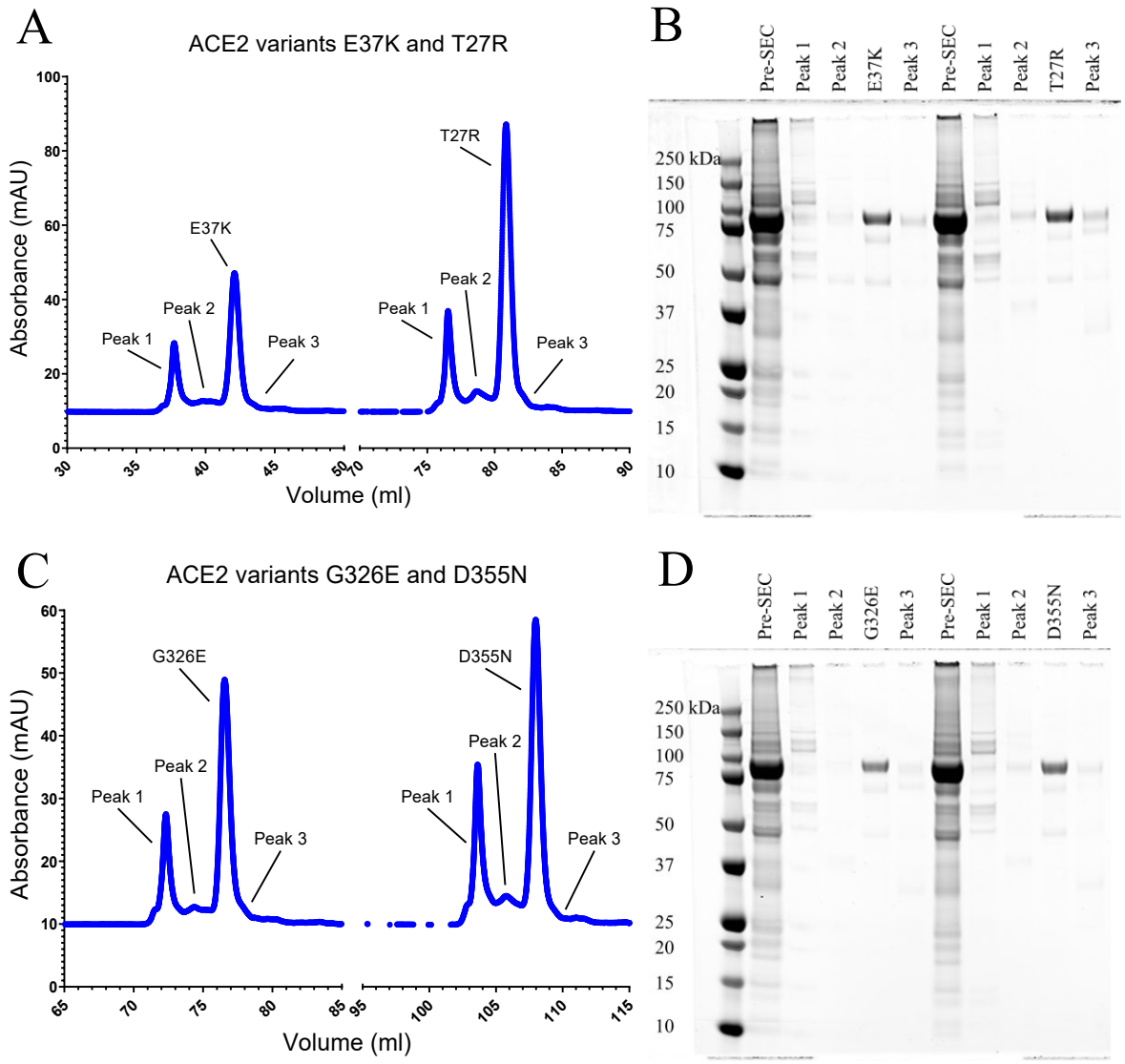


Figure 6.3: Purification of soluble human ACE2 variants E37K, T27R, G326E and D355N

(A) Size exclusion chromatography of ACE2 variants E37K and T27R. Contaminating peaks are labelled peak 1-3 with large peaks corresponding to pure ACE2. **(B)** SDS-PAGE gel, lane 1 contains a protein ladder, lanes 2 and 7 contains the material after His tag purification, lanes 3, 4, 6, 8, 9 and 11 contain contaminating proteins removed by SEC. Lane 5 contains purified E37K and lane 10 contains the purified T27R. **(C)** Size exclusion chromatography of ACE2 variants G326E and D355N. Contaminating peaks are labelled peak 1-3 with large peaks corresponding to pure ACE2. **(D)** SDS-PAGE gel, lane 1 contains a protein ladder, lanes 2 and 7 contains the material after His tag purification, lanes 3, 4, 6, 8, 9 and 11 contain contaminating proteins removed by SEC. Lane 5 contains purified G326E and lane 10 contains the purified D355N.

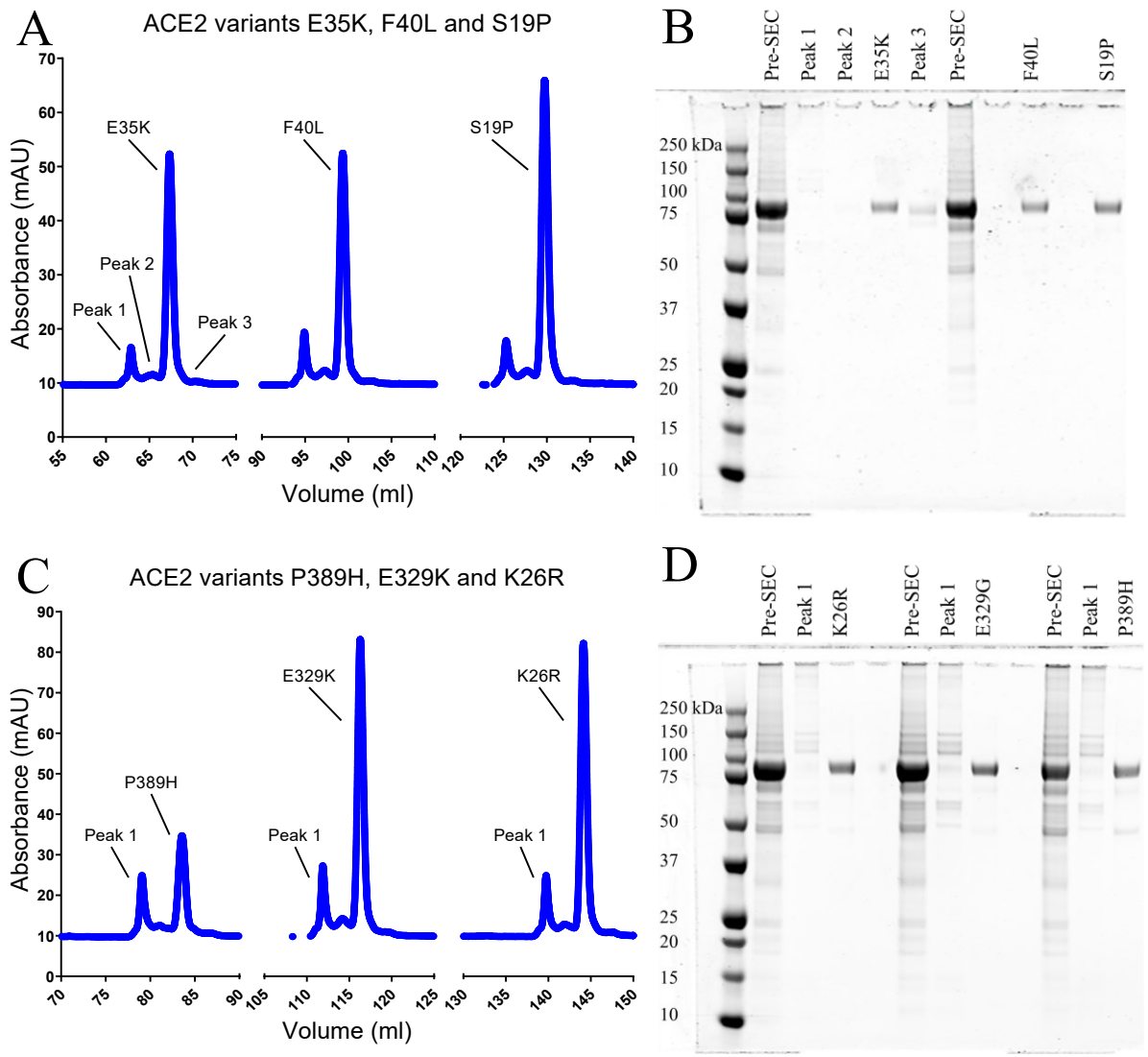


Figure 6.4: Purification of soluble human ACE2 variants E35K, F40L, S19P, P389H, E329K and K26R

(A) Size exclusion chromatography of ACE2 variants E35K, F40L and S19P. Contaminating peaks are labelled peaks 1-3 with large peaks corresponding to pure ACE2. **(B)** SDS-PAGE gel, lane 1 contains a protein ladder, lanes 2 and 7 contain the material after His tag purification for E35K and F40L respectively, lanes 3, 4 and 6 contain contaminating proteins removed by SEC. Lane 5 contains purified E35K, lane 9 contains purified F40L and lane 11 contains the purified S19P. **(C)** Size exclusion chromatography of ACE2 variants P389H, E329K and K26R. Contaminating peaks are labelled peak 1 with large peaks corresponding to pure ACE2. **(D)** SDS-PAGE gel, lane 1 contains a protein ladder, lanes 2, 6 and 10 contains the material after His tag purification, lanes 3, 7 and 11 contain contaminating proteins removed by SEC. Lane 4 contains purified K26R, lane 8 contains purified E329K and lane 12 contains the purified P389H.

6.2.3. Production of ten ACE2 variants

To generate the ACE2 variants the desired single nucleotide changes were introduced into the WT construct via site-directed mutagenesis. The protein was then produced in the same way as the WT ACE2 with the same in situ biotinylating method used during the production of all ACE2 variants. Each of these proteins behaved in a very similar way to the WT ACE2.

The SEC in Figure 6.3A and C shows each of the four protein preparations for the Phase 1 variants (E37K, T27R, G326E and D355N). The SEC in Figure 6.4A and C shows each of the six protein preparations for the Phase 2 variants (E35K, F40L, S19P, P389H, E329K and K26R). The only outlier was the slightly lower yield for the P389H variant which may be due to several factors during purification. For example, the quality of the DNA preparation, the viability of the cells or the stability of this variant. In all cases, samples from each contaminating peak and the pure ACE2 variants were run on an SDS-PAGE gel and appear identical to that of the WT ACE2 (Figure 6.3B and D and Figure 6.4B and D).

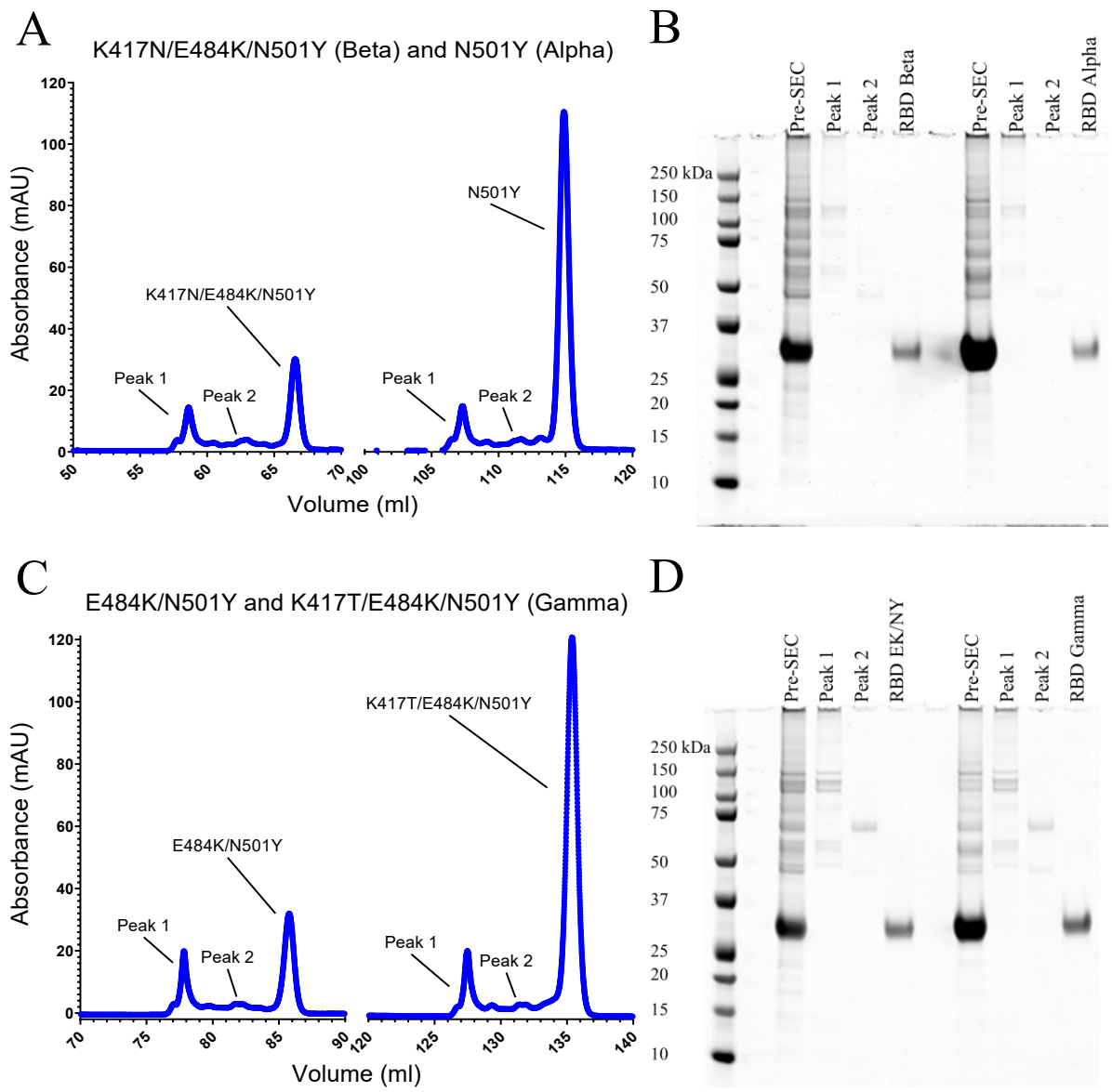


Figure 6.5: Purification of Alpha, Beta, Gamma and EK/NY SARS-CoV-2 RBD variants

(A) Size exclusion chromatography of Beta variant (K417N, E484K and N501Y) and Alpha variant (N501Y). Contaminating peaks are labelled peak 1-2 with large peaks corresponding to pure RBD. **(B)** SDS-PAGE gel, lane 1 contains a protein ladder, lanes 3 and 8 contains the material after His tag purification, lanes 4, 5, 9 and 10 contain contaminating proteins removed by SEC. Lane 6 contains purified Beta RBD and lane 11 contains the purified Alpha RBD. **(C)** Size exclusion chromatography of EK/NY variant (E484K and N501Y) and Gamma variant (K417T, E484K and N501Y). Contaminating peaks are labelled peak 1-2 with large peaks corresponding to pure RBD. **(D)** SDS-PAGE gel, lane 1 contains a protein ladder, lanes 3 and 8 contains the material after His tag purification, lanes 4, 5, 9 and 10 contain contaminating proteins removed by SEC. Lane 6 contains purified EK/NY RBD and lane 11 contains the purified Gamma RBD.

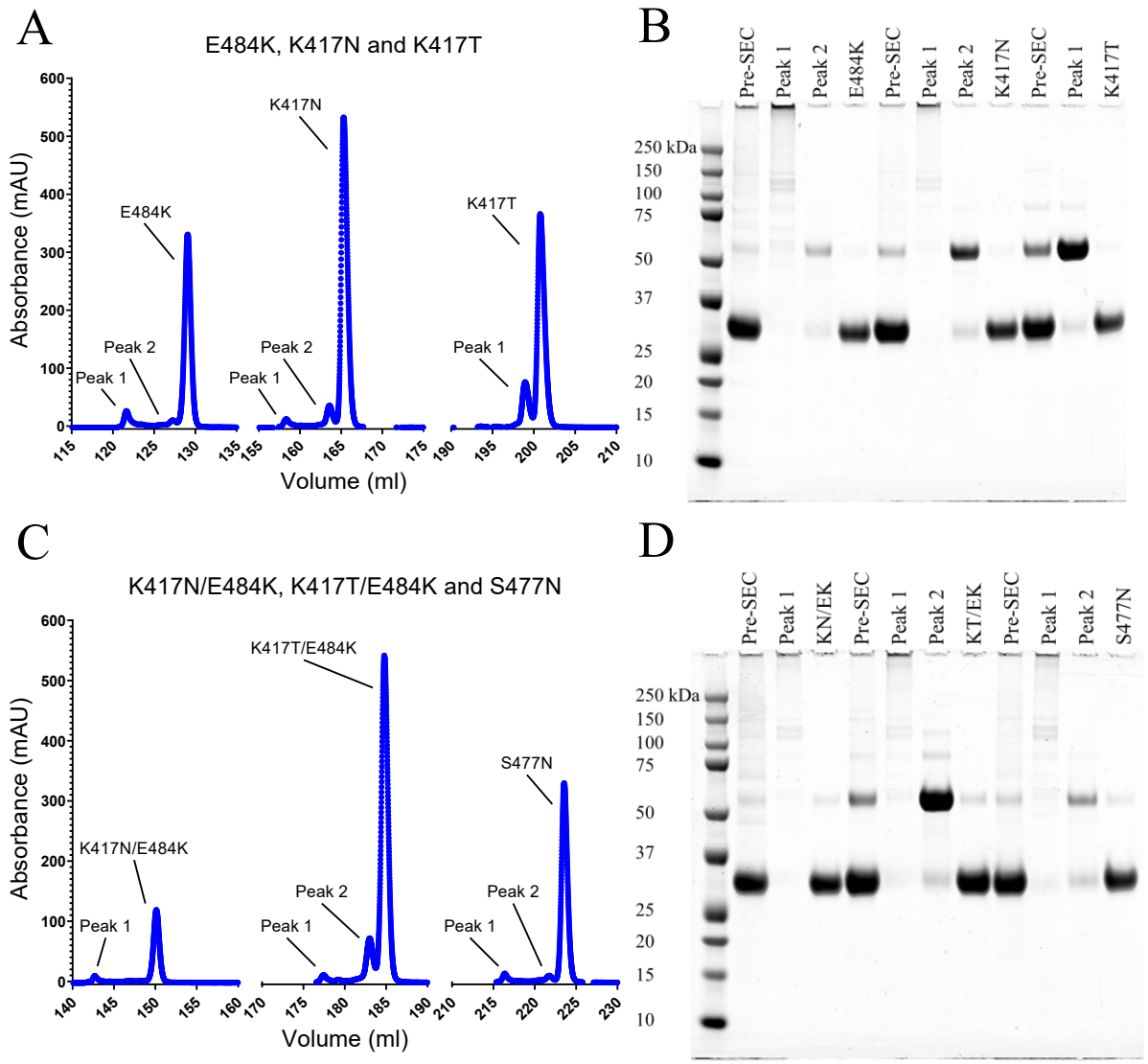


Figure 6.6: Purification of E484K, K417N, K417T, KN/EK, KT/EK and S477N SARS-CoV-2 RBD variants

(A) Size exclusion chromatography of E484K, K417N and K417T. Contaminating peaks are labelled peak 1-2 with large peaks corresponding to pure RBD. **(B)** SDS-PAGE gel, lane 1 contains a protein ladder, lanes 2, 6 and 10 contains the material after His tag purification, lanes 3,4, 7, 8 and 11 contain contaminating proteins removed by SEC. Lane 5 contains purified E484K, lane 9 contains purified K417N and lane 12 contains purified K417T. **(C)** Size exclusion chromatography of K417N/E484K, K417T/E484K and S477N. Contaminating peaks are labelled peak 1-2 with large peaks corresponding to pure RBD. **(D)** SDS-PAGE gel, lane 1 contains a protein ladder, lanes 2, 5 and 9 contains the material after His tag purification, lanes 3, 6, 7, 10 and 11 contain contaminating proteins removed by SEC. Lane 4 contains purified K417N/E484K, lane 8 contains purified K417T/E484K and lane 12 contains purified S477N.

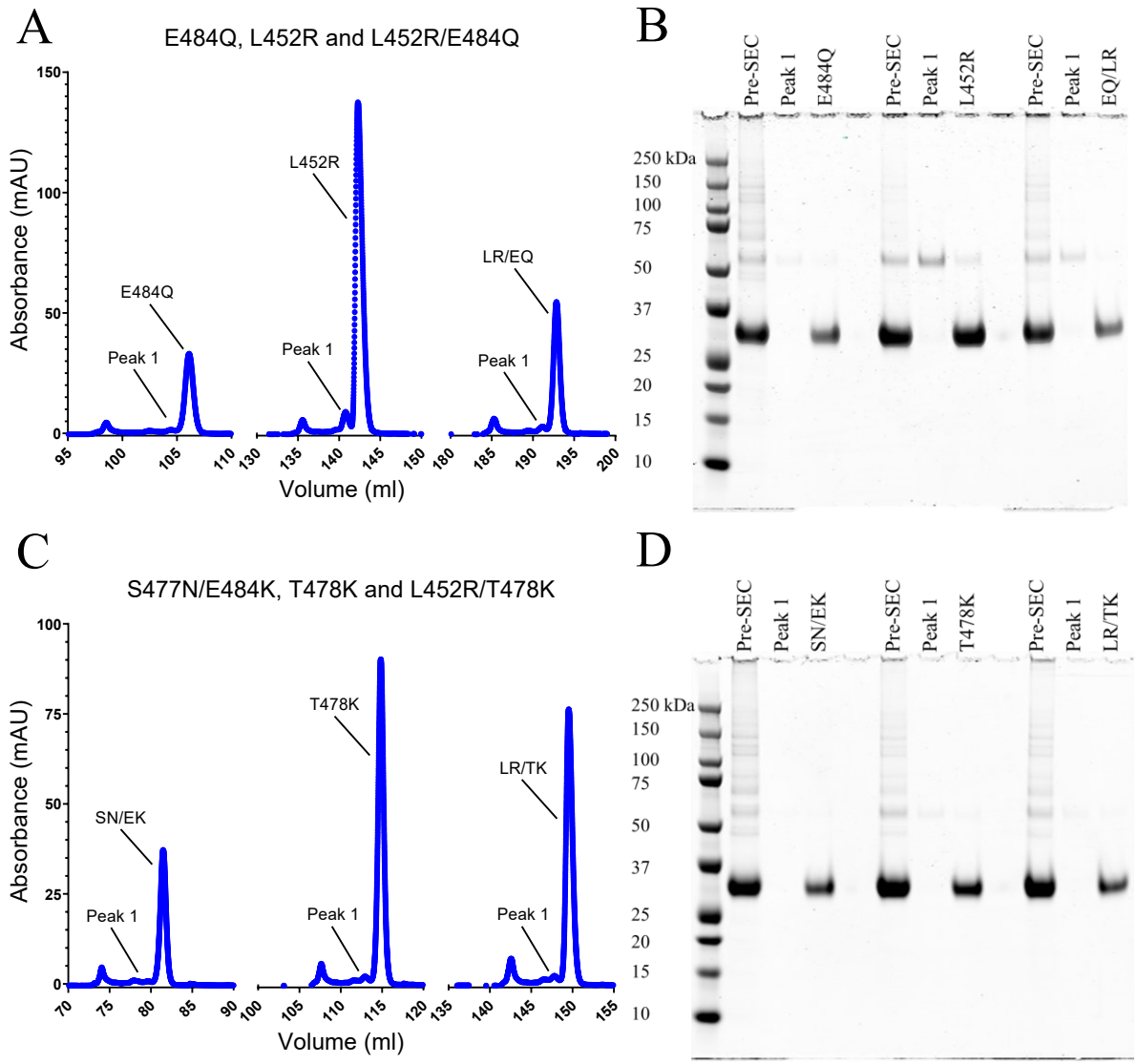


Figure 6.7: Purification of E484Q, L452R, LR/EQ, SN/EK, T478K and LR/TK SARS-CoV-2 RBD variants

(A) Size exclusion chromatography of E484Q, L452R and L542R/E484Q. Contaminating peaks are labelled peak 1 with large peaks corresponding to pure RBD. **(B)** SDS-PAGE gel, lane 1 contains a protein ladder, lanes 2, 6 and 10 contains the material after His tag purification, lanes 3, 7 and 11 contain contaminating proteins removed by SEC. Lane 4 contains purified E484Q, lane 8 contains purified L452R and lane 12 contains purified L452R/E484Q. **(C)** Size exclusion chromatography of S477N/E484K, T478K and L452R/T478K. Contaminating peaks are labelled peak 1 with large peaks corresponding to pure RBD. **(D)** SDS-PAGE gel, lane 1 contains a protein ladder, lanes 2, 6 and 10 contains the material after His tag purification, lanes 3, 7 and 11 contain contaminating proteins removed by SEC. Lane 4 contains purified S477N/E484K, lane 8 contains purified T478K and lane 12 contains purified L452R/T478K.

6.2.4. Production of sixteen RBD variants

The RBD variants were produced in a similar way to the ACE2 variants: by introducing the specific nucleotide changes into the RBD WT construct, which could then be used to purify high quality protein for each variant. Initially this was done with four variants, Alpha (N501Y), Beta (K417N/E484K/N501Y), Theta (E484K/N501Y) and Gamma (K417T/E484K/N501Y). The purification seen in Figure 6.5A-D of each of these variants was identical to that of the WT. The SDS-PAGE gel confirms that after SEC almost all contamination proteins have been removed. This was followed by a second round of purifications which again matched that of the WT, this time with a further six RBD variants (Figure 6.6A-D). This included the individual mutants E484K, S477N, K417N and K417T plus the double mutants K417N/E484K and K417T/E484K. This allowed for a detailed analysis of the binding kinetics for every combination of mutations which make up these emerging RBD variants. With the emergence of the Delta variant a further production run of six RBD variants was then completed to include Epsilon (L452R), T478K, E484Q, Delta (L452R/T478K), Kappa (L452R/E484Q) and S477N/E484K (Figure 6.7A-D). As expected, these final variants also behaved in a very similar way to those previously purified.

6.2.5. Validating the ACE2/SARS-CoV-2 RBD SPR binding assay

The biotinylated ACE2 was successfully captured on a CM5 chip surface that had been functionalised with streptavidin. An eight-point two-fold serial dilution of RBD was flown over the surface from the lowest concentration to the highest with periodic buffer injections for double referencing (see methods). The resultant double referenced traces were plotted in Figure 6.8A, showing the 30 s association and subsequent disassociation of the RBD from the surface. The association phase was fit with a single site binding model with the fit shown in blue matching the data very well (Figure 6.8B). The plateau binding was then extracted from the fit of each injection and plotted against the respective concentration of RBD (Figure

6.8C). A one-site specific binding model could then be fit (shown in blue) and the equilibrium K_D extracted.

The SPR measurements were routinely performed at 37 °C (as this has greater biological relevance and adds the potential for testing therapeutic agents in our assay). However, in one case I performed the experiment at 25 °C (as this is often used as a standard temperature for SPR measurements). As expected, the K_D value obtained at the lower temperature was approximately three-fold lower, because the lower temperature acts to stabilize the binding by decreasing the k_{off}. Overall, the values I have calculated match very well to the literature in those cases when all the necessary experimental parameters have been reported correctly and allow me to draw appropriate comparisons (Lei et al., 2020; Shang et al., 2020; Supasa et al., 2021; Wrapp et al., 2020; Zhang et al., 2021).

6.2.6. Testing the prediction that specific ACE2 variants could significantly increase or decrease RBD binding

Our collaborators had identified hundreds of candidate ACE2 variants of interest (Macgowan et al., 2022), but due to the considerable time and effort needed to make and characterise each ACE2 variant in the laboratory it was decided to start with four of them: two predicted to strongly decrease affinity to RBD (E37K and D355N), and two predicted to strongly increase affinity (T27R and G326E).

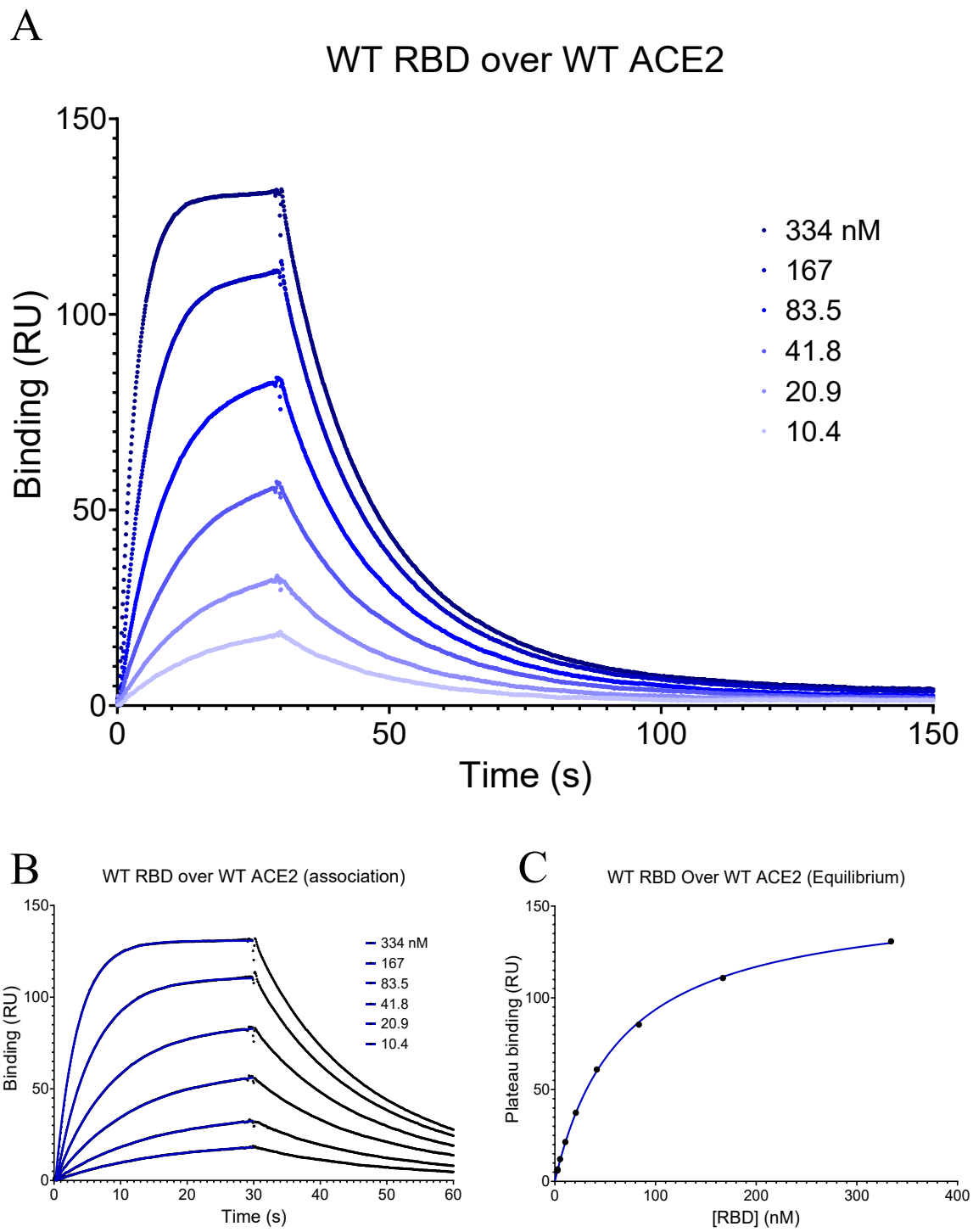


Figure 6.8: Example data set for RBD binding captured WT ACE2

(A) A representative data set with binding data for six increasing RBD concentrations run sequentially over captured ACE2. The data has been double referenced and each binding curve superimposed. **(B)** The blue line represents the fit of the association phase with a One-phase association model. **(C)** The plateau values extracted from the fit of each association phase in B plotted against the [RBD]. This was fit with a One-site specific binding model and the equilibrium K_D was extracted.

The fold change relative to WT for the equilibrium K_D for RBD binding to three of the four variants is shown in Figure 6.9A. The D355N variant produced negligible RBD binding therefore it is marked as not applicable (N/A). The antibody bound as well to D355N variant as to WT ACE2, indicating that it was correctly folded (Figure 6.10A). Interestingly, the anti-ACE2 antibody shows a complete abolition of binding for the T27R variant which has almost identical RBD binding properties to the WT. Therefore, this points towards this residue being critical for antibody recognition rather than an issue with the structural confirmation of this variant. This was interesting because at the time this antibody was the only one that had been shown to bind ACE2 on cells and was also capable of blocking RBD binding to ACE2, therefore its epitope was expected to be close to that of the RBD-ACE2 interface.

Each of these mutations was predicted to change the ΔΔG of binding by a ≥ 1 kcal mol^{-1} increase (risk variant) or decrease (protective variant) (Table 6.1). Of the two protective variants, E37K matched the prediction very closely. However, D355N abolished binding completely, and an estimate for the ΔΔG based on the experimental SPR data showed that it has significantly weaker affinity than predicted *in silico* (see methods). Furthermore, the risk variants T27R and G326E both showed significantly lower affinity than had been predicted. From these results it seemed that the prediction algorithm tended to underestimate binding affinities for the variants. While it could identify variants with reduced affinity, it did not accurately predict those that would increase affinity to RBD.

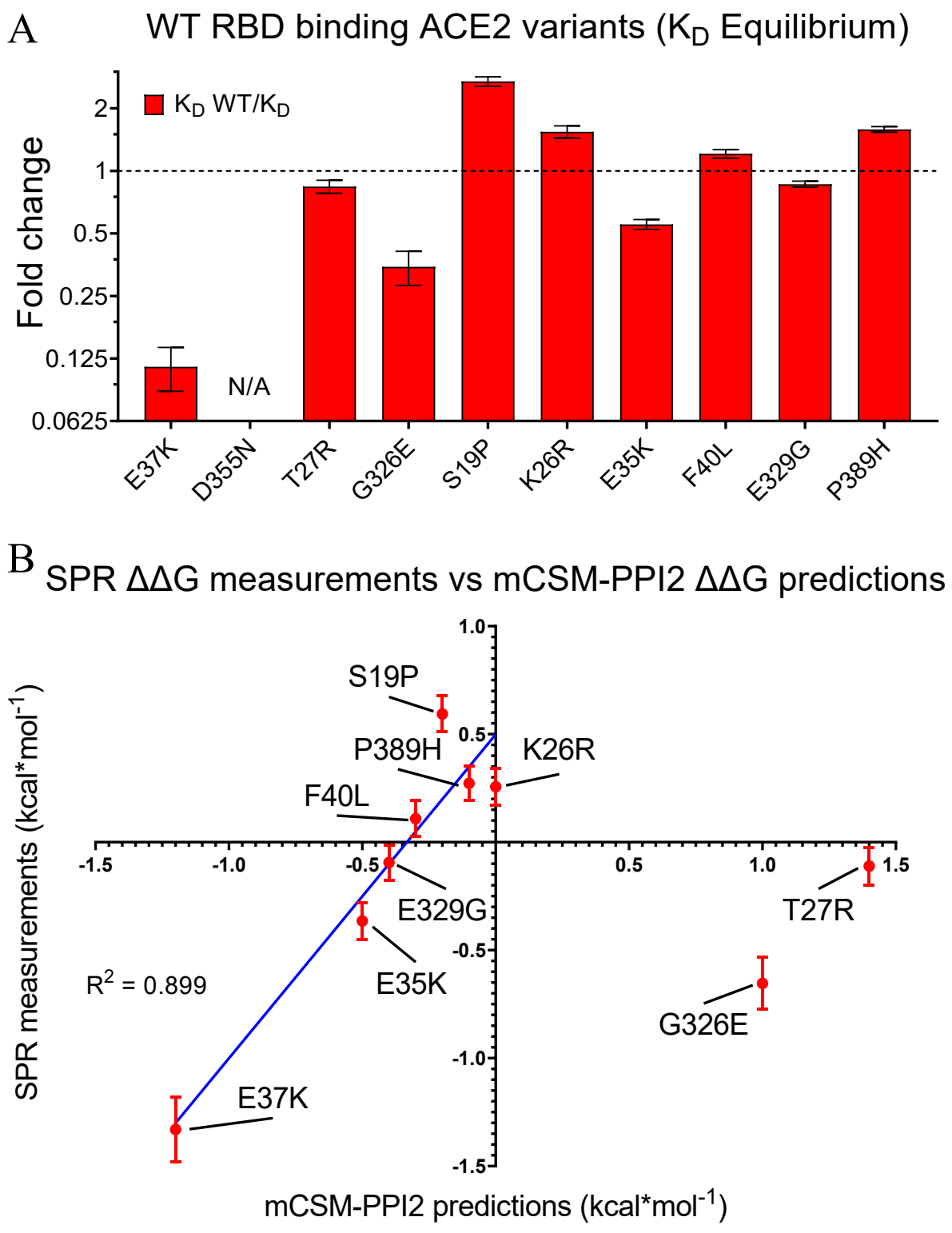


Figure 6.9: WT RBD binding to WT and ten ACE2 variants

(A) The fold change in the equilibrium K_D relative to WT for 10 ACE2 variants. The data is representative of 10 biological replicates for the WT and 3 for each variant. **(B)** Comparison of SPR ΔΔG with the mCSM-PPI2 ΔΔG prediction for 9 ACE2 mutations. T27R and G326E were excluded from the linier regression as outliers.

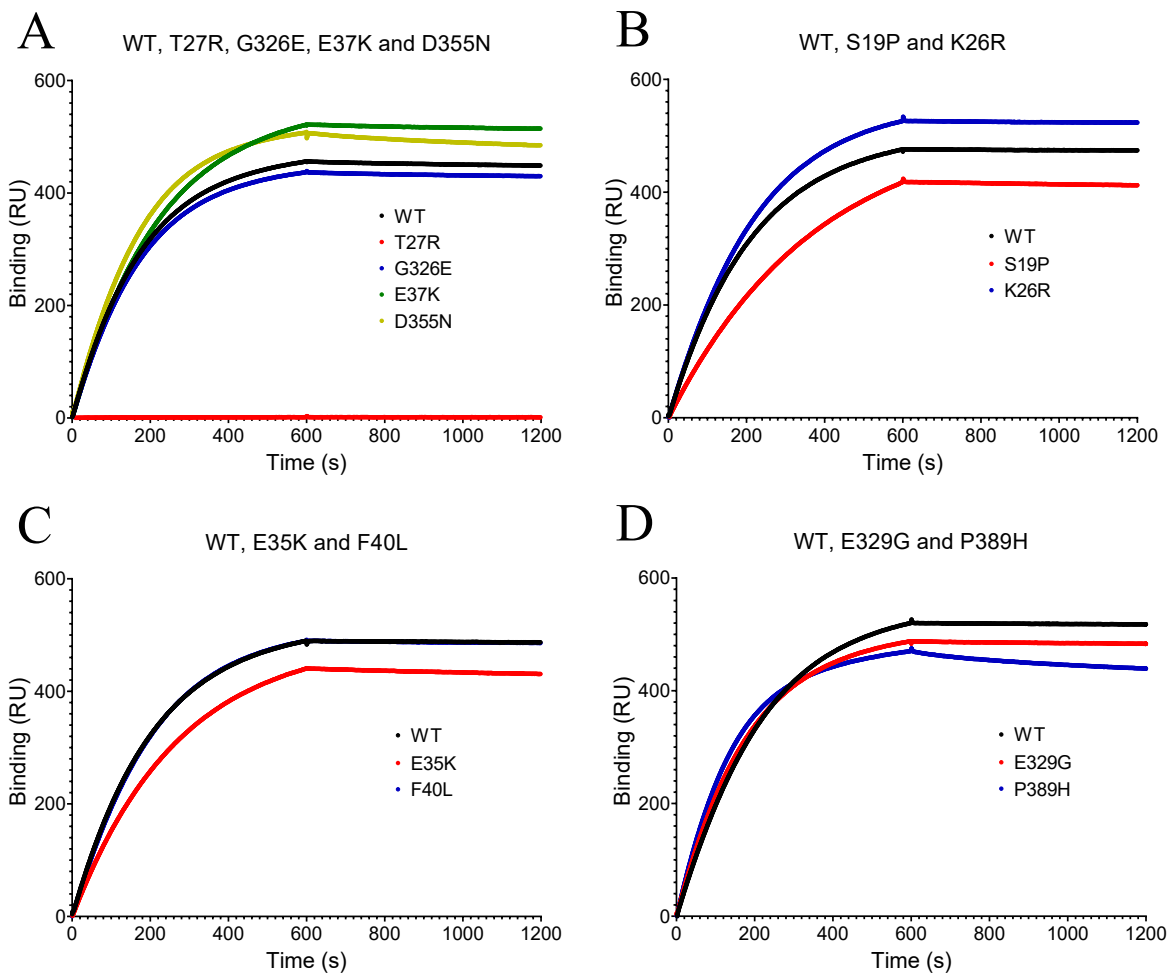


Figure 6.10: Anti ACE2 Antibody (NOVUS AC384-NBP2-80038) binding to WT and ten ACE2 variants

(A) Anti ACE2 binding to WT and the initial four ACE2 variants: T27R, G326E, E37K and D355N. **(B)** Anti ACE2 binding to WT, E35K and F40L. **(C)** Anti ACE2 binding to WT, S19P and K26R. **(D)** Anti ACE2 binding to WT, E329G and P389H. Anti ACE2 was injected for 600 s association and buffer for a further 600 s dissociation.

6.2.7. Expanding the assay to common ACE2 variants and calibrating the prediction algorithm

I then decided to test six more ACE2 variants, this time focusing on the most common variants in the human population. While these variants were not predicted to produce large changes to RBD affinity (Table 6.1), across a whole population even a small difference could have a considerable effect. The second motivation for experimentally testing the six new variants was to help calibrate the prediction algorithm, as this may allow for any systematic error in the predictor to be corrected. The six new variants looked identical to the first set during protein purification which can been seen in both the size exclusion and when running on an SDS-PAGE gel (Figure 6.4A-D). The anti-ACE2 antibody bound equally to all six variants compared to WT (Figure 6.10B-D). It was therefore possible to measure the equilibrium K_D values for each one and plot this as the fold change compared to WT (Figure 6.9A).

The results were surprising. The two most common variants (S19P and K26R) were predicted to either decrease RBD affinity or be neutral (Table 6.1). However, they were both found to increase affinity to RBD, which may have significant implications if increased affinity to RBD is confirmed to be a risk factor for SARS-CoV-2 infection outcome. While other variants also showed increased affinity for RBD they are significantly less common in the population and therefore likely have less of an impact.

ACE2 Variant	Allele count	Predicted ΔΔG (kcal mol^{-1})	Measured ΔΔG (kcal mol^{-1})
Phase 1			
E37K	8	-1.2	-1.33 ± 0.15
D355N	2	-1.3	-3*
T27R	N/A	1.4	-0.11 ± 0.09
G326E	1	1.0	-0.65 ± 0.12
Phase 2			
S19P	64	-0.2	0.59 ± 0.08
K26R	797	0.0	0.26 ± 0.09
E35K	3	-0.5	-0.36 ± 0.08
F40L	3	-0.3	0.11 ± 0.08
E329G	7	-0.4	-0.09 ± 0.08
P389H	7	-0.1	0.27 ± 0.08

Table 6.1: Summary of the ten ACE2 variants highlighting the predicted and measured ΔΔG values

(Column 1) Shows the amino acid change for each ACE2 variant. **(Column 2)** Shows the number of times each variant appears in the gnomAD database. **(Column 3)** Shows the predicted ΔΔG values obtained using the mCSM-PPI2 algorithm (Macgowan et al., 2022). **(Column 4)** Shows the ΔΔG values using the calculated K_D (see methods). The data is representative of three biological replicates plus or minus the SD. * = Estimated upper limit for ΔΔG as binding was too poor to fit accurately (see methods).

It may appear at first glance that there is a large divergence between the SPR measurements, and the predictions made by the mCSM-PPI2 algorithm. However, the measured and predicted ΔΔG values for the variants were compared by plotting one against the other (Figure 6.9B), and this plot showed a very strong corelation between the two. This confirms that there is a systematic error in the predictor where it consistently predicts a lower affinity than is measured. However, the T27R and G326E are still clear outliers, which suggests there are other issues with the prediction algorithm which need to be solved. The linear regression fit to this data will allow our collaborators to recalibrate the ΔΔG predictions for all the other possible RBD-ACE2 interface variants (Macgowan et al., 2022).

6.2.8. Effect of emergent SARS-CoV-2 RBD variants on binding WT and common ACE2 variants

So far, the focus of this chapter has been on ACE2 variants found in the human population that could alter RBD binding. However, the rapid growth of the virus combined with widespread infection means mutations are constantly occurring and therefore new viral variants are emerging quickly. As detailed in the introduction to this chapter, we initially produced and published data on how ten RBD mutations in its interface with ACE2 affected binding (Barton et al., 2021). However, the virus continued to mutate over the spring of 2021, so I produced a further 6 RBD variants that had emerged, with the primary focus being the new Delta variant. At the beginning of 2022 I then produced a further three RBD variants focused on mutations which have arisen due to the Omicron variant.

While for the ACE2 variants I calculated the K_D using the equilibrium binding, for the RBD variants I wanted to achieve very accurate information about the k_{on} and k_{off}. This is only possible when the level of immobilised protein on the chip surface is reduced to a minimum to prevent rebinding events and mass transport limitations (Myszka, 1997). Therefore, I used approximately 50 response units (RU) of ACE2 immobilised on the chip surface for all the

RBD variant measurements. This can be seen in Figure 6.11A, where the association phase and dissociation phase for WT RBD binding WT ACE2 have been fitted (see methods). The maximum binding measured is approximately 10 RU in comparison to the previous experiments in Figure 6.8A where the maximum binding is approximately 130 RU.

The k_{off} can be extracted from the fit of each dissociation phase and plotted against the RBD concentration shown in Figure 6.11B. The k_{off} is not affected by analyte concentration and so does not change, therefore the average value across the concentration range is taken as the k_{off}. To find the k_{on}, first the observed-on rate (k_{obs}) extracted from the association phase is plotted against the concentration of RBD (Figure 6.11C). The gradient of the linear regression therefore corresponds to the k_{on}. With the k_{off} and k_{on} extracted the calculated K_D can be found (see methods). However, it is also possible to measure the equilibrium binding K_D (which can be extracted from the fit in (Figure 6.11D) and compared it with the calculated K_D value (Table 6.2). To confirm that the equilibrium K_D is not affected by immobilisation level I plotted the equilibrium K_D measurements against the corresponding immobilisation of WT ACE2, and no correlation was observed (Figure 6.11E). While the equilibrium K_D is not affected by ACE2 immobilization, the k_{on} and k_{off} are. This is due to rebinding and mass transport limitations (Myszka, 1997). This can be seen in Figure 6.12A and B, where both rates slow down as ACE2 immobilisation increases. As these artifacts are enhanced with faster kinetics, I also show a further control with the E484K/N501Y RBD variant which has the fastest kinetics of any variant measured here compared to the WT and appears to confirm that an immobilisation of 50 RU of ACE2 allows for the most reliable estimation of the k_{on} and k_{off} (Figure 6.12C and D). Setting the ACE2 immobilisation below 50 RU led to very low RU values for RBD binding which increased experimental noise and made fitting the data much more difficult.

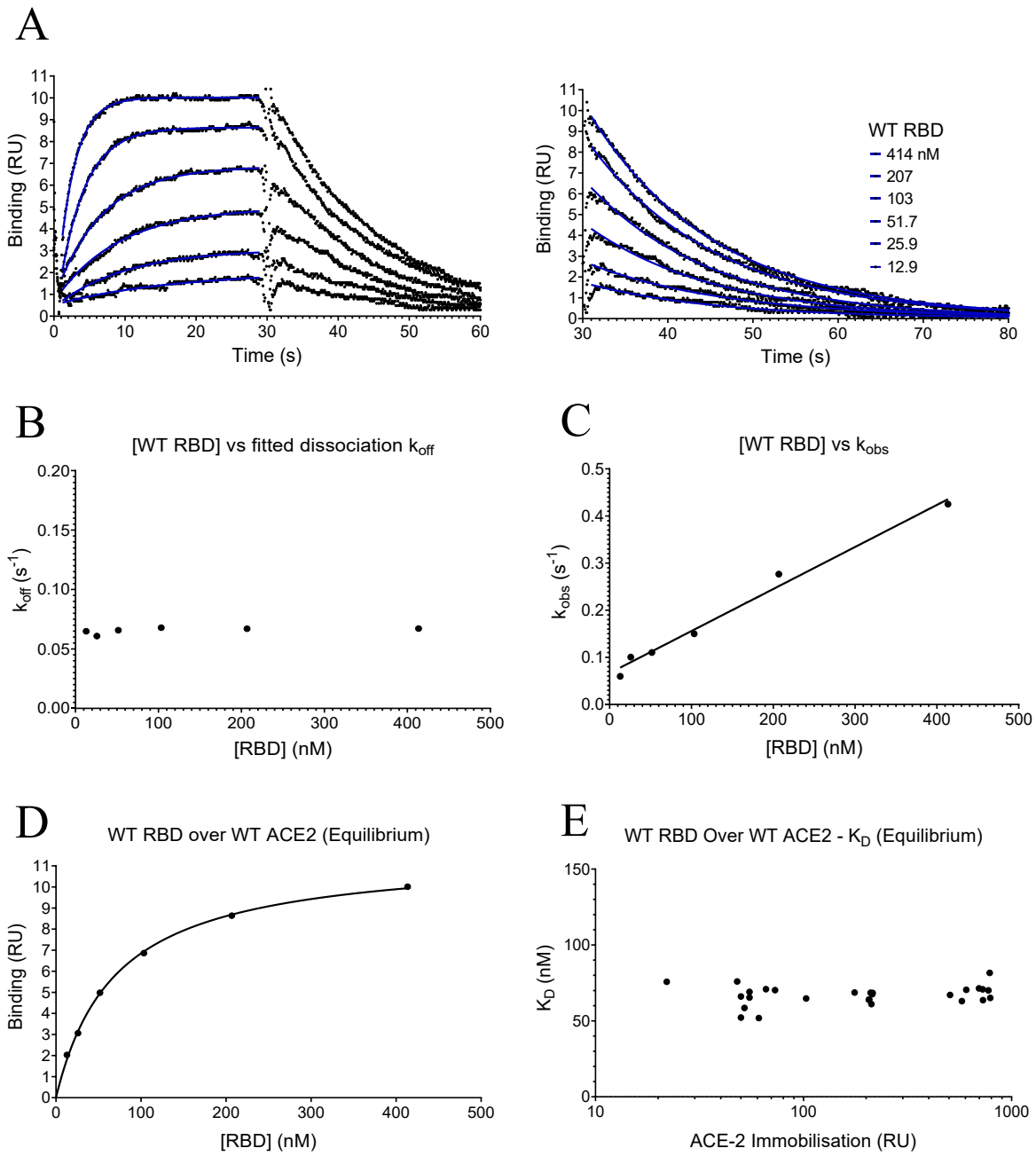


Figure 6.11: Fitting kon and koff for WT RBD binding WT ACE2

(A) WT RBD binding immobilised WT ACE2 the fits for the association and disassociation phase are shown in blue. **(B)** The k_{off} for each RBD injection plotted against its RBD concentration. **(C)** The k_{obs} for each injection plotted against its RBD concentration. The y-intercept is constrained to the average of the k_{off} from B and the slope of the linier regression represents the k_{on}. **(D)** The equilibrium binding in A plotted against the concentration of RBD injected over the surface. **(E)** The extracted equilibrium K_D values for WT RBD binding WT ACE2 at a range of surface immobilisations (n = 27).

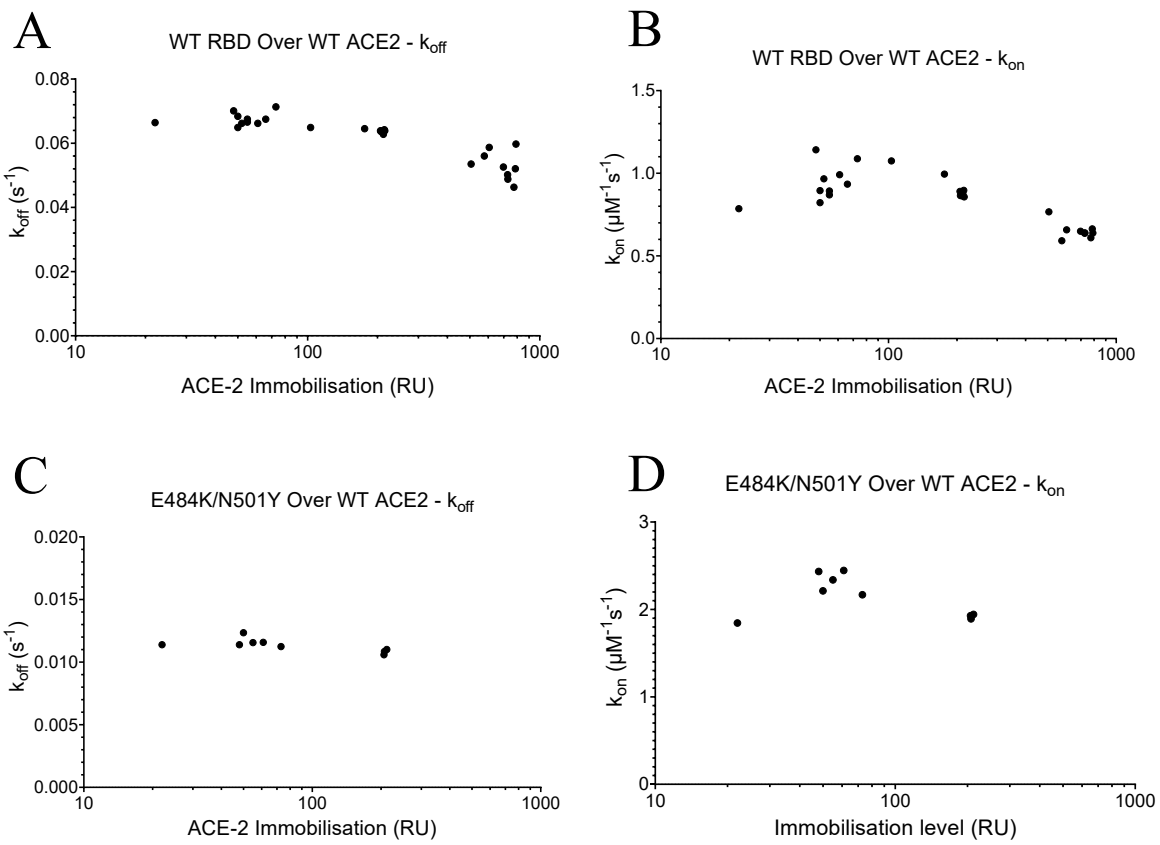


Figure 6.12: WT and E484K/N501Y binding WT ACE2 over a range of immobilisations

(A and B) The k_{off} and k_{on} respectively for WT RBD binding WT ACE2 at a range of surface immobilisations (n = 27). **(C and D)** The k_{off} and k_{on} respectively for E484K/N501Y RBD binding WT ACE2 at a range of surface immobilisations (n = 12).

With the assay now optimised for low immobilisation measurements I was then able to test all nineteen RBD variants for binding to WT ACE2 (Figure 6.13B and Figure 6.14A). This data shows that the mutations (or combinations of mutations present) in all the common new variants increase the affinity of RBD for ACE2. The Alpha variant would be a stereotypical example: the N501Y results in visibly faster k_{on} and slower k_{off} (Figure 6.13A). Combined, this gives this variant more than a 10-fold increase in affinity compared to WT RBD. Other mutations confer a more modest increase in affinity (for example, the S477N is linked to a 1.5-2-fold increase in affinity), but this may still be enough to outcompete the WT variant (Figure 6.13B). This has implications for people with ACE2 variants that increase affinity to a similar degree.

While all named variants show an overall increase in affinity with respect to WT, some of the mutations selected for within these variants do not improve affinity but something else, such as immune evasion. For example, the Beta and Gamma variants contain the K417N/T respectively which I show dramatically reduce the affinity for ACE2. This, along with the fact that these variants appeared among populations who had previously had very high levels of infection, suggests that mutations at K417 are aimed at immune evasion (Dejnirattisai et al., 2021; Hoffmann et al., 2021; Sabino et al., 2021; D. Zhou et al., 2021). The significant reduction in binding affinity due to these mutations is predominantly compensated for by the N501Y mutation and, to a lesser extent, the E484K mutation, also present in these variants. The E484K mutation has been widely suggested to lead to immune evasion through blocking antibody binding (Alenquer et al., 2021; Jangra et al., 2021) but this data suggests that it also confers a modest increase in affinity over the WT RBD.

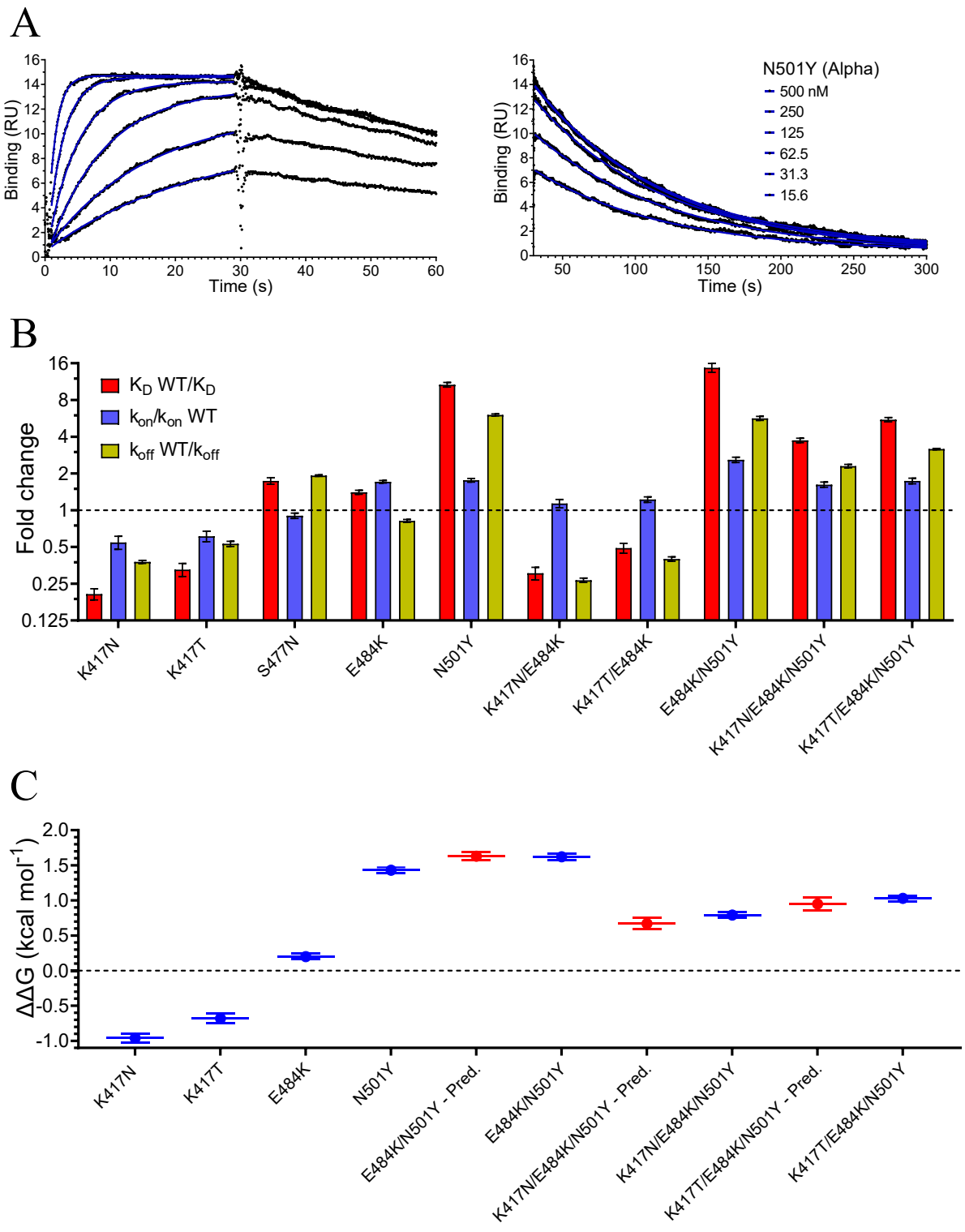


Figure 6.13: Effect of RBD variants binding WT ACE2 including Alpha, Beta, and Gamma

(A) N501Y (Alpha) binding immobilised WT ACE2 the fits for the association and disassociation phase are shown in blue. **(B)** The fold change relative to WT RBD for the k_{on}, k_{off} and K_D (Calculated) for binding to immobilised WT ACE2 (Error bars show SD) (n = 3). **(C)** The blue data points show the measured ΔΔG for a selection of single and combined RBD variants. The red data points show the predicted (Pred.) ΔΔG for the combined RBD variants by summing the relevant single mutations (Error bars show SD) (n = 3). E484K/N501Y (Theta), K417N/E484K/N501Y (Beta) and K417T/E484K/N501Y (Gamma)

The mutations studied here may affect the k_{on}, k_{off}, or both. In the case of the E484K mutation, the increase in binding is predominantly derived by an increase in the k_{on}, which may be due to electrostatic steering of the molecule when binding due to the charge change. This contrasts with S477N, which predominantly affects the k_{off}, and N501Y, which affects both. Furthermore, converting the K_D values in Figure 6.13B into ΔΔG allows me to assess whether these individual mutations are additive. For example, the individual ΔΔG for E484K and N501Y can be summed to give a predicted ΔΔG, which was then compared to the measured ΔΔG for the double mutant (Figure 6.13C). This process was also carried out for the Beta and Gamma triple mutant variants. The results show that indeed each mutation is acting independently, and therefore their individual effects are additive. This is true for both mutations which have a positive and negative effect on affinity. Looking at the RBD-ACE2 interface structure in Figure 6.1B it is possible to rationalise why this is the case as all three individual mutations are well-separated from each other in the binding interface.

Finally, the mutations which make up the Delta and Kappa variants (L452R, T478K and E484Q) have very modest effects on the binding affinity (Figure 6.14A). However, when combined the L452R/T478K of the Delta variant increase the affinity by more than predicted by additivity (Figure 6.14B). This suggests cooperativity between these two mutations, which would require a more detailed structural analysis to explain. The increase in affinity for the Delta and Omicron (BA.2) variants are not as strong an increase as was seen for Alpha, Beta and Gamma variants and therefore do not explain why they have been so successful in out competing the previous variant. It can be concluded that binding kinetics alone cannot explain the further increased transmissibility of the Delta and now Omicron variants, and therefore other mutations in the spike protein or other viral components must be responsible for the selective advantage of these variants. However, the large number of changes associated with the Omicron variant would suggest immune evasion is key to its success.

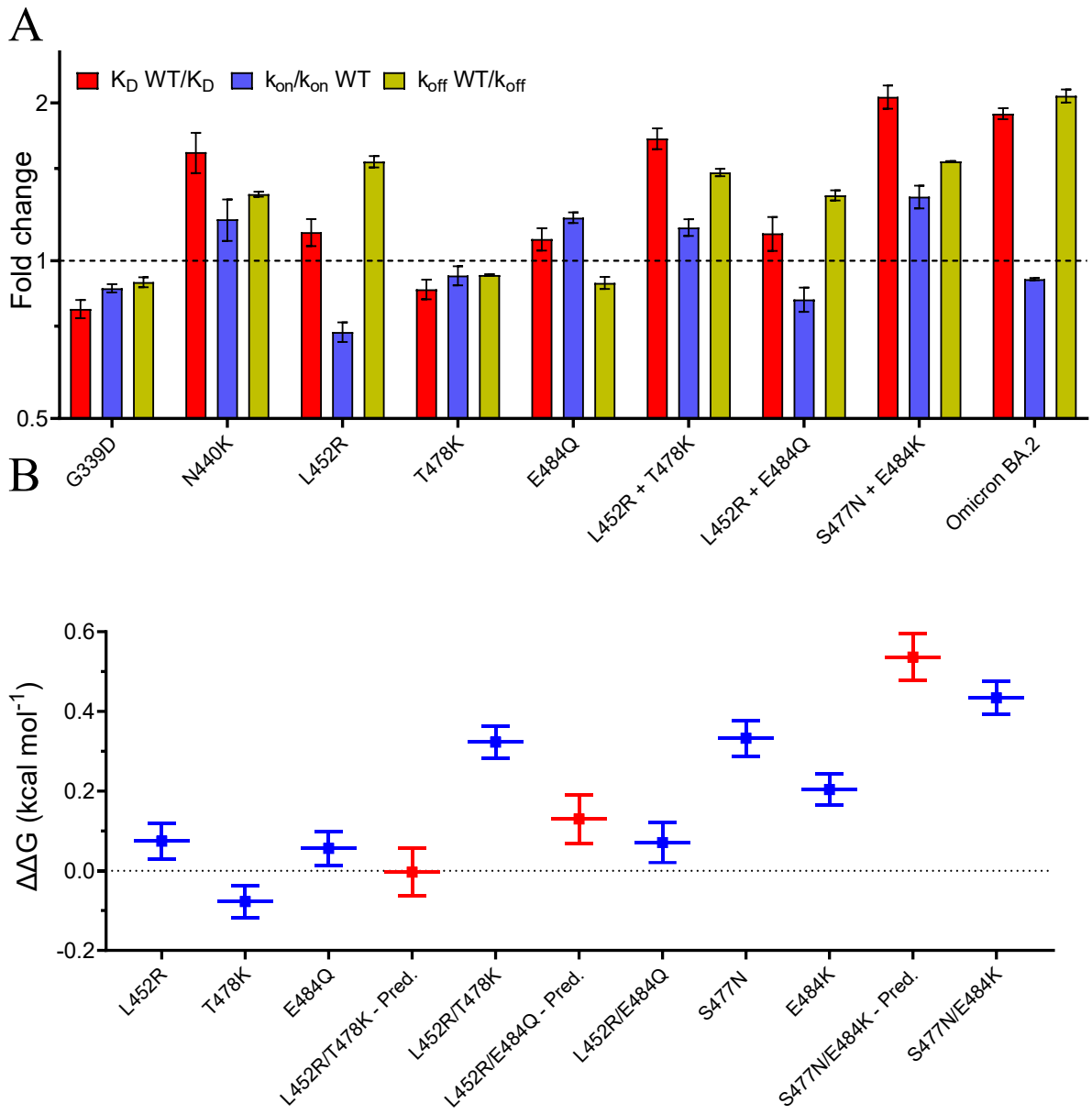


Figure 6.14: Continued, effect of RBD variants binding WT ACE2 including Epsilon, Kappa, Delta, and Omicron

(A) The fold change relative to WT RBD for the k_{on}, k_{off} and K_D (Calculated) for binding to immobilised WT ACE2 (Error bars show SD) (n = 3). **(B)** The blue data points show the measured ΔΔG the RBD variants. The red data points show the predicted (Pred.) ΔΔG for the combined RBD mutations by summing the relevant single mutations (Error bars show SD) (n = 3).

6.2.9. The combined effect of RBD variants binding common ACE2 variants S19P and K26R

I also wanted to look at what effect combining the RBD and ACE2 variants would have on affinity. However, with nineteen RBD and ten ACE2 the total number of combinations was not feasible or cost effective to test using SPR. Therefore, I chose the two most common ACE2 variants (S19P and K26R) which would also be most relevant to human health. As I showed in Figure 6.9A with the equilibrium K_D, S19P and K26R enhanced the affinity to WT RBD. A similar but slightly enhanced effect can be seen by plotting the calculated K_D under the low immobilisation conditions (Figure 6.15A). The increase in affinity for each mutation is driven by both an increase in k_{on} and a decrease in the k_{off}.

To quantify if there was an effect from combining mutations on both ACE2 and RBD, the measured ΔΔG for the S19P or K26R ACE2 variants binding RBD variants was compared to the sum of the ΔΔG for ACE2 variants binding WT RBD and the RBD variants binding WT ACE2, respectively (Table 6.3). This was plotted as the difference between the measured and predicted ΔΔG and is therefore, represented as a ΔΔΔG (Figure 6.15B-E). If the individual mutations showed negative cooperativity the ΔΔΔG would be a negative number, but if they showed positive cooperativity, it would be a positive number. As cooperativity is rare this analysis shows that all variant combinations are very close to zero. However, there is a single outlier with the RBD variant S477N binding S19P ACE2. The structure of the complex in Figure 6.1B reveals that the S19 and S477 residues can be found in close proximity in the binding interface. It is likely that the combination of the S19P and S477N mutations disrupted the same favourable interaction that benefits the individual mutations. Similarly, negative cooperativity was also observed between S19P ACE2 and RBD with the combined mutations S477N/E484K and Omicron BA.2 likely for the same reason (Figure 6.14D).

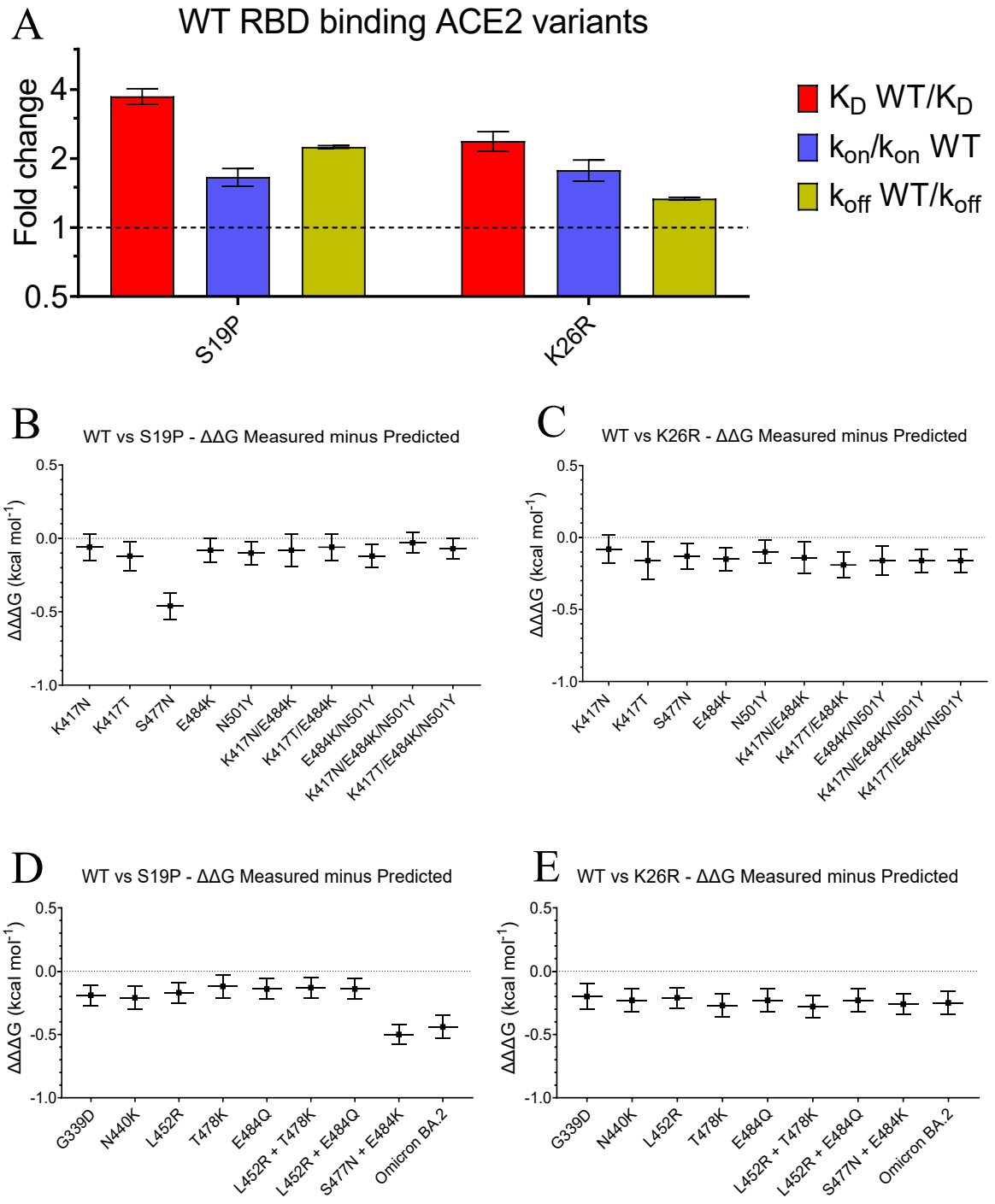


Figure 6.15: RBD variants binding S19P and K26R ACE2 variants

(A) Shows the fold change relative to WT RBD for the k_{on}, k_{off} and K_D (Calculated) for binding to immobilised S19P and K26R ACE2 (Error bars show SD) (n = 3). **(B-E)** Combining ΔΔG for WT and S19P or K26R binding RBD variants was plotted as the difference between the measured and predicted ΔΔG and is therefore represented as a ΔΔΔG (see methods).

RBD over WT ACE2	k_{off} (s^{-1})	SD	k_{on} ($\mu M^{-1} s^{-1}$)	SD	K_D Calc. (nM)	SD	K_D Equi. (nM)	SD
WT	0.0668	0.0011	0.901	0.053	74.4	4.0	62.6	7.7
G339D	0.0735	0.0013	0.798	0.012	92.1	3.1	97.1	3.8
K417N	0.177	0.0042	0.491	0.049	364	29	349	10
K417T	0.126	0.0051	0.552	0.044	230	23	226	19
N440K	0.0499	0.0004	1.08	0.080	46.4	3.5	53.4	7.0
L452R (Epsilon)	0.0433	0.0009	0.659	0.023	65.8	3.2	70.0	1.8
S477N	0.0348	0.0004	0.812	0.033	42.9	2.1	42.6	3.0
T478K	0.0712	0.0002	0.844	0.029	84.5	3.0	90.3	2.9
E484K (Eta/Iota)	0.0818	0.0018	1.54	0.031	53.1	1.7	52.6	2.0
E484Q	0.0737	0.0016	1.09	0.021	67.8	2.8	65.8	3.7
N501Y (Alpha)	0.0111	0.0002	1.59	0.043	7.0	0.2	5.5	2.4
K417N/E484K	0.251	0.0080	1.02	0.066	247	23	251	23
K417T/E484K	0.168	0.0057	1.10	0.047	153	12	147	8.6
L452R/T478K (Delta)	0.0454	0.0006	1.04	0.031	43.6	1.6	44.2	0.8
L452R/E484Q (Kappa)	0.0502	0.0009	0.760	0.033	66.2	4.2	71.2	7.2
S477N/E484K	0.0432	0.0001	1.19	0.048	36.3	1.5	39.5	0.9
E484K/N501Y (Theta)	0.0118	0.0004	2.33	0.095	5.1	0.4	3.7	2.7

K417N/E484K/N501Y (Beta)	0.0291	0.0008	1.46	0.058	20.0	0.7	17.4	3.1
K417T/E484K/N501Y (Gamma)	0.0211	0.0002	1.56	0.067	13.5	0.4	12.2	3.4
Omicron BA.2	0.0324	0.0008	0.831	0.003	39.0	0.8	37.4	4.3
RBD over S19P ACE2	**k_{off} (s^{-1})**	**SD**	**k_{on} ($\mu M^{-1} s^{-1}$)**	**SD**	**K_D Calc. (nM)**	**SD**	**K_D Equi. (nM)**	**SD**
WT	0.0298	0.0004	1.50	0.121	20.0	1.3	30.5	2.2
G339D	0.0312	0.0005	0.923	0.042	33.9	2.0	33.8	4.1
K417N	0.0782	0.0028	0.725	0.042	108	2.8	129	8.2
K417T	0.0521	0.0020	0.689	0.021	75.8	4.7	87.8	7.0
N440K	0.0217	0.0003	1.23	0.082	17.7	1.0	21.1	3.5
L452R (Epsilon)	0.0188	0.0001	0.799	0.021	23.5	0.5	23.7	7.5
S477N	0.0257	0.0002	1.05	0.074	24.6	1.7	30.3	2.7
T478K	0.0298	0.0005	1.09	0.069	27.5	2.0	34.3	1.2
E484K (Eta/Iota)	0.0325	0.0003	2.02	0.077	16.2	0.6	20.8	1.3
E484Q	0.0302	0.0002	1.32	0.037	22.8	0.5	22.9	3.6
N501Y (Alpha)	0.0051	0.0000	2.31	0.089	2.2	0.1	3.5	0.4
K417N/E484K	0.0961	0.0020	1.28	0.111	75.6	7.1	91.3	6.5
K417T/E484K	0.0660	0.0025	1.45	0.034	45.5	2.5	53.8	1.5
L452R/T478K (Delta)	0.0186	0.0001	1.29	0.057	14.5	0.6	16.1	1.2

L452R/E484Q (Kappa)	0.0205	0.0002	0.919	0.026	22.3	0.8	26.7	2.7
S477N/E484K	0.0309	0.0001	1.39	0.071	22.2	1.2	24.5	1.1
E484K/N501Y (Theta)	0.0051	0.0001	3.10	0.095	1.7	0.0	3.4	0.4
K417N/E484K/N501Y (Beta)	0.0122	0.0001	2.16	0.028	5.7	0.1	10.4	1.2
K417T/E484K/N501Y (Gamma)	0.0085	0.0001	2.11	0.052	4.0	0.1	6.1	1.3
Omicron BA.2	0.0214	0.0001	0.983	0.071	21.9	1.6	22.9	3.9
RBD over K26R ACE2	**k_{off} (s^{-1})**	**SD**	**k_{on} ($\mu M^{-1} s^{-1}$)**	**SD**	**K_D Calc. (nM)**	**SD**	**K_D Equi. (nM)**	**SD**
WT	0.0500	0.0006	1.60	0.155	31.4	2.6	48.8	2.5
G339D	0.0512	0.0013	0.950	0.073	54.3	5.3	60.5	0.9
K417N	0.154	0.0079	0.880	0.075	175	8.1	237	15
K417T	0.101	0.0008	0.811	0.121	127	17	154	2.8
N440K	0.0351	0.0004	1.22	0.063	28.8	1.4	33.3	4.4
L452R (Epsilon)	0.0300	0.0003	0.772	0.014	38.9	1.0	42.2	4.8
S477N	0.0240	0.0001	1.07	0.048	22.6	1.1	33.4	1.3
T478K	0.0542	0.0008	0.979	0.032	55.4	2.6	57.4	2.3
E484K (Eta/Iota)	0.0587	0.0011	2.03	0.033	28.9	1.0	35.9	1.5

E484Q	0.0547	0.0004	1.31	0.075	42.0	2.3	41.5	3.6
N501Y (Alpha)	0.0081	0.0000	2.34	0.093	3.5	0.1	7.5	1.5
K417N/E484K	0.191	0.0048	1.48	0.148	130	9.4	166	11
K417T/E484K	0.135	0.0041	1.53	0.023	88.0	3.9	105	0.7
L452R/T478K (Delta)	0.0335	0.0009	1.16	0.080	29.1	1.7	29.1	1.4
L452R/E484Q (Kappa)	0.0358	0.0003	0.876	0.011	40.9	0.6	44.7	3.5
S477N/E484K	0.0307	0.0004	1.32	0.047	23.3	0.9	24.3	0.2
E484K/N501Y (Theta)	0.0085	0.0002	3.06	0.230	2.8	0.2	6.4	0.3
K417N/E484K/N501Y (Beta)	0.0234	0.0004	2.13	0.054	11.0	0.3	18.7	2.0
K417T/E484K/N501Y (Gamma)	0.0164	0.0003	2.21	0.061	7.4	0.3	15.3	0.8
Omicron BA.2	0.0258	0.0004	1.04	0.086	25.0	2.1	28.8	2.7

Table 6.2: Summary of the binding parameters for RBD WT and nineteen variants

The values include the k_{off}, k_{on}, K_D (calculated) and K_D (equilibrium) binding ACE2 WT and ACE2 variants S19P and K26R. The values represent the mean and SD from three biological replicates.

ΔG values	ACE2 WT (kcal*mol $^{-1}$)	SD	ACE2 S19P (kcal*mol $^{-1}$)	SD	ACE2 K26R (kcal*mol $^{-1}$)	SD
WT	-9.93	0.03	-10.7	0.04	-10.4	0.05
G339D	-9.80	0.02	-10.4	0.04	-10.1	0.06
K417N	-8.97	0.05	-9.70	0.02	-9.41	0.03
K417T	-9.24	0.06	-9.92	0.04	-9.61	0.09
N440K	-10.2	0.04	-10.8	0.04	-10.5	0.03
L452R (Epsilon)	-10.0	0.03	-10.6	0.01	-10.3	0.02
S477N	-10.3	0.03	-10.6	0.04	-10.6	0.03
T478K	-9.85	0.02	-10.5	0.04	-10.1	0.03
E484K (Eta/Iota)	-10.1	0.02	-10.8	0.02	-10.5	0.02
E484Q	-9.98	0.02	-10.6	0.01	-10.3	0.03
N501Y (Alpha)	-11.4	0.02	-12.1	0.03	-11.8	0.03
K417N/E484K	-9.20	0.06	-9.92	0.06	-9.59	0.04
K417T/E484K	-9.49	0.05	-10.2	0.03	-9.82	0.03
L452R/T478K (Delta)	-10.2	0.02	-10.9	0.03	-10.5	0.04
L452R/E484Q (Kappa)	-10.0	0.04	-10.7	0.02	-10.3	0.01
S477N/E484K	-10.4	0.02	-10.7	0.03	-10.6	0.02
E484K/N501Y (Theta)	-11.5	0.04	-12.2	0.02	-11.9	0.04
K417N/E484K/N501Y (Beta)	-10.7	0.02	-11.5	0.01	-11.1	0.02
K417T/E484K/N501Y (Gamma)	-11.0	0.02	-11.7	0.01	-11.3	0.03
Omicron BA.2	-10.3	0.01	-10.7	0.04	-10.6	0.05

Table 6.3: Summary of the ΔG values for nineteen RBD variants binding ACE2 WT plus ACE2 S19P and ACE2 K26R.

6.3. Discussion

In this chapter I have produced functional SARS-CoV-2 RBD and human ACE2, plus variants of both. Using SPR I have characterised the binding of RBD to WT ACE2 with values comparable to the literature. This assay has then been used to test RBD binding to the ten ACE2 variants. The results with ACE2 variants E37K and D355N suggest that some ACE2 mutations could indeed confer significant resistance to viral cell entry. If the efficiency of viral entry is a continuous process based on affinity, then even a small reduction in RBD affinity for ACE2 variants could lead to increased resistance to infection and may have a large impact across a population.

While it is not as obvious what effects variants with increased affinity for RBD may have, it is likely that they would put individuals at higher risk/expose them to worse outcomes. Enhanced affinity variants may make individuals more susceptible to small initial viral loads or allow the virus to infect cell types with lower ACE2 expression. Patients with acute infections often have viral spreading to other tissues that express ACE2 such as the heart, kidney and gastrointestinal tract which can lead to further complications (Cao & Li, 2020).

Furthermore, there is evidence that ACE2 expression levels are correlated with severity of disease (Fang et al., 2020), for example, patients with type 1 or type 2 diabetes, where ACE2 expression is substantially increased. Therefore, variation in ACE2 expression levels across a population, combined with different ACE2 variants in such populations, could result in some individuals being very susceptible to the virus (if they expressed high levels of increased affinity ACE2 variants) and others very resistant (if they expressed low affinity ACE2 at low levels). This could explain to some extent the large differences in outcome for this disease observed (Tjendra et al., 2020).

This binding data will allow for other prediction algorithms to be refined in the future to aid the identification of protective or risk ACE2 variants for SARS-CoV-2. Having a set of reliable binding measurements is of great value when training new algorithms giving this data value beyond RBD-ACE2 interactions. These algorithms may then be applicable to assess future virus variants or other protein-protein interactions, which may speed up the response to future viruses with pandemic potential.

As was shown with SARS-CoV-1 and related viruses there is good evidence that increasing the affinity of the viral protein for its cellular target can increase infectivity and therefore disease progression (Hasegawa et al., 2007; Li et al., 2005). This can also reduce the number of available ligands the virus needs to allow entry into other cell types, which can quickly lead to disease complications (Cao & Li, 2020). With the emergence of virus variants with key mutations in the RBD-ACE2 binding interface such as Alpha, Beta and Gamma, the SPR assay was then further extended to measure very accurate binding kinetics for these variants through optimising the assay to work at low ACE2 immobilisations. This, combined with very pure protein containing very few aggregates, reduced artifacts such as mass transport limitations and rebinding. These adjustments, when combined with performing the assay at a physiological temperature of 37 °C, resulted in rate constants that are likely to be more accurate and hence are faster than previously reported.

The data shows that while all successful variants contain mutations which increase RBD-ACE2 affinity it is not a strait forward correlation. For example, the N501Y mutation gives rise to a ten-fold increase in affinity but has not become dominant in the same way as D614G. Equally the highest fold change in affinity was measured with the combined N501Y/E484K which led to a fifteen-fold increase in affinity. While this variant did emerge in the UK it was not able to become dominant and did not spread widely. The emergence of the Delta variant drives this point home as it contains none of these key mutations and has approximately a

two-fold increase in affinity. The ability of the Delta to out compete the Alpha variant is therefore thought to be due to mutations elsewhere in the spike protein such as P681R (Yang Liu et al., 2021). This mutation is in the furin cleavage site which leads to increased S1/S1 cleavage which aids cell entry (Jackson et al., 2021). Equally the emergence of the heavily altered Omicron variant also has a similar approximately two-fold increase in ACE2 affinity over WT. The very large number of mutations especially in the RBD mean that at the current time it is unclear why it has been so successful over the Delta variant.

While variant selection based on affinity is relatively straight forward to quantify the contribution of variants to immune evasion is not. The majority of neutralising antibodies produced after infection or immunisation target the RBD (Garcia-Beltran et al., 2021; Greaney, Loes, et al., 2021). Additionally the emergence of Beta and Gamma variants occurred in populations with high levels of prior infection by SARS-CoV-2 (Dejnirattisai et al., 2021; Hoffmann et al., 2021; Sabino et al., 2021; D. Zhou et al., 2021). The E484K mutation has been specifically associated with disruption of antibody binding (Greaney, Starr, et al., 2021; Wu et al., 2021). In addition, I find E484K also increased RBD affinity for ACE2 highlighting the dule role of this mutation.

A caveat of this work is the use monomeric RBD binding ACE2 rather than the full-length spike which forms a trimer on the viral surface. While I was able to produce the full-length spike protein it did not work in the SPR assay. I believe this was due to the protein aggregating as it could bind ACE2 but did not dissociate. There is evidence that ACE2 can form a dimer on the cell surface (Yan et al., 2020). Therefore, the spike-ACE2 interaction could be significantly aided by the receptor and ligand both having the potential to be multivalent. As I have shown with the work on NTRs this can significantly improve binding. Therefore, the SPR assay I have used here cannot study this effect. To test this, it would need

to be done in a cellular assay to quantify virus particle attachment to ACE2 using the different variants.

The virus has changed significantly since its emergence. This is common when a virus jumps from one species to another as it is not yet adapted to the new host (Geoghegan & Holmes, 2018). Therefore it is not surprising that a large number of mutations have been located in the spike and specifically the RBD binding interface with ACE2 (Chen et al., 2020). However, the question of how much further improvements the virus can make is difficult to judge. It is likely that the virus will continue to evolve due to the high number of infections and this will require yearly booster vaccines as the virus adapts to the increased immunity in the population (Luo et al., 2021).

Chapter 7 - General Discussion

This work has used reductionist assays to produce quantitative data on the activation and function of cell surface receptors. This has allowed me to use a similar set of techniques to study two different topics in the form of NTRs and SARS-CoV-2. The generic ligand system allows for fine control over receptor ligand binding and has produced evidence that NTRs share a common mechanism for activation. The outcome of these interactions is dependent on the length, valency, and affinity but not the mobility of the ligand. This generic ligand system has also helped to better understand the activation of CD5 and CD6 in the context of TCR activation. This complex system has been difficult to untangle but I have been able to confirm key results in the literature regarding their dual activatory and inhibitory roles. While there is more that can be done with this system, I have begun to define which aspects of the CD5 and CD6 molecules are responsible for their function. While different the approach for the SARS-CoV-2 work is similar in the use of a simple binding assay to better characterise the RBD/ACE2 binding interaction. This has allowed me to generate high quality affinity and kinetic binding measurements for a large number of RBD and ACE2 variants. While the work presented in this thesis is focused on fundamental biology, it has a strong relevance for therapeutic applications.

7.1. Improving immunotherapies

The field of immunotherapy is expanding extremely rapidly now due to successes in harnessing the patient's own immune systems to treat certain types of cancer, for example melanoma (Khalil et al., 2016). New immunotherapies are based either on stimulating endogenous T cells (e.g., checkpoint inhibitor antibodies and tumour vaccines) or redirecting T cells using synthetic antigen receptors. These receptors are either expressed on cell surfaces (e.g., CARs) or provided as soluble bispecific molecules (e.g., BiTEs and ImmTACs). All

these methods rely on the activation of NTRs. Therefore, the design of these therapies needs to consider the factors that influence NTR activation to design and optimise immunotherapies moving forward. Until the development of CARs, T cells required the TCR to recognise a specific peptide presented on an MHC molecule on the target cell. CARs incorporate an scFv which allows for T cells to be targeted towards any specific cell surface antigen (Eshhar et al., 1993). However, these improvements have focused on the signalling and largely ignored the extracellular domain.

There are several CAR treatments which have been approved for clinical use but, so far, they target the CD19 molecule using second generation CARs (Exley & McBlane, 2021). All these constructs contain a long hinge region derived from CD28, CD8 or IgG1 which significantly increases the overall size of the molecule. However, the data presented in this thesis is consistent with previous reports in the literature that CARs are sensitive to receptor ligand dimensions (A. A. Hombach et al., 2007; Hudecek et al., 2013, 2015; Krenciute et al., 2016; Rodgers et al., 2016). In general, the shorter the CAR constructs or the closer the epitope was to the opposing membrane, the superior the functional response.

In theory there is an optimum length which would allow CARs to take advantage of co-receptors such as CD2 which will form strong adhesion between the effector and target cell. Therefore, designing CARs to mimic the TCR as closely as possible should be a clear goal. This concept has been coined as a synthetic T cell receptor and antigen receptor (STAR) where the TCR Vβ and Vα are replaced with the VL and VH domains from the CAR (Yue Liu et al., 2021). This results in a receptor which can achieve very good antigen sensitivity on the order of the native TCR. This has not been possible with standard CARs which are inefficient at exploiting accessory adhesion molecules (Burton et al., 2021). Additionally, the target for the CARs also needs to be taken into account. If the target antigen is very large the epitope on the antigen needs to be close to the membrane. Despite the large amount of

evidence in the literature the importance of receptor ligand size on the effectiveness of CARs has not yet been widely accepted. However, the other advances which have focused on the signalling may still be significantly improved by taking this into account.

In addition to the sensitivity to length, my work would also suggest that the fact most CARs form a dimer should also improve their function. Increasing the multivalence of CARs may be achieved by cross-linking or adding multiple CARs which bind the same ligand with different epitopes. This is also being explored in terms of controlling off-tumour effects by introducing, for example, "AND gate" systems which require multiple antigens on the target cell to engage independent receptors in order to activate cell killing (Salzer et al., 2020).

While I show the mobility of the receptor is not likely to have a large impact on CAR function, the affinity of the scFv for the epitope very likely will. As the scFv is derived from an antibody it will usually have an affinity for its target higher than the typical affinity for NTRs and their ligands. This is another aspect which has not been well explored in terms of CAR design, and it may be that altering this could help improve the potency of the treatment and reduce off target side effects.

7.2. CD5 and CD6 immunotherapies

Although the anti-CD6 monoclonal antibody itolizumab is being used in the treatment of psoriasis, little is known about its mode of action (Menon & David, 2015). What is known is that it binds to the membrane-distal domain of CD6, and it does not block binding of CD166. Therefore, a potential use case for the current generic ligand system could be to test this antibody and others which bind to other domains of CD6. This will help to define how these antibodies are affecting cellular activation which has not been possible due to the lack of well controlled assays.

This is important because itolizumab is also being trialled in treating COVID-19 patents who have developed complications due to hyperinflammation of the immune system (Loganathan et al., 2020), with the aim of reducing the immune response and cytokine production. In India the treatment has been controversially approved after only phase II trials due to the urgent need for COVID-19 treatments (Atal et al., 2020). This highlights the need to better understand how this antibody is affecting CD6.

7.3. Applications for RBD/ACE2 binding data

Equally there is clear clinical relevance for the work on SARS-CoV-2 as it adds to the large body of research on the virus and how it is changing over time. The RBD/ACE2 interaction is critical for the virus to enter cells but is also a key target of antibodies. The RBD mutations are particularly interesting as they appear to be selected for both in terms of improving affinity for ACE2 but also antibody evasion. This suggests that some mutations which offer immune evasion but reduce affinity can be compensated for by those such as N501Y which greatly increased RBD/ACE2 affinity.

One of the initial aims of producing recombinant ACE2 with a higher affinity for RBD was the potential to use this as a drug to bind to and inhibit or deplete virus in patients. This has been attempted by a number of labs and appears to be capable of binding viral particles (Lei et al., 2020; Tanaka et al., 2021; Z. Zhang et al., 2021). They have also used a similar set of techniques in order to predict key mutations in ACE2 which would increase its affinity for the RBD. The production of a trimeric ACE2 was shown to be significantly better at inhibiting infection by pseudotyped virus (Guo et al., 2021). This multivalent version increases the avidity and therefore dramatically increases the binding potential to the viral particles. Early work suggested that the use of soluble ACE2 could decrease viral load in patients with severe COVID-19 (Monteil et al., 2020; Zoufaly et al., 2020). However, there

are issues with immunogenicity and the retention of recombinant proteins in the body as they can be quickly lost in the urine (Jia et al., 2021).

The work presented in this thesis builds towards a prediction model to identify how individuals with ACE2 variants may be susceptible to new viral variants. However, identifying individuals with ACE2 variants is not routinely done due to the cost associated with sequencing. If large scale sequencing was introduced, it would create ethical and privacy issues with some people not wanting to know or disclose that information as it could lead to increased health care costs. Additionally, while S19P and K26R significantly improve binding affinity for RBD it would be difficult to do trials on whether these individuals would benefit from personalised treatments or not.

It would likely be more productive to focus on predicting future variants of concern based on mutations which could alter receptor binding or evade antibody binding. Plus, further structural changes could alter the stability or number of spike proteins on the viral surface. This could be used to produce monoclonal antibodies or other treatments against future variants.

High-quality binding data for protein-protein binding interfaces is very valuable as training data to improving molecular modelling of such interactions. As we have shown current models such as mCSM-PPI2 are not there yet in terms of their accuracy (Rodrigues et al., 2019). However, with improvements in machine learning and greater availability of data sets this should improve in the future (Das & Chakrabarti, 2021; Sanchez-Garcia et al., 2019; W. Wang et al., 2017).

Bibliography

Abdiche, Y., Malashock, D., Pinkerton, A., & Pons, J. (2008). Determining kinetics and affinities of protein interactions using a parallel real-time label-free biosensor, the Octet. *Analytical Biochemistry*, *377*(2), 209–217. https://doi.org/10.1016/J.AB.2008.03.035

Aivazian, D., & Stern, L. J. (2000). Phosphorylation of T cell receptor ζ is regulated by a lipid dependent folding transition. *Nature Structural Biology 2000 7:11*, *7*(11), 1023–1026. https://doi.org/10.1038/80930

Alarcón, B., Swamy, M., van Santen, H. M., & Schamel, W. W. A. (2006). T-cell antigen-receptor stoichiometry: pre-clustering for sensitivity. *EMBO Reports*, *7*(5), 490–495. https://doi.org/10.1038/sj.embor.7400682

Aleksic, M., Dushek, O., Zhang, H., Shenderov, E., Chen, J. L., Cerundolo, V., Coombs, D., & van der Merwe, P. A. (2010). Dependence of T Cell Antigen Recognition on T Cell Receptor-Peptide MHC Confinement Time. *Immunity*, *32*(2), 163–174. https://doi.org/10.1016/J.IMMUNI.2009.11.013

Alenquer, M., Ferreira, F., Lousa, D., Valério, M., Medina-Lopes, M., Bergman, M.-L., Gonçalves, J., Demengeot, J., Leite, R. B., Lilue, J., Ning, Z., Penha-Gonçalves, C., Soares, H., Soares, C. M., & Amorim, M. J. (2021). Signatures in SARS-CoV-2 spike protein conferring escape to neutralizing antibodies. *PLOS Pathogens*, *17*(8), e1009772. https://doi.org/10.1371/JOURNAL.PPAT.1009772

Ali, S. R., Fong, J. J., Carlin, A. F., Busch, T. D., Linden, R., Angata, T., Areschoug, T., Parast, M., Varki, N., Murray, J., Nizet, V., & Varki, A. (2014). Siglec-5 and Siglec-14 are polymorphic paired receptors that modulate neutrophil and amnion signaling responses to group B Streptococcus. *Journal of Experimental Medicine*, *211*(6), 1231–1242. https://doi.org/10.1084/JEM.20131853

Alonso-Ramirez, R., Loisel, S., Buors, C., Pers, J.-O., Montero, E., Youinou, P., & Renaudineau, Y. (2010). *Rationale for Targeting CD6 as a Treatment for Autoimmune Diseases*. *2010*. https://doi.org/10.1155/2010/130646

Amanat, F., Stadlbauer, D., Strohmeier, S., Nguyen, T. H. O., Chromikova, V., McMahon, M., Jiang, K., Arunkumar, G. A., Jurczyszak, D., Polanco, J., Bermudez-Gonzalez, M., Kleiner, G., Aydillo, T., Miorin, L., Fierer, D. S., Lugo, L. A., Kojic, E. M., Stoever, J., Liu, S. T. H., … Krammer, F. (2020). A serological assay to detect SARS-CoV-2 seroconversion in humans. *Nature Medicine 2020 26:7*, *26*(7), 1033–1036. https://doi.org/10.1038/s41591-020-0913-5

Angata, T., Hayakawa, T., Yamanaka, M., Varki, A., & Nakamura, M. (2006). Discovery of Siglec-14, a novel sialic acid receptor undergoing concerted evolution with Siglec-5 in primates. *The FASEB Journal*, *20*(12), 1964–1973. https://doi.org/10.1096/fj.06-5800com

Artavanis-Tsakonas, S., Rand, M. D., & Lake, R. J. (1999). Notch Signaling: Cell Fate Control and Signal Integration in Development. *Science*, *284*(5415), 770–776. https://doi.org/10.1126/SCIENCE.284.5415.770

Aruffo, A., Melnick, M. B., Linsley, P. S., & Seed, B. (1991). The lymphocyte glycoprotein CD6 contains a repeated domain structure characteristic of a new family of cell surface and secreted proteins. *Journal of Experimental Medicine*, *174*(4), 949–952.

https://doi.org/10.1084/JEM.174.4.949

Aruffo, Stamenkovic, I., Melnick, M., Underhill, C. B., & Seed, B. (1990). CD44 is the principal cell surface receptor for hyaluronate. *Cell*, *61*(7), 1303–1313. https://doi.org/10.1016/0092-8674(90)90694-A

Atal, S., Fatima, Z., & Balakrishnan, S. (2020). Approval of Itolizumab for COVID-19: A Premature Decision or Need of The Hour? *BioDrugs 2020 34:6*, *34*(6), 705–711. https://doi.org/10.1007/S40259-020-00448-5

Axtell, R. C., Webb, M. S., Barnum, S. R., & Raman, C. (2004). Cutting Edge: Critical Role for CD5 in Experimental Autoimmune Encephalomyelitis: Inhibition of Engagement Reverses Disease in Mice. *The Journal of Immunology*, *173*(5), 2928–2932. https://doi.org/10.4049/JIMMUNOL.173.5.2928

Azuma, M., Ito, D., Yagita, H., Okumura, K., Phillips, J. H., Lanier, L. L., & Somoza, C. (1993). B70 antigen is a second ligand for CTLA-4 and CD28. *Nature 1993 366:6450*, *366*(6450), 76–79. https://doi.org/10.1038/366076a0

Azzam, H. S., DeJarnette, J. B., Huang, K., Emmons, R., Park, C.-S., Sommers, C. L., El-Khoury, D., Shores, E. W., & Love, P. E. (2001). Fine Tuning of TCR Signaling by CD5. *The Journal of Immunology*, *166*(9), 5464–5472. https://doi.org/10.4049/JIMMUNOL.166.9.5464

Azzam, H. S., Grinberg, A., Lui, K., Shen, H., Shores, E. W., & Love, P. E. (1998). CD5 Expression Is Developmentally Regulated By T Cell Receptor (TCR) Signals and TCR Avidity. *Journal of Experimental Medicine*, *188*(12), 2301–2311. https://doi.org/10.1084/JEM.188.12.2301

Baeuerle, P. A., & Reinhardt, C. (2009). Bispecific T-cell engaging antibodies for cancer therapy. *Cancer Research*, *69*(12), 4941–4944. https://doi.org/10.1158/0008-5472.CAN-09-0547

Bakalar, M. H., Joffe, A. M., Schmid, E. M., Son, S., Podolski, M., & Fletcher, D. A. (2018). Size-Dependent Segregation Controls Macrophage Phagocytosis of Antibody-Opsonized Targets. *Cell*, *174*(1), 131-142.e13. https://doi.org/10.1016/J.CELL.2018.05.059

Bamberger, M., Santos, A. M., Gonçalves, C. M., Oliveira, M. I., James, J. R., Moreira, A., Lozano, F., Davis, S. J., & Carmo, A. M. (2011). A new pathway of CD5 glycoprotein-mediated T cell inhibition dependent on inhibitory phosphorylation of fyn kinase. *Journal of Biological Chemistry*, *286*(35), 30324–30336. https://doi.org/10.1074/JBC.M111.230102/ATTACHMENT/58B1DA9E-5E86-4165-AE8C-0DA1690BEBDF/MMC1.PDF

Banaszynski, L. A., CW, L., & TJ, W. (2005). Characterization of the FKBP.rapamycin.FRB ternary complex. *Journal of the American Chemical Society*, *127*(13), 4715–4721. https://doi.org/10.1021/JA043277Y

Baniyash, M. (2004). TCR ζ-chain downregulation: curtailing an excessive inflammatory immune response. *Nature Reviews Immunology 2002 4:9*, *4*(9), 675–687. https://doi.org/10.1038/nri1434

Barclay, A. N., & Brown, M. H. (2006). The SIRP family of receptors and immune regulation. *Nature Reviews Immunology 2006 6:6*, *6*(6), 457–464. https://doi.org/10.1038/nri1859

Barclay, Brown, M. H., Law, S. K. A., McKnight, A. J., Tomlinson, M. G., & van der Merwe, P. A. (1997). *The leucocyte antigen factsbook, 2nd Edn*. Academic Press. https://books.google.co.uk/books?hl=en&lr=&id=mTbJGx7pTe4C&oi=fnd&pg=PP2&dq=the+leukocyte+antigen+factsbook&ots=C9PkH1Bl3c&sig=cT3zylYnDW-Zikt52OwO0dkzLpw#v=onepage&q=the leukocyte antigen factsbook&f=false

Barton, M. I., Macgowan, S., Kutuzov, M., Dushek, O., Barton, G. J., & Van Der Merwe, P. A. (2021). Effects of common mutations in the sars-cov-2 spike rbd and its ligand the human ace2 receptor on binding affinity and kinetics. *ELife*, *10*. https://doi.org/10.7554/ELIFE.70658

Bashour, K. T., Gondarenko, A., Chen, H., Shen, K., Liu, X., Huse, M., Hone, J. C., & Kam, L. C. (2014). CD28 and CD3 have complementary roles in T-cell traction forces. *Proceedings of the National Academy of Sciences of the United States of America*, *111*(6), 2241–2246. https://doi.org/10.1073/pnas.1315606111

Bateman, A., Martin, M. J., Orchard, S., Magrane, M., Agivetova, R., Ahmad, S., Alpi, E., Bowler-Barnett, E. H., Britto, R., Bursteinas, B., Bye-A-Jee, H., Coetzee, R., Cukura, A., Silva, A. Da, Denny, P., Dogan, T., Ebenezer, T. G., Fan, J., Castro, L. G., … Zhang, J. (2021). UniProt: the universal protein knowledgebase in 2021. *Nucleic Acids Research*, *49*(D1), D480–D489. https://doi.org/10.1093/NAR/GKAA1100

Baychelier, F., Sennepin, A., Ermonval, M., Dorgham, K., Debré, P., & Vieillard, V. (2013). Identification of a cellular ligand for the natural cytotoxicity receptor NKp44. *Blood*, *122*(17), 2935–2942. https://doi.org/10.1182/blood-2013-03-489054

Bergman, M., Mustelin, T., Oetken, C., Partanen, J., Flint, N. A., Amrein, K. E., Autero, M., Burn, P., & Alitalo, K. (1992). The human p50csk tyrosine kinase phosphorylates p56lck at Tyr-505 and down regulates its catalytic activity. *The EMBO Journal*, *11*(8), 2919–2924. https://doi.org/10.1002/J.1460-2075.1992.TB05361.X

Bernal, J. L., Andrews, N., Gower, C., Gallagher, E., Simmons, R., Thelwall, S., Stowe, J., Tessier, E., Groves, N., Dabrera, G., Myers, R., Campbell, C. N. J., Amirthalingam, G., Edmunds, M., Zambon, M., Brown, K. E., Hopkins, S., Chand, M., & Ramsay, M. (2021). Effectiveness of Covid-19 Vaccines against the B.1.617.2 (Delta) Variant. *The New England Journal of Medicine*, *385*(7), 585–594. https://doi.org/10.1056/NEJMOA2108891

Beth, M., Lewis, H., Lanier, L., Nakamura, M. C., Humphrey, M. B., & Lanier, L. L. (2005). Role of ITAM-containing adapter proteins and their receptors in the immune system and bone. *Immunological Reviews*, *208*(1), 50–65. https://doi.org/10.1111/J.0105-2896.2005.00325.X

Beum, P. V., Lindorfer, M. A., & Taylor, R. P. (2008). Within Peripheral Blood Mononuclear Cells, Antibody-Dependent Cellular Cytotoxicity of Rituximab-Opsonized Daudi cells Is Promoted by NK Cells and Inhibited by Monocytes due to Shaving. *The Journal of Immunology*, *181*(4), 2916–2924. https://doi.org/10.4049/JIMMUNOL.181.4.2916

Bhandoola, A., Bosselut, R., Yu, Q., Cowan, M. L., Feigenbaum, L., Love, P. E., & Singer, A. (2002). *CD5-mediated inhibition of TCR signaling during intrathymic selection and development does not require the CD5 extracellular domain*. https://doi.org/10.1002/1521-4141

Bluemel, C., Hausmann, S., Fluhr, P., Sriskandarajah, M., Stallcup, W. B., Baeuerle, P. A., &

Kufer, P. (2010). Epitope distance to the target cell membrane and antigen size determine the potency of T cell-mediated lysis by BiTE antibodies specific for a large melanoma surface antigen. *Cancer Immunology, Immunotherapy*, *59*(8), 1197–1209. https://doi.org/10.1007/s00262-010-0844-y

Boni, M. F., Lemey, P., Jiang, X., Lam, T. T. Y., Perry, B. W., Castoe, T. A., Rambaut, A., & Robertson, D. L. (2020). Evolutionary origins of the SARS-CoV-2 sarbecovirus lineage responsible for the COVID-19 pandemic. *Nature Microbiology 2020 5:11*, *5*(11), 1408–1417. https://doi.org/10.1038/s41564-020-0771-4

Bott, C. M., Doshi, J. B., Morimoto, C., Romain, P. L., & Fox, D. A. (1993). Activation of human T cells through CD6: functional effects of a novel anti-CD6 monoclonal antibody and definition of four epitopes of the CD6 glycoprotein. *International Immunology*, *5*(7), 783–792. https://doi.org/10.1093/INTIMM/5.7.783

Bowen, Bajorath, J., Siadak, A. W., Modrell, B., Malacko, A. R., Marquardt, H., Nadler, S. G., & Aruffo, A. (1996). The Amino-terminal Immunoglobulin-like Domain of Activated Leukocyte Cell Adhesion Molecule Binds Specifically to the Membrane-proximal Scavenger Receptor Cysteine-rich Domain of CD6 with a 1:1 Stoichiometry *. *Journal of Biological Chemistry*, *271*(29), 17390–17396. https://doi.org/10.1074/JBC.271.29.17390

Bowen, M. A., Whitney, G. S., Neubauer, M., Starling, G. C., Palmer, D., Zhang, J., Nowak, N. J., Shows, T. B., & Aruffo, A. (1997). Structure and chromosomal location of the human CD6 gene: detection of five human CD6 isoforms. *The Journal of Immunology*, *158*(3).

Bowen, Patel, D. D., Li, X., Modrell, B., Malacko, A. R., Wang, W. C., Marquardt, H., Neubauer, M., Pesando, J. M., & Francke, U. (1995). Cloning, mapping, and characterization of activated leukocyte-cell adhesion molecule (ALCAM), a CD6 ligand. *Journal of Experimental Medicine*, *181*(6), 2213–2220. https://doi.org/10.1084/JEM.181.6.2213

Brameshuber, M., Kellner, F., Rossboth, B. K., Ta, H., Alge, K., Sevcsik, E., Göhring, J., Axmann, M., Baumgart, F., Gascoigne, N. R. J., Davis, S. J., Stockinger, H., Schütz, G. J., & Huppa, J. B. (2018). Monomeric TCRs drive T cell antigen recognition. *Nature Immunology 2018 19:5*, *19*(5), 487–496. https://doi.org/10.1038/s41590-018-0092-4

Breuning, J., & Brown, M. H. (2017). T Cell Costimulation by CD6 Is Dependent on Bivalent Binding of a GADS/SLP-76 Complex. *Molecular and Cellular Biology*, *37*(11). https://doi.org/10.1128/MCB.00071-17

Breuning, J., Philip, B., & Brown, M. H. (2019). Addition of the C-terminus of CD6 to a chimeric antigen receptor enhances cytotoxicity and does not compromise expression. *Immunology*, *156*(2), 130–135. https://doi.org/10.1111/IMM.13009

Brocker, T. (2000). Chimeric Fv-ζ or Fv-ε receptors are not sufficient to induce activation or cytokine production in peripheral T cells. *Blood*, *96*(5), 1999–2001. https://doi.org/10.1182/BLOOD.V96.5.1999

Brossard, C., Semichon, M., Trautmann, A., & Bismuth, G. (2003). CD5 Inhibits Signaling at the Immunological Synapse Without Impairing Its Formation. *The Journal of Immunology*, *170*(9), 4623–4629. https://doi.org/10.4049/JIMMUNOL.170.9.4623

Brouwer, P. J. M., Caniels, T. G., van der Straten, K., Snitselaar, J. L., Aldon, Y., Bangaru,

S., Torres, J. L., Okba, N. M. A., Claireaux, M., Kerster, G., Bentlage, A. E. H., van Haaren, M. M., Guerra, D., Burger, J. A., Schermer, E. E., Verheul, K. D., van der Velde, N., van der Kooi, A., van Schooten, J., … van Gils, M. J. (2020). Potent neutralizing antibodies from COVID-19 patients define multiple targets of vulnerability. *Science*, *369*(6504), 643–650. https://doi.org/10.1126/SCIENCE.ABC5902/SUPPL_FILE/PAP.PDF

Brown, M. H., & Lacey, E. (2010). A Ligand for CD5 Is CD5. *The Journal of Immunology*, *185*(10), 6068–6074. https://doi.org/10.4049/JIMMUNOL.0903823

Bunnell, S. C., Hong, D. I., Kardon, J. R., Yamazaki, T., McGlade, C. J., Barr, V. A., & Samelson, L. E. (2002). T cell receptor ligation induces the formation of dynamically regulated signaling assemblies. *Journal of Cell Biology*, *158*(7), 1263–1275. https://doi.org/10.1083/JCB.200203043

Burgess, K. E., Yamamoto, M., Prasad, K. V, & Rudd, C. E. (1992). CD5 acts as a tyrosine kinase substrate within a receptor complex comprising T-cell receptor zeta chain/CD3 and protein-tyrosine kinases p56lck and p59fyn. *Proceedings of the National Academy of Sciences*, *89*(19), 9311–9315. https://doi.org/10.1073/PNAS.89.19.9311

Burton, J., Siller-Farfán, J. A., Pettmann, J., Salzer, B., Kutuzov, M., van der Merwe, P. A., Dushek, O., & William, S. (2021). Inefficient exploitation of accessory receptors reduces the sensitivity of chimeric antigen receptors. *BioRxiv*, 2021.10.26.465853. https://doi.org/10.1101/2021.10.26.465853

Call, M. E., & Wucherpfennig, K. W. (2004). Molecular mechanisms for the assembly of the T cell receptor–CD3 complex. *Molecular Immunology*, *40*(18), 1295–1305. https://doi.org/10.1016/J.MOLIMM.2003.11.017

Call, M. E., & Wucherpfennig, K. W. (2007). Common themes in the assembly and architecture of activating immune receptors. *Nature Reviews Immunology 2007 7:11*, *7*(11), 841–850. https://doi.org/10.1038/nri2186

Cambier, J. C. (1995). New nomenclature for the Reth motif (or ARH1/TAM/ARAM/YXXL). *Immunology Today*, *16*(2), 110. https://doi.org/10.1016/0167-5699(95)80105-7

Campi, G., Varma, R., & Dustin, M. L. (2005). Actin and agonist MHC–peptide complex–dependent T cell receptor microclusters as scaffolds for signaling. *Journal of Experimental Medicine*, *202*(8), 1031–1036. https://doi.org/10.1084/JEM.20051182

Cannon, J. L., Mody, P. D., Blaine, K. M., Chen, E. J., Nelson, A. D., Sayles, L. J., Moore, T. V., Clay, B. S., Dulin, N. O., Shilling, R. A., Burkhardt, J. K., & Sperling, A. I. (2011). CD43 interaction with ezrin-radixin-moesin (ERM) proteins regulates T-cell trafficking and CD43 phosphorylation. *Molecular Biology of the Cell*, *22*(7), 954–963. https://doi.org/10.1091/MBC.E10-07-0586/ASSET/IMAGES/LARGE/954FIG9.JPEG

Cannons, J. L., Tangye, S. G., & Schwartzberg, P. L. (2011). SLAM Family Receptors and SAP Adaptors in Immunity. *Http://Dx.Doi.Org/10.1146/Annurev-Immunol-030409-101302*, *29*, 665–705. https://doi.org/10.1146/ANNUREV-IMMUNOL-030409-101302

Cao, & Li, T. (2020). COVID-19: towards understanding of pathogenesis. *Cell Research*, *30*(5), 367–369. https://doi.org/10.1038/s41422-020-0327-4

Cao, Y., Li, L., Feng, Z., Wan, S., Huang, P., Sun, X., Wen, F., Huang, X., Ning, G., &

Wang, W. (2020). Comparative genetic analysis of the novel coronavirus (2019-nCoV/SARS-CoV-2) receptor ACE2 in different populations. In *Cell Discovery* (Vol. 6, Issue 1, pp. 1–4). Springer Nature. https://doi.org/10.1038/s41421-020-0147-1

Carbone, C. B., Kern, N., Fernandes, R. A., Hui, E., Su, X., Garcia, K. C., & Vale, R. D. (2017). In vitro reconstitution of T cell receptor-mediated segregation of the CD45 phosphatase. *Proceedings of the National Academy of Sciences of the United States of America*, *114*(44), E9338–E9345. https://doi.org/10.1073/pnas.1710358114

Cartwright, A. N. R., Griggs, J., & Davis, D. M. (2014). The immune synapse clears and excludes molecules above a size threshold. *Nature Communications*, *5*, 5479. https://doi.org/10.1038/ncomms6479

Castro, M. A. A., Oliveira, M. I., Nunes, R. J., Fabre, S., Barbosa, R., Peixoto, A., Brown, M. H., Parnes, J. R., Bismuth, G., Moreira, A., Rocha, B., & Carmo, A. M. (2007). Extracellular Isoforms of CD6 Generated by Alternative Splicing Regulate Targeting of CD6 to the Immunological Synapse. *The Journal of Immunology*, *178*(7), 4351–4361. https://doi.org/10.4049/JIMMUNOL.178.7.4351

Cayrol, R., Wosik, K., Berard, J. L., Dodelet-Devillers, A., Ifergan, I., Kebir, H., Haqqani, A. S., Kreymborg, K., Krug, S., Moumdjian, R., Bouthillier, A., Becher, B., Arbour, N., David, S., Stanimirovic, D., & Prat, A. (2007). Activated leukocyte cell adhesion molecule promotes leukocyte trafficking into the central nervous system. *Nature Immunology 2007 9:2*, *9*(2), 137–145. https://doi.org/10.1038/ni1551

Cenit, M. C., Martínez-Florensa, M., Consuegra, M., Bonet, L., Carnero-Montoro, E., Armiger, N., Caballero-Baños, M., Arias, M. T., Benitez, D., Ortego-Centeno, N., De Ramón, E., Sabio, J. M., García-Hernández, F. J., Tolosa, C., Suárez, A., González-Gay, M. A., Bosch, E., Martín, J., & Lozano, F. (2014). Analysis of Ancestral and Functionally Relevant CD5 Variants in Systemic Lupus Erythematosus Patients. *PLOS ONE*, *9*(11), e113090. https://doi.org/10.1371/JOURNAL.PONE.0113090

Cerami, A. (1992). Inflammatory cytokines. *Clinical Immunology and Immunopathology*, *62*(1), S3–S10. https://doi.org/10.1016/0090-1229(92)90035-M

Chan, A. C., & Carter, P. J. (2010). Therapeutic antibodies for autoimmunity and inflammation. *Nature Reviews Immunology*, *10*(5), 301–316. https://doi.org/10.1038/nri2761

Chan, Irving, B. A., Fraser, J. D., & Weiss, A. (1991). The zeta chain is associated with a tyrosine kinase and upon T-cell antigen receptor stimulation associates with ZAP-70, a 70-kDa tyrosine phosphoprotein. *Proceedings of the National Academy of Sciences*, *88*(20), 9166–9170. https://doi.org/10.1073/PNAS.88.20.9166

Chan, & Springer, T. A. (1992). Effect of lengthening lymphocyte function-associated antigen 3 on adhesion to CD2. *Molecular Biology of the Cell*, *3*(2), 157–166. http://www.ncbi.nlm.nih.gov/pubmed/1348006

Chang, V. T., Fernandes, R. A., Ganzinger, K. A., Lee, S. F., Siebold, C., McColl, J., Jönsson, P., Palayret, M., Harlos, K., Coles, C. H., Jones, E. Y., Lui, Y., Huang, E., Gilbert, R. J. C., Klenerman, D., Aricescu, A. R., & Davis, S. J. (2016). Initiation of T cell signaling by CD45 segregation at 'close contacts'. *Nature Immunology*, *17*(5), 574–582. https://doi.org/10.1038/ni.3392

Chappell, P. E., Garner, L. I., Yan, J., Metcalfe, C., Hatherley, D., Johnson, S., Robinson, C.

V., Lea, S. M., & Brown, M. H. (2015). Structures of CD6 and Its Ligand CD166 Give Insight into Their Interaction. *Structure*, *23*(8), 1426–1436. https://doi.org/10.1016/J.STR.2015.05.019

Chen, Al-Aghbar, M. A., Lee, C.-H., Chang, T.-C., Su, Y.-C., Li, Y.-C., Chang, S.-E., Chen, C.-C., Chung, T.-H., Liao, Y.-C., Lee, C.-H., & Roffler, S. R. (2017). The Affinity of Elongated Membrane-Tethered Ligands Determines Potency of T Cell Receptor Triggering. *Frontiers in Immunology*, *8*, 793. https://doi.org/10.3389/fimmu.2017.00793

Chen, & Flies, D. B. (2013). Molecular mechanisms of T cell co-stimulation and co-inhibition. *Nature Reviews Immunology 2013 13:4*, *13*(4), 227–242. https://doi.org/10.1038/nri3405

Chen, Gao, K., Wang, R., Nguyen, D. D., & Wei, G. W. (2021). Review of COVID-19 Antibody Therapies. *Https://Doi.Org/10.1146/Annurev-Biophys-062920-063711*, *50*, 1–30. https://doi.org/10.1146/ANNUREV-BIOPHYS-062920-063711

Chen, J.-L., Morgan, A. J., Stewart-Jones, G., Shepherd, D., Bossi, G., Wooldridge, L., Hutchinson, S. L., Sewell, A. K., Griffiths, G. M., Merwe, P. A. van der, Jones, E. Y., Galione, A., & Cerundolo, V. (2010). Ca2+ Release from the Endoplasmic Reticulum of NY-ESO-1–Specific T Cells Is Modulated by the Affinity of TCR and by the Use of the CD8 Coreceptor. *The Journal of Immunology*, *184*(4), 1829–1839. https://doi.org/10.4049/JIMMUNOL.0902103

Chen, K. Y., Jenkins, E., Körbel, M., Ponjavic, A., Lippert, A. H., Santos, A. M., Ashman, N., O'Brien-Ball, C., McBride, J., Klenerman, D., & Davis, S. J. (2021). Trapping or slowing the diffusion of T cell receptors at close contacts initiates T cell signaling. *Proceedings of the National Academy of Sciences*, *118*(39), e2024250118. https://doi.org/10.1073/PNAS.2024250118

Chen, Wang, R., Wang, M., & Wei, G. W. (2020). Mutations Strengthened SARS-CoV-2 Infectivity. *Journal of Molecular Biology*, *432*(19), 5212–5226. https://doi.org/10.1016/J.JMB.2020.07.009

Cho, Collins, J. J., & Wong, W. W. (2018). Universal Chimeric Antigen Receptors for Multiplexed and Logical Control of T Cell Responses. *Cell*, *173*(6), 1426-1438.e11. https://doi.org/10.1016/J.CELL.2018.03.038

Cho, H.-S., Mason, K., Ramyar, K. X., Stanley, A. M., Gabelli, S. B., Denney, D. W., & Leahy, D. J. (2003). Structure of the extracellular region of HER2 alone and in complex with the Herceptin Fab. *Nature*, *421*(6924), 756–760. https://doi.org/10.1038/nature01392

Choudhuri, K., Parker, M., Milicic, A., Cole, D. K., Shaw, M. K., Sewell, A. K., Stewart-Jones, G., Dong, T., Gould, K. G., & van der Merwe, P. A. (2009). Peptide-major histocompatibility complex dimensions control proximal kinase-phosphatase balance during T cell activation. *The Journal of Biological Chemistry*, *284*(38), 26096–26105. https://doi.org/10.1074/jbc.M109.039966

Choudhuri, K., & van der Merwe, P. A. (2007). Molecular mechanisms involved in T cell receptor triggering. *Seminars in Immunology*, *19*(4), 255–261. https://doi.org/10.1016/J.SMIM.2007.04.005

Choudhuri, K., Wiseman, D., Brown, M. H., Gould, K., & van der Merwe, P. A. (2005). T-cell receptor triggering is critically dependent on the dimensions of its peptide-MHC

ligand. *Nature*, *436*(7050), 578–582. https://doi.org/10.1038/nature03843

Cibrián, D., & Sánchez-Madrid, F. (2017). CD69: from activation marker to metabolic gatekeeper. *European Journal of Immunology*, *47*(6), 946–953. https://doi.org/10.1002/EJI.201646837

Cleary, K. L. S., Chan, H. T. C., James, S., Glennie, M. J., & Cragg, M. S. (2017). Antibody Distance from the Cell Membrane Regulates Antibody Effector Mechanisms. *The Journal of Immunology*, *198*(10), 3999–4011. https://doi.org/10.4049/jimmunol.1601473

Consuegra-Fernández, M., Julià, M., Martínez-Florensa, M., Aranda, F., Català, C., Armiger-Borràs, N., Arias, M.-T., Santiago, F., Guilabert, A., Esteve, A., Muñoz, C., Ferrándiz, C., Carrascosa, J.-M., Pedrosa, E., Romaní, J., Alsina, M., Mascaró-Galy, J.-M., & Lozano, F. (2017). Genetic and experimental evidence for the involvement of the CD6 lymphocyte receptor in psoriasis. *Cellular & Molecular Immunology 2017 15:10*, *15*(10), 898–906. https://doi.org/10.1038/cmi.2017.119

Cooper, J. A., & Qian, H. (2008). A Mechanism for Src Kinase-Dependent Signaling by Noncatalytic Receptors†. *Biochemistry*, *47*(21), 5681–5688. https://doi.org/10.1021/BI8003044

Cordoba, S.-P., Choudhuri, K., Zhang, H., Bridge, M., Basat, A. B., Dustin, M. L., & van der Merwe, P. A. (2013). The large ectodomains of CD45 and CD148 regulate their segregation from and inhibition of ligated T-cell receptor. *Blood*, *121*(21), 4295–4302. https://doi.org/10.1182/blood-2012-07-442251

Cornish, A. L., Freeman, S., Forbes, G., Ni, J., Zhang, M., Cepeda, M., Gentz, R., Augustus, M., Carter, K. C., & Crocker, P. R. (1998). Characterization of Siglec-5, a Novel Glycoprotein Expressed on Myeloid Cells Related to CD33. *Blood*, *92*(6), 2123–2132. https://doi.org/10.1182/BLOOD.V92.6.2123

Courtney, A. H., Lo, W. L., & Weiss, A. (2018). TCR Signaling: Mechanisms of Initiation and Propagation. *Trends in Biochemical Sciences*, *43*(2), 108–123. https://doi.org/10.1016/J.TIBS.2017.11.008

Crocker, P. R., Paulson, J. C., & Varki, A. (2007). Siglecs and their roles in the immune system. *Nature Reviews Immunology 2007 7:4*, *7*(4), 255–266. https://doi.org/10.1038/nri2056

Curtsinger, J. M., & Mescher, M. F. (2010). Inflammatory cytokines as a third signal for T cell activation. *Current Opinion in Immunology*, *22*(3), 333–340. https://doi.org/10.1016/J.COI.2010.02.013

D'Ambrosio, D., Hippen, K. L., Minskoff, S. A., Mellman, I., Pani, G., Siminovitch, K. A., & Cambier, J. C. (1995). Recruitment and Activation of PTP1C in Negative Regulation of Antigen Receptor Signaling by FcγRIIB1. *Science*, *268*(5208), 293–297. https://doi.org/10.1126/SCIENCE.7716523

D'Oro, U., Sakaguchi, K., Appella, E., & Ashwell, J. D. (1996). Mutational analysis of Lck in CD45-negative T cells: dominant role of tyrosine 394 phosphorylation in kinase activity. *Molecular and Cellular Biology*, *16*(9), 4996–5003. https://doi.org/10.1128/MCB.16.9.4996

Damle, R. N., Ghiotto, F., Valetto, A., Albesiano, E., Fais, F., Yan, X. J., Sison, C. P., Allen,

S. L., Kolitz, J., Schulman, P., Vinciguerra, V. P., Budde, P., Frey, J., Rai, K. R., Ferrarini, M., & Chiorazzi, N. (2002). B-cell chronic lymphocytic leukemia cells express a surface membrane phenotype of activated, antigen-experienced B lymphocytesPresented in part at the 42nd Annual Meeting of the American Society of Hematology, December 1-5, 2000, San Francisco, CA. *Blood*, *99*(11), 4087–4093. https://doi.org/10.1182/BLOOD.V99.11.4087

Darif, D., Hammi, I., Kihel, A., El Idrissi Saik, I., Guessous, F., & Akarid, K. (2021). The pro-inflammatory cytokines in COVID-19 pathogenesis: What goes wrong? *Microbial Pathogenesis*, *153*, 104799. https://doi.org/10.1016/J.MICPATH.2021.104799

Darowski, D., Kobold, S., Jost, C., & Klein, C. (2019). Combining the best of two worlds: highly flexible chimeric antigen receptor adaptor molecules (CAR-adaptors) for the recruitment of chimeric antigen receptor T cells. *Https://Doi.Org/10.1080/19420862.2019.1596511*, *11*(4), 621–631. https://doi.org/10.1080/19420862.2019.1596511

Das, S., & Chakrabarti, S. (2021). Classification and prediction of protein–protein interaction interface using machine learning algorithm. *Scientific Reports 2021 11:1*, *11*(1), 1–12. https://doi.org/10.1038/s41598-020-80900-2

Dasu, T., Qualls, J. E., Tuna, H., Raman, C., Cohen, D. A., & Bondada, S. (2008). CD5 plays an inhibitory role in the suppressive function of murine CD4+ CD25+ Treg cells. *Immunology Letters*, *119*(1–2), 103–113. https://doi.org/10.1016/J.IMLET.2008.05.008

Davies, N. G., Abbott, S., Barnard, R. C., Jarvis, C. I., Kucharski, A. J., Munday, J. D., Pearson, C. A. B., Russell, T. W., Tully, D. C., Washburne, A. D., Wenseleers, T., Gimma, A., Waites, W., Wong, K. L. M., van Zandvoort, K., Silverman, J. D., Diaz-Ordaz, K., Keogh, R., Eggo, R. M., … Edmunds, W. J. (2021). Estimated transmissibility and impact of SARS-CoV-2 lineage B.1.1.7 in England. *Science*, *372*(6538), eabg3055. https://doi.org/10.1126/science.abg3055

Davis, S. J., & van der Merwe, P. A. (2006). The kinetic-segregation model: TCR triggering and beyond. *Nature Immunology*, *7*(8), 803–809. https://doi.org/10.1038/ni1369

Davis, S. J., & van der Merwe, P. A. (2011). Lck and the nature of the T cell receptor trigger. *Trends in Immunology*, *32*(1), 1–5. https://doi.org/10.1016/J.IT.2010.11.003

Davis, & van der Merwe, P. A. (1996). The structure and ligand interactions of CD2: implications for T-cell function. *Immunology Today*, *17*(4), 177–187. http://www.ncbi.nlm.nih.gov/pubmed/8871350

De Jager, P. L., Jia, X., Wang, J., de Bakker, P. I. W., Ottoboni, L., Aggarwal, N. T., Piccio, L., Raychaudhuri, S., Tran, D., Aubin, C., Briskin, R., Romano, S., Baranzini, S. E., McCauley, J. L., Pericak-Vance, M. A., Haines, J. L., Gibson, R. A., Naeglin, Y., Uitdehaag, B., … Oksenberg, J. R. (2009). Meta-analysis of genome scans and replication identify CD6, IRF8 and TNFRSF1A as new multiple sclerosis susceptibility loci. *Nature Genetics 2009 41:7*, *41*(7), 776–782. https://doi.org/10.1038/ng.401

De Visser, K. E., Eichten, A., & Coussens, L. M. (2006). Paradoxical roles of the immune system during cancer development. *Nature Reviews Cancer 2006 6:1*, *6*(1), 24–37. https://doi.org/10.1038/nrc1782

Dejnirattisai, W., Zhou, D., Supasa, P., Liu, C., Mentzer, A. J., Ginn, H. M., Zhao, Y., Duyvesteyn, H. M. E., Tuekprakhon, A., Nutalai, R., Wang, B., López-Camacho, C.,

Slon-Campos, J., Walter, T. S., Skelly, D., Costa Clemens, S. A., Naveca, F. G., Nascimento, V., Nascimento, F., … Screaton, G. R. (2021). Antibody evasion by the P.1 strain of SARS-CoV-2. *Cell*. https://doi.org/10.1016/j.cell.2021.03.055

Denham, E. M., Barton, M. I., Black, S. M., Bridge, M. J., de Wet, B., Paterson, R. L., van der Merwe, P. A., & Goyette, J. (2019). A generic cell surface ligand system for studying cell–cell recognition. *PLOS Biology*, *17*(12), e3000549. https://doi.org/10.1371/journal.pbio.3000549

Depoil, D., & Dustin, M. L. (2014). Force and affinity in ligand discrimination by the TCR. *Trends in Immunology*, *35*(12), 597–603. https://doi.org/10.1016/J.IT.2014.10.007

Doty, R. T., & Clark, E. A. (1996). Subcellular localization of CD80 receptors is dependent on an intact cytoplasmic tail and is required for CD28-dependent T cell costimulation. *The Journal of Immunology*, *157*(8).

Dushek, O., Goyette, J., & van der Merwe, P. A. (2012). Non-catalytic tyrosine-phosphorylated receptors. *Immunological Reviews*, *250*(1), 258–276. https://doi.org/10.1111/imr.12008

Dustin, M. L., Olszowy, M. W., Holdorf, A. D., Li, J., Bromley, S., Desai, N., Widder, P., Rosenberger, F., van der Merwe, P. A., Allen, P. M., & Shaw, A. S. (1998). A Novel Adaptor Protein Orchestrates Receptor Patterning and Cytoskeletal Polarity in T-Cell Contacts. *Cell*, *94*(5), 667–677. https://doi.org/10.1016/S0092-8674(00)81608-6

Enyindah-Asonye, G., Li, Y., Ruth, J. H., Spassov, D. S., Hebron, K. E., Zijlstra, A., Moasser, M. M., Wang, B., Singer, N. G., Cui, H., Ohara, R. A., Rasmussen, S. M., Fox, D. A., & Lin, F. (2017). CD318 is a ligand for CD6. *Proceedings of the National Academy of Sciences of the United States of America*, *114*(33), E6912–E6921. https://doi.org/10.1073/PNAS.1704008114

Eshhar, Z., Waks, T., Gross, G., & Schindler, D. G. (1993). Specific activation and targeting of cytotoxic lymphocytes through chimeric single chains consisting of antibody-binding domains and the gamma or zeta subunits of the immunoglobulin and T-cell receptors. *Proceedings of the National Academy of Sciences*, *90*(2), 720–724. https://doi.org/10.1073/PNAS.90.2.720

Exley, A. R., & McBlane, J. (2021). Regulating innovation in the early development of cell therapies. *Immunotherapy Advances*, *1*(1), 1–18. https://doi.org/10.1093/IMMADV/LTAA011

Fan, X., Cao, D., Kong, L., & Zhang, X. (2020). Cryo-EM analysis of the post-fusion structure of the SARS-CoV spike glycoprotein. *Nature Communications 2020 11:1*, *11*(1), 1–10. https://doi.org/10.1038/s41467-020-17371-6

Fang, L., Karakiulakis, G., & Roth, M. (2020). Are patients with hypertension and diabetes mellitus at increased risk for COVID-19 infection? In *The Lancet Respiratory Medicine* (Vol. 8, Issue 4, p. e21). Lancet Publishing Group. https://doi.org/10.1016/S2213-2600(20)30116-8

Felce, J. H., Sezgin, E., Wane, M., Brouwer, H., Dustin, M. L., Eggeling, C., & Davis, S. J. (2018). CD45 exclusion– and cross-linking–based receptor signaling together broaden FceRI reactivity. *Science Signaling*, *11*(561). https://doi.org/10.1126/SCISIGNAL.AAT0756/SUPPL_FILE/AAT0756_SM.PDF

Feng, J., Call, M. E., & Wucherpfennig, K. W. (2006). The Assembly of Diverse Immune Receptors Is Focused on a Polar Membrane-Embedded Interaction Site. *PLOS Biology*, *4*(5), e142. https://doi.org/10.1371/JOURNAL.PBIO.0040142

Fernandes, R. A., Ganzinger, K. A., Tzou, J. C., Jönsson, P., Lee, S. F., Palayret, M., Santos, A. M., Carr, A. R., Ponjavic, A., Chang, V. T., Macleod, C., Christoffer Lagerholm, B., Lindsay, A. E., Dushek, O., Tilevik, A., Davis, S. J., & Klenerman, D. (2019). A cell topography-based mechanism for ligand discrimination by the T cell receptor. *Proceedings of the National Academy of Sciences of the United States of America*, *116*(28), 14002–14010. https://doi.org/10.1073/PNAS.1817255116/SUPPL_FILE/PNAS.1817255116.SM03.AVI

Fernandes, R. A., Yu, C., Carmo, A. M., Evans, E. J., Merwe, P. A. van der, & Davis, S. J. (2010). What Controls T Cell Receptor Phosphorylation? *Cell*, *142*(5), 668–669. https://doi.org/10.1016/J.CELL.2010.08.018

Fletcher, J. M., Lalor, S. J., Sweeney, C. M., Tubridy, N., & Mills, K. H. G. (2010). T cells in multiple sclerosis and experimental autoimmune encephalomyelitis. *Clinical & Experimental Immunology*, *162*(1), 1–11. https://doi.org/10.1111/J.1365-2249.2010.04143.X

Ford, J. W., & McVicar, D. W. (2009). TREM and TREM-like receptors in inflammation and disease. *Current Opinion in Immunology*, *21*(1), 38–46. https://doi.org/10.1016/J.COI.2009.01.009

Fortini, M. E. (2009). Notch Signaling: The Core Pathway and Its Posttranslational Regulation. *Developmental Cell*, *16*(5), 633–647. https://doi.org/10.1016/J.DEVCEL.2009.03.010

Freeman, Goyette, J., Furuya, W., Woods, E. C., Bertozzi, C. R., Bergmeier, W., Hinz, B., van der Merwe, P. A., Das, R., & Grinstein, S. (2016). Integrins Form an Expanding Diffusional Barrier that Coordinates Phagocytosis. *Cell*, *164*(1–2), 128–140. https://doi.org/10.1016/J.CELL.2015.11.048

Freeman, S. D., Kelm, S., Barber, E. K., & Crocker, P. R. (1995). Characterization of CD33 as a new member of the sialoadhesin family of cellular interaction molecules. *Blood*, *85*(8), 2005–2012. http://www.ncbi.nlm.nih.gov/pubmed/7718872

Freeman, Vega, A., Riedl, M., Collins, R. F., Ostrowski, P. P., Woods, E. C., Bertozzi, C. R., Tammi, M. I., Lidke, D. S., Johnson, P., Mayor, S., Jaqaman, K., & Grinstein, S. (2018). Transmembrane Pickets Connect Cyto- and Pericellular Skeletons Forming Barriers to Receptor Engagement. *Cell*, *172*(1–2), 305-317.e10. https://doi.org/10.1016/J.CELL.2017.12.023

Friedlein, G., Hage, F. El, Vergnon, I., Richon, C., Saulnier, P., Lécluse, Y., Caignard, A., Boumsell, L., Bismuth, G., Chouaib, S., & Mami-Chouaib, F. (2007). Human CD5 Protects Circulating Tumor Antigen-Specific CTL from Tumor-Mediated Activation-Induced Cell Death. *The Journal of Immunology*, *178*(11), 6821–6827. https://doi.org/10.4049/JIMMUNOL.178.11.6821

Fu, L., Han, L., Xie, C., Li, W., Lin, L., Pan, S., Zhou, Y., Li, Z., Jin, M., & Zhang, A. (2017). Identification of Extracellular Actin As a Ligand for Triggering Receptor Expressed on Myeloid Cells-1 Signaling. *Frontiers in Immunology*, *8*, 917.

https://doi.org/10.3389/fimmu.2017.00917

Fulton, R. B., Hamilton, S. E., Xing, Y., Adam Best, J., Goldrath, A. W., Hogquist, K. A., & Jameson, S. C. (2015). The TCR's sensitivity to self peptide-MHC dictates the ability of naive CD8 + T cells to respond to foreign antigens. *Nature Immunology VOLUME*, *16*. https://doi.org/10.1038/ni.3043

Furlan, G., Minowa, T., Hanagata, N., Kataoka-Hamai, C., & Kaizuka, Y. (2014). Phosphatase CD45 Both Positively and Negatively Regulates T Cell Receptor Phosphorylation in Reconstituted Membrane Protein Clusters. *Journal of Biological Chemistry*, *289*(41), 28514–28525. https://doi.org/10.1074/jbc.M114.574319

Gangemi, R. M., Swack, J. A., Gaviria, D. M., & Romain, P. L. (1989). Anti-T12, an anti-CD6 monoclonal antibody, can activate human T lymphocytes. *The Journal of Immunology*, *143*(8), 2439 LP – 2447. http://www.jimmunol.org/content/143/8/2439.abstract

Garboczi, D. N., Ghosh, P., Utz, U., Fan, Q. R., Biddison, W. E., & Wiley, D. C. (1996). Structure of the complex between human T-cell receptor, viral peptide and HLA-A2. *Nature*, *384*(6605), 134–141. https://doi.org/10.1038/384134a0

Garcia-Beltran, W. F., Lam, E. C., St. Denis, K., Nitido, A. D., Garcia, Z. H., Hauser, B. M., Feldman, J., Pavlovic, M. N., Gregory, D. J., Poznansky, M. C., Sigal, A., Schmidt, A. G., Iafrate, A. J., Naranbhai, V., & Balazs, A. B. (2021). Multiple SARS-CoV-2 variants escape neutralization by vaccine-induced humoral immunity. *Cell*, *184*(9), 2372-2383.e9. https://doi.org/10.1016/J.CELL.2021.03.013

Garcia-Santana, C. A., Tung, J. W., & Gulnik, S. (2014). Human treg cells are characterized by low/negative CD6 expression. *Cytometry Part A*, *85*(10), 901–908. https://doi.org/10.1002/CYTO.A.22513

Garcia, K. C., Degano, M., Stanfield, R. L., Brunmark, A., Jackson, M. R., Peterson, A., Teyton, L., & Wilson, I. A. (1996). *An o4 T Cell Receptor Structure at 2.5 A and Its Orientation in the TCR-MHC Complex*. http://science.sciencemag.org/

Gary-Gouy, H., Sainz-Perez, A., Marteau, J.-B., Marfaing-Koka, A., Delic, J., Merle-Beral, H., Galanaud, P., & Dalloul, A. (2007). Natural Phosphorylation of CD5 in Chronic Lymphocytic Leukemia B Cells and Analysis of CD5-Regulated Genes in a B Cell Line Suggest a Role for CD5 in Malignant Phenotype. *The Journal of Immunology*, *179*(7), 4335–4344. https://doi.org/10.4049/JIMMUNOL.179.7.4335

Gaud, G., Lesourne, R., & Love, P. E. (2018). Regulatory mechanisms in T cell receptor signalling. *Nature Reviews Immunology 2018 18:8*, *18*(8), 485–497. https://doi.org/10.1038/s41577-018-0020-8

Geoghegan, J. L., & Holmes, E. C. (2018). The phylogenomics of evolving virus virulence. *Nature Reviews Genetics 2018 19:12*, *19*(12), 756–769. https://doi.org/10.1038/s41576-018-0055-5

Gimferrer, I., Calvo, M., Mittelbrunn, M., Farnós, M., Sarrias, M. R., Enrich, C., Vives, J., Sánchez-Madrid, F., & Lozano, F. (2004). Relevance of CD6-Mediated Interactions in T Cell Activation and Proliferation. *The Journal of Immunology*, *173*(4), 2262–2270. https://doi.org/10.4049/JIMMUNOL.173.4.2262

Gonçalves, C. M., Henriques, S. N., Santos, R. F., & Carmo, A. M. (2018). CD6, a Rheostat-

Type Signalosome That Tunes T Cell Activation. *Frontiers in Immunology*, *0*, 2994. https://doi.org/10.3389/FIMMU.2018.02994

Grakoui, A., Bromley, S. K., Sumen, C., Davis, M. M., Shaw, A. S., Allen, P. M., & Dustin, M. L. (1999). The immunological synapse: a molecular machine controlling T cell activation. *Science (New York, N.Y.)*, *285*(5425), 221–227. http://www.ncbi.nlm.nih.gov/pubmed/10398592

Greaney, A. J., Loes, A. N., Crawford, K. H. D., Starr, T. N., Malone, K. D., Chu, H. Y., & Bloom, J. D. (2021). Comprehensive mapping of mutations in the SARS-CoV-2 receptor-binding domain that affect recognition by polyclonal human plasma antibodies. *Cell Host & Microbe*, *29*(3), 463-476.e6. https://doi.org/10.1016/J.CHOM.2021.02.003

Greaney, A. J., Starr, T. N., Gilchuk, P., Zost, S. J., Binshtein, E., Loes, A. N., Hilton, S. K., Huddleston, J., Eguia, R., Crawford, K. H. D., Dingens, A. S., Nargi, R. S., Sutton, R. E., Suryadevara, N., Rothlauf, P. W., Liu, Z., Whelan, S. P. J., Carnahan, R. H., Crowe, J. E., & Bloom, J. D. (2021). Complete Mapping of Mutations to the SARS-CoV-2 Spike Receptor-Binding Domain that Escape Antibody Recognition. *Cell Host & Microbe*, *29*(1), 44-57.e9. https://doi.org/10.1016/J.CHOM.2020.11.007

Green. (1990). [5] Avidin and streptavidin. *Methods in Enzymology*, *184*(C), 51–67. https://doi.org/10.1016/0076-6879(90)84259-J

Groh, V., Porcelli, S., Fabii, M., Lanier, L. L., Picker, L. J., Anderson, T., Warnke, R. A., Bhan, A. K., Strominger, J. L., & Brenner, M. B. (1989). Human lymphocytes bearing T cell receptor gamma/delta are phenotypically diverse and evenly distributed throughout the lymphoid system. *The Journal of Experimental Medicine*, *169*(4), 1277–1294. https://doi.org/10.1084/JEM.169.4.1277

Groh, V., Steinle, A., Bauer, S., & Spies, T. (1998). Recognition of stress-induced MHC molecules by intestinal epithelial gammadelta T cells. *Science (New York, N.Y.)*, *279*(5357), 1737–1740. http://www.ncbi.nlm.nih.gov/pubmed/9497295

Guan, W., Ni, Z., Hu, Y., Liang, W., Ou, C., He, J., Liu, L., Shan, H., Lei, C., Hui, D. S. C., Du, B., Li, L., Zeng, G., Yuen, K.-Y., Chen, R., Tang, C., Wang, T., Chen, P., Xiang, J., … Zhong, N. (2020). Clinical Characteristics of Coronavirus Disease 2019 in China. *New England Journal of Medicine*, *382*(18), 1708–1720. https://doi.org/10.1056/nejmoa2002032

Guest, R. D., Hawkins, R. E., Kirillova, N., Cheadle, E. J., Arnold, J., O'Neill, A., Irlam, J., Chester, K. A., Kemshead, J. T., Shaw, D. M., Embleton, M. J., Stern, P. L., & Gilham, D. E. (1997). The role of extracellular spacer regions in the optimal design of chimeric immune receptors: evaluation of four different scFvs and antigens. *Journal of Immunotherapy*, *28*(3), 203–211. http://www.ncbi.nlm.nih.gov/pubmed/15838376

Guo, L., Bi, W., Wang, X., Xu, W., Yan, R., Zhang, Y., Zhao, K., Li, Y., Zhang, M., Cai, X., Jiang, S., Xie, Y., Zhou, Q., Lu, L., & Dang, B. (2021). Engineered trimeric ACE2 binds viral spike protein and locks it in "Three-up" conformation to potently inhibit SARS-CoV-2 infection. *Cell Research*, *31*(1), 98–100. https://doi.org/10.1038/s41422-020-00438-w

Guy, C. S., & Vignali, D. A. A. (2009). Organization of proximal signal initiation at the TCR:CD3 complex. *Immunological Reviews*, *232*(1), 7–21. https://doi.org/10.1111/J.1600-065X.2009.00843.X

Hansen, J., Baum, A., Pascal, K. E., Russo, V., Giordano, S., Wloga, E., Fulton, B. O., Yan, Y., Koon, K., Patel, K., Chung, K. M., Hermann, A., Ullman, E., Cruz, J., Rafique, A., Huang, T., Fairhurst, J., Libertiny, C., Malbec, M., … Kyratsous, C. A. (2020). Studies in humanized mice and convalescent humans yield a SARS-CoV-2 antibody cocktail. *Science*, *369*(6506), 1010–1014. https://doi.org/10.1126/SCIENCE.ABD0827/SUPPL_FILE/PAP.PDF

Harty, J. T., Tvinnereim, A. R., & White, D. W. (2003). CD8+ T Cell Effector Mechanisms in Resistance to Infection. *Http://Dx.Doi.Org/10.1146/Annurev.Immunol.18.1.275*, *18*, 275–308. https://doi.org/10.1146/ANNUREV.IMMUNOL.18.1.275

Hasegawa, K., Hu, C., Nakamura, T., Marks, J. D., Russell, S. J., & Peng, K.-W. (2007). Affinity Thresholds for Membrane Fusion Triggering by Viral Glycoproteins. *Journal of Virology*, *81*(23), 13149–13157. https://doi.org/10.1128/JVI.01415-07/ASSET/54E003F1-E9AA-4A67-AF50-A4886A471406/ASSETS/GRAPHIC/ZJV0230799310005.JPEG

Haso, W., Lee, D. W., Shah, N. N., Stetler-Stevenson, M., Yuan, C. M., Pastan, I. H., Dimitrov, D. S., Morgan, R. A., FitzGerald, D. J., Barrett, D. M., Wayne, A. S., Mackall, C. L., & Orentas, R. J. (2013). Anti-CD22-chimeric antigen receptors targeting B-cell precursor acute lymphoblastic leukemia. *Blood*, *121*(7), 1165–1174. https://doi.org/10.1182/blood-2012-06-438002

Hassan, N. J., Barclay, A. N., & Brown, M. H. (2004). Frontline: Optimal T cell activation requires the engagement of CD6 and CD166. *European Journal of Immunology*, *34*(4), 930–940. https://doi.org/10.1002/EJI.200424856

Hassan, N. J., Simmonds, S. J., Clarkson, N. G., Hanrahan, S., Puklavec, M. J., Bomb, M., Barclay, A. N., & Brown, M. H. (2006). CD6 Regulates T-Cell Responses through Activation-Dependent Recruitment of the Positive Regulator SLP-76. *Molecular and Cellular Biology*, *26*(17), 6727–6738. https://doi.org/10.1128/MCB.00688-06

Hayashi, A., Ohnishi, H., Okazawa, H., Nakazawa, S., Ikeda, H., Motegi, S., Aoki, N., Kimura, S., Mikuni, M., & Matozaki, T. (2004). Positive regulation of phagocytosis by SIRPbeta and its signaling mechanism in macrophages. *The Journal of Biological Chemistry*, *279*(28), 29450–29460. https://doi.org/10.1074/jbc.M400950200

Henderson, J. G., Opejin, A., Jones, A., Gross, C., & Hawiger, D. (2015). CD5 Instructs Extrathymic Regulatory T Cell Development in Response to Self and Tolerizing Antigens. *Immunity*, *42*(3), 471–483. https://doi.org/10.1016/J.IMMUNI.2015.02.010

Hermiston, M. L., Zikherman, J., & Zhu, J. W. (2009). CD45, CD148, and Lyp/Pep: critical phosphatases regulating Src family kinase signaling networks in immune cells. *Immunological Reviews*, *228*(1), 288–311. https://doi.org/10.1111/j.1600-065X.2008.00752.x

Hernandez, C., Huebener, P., & Schwabe, R. F. (2016). Damage-associated molecular patterns in cancer: a double-edged sword. *Oncogene 2016 35:46*, *35*(46), 5931–5941. https://doi.org/10.1038/onc.2016.104

Hoffmann, M., Arora, P., Groß, R., Seidel, A., Hörnich, B. F., Hahn, A. S., Krüger, N., Graichen, L., Hofmann-Winkler, H., Kempf, A., Winkler, M. S., Schulz, S., Jäck, H. M., Jahrsdörfer, B., Schrezenmeier, H., Müller, M., Kleger, A., Münch, J., & Pöhlmann, S. (2021). SARS-CoV-2 variants B.1.351 and P.1 escape from neutralizing antibodies.

Cell, *184*(9), 2384-2393.e12. https://doi.org/10.1016/J.CELL.2021.03.036

Hoffmann, M., Kleine-Weber, H., & Pöhlmann, S. (2020). A Multibasic Cleavage Site in the Spike Protein of SARS-CoV-2 Is Essential for Infection of Human Lung Cells. *Molecular Cell*, *78*(4), 779-784.e5. https://doi.org/10.1016/J.MOLCEL.2020.04.022

Hoffmann, M., Kleine-Weber, H., Schroeder, S., Krüger, N., Herrler, T., Erichsen, S., Schiergens, T. S., Herrler, G., Wu, N. H., Nitsche, A., Müller, M. A., Drosten, C., & Pöhlmann, S. (2020). SARS-CoV-2 Cell Entry Depends on ACE2 and TMPRSS2 and Is Blocked by a Clinically Proven Protease Inhibitor. *Cell*, *181*(2), 271-280.e8. https://doi.org/10.1016/j.cell.2020.02.052

Hogquist, K. A., & Jameson, S. C. (2014). The self-obsession of T cells: how TCR signaling thresholds affect fate 'decisions' and effector function. *Nature Immunology 2014 15:9*, *15*(9), 815–823. https://doi.org/10.1038/ni.2938

Hombach, A. A., Schildgen, V., Heuser, C., Finnern, R., Gilham, D. E., & Abken, H. (2007). T cell activation by antibody-like immunoreceptors: the position of the binding epitope within the target molecule determines the efficiency of activation of redirected T cells. *Journal of Immunology (Baltimore, Md. : 1950)*, *178*(7), 4650–4657. http://www.ncbi.nlm.nih.gov/pubmed/17372024

Hombach, A., Heuser, C., Gerken, M., Fischer, B., Lewalter, K., Diehl, V., Pohl, C., & Abken, H. (2000). T cell activation by recombinant FcεRI γ-chain immune receptors: an extracellular spacer domain impairs antigen-dependent T cell activation but not antigen recognition. *Gene Therapy*, *7*(12), 1067–1075. https://doi.org/10.1038/sj.gt.3301195

Hou, Y. J., Okuda, K., Edwards, C. E., Martinez, D. R., Asakura, T., Dinnon, K. H., Kato, T., Lee, R. E., Yount, B. L., Mascenik, T. M., Chen, G., Olivier, K. N., Ghio, A., Tse, L. V., Leist, S. R., Gralinski, L. E., Schäfer, A., Dang, H., Gilmore, R., … Baric, R. S. (2020). SARS-CoV-2 Reverse Genetics Reveals a Variable Infection Gradient in the Respiratory Tract. *Cell*, *182*(2), 429-446.e14. https://doi.org/10.1016/J.CELL.2020.05.042

Hsiung, L. M., Barclay, A. N., Brandon, M. R., Sim, E., & Porter, R. R. (1982). Purification of human C3b inactivator by monoclonal-antibody affinity chromatography. *Biochemical Journal*, *203*(1), 293. https://doi.org/10.1042/BJ2030293

Huang, I. C., Bosch, B. J., Li, F., Li, W., Kyoung, H. L., Ghiran, S., Vasilieva, N., Dermody, T. S., Harrison, S. C., Dormitzer, P. R., Farzan, M., Rottier, P. J. M., & Choe, H. (2006). SARS coronavirus, but not human coronavirus NL63, utilizes cathepsin L to infect ACE2-expressing cells. *Journal of Biological Chemistry*, *281*(6), 3198–3203. https://doi.org/10.1074/JBC.M508381200/ATTACHMENT/BEDE615F-4246-4459-B7DC-7E6AF26A19EF/MMC1.PDF

Huang, J., Brameshuber, M., Zeng, X., Xie, J., Li, Q. jing, Chien, Y. hsiu, Valitutti, S., & Davis, M. M. (2013). A Single Peptide-Major Histocompatibility Complex Ligand Triggers Digital Cytokine Secretion in CD4+ T Cells. *Immunity*, *39*(5), 846–857. https://doi.org/10.1016/J.IMMUNI.2013.08.036

Hudecek, M., Lupo-Stanghellini, M.-T., Kosasih, P. L., Sommermeyer, D., Jensen, M. C., Rader, C., & Riddell, S. R. (2013). Receptor Affinity and Extracellular Domain Modifications Affect Tumor Recognition by ROR1-Specific Chimeric Antigen Receptor T Cells. *Clinical Cancer Research*, *19*(12), 3153–3164. https://doi.org/10.1158/1078-0432.CCR-13-0330

Hudecek, M., Sommermeyer, D., Kosasih, P. L., Silva-Benedict, A., Liu, L., Rader, C., Jensen, M. C., & Riddell, S. R. (2015). The Nonsignaling Extracellular Spacer Domain of Chimeric Antigen Receptors Is Decisive for In Vivo Antitumor Activity. *Cancer Immunology Research*, *3*(2), 125–135. https://doi.org/10.1158/2326-6066.CIR-14-0127

Hui, E., Cheung, J., Zhu, J., Su, X., Taylor, M. J., Wallweber, H. A., Sasmal, D. K., Huang, J., Kim, J. M., Mellman, I., & Vale, R. D. (2017). T cell costimulatory receptor CD28 is a primary target for PD-1–mediated inhibition. *Science*, *355*(6332), 1428–1433. https://doi.org/10.1126/science.aaf1292

Hui, E., & Vale, R. D. (2014). In vitro membrane reconstitution of the T-cell receptor proximal signaling network. *Nature Structural & Molecular Biology*, *21*(2), 133–142. https://doi.org/10.1038/nsmb.2762

Husson, J., Chemin, K., Bohineust, A., Hivroz, C., & Henry, N. (2011). Force generation upon T cell receptor engagement. *PloS One*, *6*(5), e19680. https://doi.org/10.1371/journal.pone.0019680

Imai, C., Mihara, K., Andreansky, M., Nicholson, I. C., Pui, C. H., Geiger, T. L., & Campana, D. (2004). Chimeric receptors with 4-1BB signaling capacity provoke potent cytotoxicity against acute lymphoblastic leukemia. *Leukemia 2004 18:4*, *18*(4), 676–684. https://doi.org/10.1038/sj.leu.2403302

Irles, C., Symons, A., Michel, F., Bakker, T. R., van der Merwe, P. A., & Acuto, O. (2003). CD45 ectodomain controls interaction with GEMs and Lck activity for optimal TCR signaling. *Nature Immunology*, *4*(2), 189–197. https://doi.org/10.1038/ni877

Irvine, D. J., Purbhoo, M. A., Krogsgaard, M., & Davis, M. M. (2002). Direct observation of ligand recognition by T cells. *Nature 2002 419:6909*, *419*(6909), 845–849. https://doi.org/10.1038/nature01076

Ito, Y., Sakata-Sogawa, K., & Tokunaga, M. (2017). Multi-color single-molecule tracking and subtrajectory analysis for quantification of spatiotemporal dynamics and kinetics upon T cell activation. *Scientific Reports*, *7*(1), 6994. https://doi.org/10.1038/s41598-017-06960-z

Jackson, C. B., Farzan, M., Chen, B., & Choe, H. (2021). Mechanisms of SARS-CoV-2 entry into cells. *Nature Reviews Molecular Cell Biology 2021*, 1–18. https://doi.org/10.1038/s41580-021-00418-x

James, J. R. (2018). Tuning ITAM multiplicity on T cell receptors can control potency and selectivity to ligand density. *Science Signaling*, *11*(531), eaan1088. https://doi.org/10.1126/scisignal.aan1088

James, S. E., Greenberg, P. D., Jensen, M. C., Lin, Y., Wang, J., Till, B. G., Raubitschek, A. A., Forman, S. J., & Press, O. W. (2008). Antigen sensitivity of CD22-specific chimeric TCR is modulated by target epitope distance from the cell membrane. *Journal of Immunology (Baltimore, Md. : 1950)*, *180*(10), 7028–7038. http://www.ncbi.nlm.nih.gov/pubmed/18453625

James, & Vale, R. D. (2012). Biophysical mechanism of T-cell receptor triggering in a reconstituted system. *Nature*, *487*(7405), 64–69. https://doi.org/10.1038/nature11220

Jangra, S., Ye, C., Rathnasinghe, R., Stadlbauer, D., Alshammary, H., Amoako, A. A., Awawda, M. H., Beach, K. F., Bermúdez-González, M. C., Chernet, R. L., Eaker, L. Q.,

Ferreri, E. D., Floda, D. L., Gleason, C. R., Kleiner, G., Jurczyszak, D., Matthews, J. C., Mendez, W. A., Mulder, L. C. F., … Schotsaert, M. (2021). SARS-CoV-2 spike E484K mutation reduces antibody neutralisation. *The Lancet Microbe*, *2*(7), e283–e284. https://doi.org/10.1016/S2666-5247(21)00068-9

Jaumouillé, V., & Grinstein, S. (2011). Receptor mobility, the cytoskeleton, and particle binding during phagocytosis. *Current Opinion in Cell Biology*, *23*(1), 22–29. https://doi.org/10.1016/J.CEB.2010.10.006

Jenkins, E., Santos, A. M., O'Brien-Ball, C., Felce, J. H., Wilcock, M. J., Hatherley, D., Dustin, M. L., Davis, S. J., Eggeling, C., & Sezgin, E. (2019). Reconstitution of immune cell interactions in free-standing membranes. *Journal of Cell Science*, *132*(4). https://doi.org/10.1242/jcs.219709

Jia, H., Neptune, E., & Cui, H. (2021). Targeting ACE2 for COVID-19 Therapy: Opportunities and challenges. *American Journal of Respiratory Cell and Molecular Biology*, *64*(4), 416–425. https://doi.org/10.1165/RCMB.2020-0322PS/SUPPL_FILE/DISCLOSURES.PDF

Judokusumo, E., Tabdanov, E., Kumari, S., Dustin, M. L., & Kam, L. C. (2012). Mechanosensing in T Lymphocyte Activation. *Biophysical Journal*, *102*(2), L5–L7. https://doi.org/10.1016/J.BPJ.2011.12.011

June, C. H., Ledbetter, J. A., Gillespie, M. M., Lindsten, T., & Thompson, C. B. (1987). T-cell proliferation involving the CD28 pathway is associated with cyclosporine-resistant interleukin 2 gene expression. *Molecular and Cellular Biology*, *7*(12), 4472–4481. https://doi.org/10.1128/MCB.7.12.4472-4481.1987/FORMAT/PDF

Junghans, V., Santos, A. M., Lui, Y., Davis, S. J., & Jönsson, P. (2018). Dimensions and Interactions of Large T-Cell Surface Proteins. *Frontiers in Immunology*, *9*, 2215. https://doi.org/10.3389/FIMMU.2018.02215/BIBTEX

Jutz, S., Hennig, A., Paster, W., Asrak, Ö., Dijanovic, D., Kellner, F., Pickl, W. F., Huppa, J. B., Leitner, J., & Steinberger, P. (2017). A cellular platform for the evaluation of immune checkpoint molecules. *Oncotarget*, *8*(39), 64892. https://doi.org/10.18632/ONCOTARGET.17615

Kaizuka, Y., Douglass, A. D., Vardhana, S., Dustin, M. L., & Vale, R. D. (2009). The coreceptor CD2 uses plasma membrane microdomains to transduce signals in T cells. *Journal of Cell Biology*, *185*(3), 521–534. https://doi.org/10.1083/JCB.200809136

Kaizuka, Y., Douglass, A. D., Varma, R., Dustin, M. L., & Vale, R. D. (2007). Mechanisms for segregating T cell receptor and adhesion molecules during immunological synapse formation in Jurkat T cells. *Proceedings of the National Academy of Sciences of the United States of America*, *104*(51), 20296–20301. https://doi.org/10.1073/pnas.0710258105

Kamphorst, A. O., Wieland, A., Nasti, T., Yang, S., Zhang, R., Barber, D. L., Konieczny, B. T., Daugherty, C. Z., Koenig, L., Yu, K., Sica, G. L., Sharpe, A. H., Freeman, G. J., Blazar, B. R., Turka, L. A., Owonikoko, T. K., Pillai, R. N., Ramalingam, S. S., Araki, K., & Ahmed, R. (2017). Rescue of exhausted CD8 T cells by PD-1-targeted therapies is CD28-dependent. *Science (New York, N.Y.)*, *355*(6332), 1423–1427. https://doi.org/10.1126/science.aaf0683

Karczewski, K. J., Francioli, L. C., Tiao, G., Cummings, B. B., Alföldi, J., Wang, Q., Collins,

R. L., Laricchia, K. M., Ganna, A., Birnbaum, D. P., Gauthier, L. D., Brand, H., Solomonson, M., Watts, N. A., Rhodes, D., Singer-Berk, M., England, E. M., Seaby, E. G., Kosmicki, J. A., … MacArthur, D. G. (2020). The mutational constraint spectrum quantified from variation in 141,456 humans. *Nature*, *581*(7809), 434–443. https://doi.org/10.1038/s41586-020-2308-7

Katzmann, D. J., Odorizzi, G., & Emr, S. D. (2002). Receptor downregulation and multivesicular-body sorting. *Nature Reviews Molecular Cell Biology 2002 3:12*, *3*(12), 893–905. https://doi.org/10.1038/nrm973

Kaye, J., & Janeway, C. A. (1984). The Fab fragment of a directly activating monoclonal antibody that precipitates a disulfide-linked heterodimer from a helper T cell clone blocks activation by either allogeneic Ia or antigen and self-Ia. *Journal of Experimental Medicine*, *159*(5), 1397–1412. https://doi.org/10.1084/JEM.159.5.1397

Keidar, S., Kaplan, M., & Gamliel-Lazarovich, A. (2007). ACE2 of the heart: From angiotensin I to angiotensin. *Cardiovascular Research*, *73*(3), 463–469. https://doi.org/10.1016/J.CARDIORES.2006.09.006/2/73-3-463-FIG1.GIF

Khalil, D. N., Smith, E. L., Brentjens, R. J., & Wolchok, J. D. (2016). The future of cancer treatment: immunomodulation, CARs and combination immunotherapy. *Nature Reviews Clinical Oncology 2016 13:5*, *13*(5), 273–290. https://doi.org/10.1038/nrclinonc.2016.25

Kharitonenkov, A., Chen, Z., Sures, I., Wang, H., Schilling, J., & Ullrich, A. (1997). A family of proteins that inhibit signalling through tyrosine kinase receptors. *Nature*, *386*(6621), 181–186. https://doi.org/10.1038/386181a0

Kieper, W. C., Burghardt, J. T., & Surh, C. D. (2004). A Role for TCR Affinity in Regulating Naive T Cell Homeostasis. *The Journal of Immunology*, *172*(1), 40–44. https://doi.org/10.4049/JIMMUNOL.172.1.40

Kihara, H., & Siraganian, R. P. (1994). Src homology 2 domains of Syk and Lyn bind to tyrosine-phosphorylated subunits of the high affinity IgE receptor. *Journal of Biological Chemistry*, *269*(35), 22427–22432. https://doi.org/10.1016/S0021-9258(17)31807-0

Klein, L., Kyewski, B., Allen, P. M., & Hogquist, K. A. (2014). Positive and negative selection of the T cell repertoire: what thymocytes see (and don't see). *Nature Reviews Immunology 2014 14:6*, *14*(6), 377–391. https://doi.org/10.1038/nri3667

Knobloch, C., Diamantstein, T., Flegel, W. A., & Friedrich, W. (1991). Stimulation of human T cells via anti-T cell receptor monoclonal antibody BMA031: Distinct cellular events involving interleukin-2 receptor and lymphocyte function antigen 1. *Cellular Immunology*, *138*(1), 150–164. https://doi.org/10.1016/0008-8749(91)90140-7

Kobarg, J., Whitney, G. S., Palmer, D., Aruffo, A., & Bowen, M. A. (1997). Analysis of the tyrosine phosphorylation and calcium fluxing of human CD6 isoforms with different cytoplasmatic domains. *European Journal of Immunology*, *27*(11), 2971–2980. https://doi.org/10.1002/EJI.1830271133

Koegl, M., Zlatkine, P., Ley, S. C., Courtneidge, S. A., & Magee, A. I. (1994). Palmitoylation of multiple Src-family kinases at a homologous N-terminal motif. *Biochemical Journal*, *303*(3), 749–753. https://doi.org/10.1042/BJ3030749

Kofler, D. M., Severson, C. A., Mousissian, N., Jager, P. L. De, & Hafler, D. A. (2011). The CD6 Multiple Sclerosis Susceptibility Allele Is Associated with Alterations in CD4+ T

Cell Proliferation. *The Journal of Immunology*, *187*(6), 3286–3291. https://doi.org/10.4049/JIMMUNOL.1100626

Köhler, K., Xiong, S., Brzostek, J., Mehrabi, M., Eissmann, P., Harrison, A., Cordoba, S.-P., Oddos, S., Miloserdov, V., Gould, K., Burroughs, N. J., van der Merwe, P. A., & Davis, D. M. (2010). Matched Sizes of Activating and Inhibitory Receptor/Ligand Pairs Are Required for Optimal Signal Integration by Human Natural Killer Cells. *PLoS ONE*, *5*(11), e15374. https://doi.org/10.1371/journal.pone.0015374

Korber, B., Fischer, W. M., Gnanakaran, S., Yoon, H., Theiler, J., Abfalterer, W., Hengartner, N., Giorgi, E. E., Bhattacharya, T., Foley, B., Hastie, K. M., Parker, M. D., Partridge, D. G., Evans, C. M., Freeman, T. M., de Silva, T. I., Angyal, A., Brown, R. L., Carrilero, L., … Montefiori, D. C. (2020). Tracking Changes in SARS-CoV-2 Spike: Evidence that D614G Increases Infectivity of the COVID-19 Virus. *Cell*, *182*(4), 812-827.e19. https://doi.org/10.1016/j.cell.2020.06.043

Korndörfer, I. P., & Skerra, A. (2002). Improved affinity of engineered streptavidin for the Strep-tag II peptide is due to a fixed open conformation of the lid-like loop at the binding site. *Protein Science*, *11*(4), 883–893. https://doi.org/10.1110/PS.4150102

Krenciute, G., Krebs, S., Torres, D., Wu, M.-F., Liu, H., Dotti, G., Li, X.-N., Lesniak, M. S., Balyasnikova, I. V, & Gottschalk, S. (2016). Characterization and Functional Analysis of scFv-based Chimeric Antigen Receptors to Redirect T Cells to IL13Rα2-positive Glioma. *Molecular Therapy*, *24*(2), 354–363. https://doi.org/10.1038/mt.2015.199

Krogsgaard, M., Li, Q., Sumen, C., Huppa, J. B., Huse, M., & Davis, M. M. (2005). Agonist/endogenous peptide–MHC heterodimers drive T cell activation and sensitivity. *Nature 2005 434:7030*, *434*(7030), 238–243. https://doi.org/10.1038/nature03391

Krupashankar, D. S., Dogra, S., Kura, M., Saraswat, A., Budamakuntla, L., Sumathy, T. K., Shah, R., Gopal, M. G., Narayana Rao, T., Srinivas, C. R., Bhat, R., Shetty, N., Manmohan, G., Sai Krishna, K., Padmaja, D., Pratap, D. V. S., Garg, V., Gupta, S., Pandey, N., … Ganapathi, P. C. (2014). Efficacy and safety of itolizumab, a novel anti-CD6 monoclonal antibody, in patients with moderate to severe chronic plaque psoriasis: Results of a double-blind, randomized, placebo-controlled, phase-III study. *Journal of the American Academy of Dermatology*, *71*(3), 484–492. https://doi.org/10.1016/J.JAAD.2014.01.897

Kuhns, M. S., & Davis, M. M. (2008). The Safety on the TCR Trigger. *Cell*, *135*(4), 594–596. https://doi.org/10.1016/J.CELL.2008.10.033

Kulenkampff, K., Lippert, A. H., McColl, J., Santos, A. M., Ponjavic, A., Jenkins, E., Humphrey, J., Winkel, A., Franze, K., Lee, S. F., Davis, S. J., & Klenerman, D. (2020). The Costs of Close Contacts: Visualizing the Energy Landscape of Cell Contacts at the Nanoscale. *Biophysical Journal*, *118*(6), 1261–1269. https://doi.org/10.1016/J.BPJ.2020.01.019

Kumar, A., Gupta, P. K., & Srivastava, A. (2020). A review of modern technologies for tackling COVID-19 pandemic. *Diabetes & Metabolic Syndrome: Clinical Research & Reviews*, *14*(4), 569–573. https://doi.org/10.1016/J.DSX.2020.05.008

Kusumi, A., Nakada, C., Ritchie, K., Murase, K., Suzuki, K., Murakoshi, H., Kasai, R. S., Kondo, J., & Fujiwara, T. (2005). Paradigm Shift of the Plasma Membrane Concept from the Two-Dimensional Continuum Fluid to the Partitioned Fluid: High-Speed

Single-Molecule Tracking of Membrane Molecules. *Http://Dx.Doi.Org/10.1146/Annurev.Biophys.34.040204.144637*, *34*, 351–378. https://doi.org/10.1146/ANNUREV.BIOPHYS.34.040204.144637

Kwak, M., Southard, K., Kim, N. H., Gopalappa, R., Kim, W. R., An, M., Lee, H. J., Farlow, J., Georgakopoulos, A., Robakis, N., Seo, D., Kim, H. B., Kim, Y. H., Cheon, J., Gartner, Z., & Jun, Y. (2020). Size-dependent protein segregation creates a spatial switch for Notch and APP signaling. *BioRxiv*, 2020.06.28.176560. https://doi.org/10.1101/2020.06.28.176560

Lam, T. T. Y., Jia, N., Zhang, Y. W., Shum, M. H. H., Jiang, J. F., Zhu, H. C., Tong, Y. G., Shi, Y. X., Ni, X. B., Liao, Y. S., Li, W. J., Jiang, B. G., Wei, W., Yuan, T. T., Zheng, K., Cui, X. M., Li, J., Pei, G. Q., Qiang, X., … Cao, W. C. (2020). Identifying SARS-CoV-2-related coronaviruses in Malayan pangolins. *Nature 2020 583:7815*, *583*(7815), 282–285. https://doi.org/10.1038/s41586-020-2169-0

Lanier, L. L. (2009). DAP10- and DAP12-associated receptors in innate immunity. *Immunological Reviews*, *227*(1), 150–160. https://doi.org/10.1111/J.1600-065X.2008.00720.X

Lanier, L. L., & Bakker, A. B. . (2000). The ITAM-bearing transmembrane adaptor DAP12 in lymphoid and myeloid cell function. *Immunology Today*, *21*(12), 611–614. https://doi.org/10.1016/S0167-5699(00)01745-X

Lanier, L. L., Corliss, B., Wu, J., & Phillips, J. H. (1998). Association of DAP12 with Activating CD94/NKG2C NK Cell Receptors. *Immunity*, *8*(6), 693–701. https://doi.org/10.1016/S1074-7613(00)80574-9

Lehrman, E. K., Wilton, D. K., Litvina, E. Y., Welsh, C. A., Chang, S. T., Frouin, A., Walker, A. J., Heller, M. D., Umemori, H., Chen, C., & Stevens, B. (2018). CD47 Protects Synapses from Excess Microglia-Mediated Pruning during Development. *Neuron*, *100*(1), 120-134.e6. https://doi.org/10.1016/J.NEURON.2018.09.017

Lei, C., Qian, K., Li, T., Zhang, S., Fu, W., Ding, M., & Hu, S. (2020). Neutralization of SARS-CoV-2 spike pseudotyped virus by recombinant ACE2-Ig. *Nature Communications 2020 11:1*, *11*(1), 1–5. https://doi.org/10.1038/s41467-020-16048-4

Lenza, M. P., Atxabal, U., Oyenarte, I., Jiménez-Barbero, J., & Ereño-Orbea, J. (2020). Current Status on Therapeutic Molecules Targeting Siglec Receptors. *Cells 2020, Vol. 9, Page 2691*, *9*(12), 2691. https://doi.org/10.3390/CELLS9122691

Lever, M., Maini, P. K., van der Merwe, P. A., & Dushek, O. (2014). Phenotypic models of T cell activation. *Nature Reviews Immunology 2014 14:9*, *14*(9), 619–629. https://doi.org/10.1038/nri3728

Li, Farzan, M., & Harrison, S. C. (2005). Structural biology: Structure of SARS coronavirus spike receptor-binding domain complexed with receptor. *Science*, *309*(5742), 1864–1868. https://doi.org/10.1126/science.1116480

Li, J., Stagg, N. J., Johnston, J., Harris, M. J., Menzies, S. A., DiCara, D., Clark, V., Hristopoulos, M., Cook, R., Slaga, D., Nakamura, R., McCarty, L., Sukumaran, S., Luis, E., Ye, Z., Wu, T. D., Sumiyoshi, T., Danilenko, D., Lee, G. Y., … Junttila, T. T. (2017). Membrane-Proximal Epitope Facilitates Efficient T Cell Synapse Formation by Anti-FcRH5/CD3 and Is a Requirement for Myeloma Cell Killing. *Cancer Cell*, *31*(3), 383–395. https://doi.org/10.1016/j.ccell.2017.02.001

Li, L., Fierer, J. O., Rapoport, T. A., & Howarth, M. (2014). Structural Analysis and Optimization of the Covalent Association between SpyCatcher and a Peptide Tag. *Journal of Molecular Biology*, *426*(2), 309–317. https://doi.org/10.1016/J.JMB.2013.10.021

Li, P., Morris, D. L., Willcox, B. E., Steinle, A., Spies, T., & Strong, R. K. (2001). Complex structure of the activating immunoreceptor NKG2D and its MHC class I–like ligand MICA. *Nature Immunology 2001 2:5*, *2*(5), 443–451. https://doi.org/10.1038/87757

Li, W., Moore, M. J., Vasllieva, N., Sui, J., Wong, S. K., Berne, M. A., Somasundaran, M., Sullivan, J. L., Luzuriaga, K., Greeneugh, T. C., Choe, H., & Farzan, M. (2003). Angiotensin-converting enzyme 2 is a functional receptor for the SARS coronavirus. *Nature 2003 426:6965*, *426*(6965), 450–454. https://doi.org/10.1038/nature02145

Li, X., Giorg, E. E., Marichannegowda, M. H., Foley, B., Xiao, C., Kong, X. P., Chen, Y., Gnanakaran, S., Korber, B., & Gao, F. (2020). Emergence of SARS-CoV-2 through recombination and strong purifying selection. *Science Advances*, *6*(27). https://doi.org/10.1126/SCIADV.ABB9153/SUPPL_FILE/PAP.PDF

Li, Y.-C., Chen, B.-M., Wu, P.-C., Cheng, T.-L., Kao, L.-S., Tao, M.-H., Lieber, A., & Roffler, S. R. (2010). Cutting Edge: mechanical forces acting on T cells immobilized via the TCR complex can trigger TCR signaling. *Journal of Immunology (Baltimore, Md. : 1950)*, *184*(11), 5959–5963. https://doi.org/10.4049/jimmunol.0900775

Li, Y., Singer, N. G., Whitbred, J., Bowen, M. A., Fox, D. A., & Lin, F. (2017). CD6 as a potential target for treating multiple sclerosis. *Proceedings of the National Academy of Sciences*, *114*(10), 2687–2692. https://doi.org/10.1073/PNAS.1615253114

Lim, H.-S., Cordoba, S.-P., Dushek, O., Goyette, J., Taylor, A., Rudd, C. E., & van der Merwe, P. A. (2015). Costimulation of IL-2 Production through CD28 Is Dependent on the Size of Its Ligand. *The Journal of Immunology*, *195*(11), 5432–5439. https://doi.org/10.4049/jimmunol.1500707

Lin, J., & Weiss, A. (2003). The tyrosine phosphatase CD148 is excluded from the immunologic synapse and down-regulates prolonged T cell signaling. *The Journal of Cell Biology*, *162*(4), 673–682. https://doi.org/10.1083/jcb.200303040

Liu, Yang, Liu, J., Johnson, B. A., Xia, H., Ku, Z., Schindewolf, C., Widen, S. G., An, Z., Weaver, S. C., Menachery, V. D., Xie, X., & Shi, P.-Y. (2021). Delta spike P681R mutation enhances SARS-CoV-2 fitness over Alpha variant. *BioRxiv : The Preprint Server for Biology*. https://doi.org/10.1101/2021.08.12.456173

Liu, Yue, Liu, G., Wang, J., Zheng, Z. Y., Jia, L., Rui, W., Huang, D., Zhou, Z. X., Zhou, L., Wu, X., Lin, S., Zhao, X., & Lin, X. (2021). Chimeric STAR receptors using TCR machinery mediate robust responses against solid tumors. *Science Translational Medicine*, *13*(586), 5191. https://doi.org/10.1126/SCITRANSLMED.ABB5191/SUPPL_FILE/ABB5191_SM.PDF

Locksley, R. M., Reiner, S. L., Hatam, F., Littman, D. R., & Killeen, N. (1993). Helper T cells without CD4: Control of leishmaniasis in CD4-deficient mice. *Science*, *261*(5127), 1448–1451. https://doi.org/10.1126/SCIENCE.8367726

Loganathan, S., Athalye, S. N., & Joshi, S. R. (2020). Itolizumab, an anti-CD6 monoclonal antibody, as a potential treatment for COVID-19 complications.

Https://Doi.Org/10.1080/14712598.2020.1798399. https://doi.org/10.1080/14712598.2020.1798399

Long, E. O. (2003). REGULATION OF IMMUNE RESPONSES THROUGH INHIBITORY RECEPTORS. *Http://Dx.Doi.Org/10.1146/Annurev.Immunol.17.1.875*, *17*, 875–904. https://doi.org/10.1146/ANNUREV.IMMUNOL.17.1.875

Lu, J., Chu, J., Zou, Z., Hamacher, N. B., Rixon, M. W., & Sun, P. D. (2015). Structure of FcγRI in complex with Fc reveals the importance of glycan recognition for high-affinity IgG binding. *Proceedings of the National Academy of Sciences of the United States of America*, *112*(3), 833–838. https://doi.org/10.1073/pnas.1418812112

Lu, R., Zhao, X., Li, J., Niu, P., Yang, B., Wu, H., Wang, W., Song, H., Huang, B., Zhu, N., Bi, Y., Ma, X., Zhan, F., Wang, L., Hu, T., Zhou, H., Hu, Z., Zhou, W., Zhao, L., … Tan, W. (2020). Genomic characterisation and epidemiology of 2019 novel coronavirus: implications for virus origins and receptor binding. *The Lancet*, *395*(10224), 565–574. https://doi.org/10.1016/S0140-6736(20)30251-8

Luo, R., Delaunay-Moisan, A., Timmis, K., & Danchin, A. (2021). SARS-CoV-2 biology and variants: anticipation of viral evolution and what needs to be done. *Environmental Microbiology*, *23*(5), 2339–2363. https://doi.org/10.1111/1462-2920.15487

Ma, Hu, Y., Kellner, A. V., Brockman, J. M., Velusamy, A., Blanchard, A. T., Evavold, B. D., Alon, R., & Salaita, K. (2022). The magnitude of LFA-1/ICAM-1 forces fine-tune TCR-triggered T cell activation. *Science Advances*, *8*(8), 4485. https://doi.org/10.1126/SCIADV.ABG4485

Ma, Z., Discher, D. E., & Finkel, T. H. (2012). Mechanical Force in T Cell Receptor Signal Initiation. *Frontiers in Immunology*, *3*, 217. https://doi.org/10.3389/fimmu.2012.00217

Ma, Z., Sharp, K. A., Janmey, P. A., & Finkel, T. H. (2008). Surface-Anchored Monomeric Agonist pMHCs Alone Trigger TCR with High Sensitivity. *PLOS Biology*, *6*(2), e43. https://doi.org/10.1371/JOURNAL.PBIO.0060043

Macgowan, S. A., Barton, M. I., Kutuzov, M., Dushek, O., Van Der Merwe, P. A., & Barton, G. J. (2022). Missense variants in human ACE2 strongly affect binding to SARS-CoV-2 Spike providing a mechanism for ACE2 mediated genetic risk in Covid-19: A case study in affinity predictions of interface variants. *PLOS Computational Biology*, *18*(3), e1009922. https://doi.org/10.1371/JOURNAL.PCBI.1009922

Madhi, S. A., Baillie, V., Cutland, C. L., Voysey, M., Koen, A. L., Fairlie, L., Padayachee, S. D., Dheda, K., Barnabas, S. L., Bhorat, Q. E., Briner, C., Kwatra, G., Ahmed, K., Aley, P., Bhikha, S., Bhiman, J. N., Bhorat, A. E., du Plessis, J., Esmail, A., … Izu, A. (2021). Efficacy of the ChAdOx1 nCoV-19 Covid-19 Vaccine against the B.1.351 Variant. *New England Journal of Medicine*. https://doi.org/10.1056/nejmoa2102214

Mahase, E. (2021). Covid-19: Where are we on vaccines and variants? *BMJ (Clinical Research Ed.)*, *372*, n597. https://doi.org/10.1136/bmj.n597

Maher, J., Brentjens, R. J., Gunset, G., Rivière, I., & Sadelain, M. (2002). Human T-lymphocyte cytotoxicity and proliferation directed by a single chimeric TCRζ /CD28 receptor. *Nature Biotechnology 2002 20:1*, *20*(1), 70–75. https://doi.org/10.1038/nbt0102-70

Mandl, J. N., Monteiro, J. P., Vrisekoop, N., & Germain, R. N. (2013). T Cell-Positive

Selection Uses Self-Ligand Binding Strength to Optimize Repertoire Recognition of Foreign Antigens. *Immunity*, *38*(2), 263–274. https://doi.org/10.1016/J.IMMUNI.2012.09.011

Masao, O., Okada, H., Bolland, S., Yanagi, S., Kurosaki, T., & Ravetch, J. V. (1997). Deletion of SHIP or SHP-1 Reveals Two Distinct Pathways for Inhibitory Signaling. *Cell*, *90*(2), 293–301. https://doi.org/10.1016/S0092-8674(00)80337-2

Matsumoto, M., Yamada, T., Yoshinaga, S. K., Boone, T., Horan, T., Fujita, S., Li, Y., & Mitani, T. (2002). Essential Role of NF-κB-Inducing Kinase in T Cell Activation Through the TCR/CD3 Pathway. *The Journal of Immunology*, *169*(3), 1151–1158. https://doi.org/10.4049/JIMMUNOL.169.3.1151

Matsuyama, S., Nagata, N., Shirato, K., Kawase, M., Takeda, M., & Taguchi, F. (2010). Efficient Activation of the Severe Acute Respiratory Syndrome Coronavirus Spike Protein by the Transmembrane Protease TMPRSS2. *Journal of Virology*, *84*(24), 12658–12664. https://doi.org/10.1128/JVI.01542-10/ASSET/749B0B9C-5052-4A37-91B2-B78340FC711E/ASSETS/GRAPHIC/ZJV9990939980005.JPEG

McCall, M. N., Shotton, D. M., & Barclay, A. N. (1992). Expression of soluble isoforms of rat CD45. Analysis by electron microscopy and use in epitope mapping of anti-CD45R monoclonal antibodies. *Immunology*, *76*(2), 310–317. http://www.ncbi.nlm.nih.gov/pubmed/1378817

Mckeithan, T. W. (1995). Kinetic proofreading in T-cell receptor signal transduction. *Proceedings of the National Academy of Sciences*, *92*(11), 5042–5046. https://doi.org/10.1073/PNAS.92.11.5042

McNeill, L., Salmond, R. J., Cooper, J. C., Carret, C. K., Cassady-Cain, R. L., Roche-Molina, M., Tandon, P., Holmes, N., & Alexander, D. R. (2007). The Differential Regulation of Lck Kinase Phosphorylation Sites by CD45 Is Critical for T Cell Receptor Signaling Responses. *Immunity*, *27*(3), 425–437. https://doi.org/10.1016/J.IMMUNI.2007.07.015

Menon, R., & David, B. G. (2015). Itolizumab – a humanized anti-CD6 monoclonal antibody with a better side effects profile for the treatment of psoriasis. *Clinical, Cosmetic and Investigational Dermatology*, *8*, 215. https://doi.org/10.2147/CCID.S47784

Meyaard, L., Adema, G. J., Chang, C., Woollatt, E., Sutherland, G. R., Lanier, L. L., & Phillips, J. H. (1997). LAIR-1, a Novel Inhibitory Receptor Expressed on Human Mononuclear Leukocytes. *Immunity*, *7*(2), 283–290. https://doi.org/10.1016/S1074-7613(00)80530-0

Milstein, O., Tseng, S.-Y., Starr, T., Llodra, J., Nans, A., Liu, M., Wild, M. K., van der Merwe, P. A., Stokes, D. L., Reisner, Y., & Dustin, M. L. (2008). Nanoscale Increases in CD2-CD48-mediated Intermembrane Spacing Decrease Adhesion and Reorganize the Immunological Synapse. *Journal of Biological Chemistry*, *283*(49), 34414–34422. https://doi.org/10.1074/jbc.M804756200

Minguet, S., Swamy, M., Alarcón, B., Luescher, I. F., & Schamel, W. W. A. (2007). Full Activation of the T Cell Receptor Requires Both Clustering and Conformational Changes at CD3. *Immunity*, *26*(1), 43–54. https://doi.org/10.1016/J.IMMUNI.2006.10.019

Minutolo, N. G., Hollander, E. E., & Powell, D. J. J. (2019). The Emergence of Universal Immune Receptor T Cell Therapy for Cancer. *Frontiers in Oncology*, *0*(MAR), 176.

https://doi.org/10.3389/FONC.2019.00176

Mishra, S., Mindermann, S., Sharma, M., Whittaker, C., Mellan, T. A., Wilton, T., Klapsa, D., Mate, R., Fritzsche, M., Zambon, M., Ahuja, J., Howes, A., Miscouridou, X., Nason, G. P., Ratmann, O., Semenova, E., Leech, G., Sandkühler, J. F., Rogers-Smith, C., … Flaxman, S. (2021). Changing composition of SARS-CoV-2 lineages and rise of Delta variant in England. *EClinicalMedicine*, *39*, 101064. https://doi.org/10.1016/J.ECLINM.2021.101064

Mizuno, R., Sugiura, D., Shimizu, K., Maruhashi, T., Watada, M., Okazaki, I. mi, & Okazaki, T. (2019). PD-1 primarily targets TCR signal in the inhibition of functional T cell activation. *Frontiers in Immunology*, *10*(MAR), 630. https://doi.org/10.3389/fimmu.2019.00630

Molina, A. (2008). A Decade of Rituximab: Improving Survival Outcomes in Non-Hodgkin's Lymphoma. *Annual Review of Medicine*, *59*(1), 237–250. https://doi.org/10.1146/annurev.med.59.060906.220345

Monteil, V., Kwon, H., Prado, P., Hagelkrüys, A., Wimmer, R. A., Stahl, M., Leopoldi, A., Garreta, E., Hurtado del Pozo, C., Prosper, F., Romero, J. P., Wirnsberger, G., Zhang, H., Slutsky, A. S., Conder, R., Montserrat, N., Mirazimi, A., & Penninger, J. M. (2020). Inhibition of SARS-CoV-2 Infections in Engineered Human Tissues Using Clinical-Grade Soluble Human ACE2. *Cell*, *181*(4), 905-913.e7. https://doi.org/10.1016/J.CELL.2020.04.004

Moretta, A., Bottino, C., Vitale, M., Pende, D., Cantoni, C., Cristina, M., Biassoni, R., & Moretta, L. (2003). Activating Receptors and Coreceptors Involved in Human Natural Killer Cell-Mediated Cytolysis. *Https://Doi.Org/10.1146/Annurev.Immunol.19.1.197*, *19*, 197–223. https://doi.org/10.1146/ANNUREV.IMMUNOL.19.1.197

Mori, D., Grégoire, C., Voisinne, G., Celis-Gutierrez, J., Aussel, R., Girard, L., Camus, M., Marcellin, M., Argenty, J., Burlet-Schiltz, O., Fiore, F., Gonzalez de Peredo, A., Malissen, M., Roncagalli, R., & Malissen, B. (2021). The T cell CD6 receptor operates a multitask signalosome with opposite functions in T cell activation. *Journal of Experimental Medicine*, *218*(2). https://doi.org/10.1084/JEM.20201011

Murphy K. (2011). *Janeway's Immunobiology* (8th editio). Garland Science.

Myszka, D. G. (1997). Kinetic analysis of macromolecular interactions using surface plasmon resonance biosensors. *Current Opinion in Biotechnology*, *8*(1), 50–57. https://doi.org/10.1016/S0958-1669(97)80157-7

Myszka, D. G. (1999). Improving biosensor analysis. *Journal of Molecular Recognition*, *12*(5), 279–284. https://doi.org/10.1002/(SICI)1099-1352(199909/10)12:5<279::AID-JMR473>3.0.CO;2-3

Nakada, C., Ritchie, K., Oba, Y., Nakamura, M., Hotta, Y., Iino, R., Kasai, R. S., Yamaguchi, K., Fujiwara, T., & Kusumi, A. (2003). Accumulation of anchored proteins forms membrane diffusion barriers during neuronal polarization. *Nature Cell Biology 2003 5:7*, *5*(7), 626–632. https://doi.org/10.1038/ncb1009

Narula, S. S., Yuan, R. W., Adams, S. E., Green, O. M., Green, J., Philips, T. B., Zydowsky, L. D., Botfield, M. C., Hatada, M., Laird, E. R., Zoller, M. J., Karas, J. L., & Dalgarno, D. C. (1995). Solution structure of the C-terminal SH2 domain of the human tyrosine kinase Syk complexed with a phosphotyrosine pentapeptide. *Structure*, *3*(10), 1061–

1073. https://doi.org/10.1016/S0969-2126(01)00242-8

Natkanski, E., Lee, W.-Y., Mistry, B., Casal, A., Molloy, J. E., & Tolar, P. (2013). B Cells Use Mechanical Energy to Discriminate Antigen Affinities. *Science*, *340*(6140), 1587–1590. https://doi.org/10.1126/science.1237572

Nishiura, H., Ito, K., Anzai, A., Kobayashi, T., Piantham, C., & Rodríguez-Morales, A. J. (2022). Relative reproduction number of SARS-CoV-2 omicron (B.1.1.529) compared with Delta variant in South Africa. *Journal of Clinical Medicine*, *11*(1), 30. https://doi.org/10.3390/JCM11010030/S1

Ofori-Acquah, S. F., & King, J. A. (2008). Activated leukocyte cell adhesion molecule: a new paradox in cancer. *Translational Research*, *151*(3), 122–128. https://doi.org/10.1016/J.TRSL.2007.09.006

Oganesyan, V., Mazor, Y., Yang, C., Cook, K. E., Woods, R. M., Ferguson, A., Bowen, M. A., Martin, T., Zhu, J., Wu, H., & Dall'Acqua, W. F. (2015). Structural insights into the interaction of human IgG1 with FcγRI: no direct role of glycans in binding. *Acta Crystallographica. Section D, Biological Crystallography*, *71*(Pt 11), 2354–2361. https://doi.org/10.1107/S1399004715018015

Okada, M., Nada, S., Yamanashi, Y., Yamamoto, T., & Nakagawa, H. (1991). CSK: a protein-tyrosine kinase involved in regulation of src family kinases. *Journal of Biological Chemistry*, *266*(36), 24249–24252. https://doi.org/10.1016/S0021-9258(18)54220-4

Oliveira, M. I., Gonçalves, C. M., Pinto, M., Fabre, S., Santos, A. M., Lee, S. F., Castro, M. A. A., Nunes, R. J., Barbosa, R. R., Parnes, J. R., Yu, C., Davis, S. J., Moreira, A., Bismuth, G., & Carmo, A. M. (2012). CD6 attenuates early and late signaling events, setting thresholds for T-cell activation. *European Journal of Immunology*, *42*(1), 195–205. https://doi.org/10.1002/EJI.201040528

Ordoñez-Rueda, D., Lozano, F., Sarukhan, A., Raman, C., Garcia-Zepeda, E. A., & Soldevila, G. (2009). Increased numbers of thymic and peripheral CD4+ CD25+Foxp3+ cells in the absence of CD5 signaling. *European Journal of Immunology*, *39*(8), 2233–2247. https://doi.org/10.1002/EJI.200839053

Orloff, D. G., Ra, C., Frank, S. J., Klausner, R. D., & Kinet, J.-P. (1990). Family of disulphide-linked dimers containing the ζ and η chains of the T-cell receptor and the γ chain of Fc receptors. *Nature 1990 347:6289*, *347*(6289), 189–191. https://doi.org/10.1038/347189a0

Osorio, L. M., Garcia, C. A., Jondal, M., & Chow, S. C. (1994). The Anti-CD6 mAb, IOR-T1, Defined a New Epitope on the Human CD6 Molecule That Induces Greater Responsiveness in T Cell Receptor/CD3-Mediated T Cell Proliferation. *Cellular Immunology*, *154*(1), 123–133. https://doi.org/10.1006/CIMM.1994.1062

Oudit, G. Y., Crackower, M. A., Backx, P. H., & Penninger, J. M. (2003). The Role of ACE2 in Cardiovascular Physiology. *Trends in Cardiovascular Medicine*, *13*(3), 93–101. https://doi.org/10.1016/S1050-1738(02)00233-5

Padilla, O., Calvo, J., Vila, J. M., Arman, M., Gimferrer, I., Places, L., Arias, M. T., Pujana, M. A., Vives, J., & Lozano, F. (2000). Genomic organization of the human CD5 gene. *Immunogenetics 2000 51:12*, *51*(12), 993–1001. https://doi.org/10.1007/S002510000235

Pageon, S. V., Tabarin, T., Yamamoto, Y., Ma, Y., Nicovich, P. R., Bridgeman, J. S., Cohnen, A., Benzing, C., Gao, Y., Crowther, M. D., Tungatt, K., Dolton, G., Sewell, A. K., Price, D. A., Acuto, O., Parton, R. G., Gooding, J. J., Rossy, J., Rossjohn, J., & Gaus, K. (2016). Functional role of T-cell receptor nanoclusters in signal initiation and antigen discrimination. *Proceedings of the National Academy of Sciences*, *113*(37), E5454–E5463. https://doi.org/10.1073/PNAS.1607436113

Paszek, M. J., DuFort, C. C., Rossier, O., Bainer, R., Mouw, J. K., Godula, K., Hudak, J. E., Lakins, J. N., Wijekoon, A. C., Cassereau, L., Rubashkin, M. G., Magbanua, M. J., Thorn, K. S., Davidson, M. W., Rugo, H. S., Park, J. W., Hammer, D. A., Giannone, G., Bertozzi, C. R., & Weaver, V. M. (2014). The cancer glycocalyx mechanically primes integrin-mediated growth and survival. *Nature 2014 511:7509*, *511*(7509), 319–325. https://doi.org/10.1038/nature13535

Paulick, M. G., Wise, A. R., Forstner, M. B., Groves, J. T., & Bertozzi, C. R. (2007). Synthetic analogues of glycosylphosphatidylinositol-anchored proteins and their behavior in supported lipid bilayers. *Journal of the American Chemical Society*, *129*(37), 11543–11550. https://doi.org/10.1021/JA073271J/SUPPL_FILE/JA073271JSI20070703_061319.PDF

Peña-Rossi, C., Zuckerman, L. A., Strong, J., Kwan, J., Ferris, W., Chan, S., Tarakhovsky, A., Beyers, A. D., & Killeen, N. (1999). Negative Regulation of CD4 Lineage Development and Responses by CD5. *The Journal of Immunology*, *163*(12), 6494 LP – 6501. http://www.jimmunol.org/content/163/12/6494.abstract

Pettmann, J., Huhn, A., Shah, E. A., Kutuzov, M. A., Wilson, D. B., Dustin, M. L., Davis, S. J., van der Merwe, P. A., & Dushek, O. (2021). The discriminatory power of the t cell receptor. *ELife*, *10*. https://doi.org/10.7554/ELIFE.67092

Pryshchep, S., Zarnitsyna, V. I., Hong, J., Evavold, B. D., & Zhu, C. (2014). Accumulation of Serial Forces on TCR and CD8 Frequently Applied by Agonist Antigenic Peptides Embedded in MHC Molecules Triggers Calcium in T Cells. *The Journal of Immunology*, *193*(1), 68–76. https://doi.org/10.4049/jimmunol.1303436

Puech, P.-H., Nevoltris, D., Robert, P., Limozin, L., Boyer, C., & Bongrand, P. (2011). Force Measurements of TCR/pMHC Recognition at T Cell Surface. *PLoS ONE*, *6*(7), e22344. https://doi.org/10.1371/journal.pone.0022344

Purbhoo, M. A., Irvine, D. J., Huppa, J. B., & Davis, M. M. (2004). T cell killing does not require the formation of a stable mature immunological synapse. *Nature Immunology 2004 5:5*, *5*(5), 524–530. https://doi.org/10.1038/ni1058

Rafiq, S., Hackett, C. S., & Brentjens, R. J. (2019). Engineering strategies to overcome the current roadblocks in CAR T cell therapy. *Nature Reviews Clinical Oncology 2019 17:3*, *17*(3), 147–167. https://doi.org/10.1038/s41571-019-0297-y

Rambaut, A., Holmes, E. C., O'Toole, Á., Hill, V., McCrone, J. T., Ruis, C., du Plessis, L., & Pybus, O. G. (2020). A dynamic nomenclature proposal for SARS-CoV-2 lineages to assist genomic epidemiology. *Nature Microbiology*, *5*(11), 1403–1407. https://doi.org/10.1038/s41564-020-0770-5

Ramsland, P. A., Farrugia, W., Bradford, T. M., Sardjono, C. T., Esparon, S., Trist, H. M., Powell, M. S., Tan, P. S., Cendron, A. C., Wines, B. D., Scott, A. M., & Hogarth, P. M. (2011). Structural basis for Fc gammaRIIa recognition of human IgG and formation of

inflammatory signaling complexes. *Journal of Immunology (Baltimore, Md. : 1950)*, *187*(6), 3208–3217. https://doi.org/10.4049/jimmunol.1101467

Ratzinger, F., Haslacher, H., Poeppl, W., Hoermann, G., Kovarik, J. J., Jutz, S., Steinberger, P., Burgmann, H., Pickl, W. F., & Schmetterer, K. G. (2014). Azithromycin suppresses CD4+ T-cell activation by direct modulation of mTOR activity. *Scientific Reports 2014 4:1*, *4*(1), 1–10. https://doi.org/10.1038/srep07438

Razvag, Y., Neve-Oz, Y., Sajman, J., Reches, M., & Sherman, E. (2018). Nanoscale kinetic segregation of TCR and CD45 in engaged microvilli facilitates early T cell activation. *Nature Communications*, *9*(1), 732. https://doi.org/10.1038/s41467-018-03127-w

Read, C. B., Kuijper, J. L., Hjorth, S. A., Heipel, M. D., Tang, X., Fleetwood, A. J., Dantzler, J. L., Grell, S. N., Kastrup, J., Wang, C., Brandt, C. S., Hansen, A. J., Wagtmann, N. R., Xu, W., & Stennicke, V. W. (2015). Cutting Edge: identification of neutrophil PGLYRP1 as a ligand for TREM-1. *Journal of Immunology (Baltimore, Md. : 1950)*, *194*(4), 1417–1421. https://doi.org/10.4049/jimmunol.1402303

Resh, M. D. (1999). Fatty acylation of proteins: new insights into membrane targeting of myristoylated and palmitoylated proteins. *Biochimica et Biophysica Acta (BBA) - Molecular Cell Research*, *1451*(1), 1–16. https://doi.org/10.1016/S0167-4889(99)00075-0

Robbiani, D. F., Gaebler, C., Muecksch, F., Lorenzi, J. C. C., Wang, Z., Cho, A., Agudelo, M., Barnes, C. O., Gazumyan, A., Finkin, S., Hägglöf, T., Oliveira, T. Y., Viant, C., Hurley, A., Hoffmann, H. H., Millard, K. G., Kost, R. G., Cipolla, M., Gordon, K., … Nussenzweig, M. C. (2020). Convergent antibody responses to SARS-CoV-2 in convalescent individuals. *Nature 2020 584:7821*, *584*(7821), 437–442. https://doi.org/10.1038/s41586-020-2456-9

Robinson, M. J., Sancho, D., Slack, E. C., LeibundGut-Landmann, S., & Sousa, C. R. e. (2006). Myeloid C-type lectins in innate immunity. *Nature Immunology 2006 7:12*, *7*(12), 1258–1265. https://doi.org/10.1038/ni1417

Rodgers, D. T., Mazagova, M., Hampton, E. N., Cao, Y., Ramadoss, N. S., Hardy, I. R., Schulman, A., Du, J., Wang, F., Singer, O., Ma, J., Nunez, V., Shen, J., Woods, A. K., Wright, T. M., Schultz, P. G., Kim, C. H., & Young, T. S. (2016). Switch-mediated activation and retargeting of CAR-T cells for B-cell malignancies. *Proceedings of the National Academy of Sciences of the United States of America*, *113*(4), E459-68. https://doi.org/10.1073/pnas.1524155113

Rodrigues, C. H. M., Myung, Y., Pires, D. E. V., & Ascher, D. B. (2019). MCSM-PPI2: predicting the effects of mutations on protein-protein interactions. *Nucleic Acids Research*, *47*(W1), W338–W344. https://doi.org/10.1093/nar/gkz383

Roncagalli, R., Hauri, S., Fiore, F., Liang, Y., Chen, Z., Sansoni, A., Kanduri, K., Joly, R., Malzac, A., Lähdesmäki, H., Lahesmaa, R., Yamasaki, S., Saito, T., Malissen, M., Aebersold, R., Gstaiger, M., & Malissen, B. (2014). Quantitative proteomics analysis of signalosome dynamics in primary T cells identifies the surface receptor CD6 as a Lat adaptor–independent TCR signaling hub. *Nature Immunology 2014 15:4*, *15*(4), 384–392. https://doi.org/10.1038/ni.2843

Rosenbaum, D. M., Rasmussen, S. G. F., & Kobilka, B. K. (2009). The structure and function of G-protein-coupled receptors. *Nature*, *459*(7245), 356–363.

https://doi.org/10.1038/nature08144

Rosental, B., Brusilovsky, M., Hadad, U., Oz, D., Appel, M. Y., Afergan, F., Yossef, R., Rosenberg, L. A., Aharoni, A., Cerwenka, A., Campbell, K. S., Braiman, A., & Porgador, A. (2011). Proliferating cell nuclear antigen is a novel inhibitory ligand for the natural cytotoxicity receptor NKp44. *Journal of Immunology (Baltimore, Md. : 1950)*, *187*(11), 5693–5702. https://doi.org/10.4049/jimmunol.1102267

Sabino, E. C., Buss, L. F., Carvalho, M. P. S., Prete, C. A., Crispim, M. A. E., Fraiji, N. A., Pereira, R. H. M., Parag, K. V., da Silva Peixoto, P., Kraemer, M. U. G., Oikawa, M. K., Salomon, T., Cucunuba, Z. M., Castro, M. C., de Souza Santos, A. A., Nascimento, V. H., Pereira, H. S., Ferguson, N. M., Pybus, O. G., … Faria, N. R. (2021). Resurgence of COVID-19 in Manaus, Brazil, despite high seroprevalence. *The Lancet*, *397*(10273), 452–455. https://doi.org/10.1016/S0140-6736(21)00183-5

Salzer, B., Schueller, C. M., Zajc, C. U., Peters, T., Schoeber, M. A., Kovacic, B., Buri, M. C., Lobner, E., Dushek, O., Huppa, J. B., Obinger, C., Putz, E. M., Holter, W., Traxlmayr, M. W., & Lehner, M. (2020). Engineering AvidCARs for combinatorial antigen recognition and reversible control of CAR function. *Nature Communications 2020 11:1*, *11*(1), 1–16. https://doi.org/10.1038/s41467-020-17970-3

Sanchez-Garcia, R., Sorzano, C. O. S., Carazo, J. M., & Segura, J. (2019). BIPSPI: a method for the prediction of partner-specific protein–protein interfaces. *Bioinformatics*, *35*(3), 470–477. https://doi.org/10.1093/BIOINFORMATICS/BTY647

Santos, R. F., Oliveira, L., Brown, M. H., & Carmo, A. M. (2019). Domain-specific CD6 monoclonal antibodies identify CD6 isoforms generated by alternative-splicing. *Immunology*, *157*(4), 296–303. https://doi.org/10.1111/IMM.13087

Schamel, W. W. A., & Alarcón, B. (2013). Organization of the resting TCR in nanoscale oligomers. *Immunological Reviews*, *251*(1), 13–20. https://doi.org/10.1111/IMR.12019

Schilham, M. W., Fung-Leung, W.-P., Rahemtulla, A., Kuendig, T., Zhang, L., Potter, J., Miller, R. G., Hengartner, H., & Mak, T. W. (1993). Alloreactive cytotoxic T cells can develop and function in mice lacking both CD4 and CD8. *European Journal of Immunology*, *23*(6), 1299–1304. https://doi.org/10.1002/EJI.1830230617

Schlessinger, J. (1994). SH2/SH3 signaling proteins. *Current Opinion in Genetics & Development*, *4*(1), 25–30. https://doi.org/10.1016/0959-437X(94)90087-6

Schmid, E. M., Bakalar, M. H., Choudhuri, K., Weichsel, J., Ann, H. S., Geissler, P. L., Dustin, M. L., & Fletcher, D. A. (2016). Size-dependent protein segregation at membrane interfaces. *Nature Physics*, *12*(7), 704–711. https://doi.org/10.1038/nphys3678

Shang, J., Ye, G., Shi, K., Wan, Y., Luo, C., Aihara, H., Geng, Q., Auerbach, A., & Li, F. (2020). Structural basis of receptor recognition by SARS-CoV-2. *Nature*, *581*(7807), 221–224. https://doi.org/10.1038/s41586-020-2179-y

Sharma, P., & Kranz, D. M. (2016). Recent advances in T-cell engineering for use in immunotherapy. *F1000Research*, *5*. https://doi.org/10.12688/f1000research.9073.1

Sheppard, K. A., Fitz, L. J., Lee, J. M., Benander, C., George, J. A., Wooters, J., Qiu, Y., Jussif, J. M., Carter, L. L., Wood, C. R., & Chaudhary, D. (2004). PD-1 inhibits T-cell receptor induced phosphorylation of the ZAP70/CD3ζ signalosome and downstream

signaling to PKCθ. *FEBS Letters*, *574*(1–3), 37–41. https://doi.org/10.1016/J.FEBSLET.2004.07.083

Shlapatska, L. M., Mikhalap, S. V., Berdova, A. G., Zelensky, O. M., Yun, T. J., Nichols, K. E., Clark, E. A., & Sidorenko, S. P. (2001). CD150 Association with Either the SH2-Containing Inositol Phosphatase or the SH2-Containing Protein Tyrosine Phosphatase Is Regulated by the Adaptor Protein SH2D1A. *The Journal of Immunology*, *166*(9), 5480–5487. https://doi.org/10.4049/JIMMUNOL.166.9.5480

Siller-Farfán, J. A., & Dushek, O. (2018). Molecular mechanisms of T cell sensitivity to antigen. *Immunological Reviews*, *285*(1), 194–205. https://doi.org/10.1111/IMR.12690

Simmons, G., Gosalia, D. N., Rennekamp, A. J., Reeves, J. D., Diamond, S. L., & Bates, P. (2005). Inhibitors of cathepsin L prevent severe acute respiratory syndrome coronavirus entry. *Proceedings of the National Academy of Sciences*, *102*(33), 11876–11881. https://doi.org/10.1073/PNAS.0505577102

Singer, N. G., Fox, D. A., Haqqi, T. M., Beretta, L., Endres, J. S., Prohaska, S., Parnes, J. R., Bromberg, J., & Sramkoski, R. M. (2002). CD6: expression during development, apoptosis and selection of human and mouse thymocytes. *International Immunology*, *14*(6), 585–597. https://doi.org/10.1093/INTIMM/DXF025

Soldevila, G., Raman, C., & Lozano, F. (2011). The immunomodulatory properties of the CD5 lymphocyte receptor in health and disease. *Current Opinion in Immunology*, *23*(3), 310–318. https://doi.org/10.1016/J.COI.2011.03.003

Soumpasis, D. M. (1983). Theoretical analysis of fluorescence photobleaching recovery experiments. *Biophysical Journal*, *41*(1), 95–97. https://doi.org/10.1016/S0006-3495(83)84410-5

Spear, P., Wu, M.-R., Sentman, M.-L., & Sentman, C. L. (2013). NKG2D ligands as therapeutic targets. *Cancer Immunity*, *13*, 8. http://www.ncbi.nlm.nih.gov/pubmed/23833565

Springer, T. A. (1990). Adhesion receptors of the immune system. *Nature*, *346*(6283), 425–434. https://doi.org/10.1038/346425a0

Srivastava, S., & Riddell, S. R. (2015). Engineering CAR-T cells: Design concepts. *Trends in Immunology*, *36*(8), 494–502. https://doi.org/10.1016/j.it.2015.06.004

Starr, T. N., Greaney, A. J., Hilton, S. K., Ellis, D., Crawford, K. H. D., Dingens, A. S., Navarro, M. J., Bowen, J. E., Tortorici, M. A., Walls, A. C., King, N. P., Veesler, D., & Bloom, J. D. (2020). Deep Mutational Scanning of SARS-CoV-2 Receptor Binding Domain Reveals Constraints on Folding and ACE2 Binding. *Cell*, *182*(5), 1295-1310.e20. https://doi.org/10.1016/j.cell.2020.08.012

Sungnak, W., Huang, N., Bécavin, C., Berg, M., Queen, R., Litvinukova, M., Talavera-López, C., Maatz, H., Reichart, D., Sampaziotis, F., Worlock, K. B., Yoshida, M., Barnes, J. L., Banovich, N. E., Barbry, P., Brazma, A., Collin, J., Desai, T. J., Duong, T. E., … Figueiredo, F. (2020). SARS-CoV-2 entry factors are highly expressed in nasal epithelial cells together with innate immune genes. *Nature Medicine 2020 26:5*, *26*(5), 681–687. https://doi.org/10.1038/s41591-020-0868-6

Supasa, P., Zhou, D., Dejnirattisai, W., Liu, C., Mentzer, A. J., Ginn, H. M., Zhao, Y., Duyvesteyn, H. M. E., Nutalai, R., Tuekprakhon, A., Wang, B., Paesen, G. C., Slon-

Campos, J., López-Camacho, C., Hallis, B., Coombes, N., Bewley, K. R., Charlton, S., Walter, T. S., … Screaton, G. R. (2021). Reduced neutralization of SARS-CoV-2 B.1.1.7 variant by convalescent and vaccine sera. *Cell*, *184*(8), 2201-2211.e7. https://doi.org/10.1016/j.cell.2021.02.033

Swaminathan, B., Cuapio, A., Alloza, I., Matesanz, F., Alcina, A., García-Barcina, M., Fedetz, M., Fernández, Ó., Lucas, M., Órpez, T., Pinto-Medel, M. J., Otaegui, D., Olascoaga, J., Urcelay, E., Ortiz, M. A., Arroyo, R., Oksenberg, J. R., Antigüedad, A., Tolosa, E., & Vandenbroeck, K. (2013). Fine Mapping and Functional Analysis of the Multiple Sclerosis Risk Gene CD6. *PLOS ONE*, *8*(4), e62376. https://doi.org/10.1371/JOURNAL.PONE.0062376

Syeda, R., Florendo, M. N., Cox, C. D., Kefauver, J. M., Santos, J. S., Martinac, B., & Patapoutian, A. (2016). Piezo1 Channels Are Inherently Mechanosensitive. *Cell Reports*, *17*(7), 1739–1746. https://doi.org/10.1016/j.celrep.2016.10.033

Sykulev, Y., Joo, M., Vturina, I., Tsomides, T. J., & Eisen, H. N. (1996). Evidence that a Single Peptide–MHC Complex on a Target Cell Can Elicit a Cytolytic T Cell Response. *Immunity*, *4*(6), 565–571. https://doi.org/10.1016/S1074-7613(00)80483-5

Tanaka, S., Nelson, G., Olson, A., Buzko, O., Higashide, W., Shin, A., Gonzales, M., Taft, J., Patel, R., Buta, S., Martin-Fernandez, M., Bogunovic, D., Spilman, P., Niazi, K., Rabizadeh, S., & Soon-Shiong, P. (2021). A recombinant 'ACE2 Triple Decoy' that traps and neutralizes SARS-CoV-2 shows enhanced affinity for highly transmissible SARS-CoV-2 variants. *BioRxiv*, 2021.03.09.434641. https://doi.org/10.1101/2021.03.09.434641

Tarakhovsky, A., Kanner, S. B., Hombach, J., Ledbetter, J. A., Müller, W., Killeen, N., & Rajewsky, K. (1995). A Role for CD5 in TCR-Mediated Signal Transduction and Thymocyte Selection. *Science*, *269*(5223), 535–537. https://doi.org/10.1126/SCIENCE.7542801

Teyssou, E., Delagrèverie, H., Visseaux, B., Lambert-Niclot, S., Brichler, S., Ferre, V., Marot, S., Jary, A., Todesco, E., Schnuriger, A., Ghidaoui, E., Abdi, B., Akhavan, S., Houhou-Fidouh, N., Charpentier, C., Morand-Joubert, L., Boutolleau, D., Descamps, D., Calvez, V., … Soulie, C. (2021). The Delta SARS-CoV-2 variant has a higher viral load than the Beta and the historical variants in nasopharyngeal samples from newly diagnosed COVID-19 patients. *Journal of Infection*, *83*(4), e1–e3. https://doi.org/10.1016/J.JINF.2021.08.027

Tjendra, Y., Al Mana, A. F., Espejo, A. P., Akgun, Y., Millan, N. C., Gomez-Fernandez, C., & Cray, C. (2020). Predicting Disease Severity and Outcome in COVID-19 Patients: A Review of Multiple Biomarkers. *Archives of Pathology & Laboratory Medicine*, *144*(12), 1465–1474. https://doi.org/10.5858/ARPA.2020-0471-SA

Tomaz, D., Pereira, P. M., Guerra, N., Dyson, J., Henriques, R., & Gould, K. (2018). Nanoscale colocalization of NK cell activating and inhibitory receptors controls signal integration. *BioRxiv*, 266429. https://doi.org/10.1101/266429

Trautmann, A., & Randriamampita, C. (2003). Initiation of TCR signalling revisited. *Trends in Immunology*, *24*(8), 425–428. https://doi.org/10.1016/S1471-4906(03)00182-0

Treumann, A., Lifely, M. R., Schneider, P., & Ferguson, M. A. J. (1995). Primary structure of CD52. *Journal of Biological Chemistry*, *270*(11), 6088–6099.

https://doi.org/10.1074/JBC.270.11.6088/ATTACHMENT/6D8C8555-F279-4C57-8DEC-CC1C25299DF0/TBL3

Trowbridge, I. S., & Thomas, M. L. (1994). *CD45: An Emerging Role as a Protein Tyrosine Phosphatase Required for Lymphocyte Activation and Development Further ANNUAL REVIEWS*. www.annualreviews.org

Tseng, S.-Y., Liu, M., & Dustin, M. L. (2005). CD80 cytoplasmic domain controls localization of CD28, CTLA-4, and protein kinase Ctheta in the immunological synapse. *Journal of Immunology (Baltimore, Md. : 1950)*, *175*(12), 7829–7836. http://www.ncbi.nlm.nih.gov/pubmed/16339518

Van Der Merwe, P., Mcnamee, P. N., Davies, E. A., Barclay, A. N., & Davis, S. J. (1995). Topology of the CD2-CD48 cell-adhesion molecule complex: implications for antigen recognition by T cells. *Current Biology*, *5*, 74–84. https://core.ac.uk/download/pdf/81952433.pdf

Van Kempen, L. C. L. T., Meier, F., Egeblad, M., Kersten-Niessen, M. J. F., Garbe, C., Weidle, U. H., Van Muijen, G. N. P., Herlyn, M., Bloemers, H. P. J., & Swart, G. W. M. (2004). Truncation of Activated Leukocyte Cell Adhesion Molecule: A Gateway to Melanoma Metastasis. *Journal of Investigative Dermatology*, *122*(5), 1293–1301. https://doi.org/10.1111/J.0022-202X.2004.22531.X

Varma, R., Campi, G., Yokosuka, T., Saito, T., & Dustin, M. L. (2006). T Cell Receptor-Proximal Signals Are Sustained in Peripheral Microclusters and Terminated in the Central Supramolecular Activation Cluster. *Immunity*, *25*(1), 117–127. https://doi.org/10.1016/J.IMMUNI.2006.04.010

Veillette, A., Dong, Z., Pérez-Quintero, L.-A., Zhong, M.-C., & Cruz-Munoz, M.-E. (2009). Importance and mechanism of 'switch' function of SAP family adapters. *Immunological Reviews*, *232*(1), 229–239. https://doi.org/10.1111/J.1600-065X.2009.00824.X

Vély, F., Olcese, L., Bléry, M., & Vivier, E. (1996). Function of killer cell inhibitory receptors for MHC class I molecules. *Immunology Letters*, *54*(2–3), 145–150. https://doi.org/10.1016/S0165-2478(96)02664-8

Vera, J., Fenutria, R., Cañadas, O., Figueras, M., Mota, R., Sarrias, M. R., Williams, D. L., Casals, C., Yelamos, J., & Lozano, F. (2009). The CD5 ectodomain interacts with conserved fungal cell wall components and protects from zymosan-induced septic shock-like syndrome. *Proceedings of the National Academy of Sciences*, *106*(5), 1506–1511. https://doi.org/10.1073/PNAS.0805846106

Verity, R., Okell, L. C., Dorigatti, I., Winskill, P., Whittaker, C., Imai, N., Cuomo-Dannenburg, G., Thompson, H., Walker, P. G. T., Fu, H., Dighe, A., Griffin, J. T., Baguelin, M., Bhatia, S., Boonyasiri, A., Cori, A., Cucunubá, Z., FitzJohn, R., Gaythorpe, K., … Ferguson, N. M. (2020). Estimates of the severity of coronavirus disease 2019: a model-based analysis. *The Lancet Infectious Diseases*, *20*(6), 669–677. https://doi.org/10.1016/S1473-3099(20)30243-7

Voisinne, G., Gonzalez de Peredo, A., & Roncagalli, R. (2018). CD5, an Undercover Regulator of TCR Signaling. *Frontiers in Immunology*, *0*, 2900. https://doi.org/10.3389/FIMMU.2018.02900

Voss, S., & Skerra, A. (1997). Mutagenesis of a flexible loop in streptavidin leads to higher affinity for the Strep-tag II peptide and improved performance in recombinant protein

purification. *Protein Engineering, Design and Selection*, *10*(8), 975–982. https://doi.org/10.1093/PROTEIN/10.8.975

Wallis, R., Mitchell, D. A., Schmid, R., Schwaeble, W. J., & Keeble, A. H. (2010). Paths reunited: Initiation of the classical and lectin pathways of complement activation. *Immunobiology*, *215*(1), 1–11. https://doi.org/10.1016/j.imbio.2009.08.006

Walls, A. C., Tortorici, M. A., Snijder, J., Xiong, X., Bosch, B. J., Rey, F. A., & Veesler, D. (2017). Tectonic conformational changes of a coronavirus spike glycoprotein promote membrane fusion. *Proceedings of the National Academy of Sciences of the United States of America*, *114*(42), 11157–11162. https://doi.org/10.1073/PNAS.1708727114/-/DCSUPPLEMENTAL

Wan, Shang, J., Graham, R., Baric, R. S., & Li, F. (2020). Receptor Recognition by the Novel Coronavirus from Wuhan: an Analysis Based on Decade-Long Structural Studies of SARS Coronavirus. *Journal of Virology*, *94*(7), 127–147. https://doi.org/10.1128/jvi.00127-20

Wan, Z., Zhang, S., Fan, Y., Liu, K., Du, F., Davey, A. M., Zhang, H., Han, W., Xiong, C., & Liu, W. (2013). B cell activation is regulated by the stiffness properties of the substrate presenting the antigens. *Journal of Immunology (Baltimore, Md. : 1950)*, *190*(9), 4661–4675. https://doi.org/10.4049/jimmunol.1202976

Wang, W., Yang, Y., Yin, J., & Gong, X. (2017). Different protein-protein interface patterns predicted by different machine learning methods. *Scientific Reports 2017 7:1*, *7*(1), 1–13. https://doi.org/10.1038/s41598-017-16397-z

Wang, Y., Wang, Y., Luo, W., Huang, L., Xiao, J., Li, F., Qin, S., Song, X., Wu, Y., Zeng, Q., Jin, F., & Wang, Y. (2020). A comprehensive investigation of the mRNA and protein level of ACE2, the putative receptor of SARS-CoV-2, in human tissues and blood cells. *International Journal of Medical Sciences*, *17*(11), 1522. https://doi.org/10.7150/IJMS.46695

Washington, N. L., Gangavarapu, K., Zeller, M., Bolze, A., Cirulli, E. T., Schiabor Barrett, K. M., Larsen, B. B., Anderson, C., White, S., Cassens, T., Jacobs, S., Levan, G., Nguyen, J., Ramirez, J. M., Rivera-Garcia, C., Sandoval, E., Wang, X., Wong, D., Spencer, E., … Andersen, K. G. (2021). Emergence and rapid transmission of SARS-CoV-2 B.1.1.7 in the United States. *Cell*. https://doi.org/10.1016/j.cell.2021.03.052

Wee, S. F., Schieven, G. L., Kirihara, J. M., Tsu, T. T., Ledbetter, J. A., & Aruffo, A. (1993). Tyrosine phosphorylation of CD6 by stimulation of CD3: augmentation by the CD4 and CD2 coreceptors. *Journal of Experimental Medicine*, *177*(1), 219–223. https://doi.org/10.1084/JEM.177.1.219

Weiskopf, K. (2017). Cancer immunotherapy targeting the CD47/SIRPα axis. *European Journal of Cancer*, *76*, 100–109. https://doi.org/10.1016/J.EJCA.2017.02.013

Wild, M. K., Cambiaggi, A., Brown, M. H., Davies, E. A., Ohno, H., Saito, T., & van der Merwe, P. A. (1999). Dependence of T cell antigen recognition on the dimensions of an accessory receptor-ligand complex. *The Journal of Experimental Medicine*, *190*(1), 31–41. https://doi.org/10.1084/JEM.190.1.31

Woodruff, M. F. A., REID, B., & JAMES, K. (1967). Effect of Antilymphocytic Antibody and Antibody Fragments on Human Lymphocytes in vitro. *Nature 1967 215:5101*, *215*(5101), 591–594. https://doi.org/10.1038/215591a0

Wrapp, D., Wang, N., Corbett, K. S., Goldsmith, J. A., Hsieh, C.-L., Abiona, O., Graham, B. S., & McLellan, J. S. (2020). Cryo-EM structure of the 2019-nCoV spike in the prefusion conformation. *Science (New York, N.Y.)*, *367*(6483), 1260. https://doi.org/10.1126/SCIENCE.ABB2507

Wu, H., Kwong, P. D., & Hendrickson, W. A. (1997). Dimeric association and segmental variability in the structure of human CD4. *Nature 1997 387:6632*, *387*(6632), 527–530. https://doi.org/10.1038/387527a0

Wu, J., Song, Y., Bakker, A. B. H., Bauer, S., Spies, T., Lanier, L. L., & Phillips, J. H. (1999). An Activating Immunoreceptor Complex Formed by NKG2D and DAP10. *Science*, *285*(5428), 730–732. https://doi.org/10.1126/SCIENCE.285.5428.730

Wu, Peng, C., Yang, Y., Shi, Y., Zhou, L., Xu, Z., & Zhu, W. (2021). Exploring the immune evasion of SARS-CoV-2 variant harboring E484K by molecular dynamics simulations. *Briefings in Bioinformatics*. https://doi.org/10.1093/BIB/BBAB383

Xiao, K., Zhai, J., Feng, Y., Zhou, N., Zhang, X., Zou, J. J., Li, N., Guo, Y., Li, X., Shen, X., Zhang, Z., Shu, F., Huang, W., Li, Y., Zhang, Z., Chen, R. A., Wu, Y. J., Peng, S. M., Huang, M., … Shen, Y. (2020). Isolation of SARS-CoV-2-related coronavirus from Malayan pangolins. *Nature 2020 583:7815*, *583*(7815), 286–289. https://doi.org/10.1038/s41586-020-2313-x

Xing, Y., & Hogquist, K. A. (2012). T-Cell Tolerance: Central and Peripheral. *Cold Spring Harbor Perspectives in Biology*, *4*(6), a006957. https://doi.org/10.1101/CSHPERSPECT.A006957

Xu, C., Gagnon, E., Call, M. E., Schnell, J. R., Schwieters, C. D., Carman, C. V., Chou, J. J., & Wucherpfennig, K. W. (2008). Regulation of T Cell Receptor Activation by Dynamic Membrane Binding of the CD3ε Cytoplasmic Tyrosine-Based Motif. *Cell*, *135*(4), 702–713. https://doi.org/10.1016/J.CELL.2008.09.044

Xu, W., Doshi, A., Lei, M., Eck, M. J., & Harrison, S. C. (1999). Crystal Structures of c-Src Reveal Features of Its Autoinhibitory Mechanism. *Molecular Cell*, *3*(5), 629–638. https://doi.org/10.1016/S1097-2765(00)80356-1

Yamaguchi, H., & Hendrickson, W. A. (1996). Structural basis for activation of human lymphocyte kinase Lck upon tyrosine phosphorylation. *Nature 1996 384:6608*, *384*(6608), 484–489. https://doi.org/10.1038/384484a0

Yan, R., Zhang, Y., Li, Y., Xia, L., Guo, Y., & Zhou, Q. (2020). Structural basis for the recognition of SARS-CoV-2 by full-length human ACE2. *Science*, *367*(6485), 1444–1448. https://doi.org/10.1126/SCIENCE.ABB2762/SUPPL_FILE/PAP.PDF

Yang, H., Rei, M., Brackenridge, S., Brenna, E., Sun, H., Abdulhaqq, S., Liu, M. K. P., Ma, W., Kurupati, P., Xu, X., Cerundolo, V., Jenkins, E., Davis, S. J., Sacha, J. B., Früh, K., Picker, L. J., Borrow, P., Gillespie, G. M., & McMichael, A. J. (2021). HLA-E-restricted, Gag-specific CD8+T cells can suppress HIV-1 infection, offering vaccine opportunities. *Science Immunology*, *6*(57), 1703. https://doi.org/10.1126/SCIIMMUNOL.ABG1703/SUPPL_FILE/ABG1703_TABLE_S2.XLSX

Yeku, O. O., Purdon, T. J., Koneru, M., Spriggs, D., & Brentjens, R. J. (2017). Armored CAR T cells enhance antitumor efficacy and overcome the tumor microenvironment. *Scientific Reports 2017 7:1*, *7*(1), 1–14. https://doi.org/10.1038/s41598-017-10940-8

Yokosuka, T., Kobayashi, W., Takamatsu, M., Sakata-Sogawa, K., Zeng, H., Hashimoto-Tane, A., Yagita, H., Tokunaga, M., & Saito, T. (2010). Spatiotemporal Basis of CTLA-4 Costimulatory Molecule-Mediated Negative Regulation of T Cell Activation. *Immunity*, *33*(3), 326–339. https://doi.org/10.1016/j.immuni.2010.09.006

Yokosuka, T., Takamatsu, M., Kobayashi-Imanishi, W., Hashimoto-Tane, A., Azuma, M., & Saito, T. (2012). Programmed cell death 1 forms negative costimulatory microclusters that directly inhibit T cell receptor signaling by recruiting phosphatase SHP2. *The Journal of Experimental Medicine*, *209*(6), 1201–1217. https://doi.org/10.1084/jem.20112741

Yonemura, S., Hirao, M., Doi, Y., Takahashi, N., Kondo, T., Tsukita, S., & Tsukita, S. (1998). Ezrin/radixin/moesin (ERM) proteins bind to a positively charged amino acid cluster in the juxta-membrane cytoplasmic domain of CD44, CD43, and ICAM-2. *Journal of Cell Biology*, *140*(4), 885–895. https://doi.org/10.1083/jcb.140.4.885

Zahradník, J., Marciano, S., Shemesh, M., Zoler, E., Chiaravalli, J., Meyer, B., Dym, O., Elad, N., & Schreiber, G. (2021). SARS-CoV-2 RBD in vitro evolution follows contagious mutation spread, yet generates an able infection inhibitor. In *bioRxiv* (p. 2021.01.06.425392). Cold Spring Harbor Laboratory. https://doi.org/10.1101/2021.01.06.425392

Zakeri, B., Fierer, J. O., Celik, E., Chittock, E. C., Schwarz-Linek, U., Moy, V. T., & Howarth, M. (2012). Peptide tag forming a rapid covalent bond to a protein, through engineering a bacterial adhesin. *Proceedings of the National Academy of Sciences of the United States of America*, *109*(12), E690-7. https://doi.org/10.1073/pnas.1115485109

Zhang, Cai, Y., Xiao, T., Lu, J., Peng, H., Sterling, S. M., WalshJr., R. M., Rits-Volloch, S., Zhu, H., Woosley, A. N., Yang, W., Sliz, P., & Chen, B. (2021). Structural impact on SARS-CoV-2 spike protein by D614G substitution. *Science*, *372*(6541), 525–530. https://doi.org/10.1126/SCIENCE.ABF2303

Zhang, F., Crise, B., Su, B., Hou, Y., Rose, J. K., Bothwell, A., & Jacobson, K. (1991). Lateral diffusion of membrane-spanning and glycosylphosphatidylinositol-linked proteins: toward establishing rules governing the lateral mobility of membrane proteins. *Journal of Cell Biology*, *115*(1), 75–84. https://doi.org/10.1083/JCB.115.1.75

Zhang, H., Cordoba, S.-P., Dushek, O., & Merwe, P. A. van der. (2011). Basic residues in the T-cell receptor ζ cytoplasmic domain mediate membrane association and modulate signaling. *Proceedings of the National Academy of Sciences*, *108*(48), 19323–19328. https://doi.org/10.1073/PNAS.1108052108

Zhang, Jackson, C. B., Mou, H., Ojha, A., Peng, H., Quinlan, B. D., Rangarajan, E. S., Pan, A., Vanderheiden, A., Suthar, M. S., Li, W., Izard, T., Rader, C., Farzan, M., & Choe, H. (2020). SARS-CoV-2 spike-protein D614G mutation increases virion spike density and infectivity. *Nature Communications*, *11*(1), 1–9. https://doi.org/10.1038/s41467-020-19808-4

Zhang, Yanbo, & Wang, H. (2012). Integrin signalling and function in immune cells. *Immunology*, *135*(4), 268–275. https://doi.org/10.1111/J.1365-2567.2011.03549.X

Zhang, Yuhao, Geng, X., Tan, Y., Li, Q., Xu, C., Xu, J., Hao, L., Zeng, Z., Luo, X., Liu, F., & Wang, H. (2020). New understanding of the damage of SARS-CoV-2 infection outside the respiratory system. *Biomedicine & Pharmacotherapy*, *127*, 110195.

https://doi.org/10.1016/J.BIOPHA.2020.110195

Zhang, Z., Zeng, E., Zhang, L., Wang, W., Jin, Y., Sun, J., Huang, S., Yin, W., Dai, J., Zhuang, Z., Chen, Z., Sun, J., Zhu, A., Li, F., Cao, W., Li, X., Shi, Y., Gan, M., Zhang, S., … Zhao, J. (2021). Potent prophylactic and therapeutic efficacy of recombinant human ACE2-Fc against SARS-CoV-2 infection in vivo. *Cell Discovery 2021 7:1*, *7*(1), 1–15. https://doi.org/10.1038/s41421-021-00302-0

Zhou, Chong, M. M. W., & Littman, D. R. (2009). Plasticity of CD4+ T Cell Lineage Differentiation. *Immunity*, *30*(5), 646–655. https://doi.org/10.1016/J.IMMUNI.2009.05.001

Zhou, D., Dejnirattisai, W., Supasa, P., Liu, C., Mentzer, A. J., Ginn, H. M., Zhao, Y., Duyvesteyn, H. M. E., Tuekprakhon, A., Nutalai, R., Wang, B., Paesen, G. C., Lopez-Camacho, C., Slon-Campos, J., Hallis, B., Coombes, N., Bewley, K., Charlton, S., Walter, T. S., … Screaton, G. R. (2021). Evidence of escape of SARS-CoV-2 variant B.1.351 from natural and vaccine-induced sera. *Cell*, *184*(9), 2348-2361.e6. https://doi.org/10.1016/J.CELL.2021.02.037

Zhou, H., Dcosta, B. M., Samanovic, M. I., Mulligan, M. J., Landau, N. R., & Tada, T. (2021). B.1.526 SARS-CoV-2 variants identified in New York City are neutralized by vaccine-elicited and therapeutic monoclonal antibodies. *BioRxiv*, 2021.03.24.436620. https://doi.org/10.1101/2021.03.24.436620

Zhou, P., Yang, X. Lou, Wang, X. G., Hu, B., Zhang, L., Zhang, W., Si, H. R., Zhu, Y., Li, B., Huang, C. L., Chen, H. D., Chen, J., Luo, Y., Guo, H., Jiang, R. Di, Liu, M. Q., Chen, Y., Shen, X. R., Wang, X., … Shi, Z. L. (2020). A pneumonia outbreak associated with a new coronavirus of probable bat origin. *Nature*, *579*(7798), 270–273. https://doi.org/10.1038/s41586-020-2012-7

Zhuang, M. W., Cheng, Y., Zhang, J., Jiang, X. M., Wang, L., Deng, J., & Wang, P. H. (2020). Increasing host cellular receptor—angiotensin-converting enzyme 2 expression by coronavirus may facilitate 2019-nCoV (or SARS-CoV-2) infection. *Journal of Medical Virology*, *92*(11), 2693–2701. https://doi.org/10.1002/JMV.26139

Zimmerman, A. W., Joosten, B., Torensma, R., Parnes, J. R., van Leeuwen, F. N., & Figdor, C. G. (2006). Long-term engagement of CD6 and ALCAM is essential for T-cell proliferation induced by dendritic cells. *Blood*, *107*(8), 3212–3220. https://doi.org/10.1182/BLOOD-2005-09-3881

Zoufaly, A., Poglitsch, M., Aberle, J. H., Hoepler, W., Seitz, T., Traugott, M., Grieb, A., Pawelka, E., Laferl, H., Wenisch, C., Neuhold, S., Haider, D., Stiasny, K., Bergthaler, A., Puchhammer-Stoeckl, E., Mirazimi, A., Montserrat, N., Zhang, H., Slutsky, A. S., & Penninger, J. M. (2020). Human recombinant soluble ACE2 in severe COVID-19. *The Lancet Respiratory Medicine*, *8*(11), 1154–1158. https://doi.org/10.1016/S2213-2600(20)30418-5/ATTACHMENT/44F7BD01-1D44-49DE-8C49-B437CD5B0BE4/MMC1.PDF